

# Random Laguerre Tessellations

Zur Erlangung des akademischen Grades eines  
DOKTORS DER NATURWISSENSCHAFTEN  
von der Fakultät für Mathematik der  
Universität Karlsruhe (TH)  
genehmigte

## DISSERTATION

von  
Dipl.-Math. Claudia Lautensack  
aus Kaiserslautern

Tag der mündlichen Prüfung: 7. Februar 2007

Referent: Prof. Dr. Günter Last  
Koreferenten: Prof. Dr. Wolfgang Weil  
Prof. Dr. Joachim Ohser



# Preface

This thesis developed during my time as a PhD student at the department “Models and Algorithms in Image Processing” at the Fraunhofer ITWM in Kaiserslautern and the Institute for Stochastics at the University of Karlsruhe. I have experienced both the daily work in Kaiserslautern and my visits and the seminars in Karlsruhe as an interesting and enriching time. At this point I wish to thank all those people who have contributed to my work in one or another way.

I am indebted to Prof. Dr. Günter Last for accepting me as his PhD student at the University of Karlsruhe. Special thanks for the valuable discussions and remarks which have helped a lot to improve the theoretical part of this thesis.

I also wish to thank Prof. Dr. Wolfgang Weil for being the co-referee of my thesis. I am pleased to have Prof. Dr. Joachim Ohser as a third referee, especially as he was the one who suggested the subject of this thesis.

I am grateful to my colleagues at the department “Models and Algorithms in Image Processing” at the Fraunhofer ITWM and the head of department Dr. Ronald Rösch who have provided a pleasant atmosphere and excellent working facilities. In particular, I wish to thank Dr. Katja Schladitz for introducing me to the interesting and challenging field of stochastic geometry. Whenever I was seeking for advice, support or encouragement, I always found her door open. Thank you for giving me the opportunity to present my work at several conferences and workshops.

Further thanks to Prof. Dr. Sergei Zuyev for giving me a starting point for my work by sharing some of his unpublished results with me.

Many thanks to Prof. Dr. Aila Särkkä for the hospitality during my visits in Gothenburg and for inviting me to the Smögen workshops.

Moreover, I would like to thank Dr. Lars Michael Hoffmann, Katharina Robb, Oliver Wirjadi, and my brother Christian for proof-reading, Tetyana Sych for generating the 3D visualizations, Andreas Dinges and Björn Wagner for computer support, and Samir Issad for some help with the Mathematica programs.

I also want to thank the producer of the polymer foam studied in Chapter 5 for providing the tomographic images and for the permission to use this data in my thesis.

Finally, I want to say thank you to my family, who have supported me in whatever I have done. Special thanks to my father for publishing my work.

Thank you, Tom, for always being by my side!



# Contents

<b>Preface</b>	<b>i</b>
<b>Introduction</b>	<b>1</b>
<b>1 Definitions and classical results</b>	<b>5</b>
1.1 General notation . . . . .	5
1.2 Point processes . . . . .	6
1.3 Marked point processes . . . . .	10
1.4 Random measures and Palm measure . . . . .	12
1.5 Tessellations . . . . .	13
1.6 Random tessellations . . . . .	14
1.7 Flat sections . . . . .	17
<b>2 Laguerre tessellations</b>	<b>20</b>
2.1 Definitions . . . . .	20
2.2 Geometric properties of Laguerre diagrams . . . . .	23
2.3 Laguerre Delaunay tessellations . . . . .	26
2.4 The class of Laguerre tessellations . . . . .	27
<b>3 Poisson Laguerre tessellations</b>	<b>31</b>
3.1 Existence of the Poisson Laguerre tessellation . . . . .	31
3.2 Palm distributions . . . . .	34
3.2.1 Notation . . . . .	34
3.2.2 A complete description of $\mathbb{Q}_k^0$ . . . . .	36
3.3 Further distributions . . . . .	50
3.3.1 Distributions of the typical Laguerre Delaunay simplex . . . . .	50
3.3.2 Distributions for typical faces . . . . .	51
3.3.3 Contact distributions . . . . .	59
3.3.4 Chord length distribution . . . . .	62
3.4 Limit theorems . . . . .	63
3.5 Summary and open problems . . . . .	71
<b>4 Special cases, examples, and simulations</b>	<b>73</b>
4.1 Simulation methods . . . . .	73
4.2 The planar case . . . . .	75
4.2.1 General formulas . . . . .	75
4.2.2 Two-atom distribution . . . . .	78

---

4.2.3	Uniform distribution . . . . .	89
4.3	The spatial case . . . . .	91
4.3.1	General formulas . . . . .	92
4.3.2	Two-atom distribution . . . . .	96
4.3.3	Uniform distribution . . . . .	109
<b>5</b>	<b>Modeling of cellular materials</b>	<b>113</b>
5.1	Modeling the microstructure of materials by random tessellations . . . . .	114
5.2	Modeling a foam structure . . . . .	116
5.2.1	The data . . . . .	117
5.2.2	Cell reconstruction . . . . .	117
5.2.3	Statistical analysis . . . . .	118
5.2.4	Choice of model structures . . . . .	120
5.2.5	Model fitting procedure . . . . .	121
5.2.6	Test of the optimization method using simulated data . . . . .	122
5.2.7	Results for foam data . . . . .	122
5.3	Discussion . . . . .	124
	<b>Bibliography</b>	<b>127</b>
	<b>List of symbols</b>	<b>134</b>

# Introduction

A tessellation (or mosaic) in  $\mathbb{R}^d$  is a locally finite subdivision of  $\mathbb{R}^d$  into closed  $d$ -dimensional subsets with pairwise distinct interiors. Often it is further assumed that these subsets, called cells or crystals, are bounded convex polytopes. Such configurations appear in many natural structures, such as polycrystalline materials, plant cells, crack patterns or foam structures. While for instance honeycombs show a deterministic structure, most real-life tessellations must be considered as random. Consequently, random tessellations belong to the central models of stochastic geometry. Typically, they are constructed from random processes of geometric objects (e.g., points, balls or hyperplanes) in space and may be regarded as either random closed sets or point processes of convex polytopes.

Information on the topological and geometric structure of a random tessellation is captured by geometric characteristics (e.g., volume, surface area or number of vertices) of its “typical” cell. This notion refers to a cell drawn at random among the cells of the tessellation, where each cell is chosen with the same probability, and is formalized by means of Palm theory. Moments or distribution functions of characteristics of their typical cells are used as a tool for the characterization and comparison of random tessellations. Therefore, the computation of these quantities for different tessellation models is one of the main tasks when studying random tessellations.

Perhaps the most important and most widely studied model is the Voronoi (or Dirichlet) tessellation generated by a locally finite set  $S$  of points in  $\mathbb{R}^d$ . The cell generated by a point  $x \in S$  consists of all points  $y \in \mathbb{R}^d$  having  $x$  as nearest neighbor in  $S$ . Alternatively, the Voronoi tessellation can be defined as the result of a growth process. The points of  $S$  act as seeds which start to grow simultaneously and with constant speed. Growth stops at the contact points to the neighboring cells but otherwise continues until space is completely filled.

The first presentations of this concept are attributed to Dirichlet (1850) and Voronoi (1907, 1908, 1909). Since then, Voronoi tessellations with respect to various processes of generators (e.g., Poisson, hard core or cluster processes) have been considered and are used in application areas such as astronomy, biology, crystallography, ecology or communication theory. However, only the Voronoi tessellation generated by a stationary Poisson process allows for a reasonable number of analytical results. The geometric characteristics of the typical Voronoi cell with respect to other processes of generators have to be studied by means of simulation.

The Voronoi construction, with cell faces being equidistant from the generators of their cells, is quite restrictive for the range of cell patterns which can be realized by Voronoi tessellations. Thus, it sometimes turns out in applications that an observed cell structure cannot be modeled satisfactorily by a Voronoi tessellation. In order to realize a larger variety of tessellation structures, the Voronoi construction has been generalized in various ways.

Voronoi tessellations of order  $k \in \mathbb{N}$  take not only the nearest but the  $k$  nearest neighbors of a generator  $x \in S$  into account. Further generalizations are obtained when replacing the Euclidean distance by other (even anisotropic) metrics or when using more general objects (e.g., balls or line segments) as generators. Another approach to generalize the concept of Voronoi tessellations is the use of weighted distances. An individual weight  $w$  is attached to each point  $x \in S$ , the distance of  $y \in \mathbb{R}^d$  to the weighted point  $(x, w)$  is then measured by a function of  $\|x - y\|$  and  $w$ . One well-known example is the Johnson-Mehl tessellation (Johnson and Mehl, 1939), which is obtained by additively weighting the Euclidean distance. It can be interpreted as the result of a growth process of seeds being generated according to a random process in time. Unlike Voronoi cells, the cells of a Johnson-Mehl tessellation are in general no longer convex. Some analytic results for Johnson-Mehl tessellations generated by a time-inhomogeneous Poisson process have been established by Møller (1992).

This work is devoted to another type of weighted Voronoi tessellation: the Laguerre tessellation, which is generated by a set  $S$  of spheres in  $\mathbb{R}^d$  and with respect to the so-called power distance

$$\text{pow}(y, (x, r)) := \|x - y\|^2 - r^2, \quad (x, r) \in S, y \in \mathbb{R}^d.$$

This distance and the radical axis, the set of points having equal power distance to two spheres in  $\mathbb{R}^d$ , have been considered by several authors (Blaschke, 1929; Coxeter, 1969; Fischer et al., 1971). The first systematic considerations of the corresponding tessellations seem to be the papers by Imai et al. (1985), Ash and Bolker (1986), and Aurenhammer (1987b). Besides the term Laguerre tessellation a great variety of other names has been introduced for these structures, e.g., power tessellation, sectional Dirichlet tessellation, radical tessellation, Voronoi diagram in the Laguerre geometry, or Laguerre tiling. So far, Laguerre tessellations have mainly been studied in the context of computational geometry, materials science, or physics. Little attention has been paid to Laguerre tessellations as challenging and promising models in stochastic geometry. This work is thought as a foundation for the systematic investigation of random Laguerre tessellations in the framework of stochastic geometry.

As a first point, geometric properties of the Laguerre cells and the resulting tessellations have to be studied. The advantage of the power distance is not obvious at the first glance, but leads to promising geometric properties of the induced tessellations. First of all, their cells are convex polytopes, which are handled more easily than curved structures both analytically and computationally. Further, under some mild assumptions on the set of generators, the Laguerre tessellation turns out to be a normal tessellation. For such structures, a general framework of results and methods has been developed (e.g., Mecke, 1984; Møller, 1989). For example, well-known formulas relating the mean values of different cell characteristics can be applied for Laguerre tessellations. It even turns out that every normal tessellation in  $\mathbb{R}^d$  for  $d \geq 3$  can be represented as a Laguerre tessellation.

However, when working with Laguerre tessellations one is also confronted with several difficulties. A sphere contained in the generating set  $S$  does not necessarily generate a cell and if it does, it is not necessarily contained in this cell. This makes Laguerre tessellations less descriptive than Voronoi tessellations. As a further consequence, some important geometric characteristics such as the cell intensity are well-known for Voronoi tessellations but cannot be computed in the Laguerre case. Even more, it is not immediately clear which of the results for (Poisson) Voronoi tessellations can be generalized to Laguerre tessellations.

Laguerre tessellations are used in various application areas. One example is computational geometry, where algorithms, for instance for the computation of the volume, the

contour, and the connected components of the union of a set of balls (Imai et al., 1985; Avis et al., 1988), or for problems related to the illumination of balls (Aurenhammer, 1987b), are based on the construction of Laguerre tessellations. Further, information on the geometric structure of binary or polydisperse packings of spheres can be derived from their Laguerre tessellations (e.g., Gervois et al., 2002, 2004). In molecular biology and biochemistry, Laguerre tessellations are used to analyze the structure of folded proteins (Sadoc et al., 2003). Finally, they are used in materials science as models for cellular and polycrystalline materials. Telley et al. (1996a,b), Xue et al. (1997), and Schüle (1996) proposed models for grain growth in polycrystalline materials which are based on Laguerre tessellations. Recent applications of Laguerre tessellations in materials science can be found in Fan et al. (2004) (polycrystalline materials), Kühn (2005) (sintered alumina), Kadashevich and Stoyan (2005) (aerated autoclaved concrete), and Kanaun and Tkachenko (2006) (open cell foams).

The use of Laguerre tessellations as models for the microstructure of materials requires an understanding of the geometric structure of their typical cells with respect to changing processes of generators and radius distributions. So far, little has been done in this field. As a starting point, we will investigate Laguerre tessellations generated by stationary marked Poisson processes in  $\mathbb{R}^d$ . The analytic formulas for Poisson Voronoi and Johnson-Mehl tessellations as well as some first unpublished results by Zuyev (2004) rise the hope that also Laguerre tessellations will prove tractable to analytic investigations. To some degree, this turns out to be indeed the case. In this work, several results for moments and distributions of characteristics of Poisson Laguerre tessellations are established. However, compared to Poisson Voronoi tessellation, a lot of technical difficulties arise. The power distance of a point in space to a sphere is not necessarily positive and depends on both the location and the radius of the sphere. Hence, the formulas obtained for Laguerre tessellations are less explicit than the ones for the Voronoi case which makes a further treatment (e.g., numerical evaluation) more difficult if not even impossible.

Nevertheless, Laguerre tessellations are promising models for the microstructure of materials. In this thesis, their application as models for cellular materials is discussed by the example of a closed polymer foam. The Laguerre model outperforms not only the Poisson Voronoi tessellation but also Voronoi tessellations generated by hard core point processes. This is a remarkable result since these models are widely used in the context of foam modeling and shows that Laguerre tessellations should be considered as a powerful alternative.

The organization of the text is as follows: In Chapter 1, we give a summary of some basic definitions and results from stochastic geometry which will be used throughout the thesis. In particular, we turn attention to point processes and random tessellations.

The concept of the Laguerre diagram and its orthogonal dual, the Laguerre Delaunay diagram, is introduced in Chapter 2. We restrict ourselves to the deterministic case, where the set of generators is a given set of spheres in  $\mathbb{R}^d$ . We study geometric properties of both diagrams and introduce some regularity conditions on the set of generators which ensure that they are tessellations of  $\mathbb{R}^d$ . Finally, we show that any normal tessellation in  $\mathbb{R}^d$  for  $d \geq 3$  can be realized as a Laguerre tessellation, which is an evidence for the generality of Laguerre tessellations.

Chapter 3, the central chapter of this thesis, is devoted to Poisson Laguerre tessellations, where the process of generators is a homogeneous independently marked Poisson process  $\Phi$  in  $\mathbb{R}^d$ . After the existence of the Poisson Laguerre tessellation is guaranteed, we provide a

complete description of the Palm distribution describing  $\Phi$  as seen from a randomly chosen point on a  $k$ -face of the tessellation. From this result, we deduce some formulas for mean values and distributions of characteristics of the typical cells of the Laguerre and the Laguerre Delaunay tessellation generated by  $\Phi$ . Further, we derive formulas for contact and chord length distributions of Poisson Laguerre tessellations. Finally, we prove some limit theorems dealing with the convergence of Poisson Laguerre to Poisson Voronoi tessellations.

Since the cases  $d = 2$  and  $d = 3$  are the most important ones for applications, they are discussed in detail in Chapter 4. For two-atom and uniform distributions of radii, we evaluate numerically some of the formulas derived in Chapter 3. To get a further impression of the sample structures, distributions of characteristics of their typical cells are determined by simulations.

In the final chapter we discuss an example of applications, the modeling of a foam structure by a random Laguerre tessellation. We estimate the characteristics of the cells of a closed polymer foam from a tomographic image. Based on these quantities we fit a Laguerre tessellation model to the microstructure of the material. The comparison of this model to some widely used Voronoi tessellation models clearly suggests the use of the Laguerre tessellation.

# Chapter 1

## Definitions and classical results

In this chapter we introduce the notation used throughout this thesis and state some classical results from stochastic geometry which will be needed in the subsequent chapters. The notation is mainly based on the book by Schneider and Weil (2000). For the proofs of most of the theorems and further details we refer to the books on stochastic geometry by Schneider and Weil (2000) and Stoyan et al. (1995). We will only include the proofs of those statements which we have not found proven in the required form in the literature. A detailed treatment of point processes can be found in the book by Daley and Vere-Jones (1988). Concerning random tessellations we refer to the work of Møller (1989, 1994).

### 1.1 General notation

- Denote the set of real numbers by  $\mathbb{R}$  and the set of positive real numbers by  $\mathbb{R}^+$ . Further, let  $\mathbb{N} := \{1, 2, 3, \dots\}$  and  $\mathbb{N}_0 := \{0, 1, 2, 3, \dots\}$ .
- Let  $E$  be a locally compact space with countable basis and write  $\mathcal{B}(E)$  for its Borel  $\sigma$ -field. The system of closed sets in  $E$  will be denoted by  $\mathcal{F}(E)$ , the system of open sets by  $\mathcal{G}(E)$ , and the system of compact sets by  $\mathcal{C}(E)$ .  $\mathcal{F}'(E) := \mathcal{F}(E) \setminus \{\emptyset\}$  and  $\mathcal{C}'(E) := \mathcal{C}(E) \setminus \{\emptyset\}$  are the non-empty closed and compact subsets of  $E$ , respectively.

The space  $\mathcal{F}(E)$  is equipped with the topology of closed convergence, which is generated by the sets

$$\{\mathcal{F}^C : C \in \mathcal{C}(E)\} \cup \{\mathcal{F}_G : G \in \mathcal{G}(E)\},$$

where

$$\begin{aligned}\mathcal{F}^C &:= \{F \in \mathcal{F}(E) : F \cap C = \emptyset\}, \quad C \in \mathcal{C}(E), \text{ and} \\ \mathcal{F}_G &:= \{F \in \mathcal{F}(E) : F \cap G \neq \emptyset\}, \quad G \in \mathcal{G}(E).\end{aligned}$$

Finally, the set  $\mathcal{F}(E)$  is equipped with the  $\sigma$ -field  $\mathcal{B}(\mathcal{F}(E))$  of Borel sets with respect to the topology defined above.

The Borel sets in  $d$ -dimensional Euclidean space  $\mathbb{R}^d$  will be denoted by  $\mathcal{B}^d$ , and we will use the abbreviations  $\mathcal{F} := \mathcal{F}(\mathbb{R}^d)$ ,  $\mathcal{G} := \mathcal{G}(\mathbb{R}^d)$ ,  $\mathcal{C} := \mathcal{C}(\mathbb{R}^d)$ ,  $\mathcal{F}' := \mathcal{F}'(\mathbb{R}^d)$ , and  $\mathcal{C}' := \mathcal{C}'(\mathbb{R}^d)$ . The translation of a set  $B \in \mathcal{B}^d$  by  $x \in \mathbb{R}^d$  is defined as

$$B + x := \{y + x : y \in B\}.$$

- Write  $\langle \cdot, \cdot \rangle$  for the Euclidean scalar product on  $\mathbb{R}^d$  and  $\|\cdot\|$  for the corresponding norm.
- For  $B \subset \mathbb{R}^d$  we write  $\text{int } B$  for the topological interior and  $\partial B$  for the boundary of  $B$ .
- The Lebesgue measure on  $\mathbb{R}^d$  is denoted by  $\lambda_d$ . For  $B \in \mathcal{B}^d$  we will use the notation  $|B|_d := \lambda_d(B)$ . When integrating with respect to  $\lambda_d$ , we will usually write  $dx$  instead of  $\lambda_d(dx)$ .
- For  $x \in \mathbb{R}^d$  and  $r \geq 0$  let  $b(x, r)$  denote the  $d$ -dimensional ball of radius  $r$  centered in  $x$ . The  $d$ -dimensional unit sphere is denoted by  $S^{d-1}$  and its surface measure by  $\mathbb{S}$ . Let  $\omega_d := |b(0, 1)|_d$  be the volume and  $\sigma_d := \mathbb{S}(S^{d-1})$  the surface area of the unit ball in  $\mathbb{R}^d$ , i.e.

$$\omega_d = \frac{\pi^{\frac{d}{2}}}{\Gamma(\frac{d}{2} + 1)} \quad \text{and} \quad \sigma_d = 2 \frac{\pi^{\frac{d}{2}}}{\Gamma(\frac{d}{2})}.$$

- Write  $SO_d$  for the group of rotations about the origin in  $\mathbb{R}^d$  and  $\nu$  for its unique rotational invariant probability measure.
- The  $k$ -dimensional Hausdorff-measure is denoted by  $\mathcal{H}^k$ .
- For real numbers  $a$  and  $b$  such that  $a < b$  we will write  $U(a, b)$  for the uniform distribution on the interval  $[a, b]$ . For  $r_0, r_1 \in \mathbb{R}$  and  $0 \leq p \leq 1$  let  $A(r_0, r_1, p)$  be the two-atom distribution which takes the values  $r_0$  and  $r_1$  with probabilities  $p$  and  $1 - p$ , respectively.

## 1.2 Point processes

### Definition 1.2.1

For  $x \in \mathbb{R}^d$  the Dirac measure  $\delta_x$  is a probability measure on  $\mathbb{R}^d$  defined by

$$\delta_x(A) := \begin{cases} 1, & \text{if } x \in A, \\ 0, & \text{if } x \notin A, \end{cases} \quad A \in \mathcal{B}^d. \quad (1.1)$$

A *counting measure* on  $\mathbb{R}^d$  is a measure defined as a finite or countable sum

$$\eta := \sum_{i=1}^k \delta_{x_i}, \quad k \in \mathbb{N}_0 \cup \{\infty\}. \quad (1.2)$$

The counting measures  $\eta$  considered here are assumed to be locally finite, i.e.  $\eta(C) < \infty$  for every  $C \in \mathcal{C}$ . A counting measure  $\eta$  is called *simple* if  $\eta(\{x\}) \leq 1$  for all  $x \in \mathbb{R}^d$ . We write  $\mathbf{N}$  for the set of all locally finite counting measures on  $\mathbb{R}^d$  and  $\mathbf{N}_s$  for the subset of all simple measures in  $\mathbf{N}$ . We equip  $\mathbf{N}$  with the  $\sigma$ -field  $\mathcal{N}$  generated by the maps  $\eta \mapsto \eta(B)$ ,  $\eta \in \mathbf{N}$ ,  $B \in \mathcal{B}^d$ . Each simple counting measure  $\eta \in \mathbf{N}_s$  can be identified with its support

$$\text{supp } \eta := \{x \in \mathbb{R}^d : \eta(\{x\}) = 1\},$$

which is a locally finite subset of  $\mathbb{R}^d$ .

**Definition 1.2.2**

A *point process* is a random variable  $\Phi$  on a probability space  $(\Omega, \mathcal{A}, \mathbb{P})$  taking values in the measurable space  $(\mathbf{N}, \mathcal{N})$ . The distribution  $\mathbb{P}_\Phi$  of a point process is now determined by the probabilities

$$\mathbb{P}_\Phi(A) = \mathbb{P}(\Phi \in A) = \mathbb{P}(\{\omega \in \Omega : \Phi(\omega) \in A\}), \quad A \in \mathcal{N}.$$

By Schneider and Weil (2000, Lemma 3.1.7), there is a sequence  $(X_i)_{i \in \mathbb{N}}$  of measurable mappings  $X_i : \Omega \rightarrow \mathbb{R}^d$  such that

$$\Phi = \sum_{i=1}^{\Phi(\mathbb{R}^d)} \delta_{X_i}. \quad (1.3)$$

The point process  $\Phi$  is called *simple* if  $\Phi \in \mathbf{N}_s$  almost surely. In this case, each realization of  $\Phi$  can be identified with its support. Therefore, we will also use the notations  $\Phi = \{X_1, X_2, \dots\}$  and  $x \in \Phi$ .

**Definition 1.2.3 (Intensity measure)**

The *intensity measure*  $\Lambda$  of a point process  $\Phi$  is given by

$$\Lambda(B) := \mathbb{E}[\Phi(B)] = \int \varphi(B) \mathbb{P}(d\varphi), \quad B \in \mathcal{B}^d.$$

Then  $\Lambda(B)$  is the mean number of points contained in  $B$ . In the following, we will always assume that  $\Lambda$  is locally finite, i.e. that  $\Lambda(C) < \infty$  for all  $C \in \mathcal{C}$ .

**Theorem 1.2.4 (Campbell theorem)**

For any measurable function  $h : \mathbb{R}^d \rightarrow [0, \infty)$  the function  $\sum_{x \in \Phi} h(x)$  is measurable with

$$\mathbb{E} \left[ \sum_{x \in \Phi} h(x) \right] = \int \sum_{x \in \varphi} h(x) \mathbb{P}(d\varphi) = \int h(x) \Lambda(dx).$$

**Definition 1.2.5 (Stationarity and isotropy)**

For any  $y \in \mathbb{R}^d$  we define the translation of  $\Phi$  by  $y \in \mathbb{R}^d$  as

$$\Phi + y := \{x + y : x \in \Phi\}.$$

A point process  $\Phi$  is called *stationary* if its distribution is invariant under translations, i.e.

$$\mathbb{P}(\Phi \in A) = \mathbb{P}(\Phi + y \in A), \quad A \in \mathcal{N}, y \in \mathbb{R}^d.$$

The *intensity*  $\lambda$  of a stationary point process  $\Phi$  is defined by

$$\lambda := \Lambda([0, 1]^n) = \mathbb{E}[\Phi([0, 1]^n)]$$

and can be interpreted as the mean number of points of  $\Phi$  per unit volume. The local finiteness of  $\Lambda$  implies that  $\lambda$  is finite. The intensity measure  $\Lambda$  of  $\Phi$  has a decomposition

$$\Lambda(B) = \lambda |B|_d, \quad B \in \mathcal{B}^d.$$

Further, we define the rotation of  $\Phi$  by  $\vartheta \in SO_d$  as

$$\vartheta\Phi := \{\vartheta x : x \in \Phi\}.$$

A point process  $\Phi$  is called *isotropic* if its distribution is invariant under rotations, i.e.

$$\mathbb{P}(\Phi \in A) = \mathbb{P}(\vartheta\Phi \in A), \quad A \in \mathcal{N}, \vartheta \in SO_d.$$

For the rest of this section, we will assume that  $\Phi$  is a stationary point process with intensity  $0 < \lambda < \infty$ .

**Definition 1.2.6 (Palm distribution of a point process)**

The *Palm distribution*  $\mathbb{P}^0$  of the point process  $\Phi$  is a probability measure on  $\mathbf{N}$  defined by

$$\mathbb{P}^0(A) := \frac{1}{\lambda} \mathbb{E} \left[ \sum_{x \in \Phi} \mathbb{1}_{[0,1]^d}(x) \mathbb{1}_A(\Phi - x) \right], \quad A \in \mathcal{N}.$$

Heuristically,  $\mathbb{P}^0$  is the distribution of the point process  $\Phi$  conditioned on  $0 \in \Phi$ . For an arbitrary point  $x \in \mathbb{R}^d$  we define  $\mathbb{P}^x(A) := \mathbb{P}^0(A - x)$ ,  $A \in \mathcal{N}$ .

The *reduced Palm distribution*  $\mathbb{P}^{0,!}$  is defined by

$$\mathbb{P}^{0,!}(A) := \frac{1}{\lambda} \mathbb{E} \left[ \sum_{x \in \Phi} \mathbb{1}_{[0,1]^d}(x) \mathbb{1}_A((\Phi - x) \setminus \{0\}) \right], \quad A \in \mathcal{N}.$$

It is the distribution of  $\Phi \setminus \{0\}$  conditioned on  $0 \in \Phi$ .

**Definition 1.2.7 (Generating functional)**

Let  $U$  be the family of all non-negative bounded measurable functions  $u$  on  $\mathbb{R}^d$  whose support is bounded. Furthermore, let  $V$  be the family of all functions  $v = 1 - u$  for  $u \in U$  with  $0 \leq u \leq 1$ . Then the generating functional  $G_\Phi$  of a point process  $\Phi$  is defined by

$$G_\Phi(v) := \mathbb{E} \left[ \prod_{x \in \Phi} v(x) \right] = \int \prod_{x \in \varphi} v(x) \mathbb{P}(d\varphi), \quad v \in V.$$

The distribution of  $\Phi$  is uniquely determined by  $G_\Phi$ .

**Theorem 1.2.8 (Refined Campbell theorem)**

For any measurable function  $h : \mathbb{R}^d \times \mathbf{N} \rightarrow [0, \infty)$  the function  $\sum_{x \in \Phi} h(x, \Phi)$  is measurable with

$$\mathbb{E} \left[ \sum_{x \in \Phi} h(x, \Phi) \right] = \int \sum_{x \in \varphi} h(x, \varphi) \mathbb{P}(d\varphi) = \lambda \int \int h(x, \varphi + x) \mathbb{P}^0(d\varphi) dx.$$

**Definition 1.2.9 (Poisson point process)**

A *Poisson point process* on  $\mathbb{R}^d$  with locally finite intensity measure  $\Lambda$  is characterized by the following properties:

- (i) The number of points contained in a bounded Borel set  $B \in \mathcal{B}^d$  has a Poisson distribution with mean  $\Lambda(B)$ .
- (ii) For arbitrary  $k \in \mathbb{N}$  the numbers of points of  $\Phi$  in  $k$  disjoint Borel sets form  $k$  independent random variables.

A point process  $\Phi$  satisfying condition (i) is simple if and only if its intensity measure  $\Lambda$  is free of atoms. For simple point processes condition (i) implies condition (ii). Including condition (ii) in the definition guarantees that the Poisson process  $\Phi$  is uniquely determined by  $\Lambda$  irrespective of  $\Phi$  being simple or not (Schneider and Weil, 2000, p. 103).

**Proposition 1.2.10**

Let  $\Phi$  be a stationary Poisson process on  $\mathbb{R}^d$  with intensity  $\lambda$ .

(i) *Generalized Campbell theorem*

Let  $h : (\mathbb{R}^d)^n \rightarrow [0, \infty)$  be a measurable function. Then

$$\mathbb{E} \left[ \sum_{x_1, \dots, x_n \in \Phi}^{\neq} h(x_1, \dots, x_n) \right] = \lambda^n \int \dots \int h(x_1, \dots, x_n) dx_1 \dots dx_n,$$

where  $\sum^{\neq}$  denotes summation over  $n$ -tuples of pairwise distinct points of  $\Phi$ .

(ii) *The generating functional of  $\Phi$  has the form*

$$G_{\Phi}(v) = \exp \left( -\lambda \int (1 - v(x)) dx \right), \quad v \in V.$$

(iii) *Slivnyak-Theorem*

The Palm distribution of  $\Phi$  is given by  $\mathbb{P}^0 = \mathbb{P} * \delta_{\delta_0}$ , where  $\delta_{\delta_0}$  is the distribution of the point process consisting only of the fixed point 0. This means

$$\int h(\varphi) \mathbb{P}^0(d\varphi) = \int h(\varphi \cup \{0\}) \mathbb{P}(d\varphi)$$

for any measurable function  $h : \mathbf{N} \rightarrow [0, \infty)$ . For  $x \in \mathbb{R}^d$  we have  $\mathbb{P}^x = \mathbb{P} * \delta_{\delta_x}$ .

(iv) *The reduced Palm distribution of  $\Phi$  is just the original distribution of  $\Phi$ , i.e.  $\mathbb{P}^{0,1} = \mathbb{P}$ .*

**Theorem 1.2.11 (Slivnyak-Mecke formula)**

Let  $\Phi$  be a stationary Poisson process on  $\mathbb{R}^d$  with intensity  $\lambda$  and let  $h : (\mathbb{R}^d)^n \times \mathbf{N} \rightarrow [0, \infty)$  be a measurable function. Then we have

$$\mathbb{E} \left[ \sum_{x_1, \dots, x_n \in \Phi}^{\neq} h(x_1, \dots, x_n, \Phi) \right] = \lambda^n \int \dots \int \mathbb{E} [h(x_1, \dots, x_n, \Phi \cup \{x_1, \dots, x_n\})] dx_1 \dots dx_n.$$

**Proof:**

Application of the refined Campbell theorem and the Slivnyak theorem yields

$$\begin{aligned} & \mathbb{E} \left[ \sum_{x_1, \dots, x_n \in \Phi}^{\neq} h(x_1, \dots, x_n, \Phi) \right] \\ &= \mathbb{E} \left[ \sum_{x_1 \in \Phi} \sum_{x_2, \dots, x_n \in \Phi \setminus \{x_1\}}^{\neq} h(x_1, \dots, x_n, \Phi) \right] \\ &= \lambda \int \int \sum_{x_2, \dots, x_n \in (\varphi + x_1) \setminus \{x_1\}}^{\neq} h(x_1, \dots, x_n, (\varphi + x_1)) \mathbb{P}^0(d\varphi) dx_1 \\ &= \lambda \int \int \sum_{x_2, \dots, x_n \in \varphi \setminus \{x_1\}}^{\neq} h(x_1, \dots, x_n, \varphi) \mathbb{P}^{x_1}(d\varphi) dx_1 \\ &= \lambda \int \int \sum_{x_2, \dots, x_n \in \varphi}^{\neq} h(x_1, \dots, x_n, \varphi \cup \{x_1\}) \mathbb{P}(d\varphi) dx_1. \end{aligned}$$

The result is obtained by iteration of this procedure for the remaining points.  $\square$

### 1.3 Marked point processes

#### Definition 1.3.1

Let  $E$  be a locally compact space with countable basis. Analogous to (1.1) and (1.2) we may define the notion of Dirac and counting measures on  $\mathbb{R}^d \times E$ . Denote by  $\mathbf{N}(E)$  the set of all counting measures  $\eta$  on  $\mathbb{R}^d \times E$  satisfying the conditions

- (i)  $\eta(\cdot \times E) \in \mathbf{N}_s$  and
- (ii) for each  $x \in \eta(\cdot \times E)$  there is exactly one  $m \in E$  such that  $(x, m) \in \eta$ .

We equip  $\mathbf{N}(E)$  with the  $\sigma$ -field  $\mathcal{N}(E)$  generated by the maps  $\eta \mapsto \eta(A)$ ,  $A \in \mathcal{B}(\mathbb{R}^d \times E)$ .

#### Definition 1.3.2

A *marked point process*  $\Phi$  on  $\mathbb{R}^d$  with *mark space*  $E$  is a random variable on a probability space  $(\Omega, \mathcal{A}, \mathbb{P})$  taking values in the measurable space  $(\mathbf{N}(E), \mathcal{N}(E))$ . There are sequences of measurable mappings  $X_i : \Omega \rightarrow \mathbb{R}^d$ ,  $i \in \mathbb{N}$ , and  $M_i : \Omega \rightarrow E$ ,  $i \in \mathbb{N}$ , such that

$$\Phi = \sum_{i=1}^{\tau} \delta_{(X_i, M_i)},$$

where  $\tau := \Phi(\mathbb{R}^d \times E)$ . The marked point process  $\Phi$  is called *independently marked*, if the random marks  $(M_i)_{i \in \mathbb{N}}$  are independently identically distributed and independent of  $((X_i)_{i \in \mathbb{N}}, \tau)$ . The distribution  $\mathbb{F}$  of the random variables  $M_i$  is called the *mark distribution* of  $\Phi$ .

We define the translation of  $\Phi$  by  $y \in \mathbb{R}^d$  as

$$\Phi + y := \{(x + y, m) : (x, m) \in \Phi\}, \quad y \in \mathbb{R}^d,$$

and call  $\Phi$  *stationary* if its distribution is invariant under translations. We further define the rotation of  $\Phi$  by  $\vartheta \in SO_d$  as

$$\vartheta\Phi := \{(\vartheta x, m) : (x, m) \in \Phi\}, \quad \vartheta \in SO_d.$$

#### Theorem 1.3.3

The intensity measure  $\Lambda$  of a stationary marked point process  $\Phi$  on  $\mathbb{R}^d$  with mark space  $E$  is given by

$$\Lambda = \lambda \mathcal{H}^d \otimes \mathbb{Q},$$

where  $\lambda$  is the intensity of the unmarked point process  $\Phi(\cdot \times E)$  and  $\mathbb{Q}$  is a probability measure on  $E$ .

Again we assume  $0 < \lambda < \infty$ . Then

$$\mathbb{Q}(B) = \frac{1}{\lambda} \mathbb{E} \left[ \sum_{(y, m) \in \Phi} \mathbb{1}_{[0,1]^d}(y) \mathbb{1}_B(m) \right], \quad B \in \mathcal{B}(E).$$

If  $\Phi$  is an independently marked point process, then  $\mathbb{Q}$  equals the mark distribution  $\mathbb{F}$ .

**Definition 1.3.4 (Palm distribution)**

Let  $\Phi$  be a stationary marked point process on  $\mathbb{R}^d$  with mark space  $E$  and intensity  $\lambda > 0$ . The Palm distribution  $\mathbb{P}^0$  of  $\Phi$  is defined by

$$\mathbb{P}^0(A) := \frac{1}{\lambda} \mathbb{E} \left[ \sum_{(y,m) \in \Phi} \mathbb{1}_{[0,1]^d}(y) \mathbb{1}_A(\Phi - y) \right], \quad A \in \mathcal{N}(E).$$

The results for point processes given in the last section can be generalized to the case of marked point processes.

**Theorem 1.3.5 (Refined Campbell theorem)**

Let  $\Phi$  be a stationary marked point process on  $\mathbb{R}^d$  with mark space  $E$  and intensity  $\lambda > 0$ . Let  $h : \mathbb{R}^d \times E \times \mathbf{N}(E) \rightarrow [0, \infty)$  be a measurable function. Then the function  $\sum_{(y,m) \in \Phi} h(y, m, \Phi)$

is measurable and

$$\mathbb{E} \left[ \sum_{(y,m) \in \Phi} h(y, m, \Phi) \right] = \lambda \int_E \int_{\mathbb{R}^d} \int_{\mathbf{N}(E)} h(y, m, \varphi + y) \mathbb{P}^0(d\varphi) dy \mathbb{F}(dm).$$

**Definition 1.3.6**

A Poisson process on  $\mathbb{R}^d \times E$  can be defined analogously to Definition 1.2.9, where the word “bounded” in (i) is replaced by  $\Lambda(B) < \infty$ . One way to construct such a process is by independent marking of a Poisson process on  $\mathbb{R}^d$  (Schneider and Weil, 2000, Satz 3.4.7). For the stationary case, any Poisson process on  $\mathbb{R}^d \times E$  which satisfies the conditions in Definition 1.3.1 is independently marked. Therefore, we will understand by a *stationary marked Poisson process* on  $\mathbb{R}^d$  with mark space  $E$  a point process on  $\mathbb{R}^d \times E$  which is obtained by independent marking of a stationary Poisson process on  $\mathbb{R}^d$ .

**Proposition 1.3.7**

Let  $\Phi$  be a stationary marked Poisson process on  $\mathbb{R}^d$  with mark space  $E$  and intensity  $\lambda$ .

(i) *Generalized Campbell theorem*

Let  $h : (\mathbb{R}^d \times E)^n \rightarrow [0, \infty)$  be a measurable function. Then

$$\begin{aligned} & \mathbb{E} \left[ \sum_{(x_1, m_1), \dots, (x_n, m_n) \in \Phi}^{\neq} h(x_1, m_1, \dots, x_n, m_n) \right] \\ &= \lambda^n \int_E \dots \int_E \int_{\mathbb{R}^d} \dots \int_{\mathbb{R}^d} h(x_1, m_1, \dots, x_n, m_n) dx_1 \dots dx_n \mathbb{F}(dm_1) \dots \mathbb{F}(dm_n). \end{aligned}$$

(ii) Define the set  $V$  as a set of functions on  $\mathbb{R}^d \times E$  analogously to Definition 1.2.7. The generating functional of  $\Phi$  has the form

$$G_\Phi(v) = \exp \left( -\lambda \int_E \int_{\mathbb{R}^d} (1 - v(x, m)) dx \mathbb{F}(dm) \right), \quad v \in V. \quad (1.4)$$

(iii) *Slivnyak-Theorem*

If  $\Phi$  is a Poisson process with mark distribution  $\mathbb{F}$ , then

$$\mathbb{P}^0(A) = \int_E \mathbb{P}(\Phi \cup \{(0, m)\} \in A) \mathbb{F}(dm), \quad A \in \mathcal{N}(E).$$

**Theorem 1.3.8 (Slivnyak-Mecke formula)**

Let  $\Phi$  be a stationary Poisson process of intensity  $\lambda$  and let  $h : (\mathbb{R}^d \times E)^n \times \mathbf{N}(E) \rightarrow [0, \infty)$  be a measurable function. Then we have

$$\begin{aligned} & \mathbb{E} \left[ \sum_{(x_1, m_1), \dots, (x_n, m_n) \in \Phi}^{\neq} h(x_1, m_1, \dots, x_n, m_n, \Phi) \right] \\ &= \lambda^n \int_E \dots \int_E \int_{\mathbb{R}^d} \dots \int_{\mathbb{R}^d} \mathbb{E} [h(x_1, m_1, \dots, x_n, m_n, \Phi \cup \{(x_1, m_1), \dots, (x_n, m_n)\})] dx_1 \dots dx_n \\ & \quad \mathbb{F}(dm_1) \dots \mathbb{F}(dm_n). \end{aligned}$$

**Proof:**

Works as the proof of Theorem 1.2.11. □

## 1.4 Random measures and Palm measure

In the following, we will work with the canonical setting  $(\Omega, \mathcal{A}, \mathbb{P}) = (\mathbf{N}(E), \mathcal{N}(E), \mathbb{P})$ , where  $\mathbb{P}$  is a probability measure on  $(\mathbf{N}(E), \mathcal{N}(E))$ . For the moment, we assume that  $\mathbb{P}$  is the distribution of a stationary point process  $\Phi$  defined by the identical mapping on  $\mathbf{N}(E)$ . Later, we will also consider other choices of  $\mathbb{P}$ .

**Definition 1.4.1**

Denote the space of all locally finite measures on  $\mathbb{R}^d$  by  $\mathbf{M}$ . Equip  $\mathbf{M}$  with the  $\sigma$ -field  $\mathcal{M}$  generated by the mappings  $\alpha \mapsto \alpha(B)$ ,  $\alpha \in \mathbf{M}$ ,  $B \in \mathcal{B}^d$ .

- (i) A *random measure*  $M$  (adapted to the point process  $\Phi$ ) is a measurable mapping from  $\mathbf{N}(E)$  to  $\mathbf{M}$ . It is called *stationary* if

$$M(\varphi, B + x) = M(\varphi - x, B), \quad \varphi \in \mathbf{N}(E), x \in \mathbb{R}^d, B \in \mathcal{B}^d.$$

- (ii) The *intensity measure* of a random measure  $M$  is given by

$$\Lambda(B) := \mathbb{E}[M(B)], \quad B \in \mathcal{B}^d.$$

For a stationary random measure  $M$  we have  $\Lambda(dx) = \lambda_M dx$ , where  $\lambda_M = \mathbb{E}[M([0, 1]^d)]$  is the *intensity* of  $M$ .

- (iii) Let  $M$  be a stationary random measure. The measure

$$\mathbb{P}_M(A) := \int \int \mathbb{I}\{\varphi - x \in A, x \in [0, 1]^d\} M(\varphi)(dx) \mathbb{P}(d\varphi), \quad A \in \mathcal{N}(E), \quad (1.5)$$

is called the *Palm measure* of  $\mathbb{P}$  with respect to  $M$ .  $\mathbb{P}_M$  is a  $\sigma$ -finite measure satisfying the *refined Campbell theorem*

$$\mathbb{E} \left[ \int h(x, \Phi - x) M(dx) \right] = \mathbb{E}_M \left[ \int h(x, \Phi) dx \right]$$

for all measurable functions  $h : \mathbb{R}^d \times \mathbf{N}(E) \rightarrow [0, \infty)$ . Here,  $\mathbb{E}_M$  denotes integration with respect to  $\mathbb{P}_M$ .

If  $0 < \lambda_M < \infty$ , we define the *Palm probability measure* of  $M$  via  $\mathbb{P}_M^0 := \lambda_M^{-1} \mathbb{P}_M$ .

An important result relating the Palm measures of two stationary random measures is Neveu's exchange formula (Neveu, 1977).

### Theorem 1.4.2

Let  $M$  and  $M'$  be stationary random measures and  $h : \mathbb{R}^d \times \mathbf{N}(E) \rightarrow [0, \infty)$  a measurable function. Then

$$\mathbb{E}_M \left[ \int h(-x, \Phi - x) M'(dx) \right] = \mathbb{E}_{M'} \left[ \int h(x, \Phi) M(dx) \right]. \quad (1.6)$$

## 1.5 Tessellations

### Definition 1.5.1 (Tessellation)

A *tessellation* of  $\mathbb{R}^d$  is a countable set  $T = \{C_i : i \in \mathbb{N}\}$  sets  $C_i \in \mathcal{C}'$  (the *cells* of the tessellation) such that

- (i)  $\text{int}(C_i) \cap \text{int}(C_j) = \emptyset$ ,  $i \neq j$ ,
- (ii)  $\bigcup_i C_i = \mathbb{R}^d$ ,
- (iii)  $T$  is locally finite, i.e.  $\#\{C_i \in T : C_i \cap B \neq \emptyset\} < \infty$  for all bounded  $B \subset \mathbb{R}^d$ , and
- (iv) each cell of the tessellation is a compact convex set with interior points.

By Schneider and Weil (2000, Lemma 6.1.1), (iv) implies that the cells are bounded  $d$ -dimensional polytopes.

### Definition 1.5.2

Suppose  $T$  is a tessellation of  $\mathbb{R}^d$ .

- (i) The *faces* of a convex polytope  $P$  are the intersections of  $P$  with its supporting hyperplanes (Schneider, 1993, Section 2.4). Let  $P$  be a  $d$ -dimensional polytope and  $s \in \{0, \dots, d-1\}$ . We call a face of  $P$  of dimension  $s$  an *s-face* of  $P$ . Then the 0-faces of  $P$  are the vertices, the 1-faces the edges, and the  $(d-1)$ -faces the facets. For convenience, the polytope  $P$  is considered as a  $d$ -face.

Write  $\Delta_s(P)$  for the set of  $s$ -faces of a polytope  $P$  and  $\Delta_s(T) := \bigcup_{C \in T} \Delta_s(C)$  for the set of  $s$ -faces of all cells  $C$  of  $T$ . Further, let

$$F(y) := \bigcap_{C \in T, y \in C} C, \quad y \in \mathbb{R}^d,$$

be the intersection of all cells of the tessellation containing the point  $y$ . Then  $F(y)$  is a finite intersection of  $d$ -polytopes and, since it is non-empty,  $F(y)$  is an  $s$ -dimensional polytope for some  $s \in \{0, \dots, d\}$ . Therefore, we may introduce

$$\mathcal{S}_s(T) := \{F(y) : \dim F(y) = s, y \in \mathbb{R}^d\}, \quad s = 0, \dots, d,$$

the set of  $s$ -faces of the tessellation  $T$ . Then an  $s$ -face  $H \in \Delta_s(T)$  of a cell  $C$  of  $T$  is the union of all those  $s$ -faces  $F \in \mathcal{S}_s(T)$  of the tessellation contained in  $H$ .

- (ii) A tessellation  $T$  is called *face-to-face* if the faces of the cells and the faces of the tessellation coincide, i.e. if  $\Delta_s(T) = \mathcal{S}_s(T)$  for  $s = 0, \dots, d$ . For  $s = 0$  and  $s = d$  this is always true. For face-to-face tessellations we will unify notations writing  $\mathcal{S}_s(C)$  for the set of  $s$ -faces of a cell  $C$  of  $T$ .
- (iii) A tessellation  $T$  is called *normal* if it is face-to-face and every  $s$ -face of  $T$  is contained in the boundary of exactly  $d - s + 1$  cells for  $s = 0, \dots, d - 1$ .

## 1.6 Random tessellations

Write  $\mathbf{T}$  for the set of all tessellations in  $\mathbb{R}^d$ , and  $\mathbf{T}_n$  and  $\mathbf{T}_f$  for the subset of normal and face-to-face tessellations.  $\mathcal{F}'$  equipped with the topology of closed convergence is a locally compact space with countable basis (Schneider and Weil, 2000, Satz 1.1.1). Hence, the topology of closed convergence can also be defined for the system  $\mathcal{F}(\mathcal{F}')$ . The sets  $\mathbf{T}$  and  $\mathbf{T}_f$  are Borel sets in  $\mathcal{F}(\mathcal{F}')$  and the mappings  $T \mapsto \mathcal{S}_k(T)$ ,  $T \in \mathbf{T}_f$ ,  $k = 0, \dots, d - 1$ , are measurable (Schneider and Weil, 2000, Lemma 6.1.2). Schneider and Weil (2000, Lemma 6.1.3) further implies that  $\mathbf{T}_n$  is a Borel set in  $\mathcal{F}(\mathcal{F}')$ .

### Definition 1.6.1 (Random tessellation)

A *random tessellation* in  $\mathbb{R}^d$  is a random variable  $X$  on a probability space  $(\Omega, \mathcal{A}, \mathbb{P})$  with range  $\mathbf{T}$ . It is called *normal* or *face-to-face* if its realizations are almost surely normal or face-to-face, respectively.

The translation and the rotation of a tessellation  $T \in \mathbf{T}$  are defined via

$$\begin{aligned} T + y &:= \{C + y : C \in T\}, \quad y \in \mathbb{R}^d, \text{ and} \\ \vartheta T &:= \{\vartheta C : C \in T\}, \quad \vartheta \in SO_d. \end{aligned}$$

A random tessellation is called *stationary* if its distribution is invariant under translations and *isotropic* if it is invariant under rotations.

### Definition 1.6.2 (Centroid of a compact set)

Let  $c : \mathcal{C}' \rightarrow \mathbb{R}^d$  be a measurable function such that

$$c(C + y) = y + c(C), \quad y \in \mathbb{R}^d. \quad (1.7)$$

The point  $c(C)$  is called the *centroid* of the set  $C$ . A *generalized centroid function* is a measurable function  $c : \mathcal{C}' \times \mathbf{N}(\mathcal{C}') \rightarrow \mathbb{R}^d$  such that

$$c(C + x, \eta + x) = c(C, \eta) + x, \quad x \in \mathbb{R}^d, \eta \in \mathbf{N}(\mathcal{C}'), C \in \eta,$$

where  $\mathbf{N}(\mathcal{C}')$  denotes the set of all counting measures on  $\mathcal{C}'$ .

Typical choices of centroids are the center of gravity of the set  $C$ , the center of its surrounding ball, or the “extreme” point of  $C$  with respect to a given direction. Given a generalized centroid function  $c$ , each stationary random tessellation  $X$  may be interpreted as a stationary marked point process (also called  $X$ ) on  $\mathbb{R}^d$  with mark space  $\mathcal{C}'$  via

$$X = \sum_{C \in X} \delta_{(c(C,X), C - c(C,X))}.$$

Let  $c_k$  denote a generalized centroid function acting on the set of  $k$ -faces of a random tessellation  $X$ . Then we can define the point process  $N_k$  of centers of the  $k$ -faces of  $X$  as

$$N_k(X) := \sum_{F \in \mathcal{S}_k(X)} \delta_{c_k(F,X)}.$$

We assume that  $N_k \in \mathbf{N}_s$   $\mathbb{P}$ -almost surely, which guarantees that  $c_k(F) \neq c_k(F')$  for different  $k$ -faces  $F, F' \in \mathcal{S}_k(X)$  as well as the local finiteness of  $N_k$ . Note that this is an assumption on both  $X$  and the choice of  $c_k$ . Property (1.7) implies that  $N_k$  is a stationary point process.

Now the intensity  $\gamma_k$  of  $N_k$  is given by the formula

$$\gamma_k = \mathbb{E} \left[ \sum_{F \in \mathcal{S}_k(X)} \mathbb{1}_{[0,1]^d}(c_k(F, X)) \right], \quad k = 0, \dots, d,$$

and can be interpreted as the mean number of  $k$ -faces per unit volume. The values of  $\gamma_k$  do not depend on the choice of the (generalized) centroid function  $c_k$  (see Møller, 1989, p. 47).

Under the Palm distribution  $\mathbb{P}_{N_k}^0$  there is a  $k$ -face  $C_k(0)$  with center in the origin. Its distribution is called the *distribution of the typical  $k$ -face* of the tessellation  $X$ . Let  $T$  be a realization of  $X$ . By assumption,  $\psi_k := N_k(T) \in \mathbf{N}_s$  almost surely. In this case any  $x \in \psi_k$  is the center of a unique  $k$ -face  $C_k(x, T) \in \mathcal{S}_k(T)$  defined via

$$C_k(x, T) = F \iff c_k(F, T) = x.$$

For  $x \in \mathbb{R}^d \setminus \psi_k$  we set  $C_k(x, T) := \{x\}$ . If  $\psi_k \notin \mathbf{N}_s$  we define  $C_k(x, T) := \{x\}$  for all  $x \in \mathbb{R}^d$ .

Fix  $k \in \{0, \dots, d\}$  and define  $F_k(x, T) := F$  and  $c_k(x, T) := c_k(F_k(x, T), T)$  whenever the point  $x \in \mathbb{R}^d$  is contained in the relative interior of some  $k$ -face  $F \in \mathcal{S}_k(T)$ . If  $x \in \mathbb{R}^d$  is not contained in the relative interior of any  $k$ -face, we set  $F_k(x, T) := \{x\}$  and  $c_k(x, T) := x$ . Then

$$\begin{aligned} C_k(x, T) &= C_k(0, T - x) + x, & T \in \mathbf{T}, x \in \mathbb{R}^d, \\ c_k(x, T) &= c_k(0, T - x) + x, & T \in \mathbf{T}, x \in \mathbb{R}^d. \end{aligned} \tag{1.8}$$

Further random measures induced by a random tessellation are the measures

$$M_k(B) := \sum_{F \in \mathcal{S}_k(X)} \mathcal{H}^k(F \cap B), \quad k = 0, \dots, d, B \in \mathcal{B}^d.$$

Their intensities

$$\mu_k = \mathbb{E} \left[ \sum_{C \in \mathcal{S}_k(X)} \mathcal{H}^k(C \cap [0, 1]^d) \right], \quad k = 0, \dots, d,$$

can also be written as

$$\mu_k = \mathbb{E} \left[ \sum_{C \in \mathcal{S}_k(X)} \mathcal{H}^k(C) \mathbb{1}_{[0,1]^d}(c_k(C)) \right], \quad k = 0, \dots, d,$$

with the interpretation of mean total  $k$ -content of the  $k$ -faces of the tessellation per unit volume. The measures  $M_k$  and their Palm measures will be studied in detail in Chapter 3. Here, we will only state some formulas connecting the Palm measures of  $N_k$  and  $M_k$ .

### Theorem 1.6.3

For measurable functions  $f, g : \mathbf{T} \rightarrow [0, \infty)$  we have

$$\mathbb{E}_{M_k} \left[ f(X)g(X - c_k(0, X)) \right] = \mathbb{E}_{N_k} \left[ g(X) \int_{C_k(0)} f(X - x) \mathcal{H}^k(dx) \right].$$

#### Proof:

Using the representation of  $X$  as a marked point process and (1.8), the formula follows from (1.6) with  $M = M_k$ ,  $M' = N_k$ , and  $h(x, X) := \mathbb{1}\{c_k(x, X) = 0\}f(X - x)g(X)$ .  $\square$

### Corollary 1.6.4

For each measurable function  $g : \mathbf{T} \rightarrow [0, \infty)$  we have

$$\begin{aligned} \mathbb{E}_{M_k} \left[ g(X - c_k(0, X)) \right] &= \mathbb{E}_{N_k} \left[ \mathcal{H}^k(C_k(0))g(X) \right] \text{ and} \\ \mathbb{E}_{N_k} \left[ g(X) \right] &= \mathbb{E}_{M_k} \left[ \mathcal{H}^k(F_k(0, X))^{-1} \cdot g(X - c_k(0, X)) \right]. \end{aligned}$$

For the intensities  $\mu_k$  and  $\gamma_k$  we get the relation

$$\mu_k = \gamma_k \mathbb{E}_{N_k} \left[ \mathcal{H}^k(C_k(0)) \right].$$

In the following theorem let  $\mathcal{P}_d$  denote the set of all  $d$ -dimensional convex polytopes in  $\mathbb{R}^d$ . For  $k = 0, \dots, d$  consider the functions  $n_k : \mathcal{P}_d \rightarrow \mathbb{N}$ , where  $n_k(P)$  is the number of  $k$ -faces of  $P \in \mathcal{P}_d$ . Then  $\mathcal{P}_d$  is a Borel set in  $\mathcal{F}$  and the function  $n_k$  is measurable (Schneider and Weil, 2000, proof of Lemma 6.1.2).

### Theorem 1.6.5

If the random tessellation is normal we have

$$(1 - (-1)^k)\gamma_k = \sum_{j=0}^{k-1} (-1)^j \binom{d-j+1}{k-j} \gamma_j$$

and

$$\gamma_k = \gamma_d \frac{\mathbb{E}_{N_d} [n_k(C_d(0))]}{d - k + 1}. \quad (1.9)$$

In particular,

$$\begin{aligned} 2\gamma_1 &= (d+1)\gamma_0, \\ 3\gamma_0 &= 2\gamma_1 = 6\gamma_2, \quad \text{if } d = 2, \\ 2\gamma_0 &= \gamma_1 = 2(\gamma_2 - \gamma_3), \quad \text{if } d = 3. \end{aligned}$$

Typical examples for  $f$  and  $g$  in Theorem 1.6.3 are functions measuring geometric characteristics of the cells of the random tessellation  $X$ , e.g., the cell volume, the edge length or the number of  $k$ -faces of the cells. The formulas stated above indicate that a lot of relations between different cell characteristics exist.

In fact, Mecke (1984) has shown that for a planar face-to-face tessellation the mean values of its cell characteristics are completely determined by the values of  $\mu_0$  and  $\mu_1$  (usually denoted by  $L_A$ ). For a spatial tessellation the required parameters are  $\mu_0$ ,  $\mu_1$  ( $L_V$ ),  $\mu_2$  ( $S_V$ ), and the cell intensity  $\gamma_3$ .

**Theorem 1.6.6**

*For a stationary and normal random tessellation of  $\mathbb{R}^2$  let  $a_2$  and  $u_2$  be the expected area and perimeter of the typical cell, respectively, and let  $l_1$  be the expected length of the typical edge. Then the following relations hold*

$$\begin{aligned} 2\gamma_2 &= \gamma_0, \\ \gamma_1 &= \frac{3}{2}\gamma_0, \\ l_1 &= \frac{L_A}{\gamma_1} = \frac{2L_A}{3\gamma_0}, \\ a_2 &= \frac{1}{\gamma_2} = \frac{2}{\gamma_0}, \text{ and} \\ u_2 &= \frac{2L_A}{\gamma_2} = \frac{4L_A}{\gamma_0}. \end{aligned}$$

**Theorem 1.6.7**

*For a stationary and normal random tessellation of  $\mathbb{R}^3$  let  $l_3$ ,  $s_3$ ,  $v_3$ , and  $\bar{b}_3$  be the expected total edge length, surface area, volume, and mean width, respectively, of the typical cell, let  $a_2$  and  $u_2$  be the expected area and perimeter of the typical facet, and let  $l_1$  be the expected length of the typical edge. Finally, write  $n_0$ ,  $n_1$ , and  $n_2$  for the mean number of vertices, edges, and facets, respectively, of the typical cell. Then the following relations hold*

$$\begin{aligned} \gamma_2 &= \gamma_0 + \gamma_3, & \gamma_1 &= 2\gamma_0, \\ l_3 &= \frac{3L_V}{\gamma_3}, & s_3 &= \frac{2S_V}{\gamma_3}, & v_3 &= \frac{1}{\gamma_3}, & \bar{b}_3 &= \frac{L_V}{4\gamma_3}, \\ a_2 &= \frac{S_V}{\gamma_2} = \frac{S_V}{\gamma_0 + \gamma_3}, & u_2 &= \frac{3L_V}{\gamma_2} = \frac{3L_V}{\gamma_0 + \gamma_3}, \\ l_1 &= \frac{L_V}{\gamma_1} = \frac{L_V}{2\gamma_0}, \\ n_0 &= \frac{4\gamma_0}{\gamma_3}, & n_1 &= \frac{6\gamma_0}{\gamma_3}, & \text{and} & n_2 &= \frac{2(\gamma_0 + \gamma_3)}{\gamma_3}. \end{aligned}$$

## 1.7 Flat sections

Here, we summarize some results concerning the intersection of a random tessellation of  $\mathbb{R}^d$  with an affine subspace  $F_s$  of  $\mathbb{R}^d$  of dimension  $0 < s < d$ . Let  $X$  be a stationary random

tessellation with finite intensities  $\gamma_0, \dots, \gamma_d$ . Then  $X_s := X \cap F_s$  is a stationary tessellation of  $F_s$ , so the results given for stationary random tessellations also hold for  $X_s$ . Further, some relations between the characteristics of the tessellations  $X$  and  $X_s$  exist. Details are again to be found in Møller (1989, Section 6). Since  $X$  is stationary, we may assume that  $F_s$  is an  $s$ -dimensional linear subspace  $L_s$  of  $\mathbb{R}^d$ .

**Lemma 1.7.1**

Let  $k \in \{0, \dots, s\}$ . A  $k$ -face  $F$  of  $X_s$  is almost surely given by the intersection of  $L_s$  and a  $(d-s+k)$ -face  $F'$  of  $X$ , i.e.  $F = F' \cap L_s$ .

We will mark intensities, typical cells and expectations with respect to  $X_s$  with superscript  $(s)$ . Then the following relations hold.

**Theorem 1.7.2**

For  $k = 0, \dots, d$  we have

$$\gamma_k^{(s)} = \gamma_{d-s+k} \mathbb{E}_{N_{d-s+k}} \left[ \mathcal{H}^{d-s} \left( \pi_{L_s^\perp} (C_{d-s+k}(0)) \right) \right]$$

and

$$\gamma_k^{(s)} \mathbb{E}_{N_k^{(s)}} \left[ f(C_k^{(s)}(0)) \right] = \gamma_{d-s+k} \mathbb{E}_{N_{d-s+k}} \left[ \int_{\pi_{L_s^\perp}(C_{d-s+k}(0))} f(C_{d-s+k}(0) \cap (y + L_s)) \mathcal{H}^{d-s}(dy) \right]$$

for each non-negative measurable function  $f$  which is invariant under translations in  $\mathbb{R}^d$ .  $\pi_{L_s^\perp}$  denotes the projection onto the orthogonal complement of  $L_s$  in  $\mathbb{R}^d$ .

For the cases  $d = 2$  and  $d = 3$ , which are important for applications, we obtain the following results.

**Corollary 1.7.3**

(i)  $d = 2, s = 1$

Let  $l_1^{(1)}$  and  $l_1$  be the expected length of the typical edge of  $X_1$  and  $X$ , respectively. Further, let  $u_2$  and  $a_2$  denote the expected perimeter and area, respectively, of the typical cell of  $X$ . Then

$$\begin{aligned} \gamma_0^{(1)} &= \frac{2}{\pi} \gamma_1 l_1 = \frac{2L_A}{\pi}, \\ \gamma_1^{(1)} &= \frac{1}{\pi} \gamma_2 u_2 = \frac{2L_A}{\pi}, \text{ and} \\ l_1^{(1)} &= \pi \frac{a_2}{u_2} = \frac{\pi}{2L_A}. \end{aligned}$$

(ii)  $d = 3, s = 1$

Let  $l_1^{(1)}$  be the expected length of the typical edge of  $X_1$ ,  $a_2$  the expected area of the typical facet of  $X$ , and let  $s_3$  and  $v_3$  be the expected surface area and volume, respectively, of

the typical cell of  $X$ . Then we have

$$\begin{aligned}\gamma_0^{(1)} &= \frac{1}{2}\gamma_2 a_2 = \frac{S_V}{2}, \\ \gamma_1^{(1)} &= \frac{1}{4}\gamma_3 s_3 = \frac{S_V}{2}, \text{ and} \\ l_1^{(1)} &= 4\frac{v_3}{s_3} = \frac{2}{S_V}.\end{aligned}$$

(iii)  $d = 3, s = 2$

Let  $l_1^{(2)}$  be the expected length of the typical edge of  $X_2$ , let  $n_2^{(2)}, u_2^{(2)}$ , and  $a_2^{(2)}$  be the expected number of vertices, perimeter, and area, respectively, of the typical cell of  $X_2$ . Further, let  $l_1$  be the expected length of the typical edge of  $X$ , let  $u_2$  and  $a_2$  be the expected perimeter and area, respectively, of the typical facet of  $X$ , and let  $\bar{b}_3, s_3$ , and  $v_3$  be the expected mean width, surface area, and volume, respectively, of the typical cell of  $X$ . Then

$$\begin{aligned}\gamma_0^{(2)} &= \frac{1}{2}\gamma_1 l_1 = \frac{L_V}{2}, \\ \gamma_1^{(2)} &= \frac{1}{4}\gamma_2 u_2 = \frac{3L_V}{4}, \\ \gamma_2^{(2)} &= \gamma_3 \bar{b}_3 = \frac{L_V}{4}, \\ l_1^{(2)} &= \pi \frac{a_2}{u_2} = \frac{\pi S_V}{3L_V}, \\ n_2^{(2)} &= 6, \\ u_2^{(2)} &= \frac{\pi s_3}{4\bar{b}_3} = \frac{2\pi S_V}{L_V}, \text{ and} \\ a_2^{(2)} &= \frac{v_3}{\bar{b}_3} = \frac{4}{L_V}.\end{aligned}$$

# Chapter 2

## Laguerre tessellations

In this chapter we will introduce the notion of a Laguerre diagram generated by a set of spheres in  $\mathbb{R}^d$  which is a generalized (weighted) version of the well-known Voronoi diagram (Møller, 1994; Stoyan et al., 1995; Okabe et al., 2000; Schneider and Weil, 2000). We will study geometric properties of this diagram and investigate under which conditions it forms a tessellation of  $\mathbb{R}^d$ .

Besides Voronoi tessellations also their duals, the Delaunay tessellations, are of special interest. Their construction can be generalized to Laguerre tessellations leading to Laguerre Delaunay tessellations. Using these structures we derive a characterization of the class of Laguerre tessellations in  $\mathbb{R}^d$ . It turns out that any normal tessellation of  $\mathbb{R}^d$  with  $d \geq 3$  can be represented as a Laguerre tessellation.

For further reading on Laguerre diagrams we refer to Imai et al. (1985), Aurenhammer (1987b), Edelsbrunner and Seidel (1986), Schlottmann (1993), and the book by Okabe et al. (2000). Laguerre Delaunay diagrams are considered for instance in Aurenhammer (1987a) and Schlottmann (1993).

### 2.1 Definitions

For  $y, x \in \mathbb{R}^d$  and  $w \in \mathbb{R}$  define the *power* of  $y$  with respect to the pair  $(x, w)$  as

$$\text{pow}(y, (x, w)) := \|y - x\|^2 - w. \quad (2.1)$$

Let  $\varphi \subset \mathbb{R}^d \times \mathbb{R}$  be a countable set such that  $\min_{(x,w) \in \varphi} \text{pow}(y, (x, w))$  exists for each  $y \in \mathbb{R}^d$ . Then the *Laguerre cell* of  $(x, w) \in \varphi$  is defined as

$$C((x, w), \varphi) := \{y \in \mathbb{R}^d : \text{pow}(y, (x, w)) \leq \text{pow}(y, (x', w')), \quad (x', w') \in \varphi\}.$$

The point  $x$  is called the *nucleus* of the cell  $C((x, w), \varphi)$ . The *Laguerre diagram*  $L(\varphi)$  is the set of the non-empty Laguerre cells of  $\varphi$ , i.e.

$$L(\varphi) := \{C((x, w), \varphi) : (x, w) \in \varphi, C((x, w), \varphi) \neq \emptyset\}.$$

When considering the special case of positive weights, the elements  $(x, r) \in \varphi$  can be interpreted as spheres with radii  $r = \sqrt{w} \geq 0$  centered in the points  $x \in \mathbb{R}^d$ . So let  $s(x, r)$  denote a sphere in  $\mathbb{R}^d$  centered in  $x$  with radius  $r$ , i.e.

$$s(x, r) := \{y \in \mathbb{R}^d : \|y - x\| = r\}, \quad x \in \mathbb{R}^d, r \geq 0.$$

Then the *power* of a point  $y \in \mathbb{R}^d$  with respect to a sphere  $s(x, r)$  is given by

$$\text{pow}(y, s(x, r)) = \|y - x\|^2 - r^2. \quad (2.2)$$

In this case the power distance has the following geometric interpretation: For each point  $y \in \mathbb{R}^d$  outside the sphere  $s(x, r)$  the value  $\text{pow}(y, s(x, r))$  equals the squared length of the tangent line from  $y$  to the sphere. The power of a point  $y$  with respect to the sphere  $s(x, r)$  is smaller than 0 if  $y$  lies inside the sphere, equals 0 if  $y$  is contained in the boundary of the sphere, and is larger than 0 if  $y$  is outside the sphere. In order to treat also the case of negative weights, Aurenhammer has introduced the notion of an *imaginary sphere*, a sphere with imaginary radius  $r' = ir$ ,  $r \geq 0$  and  $i = \sqrt{-1}$  (Aurenhammer, 1987a). In the following we call a sphere with either real or imaginary radius a *generalized sphere*. We will often identify a pair  $(x, r)$  with the sphere  $s(x, r)$  and use both notations synonymously. In both cases, we will use the definition (2.2) of the power distance. At some points, especially when working with more than one sphere, we will also use the abbreviation  $s_i := s(x_i, r_i)$ .

Note that a Laguerre cell does not necessarily contain its nucleus and that a nucleus does not necessarily generate a cell. A necessary condition for a cell to be empty is that the generating sphere is completely contained in the union of the remaining spheres. However, this is not a sufficient condition as Figure 2.1 shows.

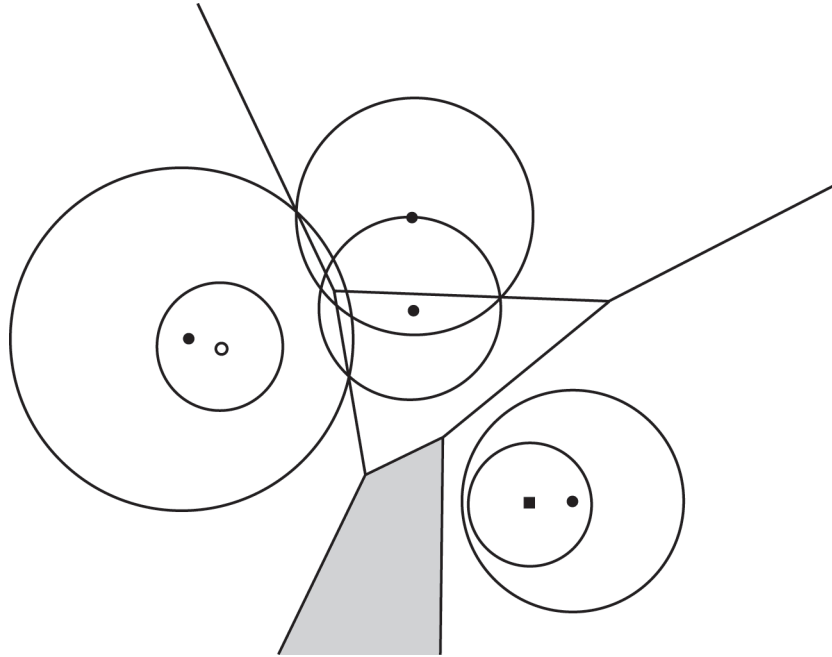


Figure 2.1: The Laguerre diagram of a set of six spheres in  $\mathbb{R}^2$ . The point centered in  $\circ$  does not generate a cell. The sphere centered in  $\blacksquare$  is completely contained in one of the other spheres. Nevertheless, it generates the cell printed in gray.

Given two spheres  $s_1 = s(x_1, r_1)$  and  $s_2 = s(x_2, r_2)$  in  $\mathbb{R}^d$ , the points  $z \in \mathbb{R}^d$  satisfying  $\text{pow}(z, s_1) = \text{pow}(z, s_2)$  form a hyperplane  $\text{Ra}(s_1, s_2)$  given by

$$\text{Ra}(s_1, s_2) = \{z \in \mathbb{R}^d : 2\langle z, x_1 - x_2 \rangle = \|x_1\|^2 - \|x_2\|^2 + r_2^2 - r_1^2\}, \quad (2.3)$$

which is perpendicular to the line joining  $x_1$  and  $x_2$  and called the *radical axis* of  $s_1$  and  $s_2$ . Then

$$H(s_1, s_2) := \{z \in \mathbb{R}^d : 2\langle z, x_1 - x_2 \rangle \geq \|x_1\|^2 - \|x_2\|^2 + r_2^2 - r_1^2\}$$

is the closed half space dominated by  $s_1$  (but not necessarily containing  $x_1$ ) and bounded by  $\text{Ra}(s_1, s_2)$ .

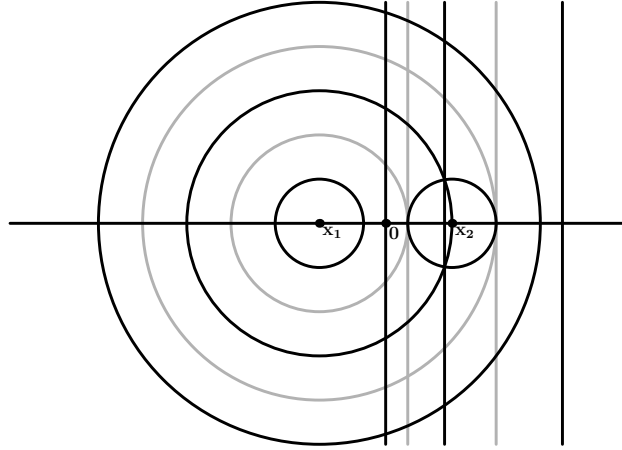


Figure 2.2: The radical axes for the spheres  $s(x_1, r_1)$  and  $s(x_2, r_2)$  with  $x_1 = (-1.5, 0)$ ,  $x_2 = (1.5, 0)$ ,  $r_1 = 1, 2, 3, 4, 5$ , and  $r_2 = 1$ .

If two spheres intersect, then their radical axis passes through their intersections. Otherwise, the two spheres are contained in the same open half space bounded by their radical axis if and only if one of the spheres is contained in the other. If two spheres have equal radii, their radical axis is the perpendicular bisector of the line joining their centers.

Obviously, the Laguerre cells are also defined by the equality

$$C(s_0, \varphi) = \bigcap_{s \in \varphi, s \neq s_0} H(s_0, s), \quad s_0 \in \varphi. \quad (2.4)$$

Hence, every  $s$ -face  $F \in \mathcal{S}_s(L(\varphi))$  can be written as

$$F = F(s_0, \dots, s_k, \varphi) = \bigcap_{i=0}^k C(s_i, \varphi), \quad s_0, \dots, s_k \in \varphi,$$

with a suitable number of cells involved. Then  $F(s_0, \dots, s_k, \varphi)$  is included in the affine subspace

$$G(s_0, \dots, s_k) = \{y \in \mathbb{R}^d : \text{pow}(y, s_0) = \dots = \text{pow}(y, s_k)\}.$$

### Remarks 2.1.1

- (i) If the radii of all spheres in  $\varphi$  are equal, the Laguerre diagram of  $\varphi$  equals the Voronoi diagram of the set  $\{x : (x, r) \in \varphi\}$ .
- (ii) Since the cells of the diagram are determined by the inequality

$$\|x_1 - y\|^2 - r_1^2 \leq \|x_2 - y\|^2 - r_2^2, \quad y \in \mathbb{R}^d, (x_1, r_1), (x_2, r_2) \in \varphi,$$

adding the same constant on both sides of the equality will leave the Laguerre diagram unchanged. Therefore, the tessellation is invariant under transformations of the form  $r \mapsto (r^2 + t)^{\frac{1}{2}}$ , with a fixed value  $t \in \mathbb{R}$  such that all radii remain positive.

## 2.2 Geometric properties of Laguerre diagrams

In this section we determine some geometric properties of the Laguerre diagram of a set of spheres in  $\mathbb{R}^d$ . In particular, we are interested in conditions on the set of generators which make the Laguerre diagram a tessellation of  $\mathbb{R}^d$ .

The representation (2.4) shows that the Laguerre cells are closed convex sets. As the intersection of two cells is included in their radical axis the cells clearly have disjoint topological interiors. So what remains to show is that the Laguerre cells form a locally finite and space-filling system of bounded  $d$ -dimensional polytopes.

For applications, it is often required that tessellations are face-to-face or normal, as these properties are present in many structures appearing in nature. Furthermore, many formulas relating different characteristics of normal tessellations exist (cf. Section 1.6 and Møller (1989)). Therefore, sufficient conditions for the Laguerre tessellation being normal are studied as well.

In 2.2.2 to 2.2.4 we mainly follow the argumentation of Schlottmann (1993), who gives some results for geometric properties of Laguerre tessellations. Analogous results for the special case of Voronoi tessellations are derived in Schneider and Weil (2000, Chapter 6).

The results of this section are formulated using positive weights and the definition (2.2) of the power distance. However, the argumentation also carries over to the case of arbitrary weights and the power distance defined via (2.1).

### Definition 2.2.1

We say that  $\varphi \subset \mathbb{R}^d \times \mathbb{R}^+$  fulfills regularity condition

- (R1) if for every  $y \in \mathbb{R}^d$  and every  $t \in \mathbb{R}$  only finitely many elements  $(x, r) \in \varphi$  satisfy  $\|y - x\|^2 - r^2 \leq t$ , and
- (R2) if  $\text{conv}\{x : (x, r) \in \varphi\} = \mathbb{R}^d$ .

If the set of radii is bounded, condition (R1) implies the local finiteness of the set of points  $\{x : (x, r) \in \varphi\}$ .

Further, we say that the points of  $\varphi$  are in *general position* if the following conditions hold.

- (GP1) No  $k + 1$  nuclei are contained in a  $(k - 1)$ -dimensional affine subspace of  $\mathbb{R}^d$  for  $k = 2, \dots, d$ , and
- (GP2) no  $d + 2$  points have equal power with respect to some point in  $\mathbb{R}^d$ .

In the case of equal radii (which is the Voronoi case) this is exactly the property addressed as general quadratic position in Møller (1994).

### Proposition 2.2.2

Let  $\varphi$  satisfy (R1) and (R2). Then every cell of  $L(\varphi)$  is compact.

**Proof:**

It remains to prove the boundedness of the Laguerre cells. Fix  $(x_0, r_0) \in \varphi$  and choose a unit vector  $u \in S^{d-1}$ . By condition (R2) we find  $(x, r) \in \varphi$  such that  $0 < \langle u, x - x_0 \rangle$ . Now for a suitable  $\delta > 0$  all  $u'$  within a neighborhood of  $u$  on the unit sphere satisfy  $\delta \|x_0 - x\| < \langle u', x - x_0 \rangle$ . Then

$$\begin{aligned} \|x_0 + \lambda u' - x\|^2 - r^2 &= \|x_0 - x\|^2 + \lambda^2 - 2\lambda \langle u', x - x_0 \rangle - r^2 \\ &< \|x_0 - x\|^2 + \lambda^2 - 2\lambda \delta \|x_0 - x\| - r^2 \end{aligned}$$

for any  $\lambda > 0$ . Since  $\|x_0 + \lambda u' - x_0\|^2 - r_0^2 = \lambda^2 - r_0^2$ , we have

$$\|x_0 + \lambda u' - x_0\|^2 - r_0^2 > \|x_0 + \lambda u' - x\|^2 - r^2 \text{ for } \lambda > \frac{1}{2} \left| 1 - \frac{r^2 - r_0^2}{\|x_0 - x\|^2} \right| \frac{\|x_0 - x\|}{\delta},$$

i.e.,  $x_0 + \lambda u' \notin C((x_0, r_0), \varphi)$ . This shows that the mapping

$$u \mapsto \sup\{\lambda \geq 0 : \lambda = 0 \text{ or } x_0 + \lambda u \in C((x_0, r_0), \varphi)\}$$

is locally bounded and therefore bounded on the unit sphere. Therefore, the boundedness of  $C((x_0, r_0), \varphi)$  is shown.  $\square$

**Lemma 2.2.3**

Let  $\varphi$  satisfy (R1) and (R2). For every bounded subset  $B$  of  $\mathbb{R}^d$  and every  $t \in \mathbb{R}$  only finitely many  $(x, r) \in \varphi$  fulfill  $\|y - x\|^2 - r^2 \leq t$  for at least one point  $y \in B$ . In other words, the set  $B$  is intersected only by a finite number of balls  $b\left(x, \sqrt{[t + r^2]^+}\right)$ , where  $[t + r^2]^+ := \max(t + r^2, 0)$ .

**Proof:**

If this was not the case, we would find a bounded set  $B$ , a number  $t \in \mathbb{R}$  and sequences  $((x_n, r_n))_n$  of pairwise distinct elements of  $\varphi$  and  $(y_n)_n$  in  $B$  such that  $\|y_n - x_n\|^2 - r_n^2 \leq t$ . Since the closure of  $B$  is compact, we may pass to a suitable subsequence such that  $\|y_n - y_0\| \leq \frac{1}{2}$  for all  $n$ . Further, again passing to a subsequence, we may assume that  $\langle y_0 - x_n, u \rangle \geq \frac{1}{2} \|y_0 - x_n\|$  for a suitable unit vector  $u$  and all  $n$ . Then

$$\begin{aligned} &\|y_0 - u - x_n\|^2 - r_n^2 \\ &= \|y_0 - x_n\|^2 + 1 - 2\langle y_0 - x_n, u \rangle - r_n^2 \\ &\leq \|y_0 - y_n\|^2 + \|y_n - x_n\|^2 + 2\|y_0 - y_n\| \|y_n - x_n\| + 1 - \|y_0 - x_n\| - r_n^2 \\ &\leq t + \frac{5}{4} + \left| \|y_n - x_n\| - \|y_0 - x_n\| \right| \\ &\leq t + \frac{5}{4} + \|y_n - y_0\| \leq t + \frac{7}{4}, \end{aligned}$$

for all  $n$ , a contradiction to (R1).  $\square$

**Proposition 2.2.4**

Let  $\varphi$  satisfy (R1) and (R2). Then the set of cells of  $L(\varphi)$  is locally finite and space filling.

**Proof:**

Choose  $y_0 \in \mathbb{R}^d$  and  $(x_0, r_0) \in \varphi$ . From (R1), it follows that there are only finitely many elements  $(x, r) \in \varphi$  such that

$$\|y_0 - x\|^2 - r^2 \leq \|y_0 - x_0\|^2 - r_0^2.$$

Therefore, there is at least one  $(x', r')$  minimizing this expression, i.e.,  $y_0 \in C((x', r'), \varphi)$ .

Now let  $K$  be a compact subset of  $\mathbb{R}^d$ . There exists an  $R > 0$  such that  $\|y - x_0\|^2 - r_0^2 \leq R$  for all  $y \in K$ . Lemma 2.2.3 shows that the set  $\varphi'$  of  $(x, r) \in \varphi$  satisfying  $\|y - x\|^2 - r^2 \leq R$  for at least one  $y \in K$  is finite. Then any cell  $C((x, r), \varphi)$  with  $(x, r) \in \varphi \setminus \varphi'$  does not intersect  $K$ . Hence, the set of Laguerre cells is locally finite.  $\square$

**Proposition 2.2.5**

Let  $\varphi$  satisfy (R1) and (R2). Then the Laguerre diagram  $L(\varphi)$  is face-to-face.

**Proof:**

Suppose it is not. Then there exist some cells  $C_i = C((x_i, r_i), \varphi)$ ,  $i = 1, \dots, n$ , such that  $F := \bigcap_i C_i \neq \emptyset$  is not a face of  $C_1$ . This means that the affine hull  $G$  of  $F$  contains a point  $z \in C_1$  which is not contained in  $F$ , say  $z \notin C_2$ . As  $G$  is contained in the radical axis  $\text{Ra}((x_1, r_1), (x_2, r_2))$ , we have

$$\langle z, x_2 - x_1 \rangle = \frac{1}{2} \left( \|x_2\|^2 - \|x_1\|^2 + r_1^2 - r_2^2 \right). \quad (2.5)$$

Since  $z$  is not contained in  $C_2$ , there is a point  $(x, r) \in \varphi$  distinct from  $(x_i, r_i)$ ,  $i = 1, \dots, n$ , such that

$$\langle z, x - x_2 \rangle > \frac{1}{2} \left( \|x\|^2 - \|x_2\|^2 + r_2^2 - r^2 \right).$$

Now  $z \in C_1$  yields

$$\langle z, x - x_1 \rangle \leq \frac{1}{2} \left( \|x\|^2 - \|x_1\|^2 + r_1^2 - r^2 \right).$$

Both inequalities combined show

$$\langle z, x_2 - x_1 \rangle < \frac{1}{2} \left( \|x_2\|^2 - \|x_1\|^2 + r_1^2 - r_2^2 \right),$$

contradictory to (2.5).  $\square$

Suppose that a non-empty Laguerre cell  $C(s_0, \varphi)$  with dimension smaller than  $d$  exists. Then this cell is contained in the radical axis  $\text{Ra}(s_1, s_2)$  formed by two other cells  $C(s_1, \varphi)$  and  $C(s_2, \varphi)$ . This is only possible if  $\text{Ra}(s_0, s_1) = \text{Ra}(s_0, s_2)$  which means that the points  $x_0, x_1$ , and  $x_2$  are contained in a line. Hence the Laguerre cells of a set  $\varphi$  in general position are either empty or have dimension  $d$ .

**Lemma 2.2.6**

Assume that  $\varphi$  satisfies (R1), (R2), and (GP 1). Let  $1 \leq k \leq d$  and choose  $k + 1$  spheres  $s_0, \dots, s_k \in \varphi$ . Further let  $L = L(x_0, \dots, x_k)$  be the  $k$ -dimensional linear subspace spanned by  $x_1 - x_0, \dots, x_k - x_0$ . Then the  $s_i$  define a unique point  $z = z(s_0, \dots, s_k) \in L$  such that  $\text{pow}(z, s_0) = \dots = \text{pow}(z, s_k)$  and  $G(s_0, \dots, s_k)$  equals the  $(d - k)$ -dimensional affine subspace  $z + L^\perp$ .

**Proof:**

According to (2.3)  $G(s_0, \dots, s_k)$  is the space of solutions of the system of linear equations

$$\langle x_i - x_0, z \rangle = \frac{1}{2} (\|x_i\|^2 - \|x_0\|^2 + r_0^2 - r_i^2), \quad i = 1, \dots, k. \quad (2.6)$$

Condition (GP1) shows that these equations are linearly independent, hence the system has a unique solution  $z$  in the  $k$ -dimensional space  $L$ . Further, the space of solutions of the homogeneous system is just the  $(d - k)$ -dimensional orthogonal complement of  $L$ .  $\square$

**Corollary 2.2.7**

*Assume that  $\varphi$  satisfies (R1) and (R2) and is in general position. Then the Laguerre diagram of  $\varphi$  is normal.*

**Proof:**

Let  $F \in \mathcal{S}_k(L(\varphi))$ ,  $0 \leq k \leq d$ , be a  $k$ -face of  $L(\varphi)$ . Then Lemma 2.2.6 tells us that  $F$  can be represented as  $F = F(s_0, \dots, s_{d-k+1}, \varphi)$ . For  $1 \leq k \leq d$  it further implies that  $F$  belongs to exactly  $d - k + 1$  cells of  $L(\varphi)$ . For  $k = 0$ , this is a consequence of condition (GP2).  $\square$

The combination of the preceding results yields the following theorem.

**Theorem 2.2.8**

*If the set  $\varphi \subset \mathbb{R}^d \times \mathbb{R}^+$  satisfies the regularity conditions (R1) and (R2) then the set of the Laguerre cells  $C((x, r), \varphi)$ ,  $(x, r) \in \varphi$ , with non-vanishing interior is a face-to-face tessellation of  $\mathbb{R}^d$ . If the points of  $\varphi$  are further in general position then all cells of  $L(\varphi)$  have dimension  $d$  and the Laguerre tessellation  $L(\varphi)$  is normal.*

## 2.3 Laguerre Delaunay tessellations

We will now come to the definition of the dual of the Laguerre tessellation. However, since the focus of this thesis is on the Laguerre tessellation itself, we will not go into detail here. In fact, we will restrict ourselves to the summary of the most important definitions and results. For further details we refer to Schlottmann (1993).

**Definition 2.3.1**

Let  $\varphi \subset \mathbb{R}^d \times \mathbb{R}^+$  be a set in general position which fulfills the regularity conditions (R1) and (R2). Then the Laguerre diagram  $L(\varphi)$  is a tessellation of  $\mathbb{R}^d$ . For each vertex  $z \in \mathcal{S}_0(L(\varphi))$  we consider the set

$$D(z, \varphi) := \text{conv} \{x : (x, r) \in \varphi, z \in \mathcal{S}_0(C((x, r), \varphi))\}.$$

We call  $D(z, \varphi)$  the *Laguerre Delaunay cell* of the vertex  $z$ .

Let  $z \in \mathcal{S}_0(L(\varphi))$  be a vertex of  $L(\varphi)$ . Then there is a number  $p \in \mathbb{R}$  such that for  $(x, r) \in \varphi$

$$z \in C((x, r), \varphi) \iff \text{pow}(z, (x, r)) = p$$

and there is no  $(x, r) \in \varphi$  with  $\text{pow}(z, (x, r)) < p$ . Let  $z, z' \in \mathcal{S}_0(L(\varphi))$  such that  $z \neq z'$  and  $D(z, \varphi) \cap D(z', \varphi) \neq \emptyset$ . Then, we find  $p, p' \in \mathbb{R}$  such that for each  $(x, r) \in \varphi$  with  $x \in D(z, \varphi) \cap D(z', \varphi)$  we have

$$\text{pow}(z, (x, r)) = p \quad \text{and} \quad \text{pow}(z', (x, r)) = p'.$$

This means  $x$  is contained in the hyperplane  $H$  defined by the equation

$$y \in H \iff 2\langle y, z - z' \rangle = p' - p + \|z\|^2 - \|z'\|^2.$$

This equation reminds us of (2.3), the equation defining the radical axis of two generalized spheres. Indeed, Schlottmann (1993) has shown that it is possible to define a set  $\varphi^*$  of generalized spheres in  $\mathbb{R}^d$  such that the Delaunay tessellation of  $\varphi$  is the Laguerre tessellation of  $\varphi^*$ . Namely, let  $z$  be a vertex of the Laguerre tessellation of  $\varphi$ . Then there are  $d + 1$  pairs  $(x_0, r_0), \dots, (x_d, r_d) \in \varphi$  such that  $z \in C((x_i, r_i), \varphi)$  and a real number  $p(z)$  such that  $\text{pow}(z, (x_i, r_i)) = p(z)$  for  $i = 0, \dots, d$ . Now we define

$$\varphi^* := \{(z, p(z)) : z \in \mathcal{S}_0(L(\varphi))\}.$$

**Theorem 2.3.2**

*The set  $\varphi^*$  fulfills the regularity conditions (R1) and (R2). Every Laguerre cell of  $\varphi^*$  is non-empty and we have  $D(\varphi) = L(\varphi^*)$ .*

**Proof:**

Schlottmann (1993, Proposition 2)

□

**Corollary 2.3.3**

*Let  $\varphi \subset \mathbb{R}^d \times \mathbb{R}^+$  be a set in general position which fulfills the regularity conditions (R1) and (R2). Then the set*

$$D(\varphi) := \{D(z, \varphi) : z \in \mathcal{S}_0(L(\varphi))\}$$

*is a face-to-face tessellation of  $\mathbb{R}^d$ .*

We call  $D(\varphi)$  the *Laguerre Delaunay tessellation* of  $\varphi$ . Since the Laguerre tessellation of  $\varphi$  is a normal tessellation, the cells of  $D(\varphi)$  have exactly  $d + 1$  vertices. Hence, all  $k$ -faces of  $D$  are  $k$ -simplices.

**Remark 2.3.4**

The vertices of the Delaunay tessellation are exactly those elements of  $\varphi$  whose Laguerre cell is not empty. If we denote this set by  $\varphi^0$ , this means  $D(\varphi) = D(\varphi^0)$  (and  $L(\varphi) = L(\varphi^0)$ ).

## 2.4 The class of Laguerre tessellations

In this section we discuss conditions on a tessellation  $T$  of  $\mathbb{R}^d$  which guarantee that  $T$  can be represented as a Laguerre tessellation. Aurenhammer (1987a) has given a complete characterization of the set of Laguerre diagrams generated by finite sets of spheres. A very pleasing result is that each normal (finite) cell complex can be realized as a Laguerre diagram. However, diagrams with finitely many cells necessarily contain unbounded cells, hence do not belong to **T**. Here, we will formulate Aurenhammer's results for the case of infinitely many spheres (or cells) which then also applies to tessellations in the sense of Definition 1.5.1.

**Definition 2.4.1**

Consider a tessellation  $T = \{C_i : i \in \mathbb{N}\}$  of  $\mathbb{R}^d$ . An *orthogonal dual* of  $T$  is a point set  $\mathcal{D}(T) := \{x_i : i \in \mathbb{N}\}$  in  $\mathbb{R}^d$  with the following properties.

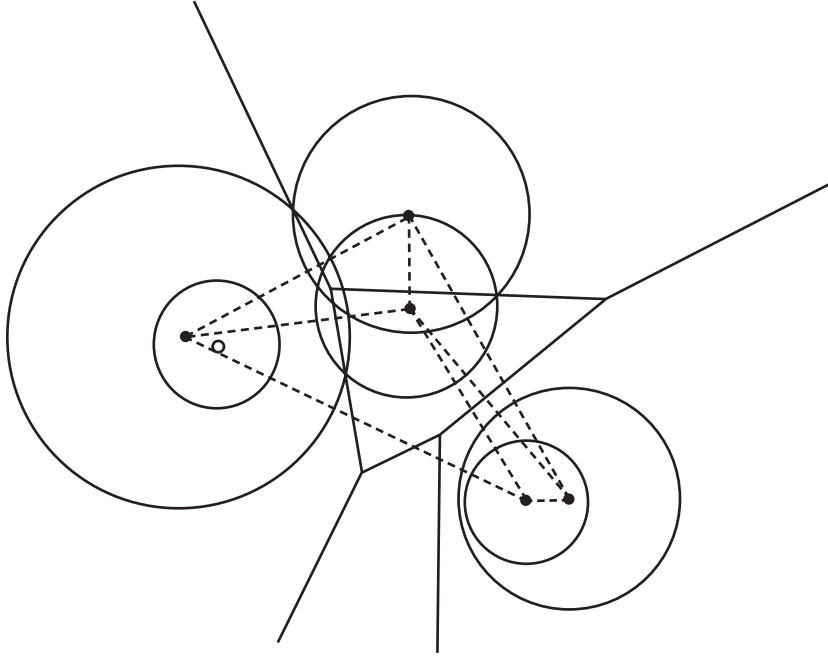


Figure 2.3: The Laguerre Delaunay diagram (dashed) of a set of six spheres in  $\mathbb{R}^2$ . The point generating an empty Laguerre cell does not contribute to the Delaunay diagram.

- (i) Each cell  $C_i$  of  $T$  is associated with exactly one point  $x_i \in \mathcal{D}(T)$  such that  $x_i \neq x_j$  for  $i \neq j$ . (Duality)
- (ii) For cells  $C_i$  and  $C_j$ ,  $i \neq j$ , of  $T$  let  $L_{i,j}$  denote the line connecting  $x_i$  and  $x_j$ . Then  $L_{i,j}$  is orthogonal to  $C_i \cap C_j$ . (Orthogonality)
- (iii) Any ray parallel to  $L_{i,j}$  directed from  $x_i$  to  $x_j$  and intersecting both of  $C_i$  and  $C_j$  first meets  $C_i$ . (Orientation)

### Theorem 2.4.2

A tessellation  $T$  of  $\mathbb{R}^d$  is the Laguerre tessellation of some set  $\varphi$  of generalized spheres if and only if an orthogonal dual  $\mathcal{D}(T)$  of  $T$  exists.

#### Proof:

If  $T$  is a Laguerre tessellation of  $\mathbb{R}^d$ , the set of cell centers of the corresponding Delaunay tessellation yields the required orthogonal dual. Conversely, consider a tessellation  $T = \{C_i : i \in \mathbb{N}\}$  of  $\mathbb{R}^d$  and assume the existence of an orthogonal dual  $\mathcal{D}(T) = \{x_i : i \in \mathbb{N}\}$ . We have to show the existence of a set  $\varphi = \{s_i : i \in \mathbb{N}\}$  of generalized spheres centered in the points  $x_i \in \mathcal{D}(T)$  such that  $T = L(\varphi)$ .

We will write  $s_i \sim s_j$  if  $C_i \subseteq H(s_i, s_j)$  and  $C_j \subseteq H(s_j, s_i)$  for the cells  $C_i$  and  $C_j$  belonging to  $x_i$  and  $x_j$ , respectively. Then,  $T = L(\varphi)$  is equivalent to  $s_i \sim s_j$  for  $s_i, s_j \in \varphi$  with  $i \neq j$ . Sort the points  $x_i$  in increasing distance to the origin, where points with equal distance are ordered lexicographically. We will now iteratively assign radii  $r_i$  to the points  $x_i$  such that  $T$  is the Laguerre tessellation of the set  $\varphi = \{s_i : s_i = s(x_i, r_i), i \in \mathbb{N}\}$ . The radius  $r_1$  can be chosen arbitrarily. Consider three cells  $C_i, C_j$ , and  $C_m$ ,  $i < j < m$ , such that

$F := C_i \cap C_j \cap C_m \neq \emptyset$  and assume that a radius  $r_i$  has already been constructed. A result by Aurenhammer (1987a, Fact 1) shows that for any radius  $r_i$  of  $s_i$  and for any cell  $C_j$  distinct from  $C_i$  there exists a generalized sphere  $s_j$  such that  $s_j \sim s_i$ . Hence, we find generalized spheres  $s_j$  and  $s_m$  such that  $s_j \sim s_i$  and  $s_m \sim s_i$ . Then  $F \subset \text{Ra}(s_i, s_j) \cap \text{Ra}(s_i, s_m)$ . Since the radical axes of the three spheres  $s_i$ ,  $s_j$ , and  $s_m$  are not parallel, they intersect in a common  $(d - 2)$ -dimensional subspace of  $\mathbb{R}^d$ . Therefore, we also have  $F \subset \text{Ra}(s_j, s_m)$ . Obviously,  $F \subset C_j \cap C_m$ . Since both  $C_j \cap C_m$  and  $\text{Ra}(s_j, s_m)$  are orthogonal to the line joining  $x_j$  and  $x_m$  and contain  $F$ , we conclude  $C_j \cap C_m \subset \text{Ra}(s_j, s_m)$ . Further, the orientation of  $\mathcal{D}(T)$  yields  $C_j \subset H(s_j, s_m)$ . This implies transitivity of the relation  $\sim$  for  $F \neq \emptyset$  which allows the construction of a set  $\varphi := \{s_i : i \in \mathbb{N}\}$  of generalized spheres such that  $T = L(\varphi)$ .  $\square$

In order to give the proof of the following theorem, we first fix some notations. Let  $T = \{C_i : i \in \mathbb{N}\}$  be a normal tessellation of  $\mathbb{R}^d$ . For  $i \geq d$  define  $Q_i = \cup_{j=1}^i C_j$  and let  $v$  be a vertex in the boundary of  $Q_i$ . Denote by  $e_1, \dots, e_s$  the edges in  $\partial Q_i$  having  $v$  as a vertex. We say that  $Q_i$  is *concave* at  $v$  if the convex hull  $\text{conv}\{e_1, \dots, e_s\}$  is not contained in  $Q_i$ . Since  $T$  is normal, concavity of  $Q_i$  implies the existence of a unique cell  $C$  of  $T$  containing all faces  $F$  in  $\partial Q_i$  with  $v \in F$ . This cell is called *proper* with respect to  $Q_i$ .

### Theorem 2.4.3

*Every normal tessellation of  $\mathbb{R}^d$  for  $d \geq 3$  is a Laguerre tessellation.*

#### Proof:

Let  $T$  be a normal tessellation of  $\mathbb{R}^d$  with  $d \geq 3$ . We will introduce a certain ordering  $C_1, C_2, \dots$  of the cells of  $T$  which can then be used for an iterative construction of an orthogonal dual  $\mathcal{D}(T) = \{x_1, x_2, \dots\}$ .

Choose  $C_1, \dots, C_d$  such that they share a common edge. A set of points  $x_1, \dots, x_d$  that satisfies duality, orthogonality and orientation can easily be found. For  $i > d$  choose  $C_i$  proper with respect to  $Q_{i-1}$  such that  $Q_i$  is simply connected. For  $j < i$  denote by  $F_{j,i}$  the face  $C_i \cap C_j$  (if it exists) and by  $L_{j,i}$  the line orthogonal to  $F_{j,i}$  through  $x_j$ . So we have to construct a suitable point  $x_i \in \mathcal{D}(T)$  using the points  $\{x_1, \dots, x_{i-1}\} \subset \mathcal{D}(T)$ . Define  $F_i := Q_{i-1} \cap C_i$  and define an inner vertex of  $F_i$  as a vertex in  $F_i \setminus \partial Q_i$ .

If we can show that  $\bigcap_{F_{j,i} \in F_i} L_{j,i}$  is a single point we can define

$$x_i := \bigcap_{F_{j,i} \in F_i} L_{j,i}.$$

This implies orthogonality of the set  $X_i := \{x_1, \dots, x_i\}$ . Duality and orientation of  $S_i$  follow from the convexity of  $C_i$ .

Let  $v$  and  $v'$  be two inner vertices joined by the edge  $e$ . Aurenhammer (1987a, Claim 1) shows that for any inner vertex  $v$  of  $F_i$   $g := \bigcap_{v \in F_{j,i}} L_{j,i}$  is a single point. Hence, there exist unique points  $p = \bigcap_{v \in F_{j,i}} L_{j,i}$  and  $p' = \bigcap_{v' \in F_{t,i}} L_{t,i}$ . Further, by Aurenhammer (1987a, Claim 2) the graph consisting of the inner vertices of  $F_i$  and the edges joining them is connected. Therefore, it is sufficient to show that for any such  $v$  and  $v'$  the points  $p$  and  $p'$  coincide. Now the edge  $e$  is contained in exactly  $(d - 1)$  2-faces of  $F_i$ , thus  $j = t$  occurs for  $(d - 1)$  values of  $j$ . Since  $d \geq 3$ , the intersection point  $p = p'$  is uniquely determined by the  $(d - 1)$  lines corresponding to these indices.

Repeating this construction, the set  $\bigcup_i X_i$  yields an orthogonal dual  $\mathcal{D}(T)$  of  $T$ . Now Theorem 2.4.2 tells us that  $T$  is a Laguerre tessellation.  $\square$

**Remarks 2.4.4**

- (i) The proof of Theorem 2.4.3 does not only yield the existence of a set of generators but also a way to construct it. This construction, however, does not lead to a unique solution.
- (ii) A counter-example to Theorem 2.4.3 for the case  $d = 2$  is given in Aurenhammer (1987a).

# Chapter 3

## Poisson Laguerre tessellations

Voronoi and generalized Voronoi tessellations generated by stationary point processes are used in various fields of application and have therefore raised the interest of many researchers for a long time. The appearance of such tessellations is mainly governed by the distribution of the geometric characteristics of their typical cells.

The easiest and most well-known model is the Voronoi tessellation generated by a stationary Poisson point process on  $\mathbb{R}^d$ . Fundamental properties of the Poisson process such as the Slivnyak theorem or the formula for the generating functional make this model tractable for the analytical derivation of mean values and even distribution functions of several characteristics of its typical cell. First results for mean values have been provided by Meijering (1953), Gilbert (1962), and Miles (1971, 1972). A derivation of these results using methods from Palm theory can be found in the work of Møller (1989, 1992). Later also formulas for several distribution functions became available. For example, Muche and Schlather studied the edge length distribution function (Muche, 1996b, 2005; Schlather, 2000), Muche and Stoyan (1992) considered contact and chord length distributions, and Calka (2003b) studied the distribution of the number of faces and of the area of a planar Voronoi tessellation. A summary of results can be found in the book by Okabe et al. (2000). Recently, Baumstark and Last (2007) provided very general results for distributions of the generators of the typical  $k$ -face of a Poisson Voronoi tessellation.

Few analytic results have been obtained for generalized random Voronoi tessellations. Several mean value formulas for the Johnson-Mehl tessellation have been derived by Møller (1992). To the best of our knowledge, the only investigation of random Laguerre tessellations is an unpublished manuscript of Zuyev (2004).

### 3.1 Existence of the Poisson Laguerre tessellation

In this chapter we study the Laguerre tessellation generated by a stationary marked Poisson process. As in Section 1.4 we will work in the canonical setting, i.e. we choose the probability space  $(\Omega, \mathcal{A}, \mathbb{P}) = (\mathbf{N}(\mathbb{R}^+), \mathcal{N}(\mathbb{R}^+), \mathbb{P})$ , where  $\mathbb{P}$  is the distribution of a stationary marked Poisson process  $\Phi$  on  $\mathbb{R}^d$  with intensity  $\lambda > 0$  and mark space  $\mathbb{R}^+$ . The marks are supposed to be independently identically distributed with distribution  $\mathbb{F}$ . We will always interpret the set of generators as a set of spheres in  $\mathbb{R}^d$ , in particular we will work with a distribution of (non-negative) radii of the spheres rather than a distribution of weights.

The definition of a point process implies that we are working with a locally finite set of generators. While this already guarantees the existence of the Poisson Voronoi tessellation, the existence of the Poisson Laguerre tessellation requires some restrictions on the distribution of radii.

**Definition 3.1.1**

For  $\varphi \in \mathbf{N}(\mathbb{R}^+)$  and  $t \in \mathbb{R}$  we define

$$\varphi^t := \varphi \cap \{(x, r) \in \mathbb{R}^d \times \mathbb{R}^+ : \text{pow}(0, (x, r)) > t\}. \quad (3.1)$$

Since  $\Phi$  is stationary, the distribution of  $\Phi^t$  is not changed when replacing the origin by an arbitrary point  $y \in \mathbb{R}^d$  in (3.1).

**Proposition 3.1.2 (Zuyev (2004))**

Choose  $y \in \mathbb{R}^d$  and write

$$p(t) := \mathbb{P}(\text{pow}(y, (x, r)) > t, (x, r) \in \Phi) = \mathbb{P}(\Phi^t = \Phi), \quad t \in \mathbb{R}, \quad (3.2)$$

for the probability that the power from  $y$  to each point of  $\Phi$  exceeds  $t$ . Then  $p(t)$  does not depend on  $y$  and is given by

$$p(t) = \exp\left(-\lambda\omega_d \int_0^\infty ([t + r^2]^+)^{\frac{d}{2}} \mathbb{F}(dr)\right)$$

where  $t^+ := \max(t, 0)$ .

**Proof:**

Let  $y \in \mathbb{R}^d$  be an arbitrary point. Using (1.4) we obtain

$$\begin{aligned} p(t) &= \mathbb{E} \left[ \prod_{(x,r) \in \Phi} \mathbb{I}\{\text{pow}(y, (x, r)) > t\} \right] \\ &= \exp\left(-\lambda \int_0^\infty \int_{\mathbb{R}^d} \mathbb{I}\{\text{pow}(y, (x, r)) \leq t\} dx \mathbb{F}(dr)\right) \\ &= \exp\left(-\lambda \int_0^\infty \int_{\mathbb{R}^d} \mathbb{I}\{\|y - x\|^2 \leq t + r^2\} dx \mathbb{F}(dr)\right) \\ &= \exp\left(-\lambda\omega_d \int_0^\infty ([t + r^2]^+)^{\frac{d}{2}} \mathbb{F}(dr)\right). \quad \square \end{aligned}$$

**Remark 3.1.3**

For any point  $y \in \mathbb{R}^d$  the property  $\text{pow}(y, (x, r)) > t$  for all  $(x, r) \in \Phi$  is equivalent to  $y \notin b(x, \sqrt{[t + r^2]^+})$  for all  $(x, r) \in \Phi$ . Hence,  $1 - p(t)$  is the volume fraction of the Boolean model of balls centered in  $x$  and with radii  $\sqrt{[t + r^2]^+}$ ,  $(x, r) \in \Phi$ .

**Proposition 3.1.4 (Zuyev (2004))**

Let  $\Phi$  be a stationary marked Poisson process on  $\mathbb{R}^d$  with intensity  $\lambda > 0$  and mark distribution  $\mathbb{F}$ . Suppose  $R$  is a random variable with distribution  $\mathbb{F}$ . Then the following statements are equivalent:

(i) The Laguerre tessellation of  $\Phi$  exists, i.e.  $\min_{(x,r) \in \Phi} \text{pow}(y, (x, r))$  almost surely exists for all  $y \in \mathbb{R}^d$ .

(ii) We have

$$\mathbb{E}[R^d] < \infty. \quad (3.3)$$

**Proof:**

Fix a point  $y \in \mathbb{R}^d$ . If (ii) holds, we have

$$\mathbb{P}\left(\inf_{(x,r) \in \Phi} \text{pow}(y, (x, r)) = -\infty\right) = \lim_{t \rightarrow -\infty} \mathbb{P}\left(\inf_{(x,r) \in \Phi} \text{pow}(y, (x, r)) < t\right) = \lim_{t \rightarrow -\infty} (1 - p(t)) = 0.$$

This means that for each  $y \in \mathbb{R}^d$  we have at least one  $(x, r) \in \Phi$  minimizing  $\text{pow}(y, (x, r))$ . Hence,  $y \in C((x, r), \Phi)$ . On the other hand,  $\mathbb{E}[R^d] = \infty$  implies  $p(t) = 0$  for each  $t \in \mathbb{R}$  and therefore  $\inf_{(x,r) \in \Phi} \text{pow}(y, (x, r)) = -\infty$  with probability 1.  $\square$

From now on we will assume that the mark distribution  $\mathbb{F}$  of  $\Phi$  satisfies (3.3). From the theory of Boolean models (see Hall, 1988, Chapter 4.2) we see that Proposition 3.1.4 can be extended by the following equivalent statements.

(iii) For each point of  $y \in \mathbb{R}^d$  the set  $\{(x, r) \in \Phi : y \in b(x, r)\}$  is almost surely finite.

(iv) For each bounded set  $B \subset \mathbb{R}^d$  the set  $\{(x, r) \in \Phi : b(x, r) \cap B \neq \emptyset\}$  is almost surely finite.

Therefore, Proposition 3.1.4 is in line with regularity condition (R1). Regularity condition (R2) is a consequence of the stationarity of  $\Phi$  (Schneider and Weil, 2000, Satz 1.3.5). So it remains to check whether the general position conditions (GP1) and (GP2) are satisfied in this context.

**Proposition 3.1.5**

$\Phi$  almost surely fulfills the general position conditions (GP1) and (GP2).

**Proof:**

It is well known (and can be shown by arguments similar to the ones below) that the points of a Poisson point process are almost surely in general quadratic position (Møller, 1992, Proposition 4.1.2). Therefore,  $\Phi$  conforms to condition (GP1). By Lemma 2.2.6, any  $d+1$  points  $(x_0, r_0), \dots, (x_d, r_d)$  in  $\Phi$  define a unique point  $z := z((x_0, r_0), \dots, (x_d, r_d)) \in \mathbb{R}^d$  such that

$$\text{pow}(z, (x_0, r_0)) = \dots = \text{pow}(z, (x_d, r_d)) =: \rho((x_0, r_0), \dots, (x_d, r_d)).$$

The expected number of points in  $\mathbb{R}^d$  having equal power to at least  $(d+2)$  points of  $\Phi$  is given by

$$\begin{aligned} & \frac{1}{(d+2)!} \mathbb{E} \left[ \sum_{s_0, \dots, s_{d+1} \in \Phi}^{\neq} \mathbb{I}\{\text{pow}(s_{d+1}, z(s_0, \dots, s_d)) = \rho(s_0, \dots, s_d)\} \right] \\ &= \lambda^{d+2} \int_0^\infty \dots \int_0^\infty \int_{\mathbb{R}^d} \dots \int_{\mathbb{R}^d} \int_0^\infty \int_{\mathbb{R}^d} \\ & \quad \mathbb{I}\{\|x_{d+1} - z((x_0, r_0), \dots, (x_d, r_d))\|^2 - r_{d+1}^2 = \rho((x_0, r_0), \dots, (x_d, r_d))\} dx_{d+1} \mathbb{F}(dr_{d+1}) \\ & \quad dx_0 \dots dx_d \mathbb{F}(dr_0) \dots \mathbb{F}(dr_d) \end{aligned}$$

The inner integral is of the form  $\int_{\mathbb{R}^d} \mathbb{I}\{\|x - z\|^2 = c\} dx$  with fixed  $z \in \mathbb{R}^d$  and  $c \in \mathbb{R}$ , and therefore equals 0. Hence, regularity condition (GP2) holds as well.  $\square$

This shows that the Laguerre tessellation of  $\Phi$  is a tessellation of  $\mathbb{R}^d$  which is almost surely normal and face-to-face.

### Remark 3.1.6

Ash and Bolker (1986, Theorem 18) show, that a Laguerre tessellation generated by a marked Poisson process on  $\mathbb{R}^2$  almost surely has no vertex which belongs to more than 3 cells. Their proof uses differential geometric methods based on the Transversality Theorem. A generalization to higher dimensions seems straightforward.

## 3.2 Palm distributions

### 3.2.1 Notation

As we have seen in Section 1.6, a random tessellation gives rise to several random measures. In this section we consider random measures induced by a Poisson Laguerre tessellation  $L(\Phi)$ , namely the measures  $M_k$  on  $\mathbb{R}^d$  introduced in (1.5) which are defined via

$$M_k(\cdot) = \sum_{S \in \mathcal{S}_k(L(\Phi))} \mathcal{H}^k(S \cap \cdot), \quad k \in \{0, \dots, d\}.$$

The intensity of  $M_k$  will be denoted by  $\mu_k$ .

The Palm measure  $\mathbb{Q}_k$  of  $M_k$  is a measure on  $\mathbf{N}(\mathbb{R}^+)$  given by

$$\mathbb{Q}_k(\cdot) = \mathbb{E} \left[ \int_{[0,1]^d} \mathbb{I}\{\Phi - y \in \cdot\} M_k(dy) \right].$$

We will prove later that  $\mu_k < \infty$  for  $k = 0, \dots, d-1$ . Hence, we can define the Palm probability measure of  $M_k$  as  $\mathbb{Q}_k^0 := \mu_k^{-1} \mathbb{Q}_k$ . With respect to this measure the origin  $0 \in \mathbb{R}^d$  is almost surely contained in a  $k$ -face of  $L(\Phi)$ . Integration with respect to  $\mathbb{Q}_k$  and  $\mathbb{Q}_k^0$  will be denoted by  $\mathbb{E}_{M_k}$  and  $\mathbb{E}_{M_k}^0$ , respectively.

For  $\varphi \in \mathbf{N}(\mathbb{R}^+)$  let  $F \in \mathcal{S}_k(L(\varphi))$  be a  $k$ -face of  $L(\varphi)$  for  $k \in \{0, \dots, d\}$ . Then there are  $m = d - k$  points  $s_0 = (x_0, r_0), \dots, s_m = (x_m, r_m)$  in  $\varphi$  which satisfy  $F = F(s_0, \dots, s_m, \varphi)$ .

Let  $x \in \mathbb{R}^d$  be contained in the relative interior of the face  $F$  and define

$$P_k(x, \varphi) := \text{pow}(x, s_0) = \dots = \text{pow}(x, s_m).$$

The points  $s_0, \dots, s_m \in \varphi$  are uniquely determined if

$$\varphi \left( \{ (y, r) : \text{pow}(x, (y, r)) = P_k(x, \varphi) \} \right) = m + 1, \quad (3.4)$$

which is always the case if  $\varphi$  is in general position. In this case, the points  $x_0, \dots, x_m$  are contained in a  $(d - k)$ -plane  $E$ . Then for  $k \leq d - 1$  there is a unique point  $z(s_0, \dots, s_m) \in E$ , such that

$$\text{pow}(z(s_0, \dots, s_m), s_0) = \dots = \text{pow}(z(s_0, \dots, s_m), s_m). \quad (3.5)$$

For  $k = d$  we have  $E = \{x_0\}$  and define  $z(s_0) := x_0$ . Thus, we may further define

$$\begin{aligned} S_{k,i}(x, \varphi) &:= (X_{k,i}(x, \varphi), R_{k,i}(x, \varphi)) := (x_i, r_i), \quad i = 0, \dots, m, \\ Z_k(x, \varphi) &:= z(s_0, \dots, s_m), \end{aligned} \quad (3.6)$$

where the order of  $S_{k,i}(x, \varphi)$  is determined by the lexicographic order of  $x_0, \dots, x_m$ . For  $k = 0$  we always have  $Z_k(x, \varphi) = x$ . If (3.4) does not hold we define  $S_{k,i}(x, \varphi) := (x, 0)$  and  $Z_k(x, \varphi) := x$ . For each point  $x \in \mathbb{R}^d$  which is not contained in the relative interior of a  $k$ -face  $F \in \mathcal{S}_k(L(\varphi))$ , let  $P_k(x, \varphi) := 0$ ,  $S_{k,0}(x, \varphi) = \dots = S_{k,m}(x, \varphi) := (x, 0)$ , and  $Z_k(x, \varphi) := x$ .

The power of  $Z_k(x, \varphi)$  to the generators of  $F$  is denoted by

$$P'_k(x, \varphi) := \text{pow}(Z_k(x, \varphi), S_{k,0}(x, \varphi)).$$

Then for  $k \leq d - 1$  the distance  $\|X_{k,i}(x, \varphi) - Z_k(x, \varphi)\| = \sqrt{P'_k(x, \varphi) + R_{k,i}(x, \varphi)^2}$  is  $\mathbb{Q}_k$ -almost everywhere a positive number and we may further define the unit vectors

$$U_{k,i}(x, \varphi) := \frac{X_{k,i}(x, \varphi) - Z_k(x, \varphi)}{\sqrt{P'_k(x, \varphi) + R_{k,i}(x, \varphi)^2}}, \quad i = 0, \dots, m.$$

For  $k = d$  we have  $P'_d(x, \varphi) = -R_{d,0}(x, \varphi)^2$  and define  $U_{d,0}(x, \varphi) := 0$ .

If  $k \geq 1$  we fix a unit vector  $u \in S^{d-1} \cap E^\perp$  and define

$$P''_k(x, \varphi) := \|x - Z_k(x, \varphi)\|^2$$

and

$$U_k(x, \varphi) := \begin{cases} \frac{Z_k(x, \varphi) - x}{\sqrt{P''_k(x, \varphi)}}, & \text{if } P''_k(x, \varphi) > 0, \\ u, & \text{otherwise.} \end{cases}$$

For any  $x \in \mathbb{R}^d$  which is not contained in the relative interior of a  $k$ -face these definitions yield  $P'_k(x, \varphi) = P''_k(x, \varphi) = 0$  and we set  $U_{k,0}(x, \varphi) = \dots = U_{k,m}(x, \varphi) := u_{d-k}$  and  $U_k(x, \varphi) := u_k$  with arbitrary  $u_{d-k} \in S^{d-1} \cap E$  and  $u_k \in S^{d-1} \cap E^\perp$ . If  $k = 0$  we define  $U_k(x, \varphi) := 0$ .

Both  $x$  and  $Z_k(x, \varphi)$  are contained in the affine hull of the face  $F$ , which is orthogonal to the linear hull of the points  $X_{k,0}(x, \varphi), \dots, X_{k,m}(x, \varphi)$  (Lemma 2.2.6). Hence, we have

$$P_k(x, \varphi) = P'_k(x, \varphi) + P''_k(x, \varphi)$$

and the mappings defined above show the following behavior with respect to translations

$$\begin{aligned} Z_k(x, \varphi) &= Z_k(0, \varphi - x) + x, \\ P_k(x, \varphi) &= P_k(0, \varphi - x), \quad P'_k(x, \varphi) = P'_k(0, \varphi - x), \quad P''_k(x, \varphi) = P''_k(0, \varphi - x), \\ U_k(x, \varphi) &= U_k(0, \varphi - x), \quad \text{and } U_{k,i}(x, \varphi) = U_{k,i}(0, \varphi - x), \end{aligned}$$

for each  $\varphi \in \mathbf{N}(\mathbb{R}^+)$ ,  $x \in \mathbb{R}^d$ , and  $i = 0, \dots, m$ .

With respect to the measure  $\mathbb{Q}_k$  the origin is almost everywhere contained in a unique  $k$ -face  $F_k(0) := F(S_{k,0}(0, \Phi), \dots, S_{k,m}(0, \Phi), \Phi) \in \mathcal{S}_k(L(\Phi))$ . Therefore, the following random variables are of special interest:

- $Z_k := Z_k(0, \Phi)$ , the center of the face  $F_k(0)$ ,
- $P_k := P_k(0, \Phi)$ , the power of the origin to the generators of  $F_k(0)$ ,
- $P'_k := P'_k(0, \Phi)$ , the power of  $Z_k$  to the generators of  $F_k(0)$ ,
- $P''_k := P''_k(0, \Phi)$ , the squared distance of  $Z_k$  to the origin,
- $U_{k,i} := U_{k,i}(0, \Phi)$ ,  $i = 0, \dots, m$ , the directions from  $Z_k$  to the generators,
- $R_{k,i} := R_{k,i}(0, \Phi)$ ,  $i = 0, \dots, m$ , the weights of the generators,
- $U_k := U_k(0, \Phi)$ , the direction from the origin to  $Z_k$ .

For abbreviation and in order to neglect the enumeration we define

$$\Psi_k := \{(U_{k,0}, R_{k,0}), \dots, (U_{k,m}, R_{k,m})\}.$$

An illustration of these notations for  $d = 2$  and  $k = 1$  is given in Figure 3.1.

### 3.2.2 A complete description of $\mathbb{Q}_k^0$

For  $0 < m \leq d$  and  $x_0, \dots, x_m \in \mathbb{R}^d$  let  $\Delta_m(x_0, \dots, x_m)$  be the  $m$ -dimensional volume of the convex hull of  $x_0, \dots, x_m$  in  $\mathbb{R}^d$ . Further, write  $\mathcal{L}_m^d$  and  $\mathcal{E}_m^d$  for the set of all  $m$ -dimensional linear and affine subspaces of  $\mathbb{R}^d$ , respectively.

#### Theorem 3.2.1

There exist unique invariant measures  $\nu_m$  on  $\mathcal{L}_m^d$  and  $\mu_m$  on  $\mathcal{E}_m^d$  such that  $\nu_m(\mathcal{L}_m^d) = 1$  and

$$\int_{\mathcal{E}_m^d} f(E) \mu_m(dE) = \int_{\mathcal{L}_m^d} \int_{L^\perp} f(L + y) \mathcal{H}^{d-m}(dy) \nu_m(dL) = \int_{SO_d} \int_{L_0^\perp} f(\vartheta(y + L_0)) \mathcal{H}^{d-m}(dy) \nu(d\vartheta),$$

where  $f : \mathcal{E}_m^d \rightarrow [0, \infty)$  is a measurable function and  $L_0 \in \mathcal{L}_m^d$  is a fixed linear subspace of  $\mathbb{R}^d$ .

#### Proof:

(Schneider and Weil, 1992, Satz 1.3.3, Satz 1.3.4, and p. 29).

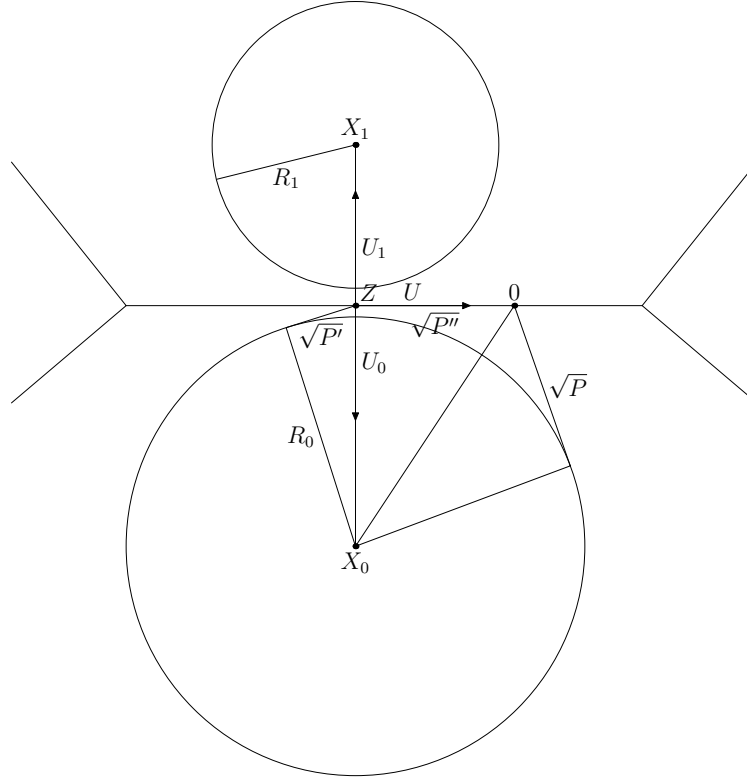


Figure 3.1: Illustration of the notation for  $d = 2$  and  $k = 1$ . The subscript 1 is omitted in the labels.

**Theorem 3.2.2 (Blaschke-Petkantschin formula)**

Suppose  $1 \leq m \leq d$  and  $f : (\mathbb{R}^d)^{m+1} \rightarrow [0, \infty)$  is a measurable function. Then

$$\begin{aligned} & \int_{\mathbb{R}^d} \dots \int_{\mathbb{R}^d} f(x_0, \dots, x_m) dx_0 \dots dx_m \\ &= c_{dm} (m!)^{d-m} \int_{\mathcal{E}_m^d} \int_E \dots \int_E f(x_0, \dots, x_m) \Delta_m(x_0, \dots, x_m)^{d-m} \mathcal{H}^m(dx_0) \dots \mathcal{H}^m(dx_m) \mu_m(dE), \end{aligned}$$

$$\text{where } c_{dm} = \frac{\sigma_{d-m+1} \dots \sigma_d}{\sigma_1 \dots \sigma_m}.$$

**Proof:**

(Schneider and Weil, 1992, Satz 6.1.5).

Finally, we prove a generalized version of a transformation formula given in Schneider and Weil (2000).

**Lemma 3.2.3**

Let  $L$  be a  $k$ -dimensional linear subspace of  $\mathbb{R}^d$  and  $f : L^{k+1} \rightarrow [0, \infty)$  a measurable function. Further, consider strictly monotonic increasing, differentiable functions  $r_i : [a, \infty) \rightarrow [0, \infty)$ ,

$i = 0, \dots, k$ , with an arbitrary real number  $a$ . Then we have

$$\begin{aligned} & \int_L \dots \int_L f(x_0, \dots, x_k) dx_0 \dots dx_k \\ &= k! \int_L \int_a^\infty \int_{S^{d-1} \cap L} \dots \int_{S^{d-1} \cap L} f(y + r_0(t)u_0, \dots, y + r_k(t)u_k) \prod_{i=0}^k (r_i(t)^{k-1} \dot{r}_i(t)) \\ & \quad \Delta_k \left( \frac{1}{\dot{r}_0(t)} u_0, \dots, \frac{1}{\dot{r}_k(t)} u_k \right) \mathbb{S}_L(du_0) \dots \mathbb{S}_L(du_k) dt \mathcal{H}^k(dy), \end{aligned}$$

where  $\mathbb{S}_L$  is the surface measure on the  $k$ -dimensional sphere  $S^{d-1} \cap L$  and  $\dot{r}_i$  is the derivative of the function  $r_i$ ,  $i = 0, \dots, k$ .

**Proof:**

We will only prove this lemma for  $L = \mathbb{R}^k \subset \mathbb{R}^d$ . The assertion is then obtained by introducing an appropriate coordinate system on  $L$ . We define a mapping

$$\begin{aligned} T : \mathbb{R}^k \times [a, \infty) \times S^{k-1} \times \dots \times S^{k-1} &\rightarrow (\mathbb{R}^k)^{k+1} \\ (y, t, u_0, \dots, u_k) &\mapsto \begin{pmatrix} y + r_0(t)u_0 \\ \vdots \\ y + r_k(t)u_k \end{pmatrix}. \end{aligned}$$

It is easy to see that  $T$  is injective. We have to show that the determinant of the Jacobian of  $T$  is given by

$$D := D(y, t, u_0, \dots, u_k) = k! \prod_{i=0}^k (r_i(t)^{k-1} \dot{r}_i(t)) \Delta_k \left( \frac{1}{\dot{r}_0(t)} u_0, \dots, \frac{1}{\dot{r}_k(t)} u_k \right).$$

Assume that the unit vectors  $u_i$  are given in spherical coordinates and let  $\dot{u}_i$  denote the derivative of  $u_i$  with respect to these coordinates. Writing  $E_k$  for the  $k$ -dimensional unit matrix we obtain

$$D = \begin{vmatrix} E_k & \dot{r}_0(t)u_0 & r_0(t)\dot{u}_0 & 0 & \dots & 0 \\ E_k & \dot{r}_1(t)u_1 & 0 & r_1(t)\dot{u}_1 & \dots & 0 \\ \vdots & \vdots & \vdots & \vdots & \ddots & \vdots \\ E_k & \dot{r}_k(t)u_k & 0 & 0 & \dots & r_k(t)\dot{u}_k \end{vmatrix}.$$

For  $\tilde{D} = \left( \prod_{i=0}^k \frac{1}{r_i(t)} \right)^{k-1} D$  this leads to

$$\tilde{D}^2 = \begin{vmatrix} E_k & E_k & \dots & E_k \\ \dot{r}_0(t)u_0^t & \dot{r}_1(t)u_1^t & \dots & \dot{r}_k(t)u_k^t \\ \dot{u}_0^t & 0 & \dots & 0 \\ 0 & \dot{u}_1^t & \dots & 0 \\ \vdots & \vdots & \ddots & \vdots \\ 0 & 0 & \dots & \dot{u}_k^t \end{vmatrix} \cdot \begin{vmatrix} E_k & \dot{r}_0(t)u_0 & \dot{u}_0 & 0 & \dots & 0 \\ E_k & \dot{r}_1(t)u_1 & 0 & \dot{u}_1 & \dots & 0 \\ \vdots & \vdots & \vdots & \vdots & \ddots & \vdots \\ E_k & \dot{r}_k(t)u_k & 0 & 0 & \dots & \dot{u}_k \end{vmatrix}$$

$$= \begin{vmatrix} (k+1)E_k & \sum \dot{r}_i(t)u_i & \dot{u}_0 & \dot{u}_1 & \cdots & \dot{u}_k \\ \sum \dot{r}_i(t)u_i^t & \sum \dot{r}_i(t)^2 & 0 & 0 & \cdots & 0 \\ \dot{u}_0^t & 0 & E_{k-1} & 0 & \cdots & 0 \\ \dot{u}_1^t & 0 & 0 & E_{k-1} & \cdots & 0 \\ \vdots & \vdots & \vdots & & \ddots & \vdots \\ \dot{u}_k^t & 0 & 0 & 0 & \cdots & E_{k-1} \end{vmatrix}$$

Now we will use the formula  $|A| = |B||A_{22}|$ , where

$$A = \begin{pmatrix} A_{11} & A_{12} \\ A_{21} & A_{22} \end{pmatrix} \text{ and } B = A_{11} - A_{12}A_{22}^{-1}A_{21},$$

if the matrix  $A$  is symmetric and  $A_{22}^{-1}$  exists. In our case we have  $A_{22} = E_{(k+1)(k-1)}$ . Further note that  $E_k - \dot{u}_i\dot{u}_i^t = u_iu_i^t$  as the matrix  $u_iu_i^t$  is orthogonal. Using this relation we obtain

$$\begin{aligned} \tilde{D}^2 &= \begin{vmatrix} (k+1)E_k - \sum \dot{u}_i\dot{u}_i^t & \sum \dot{r}_i(t)u_i \\ \sum \dot{r}_i(t)u_i^t & \sum \dot{r}_i(t)^2 \end{vmatrix} \\ &= \begin{vmatrix} \sum u_iu_i^t & \sum \dot{r}_i(t)u_i \\ \sum \dot{r}_i(t)u_i^t & \sum \dot{r}_i(t)^2 \end{vmatrix} \\ &= \begin{vmatrix} \begin{pmatrix} u_0 & \cdots & u_k \\ \dot{r}_0(t) & \cdots & \dot{r}_k(t) \end{pmatrix} & \begin{pmatrix} u_0^t & \dot{r}_0(t) \\ \vdots & \vdots \\ u_k^t & \dot{r}_k(t) \end{pmatrix} \end{vmatrix} \\ &= (k!)^2 \prod_{i=0}^k \dot{r}_i(t)^2 \Delta_k^2 \left( \frac{1}{\dot{r}_0(t)}u_0, \dots, \frac{1}{\dot{r}_k(t)}u_k \right), \end{aligned}$$

which completes the proof.  $\square$

Let  $\Phi$  be the (marked) point process of generators of a random Laguerre tessellation and recall that

$$\Phi^t = \Phi \cap \{(x, r) : \text{pow}(0, (x, r)) > t\}.$$

With respect to  $\mathbb{Q}_k$ ,  $1 \leq k \leq d-1$ , the point process  $\Phi$  is determined by the following tuple of random variables

$$(\Phi^{P_k}, P'_k, P''_k, \Psi_k, U_k) \quad (3.7)$$

which have been defined in Section 3.2.1. In fact we have for any measurable function  $h$  on  $\mathbb{R}^d \times \mathbb{R}^+$  that

$$\sum_{(x,r) \in \Phi} h(x, r) = \sum_{(x,r) \in \Phi^{P_k}} h(x, r) + \sum_{(u,r) \in \Psi_k} h((P'_k + r^2)^{\frac{1}{2}}u + P''_k^{\frac{1}{2}}U_k). \quad (3.8)$$

For  $k=0$  the decomposition simplifies to  $(\Phi^{P_0}, P_0, \Psi_0)$ . Finally, for  $k=d$  we have  $\mathbb{Q}_d = \mathbb{Q}_d^0 = \mathbb{P}$  and the corresponding representation is  $(\Phi^{P_d}, P_d, U_d, R_{d,0})$ .

### Theorem 3.2.4

Let  $\Phi$  be a stationary marked Poisson process with intensity  $\lambda > 0$  and mark distribution  $\mathbb{F}$  with property (3.3). Denote integration with respect to the Palm measure  $\mathbb{Q}_k$  by  $\mathbb{E}_{M_k}$  and let

$h$  be a non-negative measurable function defined on a suitable domain. For  $1 \leq k \leq d-1$  and  $m = d-k$  we have

$$\begin{aligned} & \mathbb{E}_{M_k} [h(\Phi^{P_k}, P'_k, P''_k, \Psi_k, U_k)] \\ &= \frac{\lambda^{m+1}}{4(m+1)!} c_{dm} (m!)^{k+1} \int_0^\infty \dots \int_0^\infty \int_{-\min_i r_i^2}^\infty \prod_{i=0}^m (t+r_i^2)^{\frac{m-2}{2}} \int_0^\infty p(t+s) s^{\frac{k-2}{2}} \\ & \quad \int_{S^{d-1} \cap L} \dots \int_{S^{d-1} \cap L} \int_{S^{d-1} \cap L^\perp} \int_{SO_d} \mathbb{E} [h(\Phi^{t+s}, t, s, \{(\vartheta u_0, r_0), \dots, (\vartheta u_m, r_m)\}, \vartheta u)] \nu(d\vartheta) \mathbb{S}_{L^\perp}(du) \\ & \quad \Delta_m^{k+1} \left( (t+r_0^2)^{\frac{1}{2}} u_0, \dots, (t+r_m^2)^{\frac{1}{2}} u_m \right) \mathbb{S}_L(du_0) \dots \mathbb{S}_L(du_m) ds dt \mathbb{F}(dr_0) \dots \mathbb{F}(dr_m). \end{aligned}$$

For  $k=0$  the following formula holds

$$\begin{aligned} & \mathbb{E}_{M_0} [h(\Phi^{P_0}, P_0, \Psi_0)] \\ &= \frac{\lambda^{d+1}}{2(d+1)} \int_0^\infty \dots \int_0^\infty \int_{-\min_i r_i^2}^\infty \prod_{i=0}^d (t+r_i^2)^{\frac{d-2}{2}} p(t) \int_{S^{d-1}} \dots \int_{S^{d-1}} \mathbb{E} [h(\Phi^t, t, \{(u_0, r_0), \dots, (u_d, r_d)\})] \\ & \quad \Delta_d \left( (t+r_0^2)^{\frac{1}{2}} u_0, \dots, (t+r_d^2)^{\frac{1}{2}} u_d \right) \mathbb{S}(du_0) \dots \mathbb{S}(du_d) dt \mathbb{F}(dr_0) \dots \mathbb{F}(dr_d). \end{aligned}$$

Finally, for  $k=d$  the representation with respect to  $(\Phi^{P_d}, P_d, U_d, R_{d,0})$  reads

$$\mathbb{E}_{M_d} [h(\Phi^{P_d}, P_d, U_d, R_{d,0})] = \frac{\lambda}{2} \int_0^\infty \int_{-r_0^2}^\infty p(t) (t+r_0^2)^{\frac{d-2}{2}} \int_{S^{d-1}} \mathbb{E} [h(\Phi^t, t, u, r_0)] \mathbb{S}(du) dt \mathbb{F}(dr_0).$$

**Proof:**

We will concentrate on the case  $1 \leq k \leq d-1$ . The proofs for the cases  $k=0$  and  $k=d$  work similarly. Let  $h_1 : \mathbf{N} \rightarrow [0, \infty)$  be a measurable function defined by

$$h_1(\varphi) := h(\varphi^{P_k(0,\varphi)}, P'_k(0, \varphi), P''_k(0, \varphi), \Psi_k(0, \varphi), U_k(0, \varphi))$$

and write  $m := d-k$ . Using the definition of  $M_k$  and Theorem 1.3.8 we get

$$\begin{aligned} & \mathbb{E}_{M_k} [h_1(\Phi)] \\ &= \mathbb{E} \left[ \int_{[0,1]^d} h_1(\Phi - y) M_k(dy) \right] \\ &= \frac{1}{(m+1)!} \mathbb{E} \left[ \sum_{s_0, \dots, s_m \in \Phi}^{\neq} \int \mathbb{I} \{y \in [0,1]^d \cap F(s_0, \dots, s_m, \Phi)\} h_1(\Phi - y) \mathcal{H}^k(dy) \right] \\ &= \frac{\lambda^{m+1}}{(m+1)!} \int_0^\infty \dots \int_0^\infty \int_{\mathbb{R}^d} \dots \int_{\mathbb{R}^d} \mathbb{E} \left[ \mathbb{I} \{y \in [0,1]^d \cap F((x_0, r_0), \dots, (x_m, r_m), \Phi)\} \right. \\ & \quad \left. h_1 \left( [\Phi \cup \{(x_0, r_0), \dots, (x_m, r_m)\}] - y \right) \right] \mathcal{H}^k(dy) dx_0 \dots dx_m \mathbb{F}(dr_0) \dots \mathbb{F}(dr_m). \end{aligned}$$

Using the decomposition of  $\Phi$  we have

$$\begin{aligned} & \mathbb{E}_{M_k} [h(\Phi^{P_k}, P'_k, P''_k, \Psi_k, U_k)] \\ &= \frac{\lambda^{m+1}}{(m+1)!} \int_0^\infty \cdots \int_0^\infty \int_{\mathbb{R}^d} \cdots \int_{\mathbb{R}^d} \int \mathbb{E} \left[ \mathbb{1} \{y \in [0, 1]^d \cap F((x_0, r_0), \dots, (x_m, r_m), \Phi)\} \right. \\ & \quad h\left((\Phi - y)^{P_k(y, \Phi \cup \{(x_0, r_0), \dots, (x_m, r_m)\})}, P'_k(y, \Phi \cup \{(x_0, r_0), \dots, (x_m, r_m)\})\right), \\ & \quad P''_k(y, \Phi \cup \{(x_0, r_0), \dots, (x_m, r_m)\}), \Psi_k(y, \Phi \cup \{(x_0, r_0), \dots, (x_m, r_m)\})\right) \\ & \quad \left. U_k(y, \Phi \cup \{(x_0, r_0), \dots, (x_m, r_m)\})\right] \mathcal{H}^k(dy) dx_0 \dots dx_m \mathbb{F}(dr_0) \dots \mathbb{F}(dr_m). \end{aligned}$$

If  $x_0, \dots, x_m$  are in general position and  $y \in F((x_0, r_0), \dots, (x_m, r_m), \Phi)$ , we have

$$\begin{aligned} P_k(y, \Phi \cup \{(x_0, r_0), \dots, (x_m, r_m)\}) &= \text{pow}(y, (x_0, r_0)), \\ P'_k(y, \Phi \cup \{(x_0, r_0), \dots, (x_m, r_m)\}) &= \text{pow}(z((x_0, r_0), \dots, (x_m, r_m)), (x_0, r_0)), \\ P''_k(y, \Phi \cup \{(x_0, r_0), \dots, (x_m, r_m)\}) &= \|z((x_0, r_0), \dots, (x_m, r_m)) - y\|^2, \\ \Psi_k(y, \Phi \cup \{(x_0, r_0), \dots, (x_m, r_m)\}) &= \tilde{\Psi}_k((x_0, r_0), \dots, (x_m, r_m)) \text{ and} \\ U_k(y, \Phi \cup \{(x_0, r_0), \dots, (x_m, r_m)\}) &= \tilde{U}_k(y, (x_0, r_0), \dots, (x_m, r_m)), \end{aligned}$$

where

$$\begin{aligned} \tilde{\Psi}_k(s_0, \dots, s_m) &:= \left\{ \left( \frac{x_0 - z(s_0, \dots, s_m)}{\|x_0 - z(s_0, \dots, s_m)\|}, r_0 \right), \dots, \left( \frac{x_m - z(s_0, \dots, s_m)}{\|x_m - z(s_0, \dots, s_m)\|}, r_m \right) \right\} \text{ and} \\ \tilde{U}_k(y, s_0, \dots, s_m) &:= \frac{z(s_0, \dots, s_m) - y}{\|z(s_0, \dots, s_m) - y\|}. \end{aligned}$$

If  $z((x_0, r_0), \dots, (x_m, r_m)) = y$  we define  $\tilde{U}_k(y, (x_0, r_0), \dots, (x_m, r_m))$  to be some fixed unit vector. If  $x_0, \dots, x_m$  are not in general position, all functions can be defined arbitrarily. Thus, we get

$$\begin{aligned} & \mathbb{E}_{M_k} [h(\Phi^{P_k}, P'_k, P''_k, \Psi_k, U_k)] \\ &= \frac{\lambda^{m+1}}{(m+1)!} \int_0^\infty \cdots \int_0^\infty \int_{\mathbb{R}^d} \cdots \int_{\mathbb{R}^d} \int \mathbb{E} \left[ \mathbb{1} \{y \in [0, 1]^d \cap F((x_0, r_0), \dots, (x_m, r_m), \Phi)\} \right. \\ & \quad h\left((\Phi - y)^{\text{pow}(y, (x_0, r_0))}, \text{pow}(z((x_0, r_0), \dots, (x_m, r_m)), (x_0, r_0)), \right. \\ & \quad \left. \|z((x_0, r_0), \dots, (x_m, r_m)) - y\|^2, \tilde{\Psi}_k((x_0, r_0), \dots, (x_m, r_m)), \tilde{U}_k(y, (x_0, r_0), \dots, (x_m, r_m))\right) \\ & \quad \left. \mathcal{H}^k(dy) dx_0 \dots dx_m \mathbb{F}(dr_0) \dots \mathbb{F}(dr_m). \right] \end{aligned}$$

Since  $\Phi$  is stationary and using (3.2) we have

$$\begin{aligned} & \mathbb{E}_{M_k} [h(\Phi^{P_k}, P'_k, P''_k, \Psi_k, U_k)] \\ &= \frac{\lambda^{m+1}}{(m+1)!} \int_0^\infty \cdots \int_0^\infty \int_{\mathbb{R}^d} \cdots \int_{\mathbb{R}^d} \mathbb{I}\{y \in [0, 1]^d \cap G((x_0, r_0), \dots, (x_m, r_m))\} p(\text{pow}(y, (x_0, r_0))) \\ & \mathbb{E} \left[ h \left( \Phi^{\text{pow}(y, (x_0, r_0))}, \text{pow}(z((x_0, r_0), \dots, (x_m, r_m)), (x_0, r_0)), \|z((x_0, r_0), \dots, (x_m, r_m)) - y\|^2, \right. \right. \\ & \left. \left. \tilde{\Psi}_k((x_0, r_0), \dots, (x_m, r_m)), \tilde{U}_k(y, (x_0, r_0), \dots, (x_m, r_m)) \right) \right] \mathcal{H}^k(dy) dx_0 \dots dx_m \\ & \mathbb{F}(dr_0) \dots \mathbb{F}(dr_m). \end{aligned}$$

Using the affine Blaschke-Petkantschin formula (Theorem 3.2.2) we obtain

$$\begin{aligned} & \mathbb{E}_{M_k} [h(\Phi^{P_k}, P'_k, P''_k, \Psi_k, U_k)] \\ &= \frac{\lambda^{m+1}}{(m+1)!} c_{dm}(m!)^k \int_0^\infty \cdots \int_0^\infty \int_{\mathcal{E}_m^d} \int_E \cdots \int_E \mathbb{I}\{y \in [0, 1]^d \cap G((x_0, r_0), \dots, (x_m, r_m))\} \\ & \mathbb{E} \left[ h \left( \Phi^{\text{pow}(y, (x_0, r_0))}, \text{pow}(z((x_0, r_0), \dots, (x_m, r_m)), (x_0, r_0)), \|z((x_0, r_0), \dots, (x_m, r_m)) - y\|^2, \right. \right. \\ & \left. \left. \tilde{\Psi}_k((x_0, r_0), \dots, (x_m, r_m)), \tilde{U}_k(y, (x_0, r_0), \dots, (x_m, r_m)) \right) \right] p(\text{pow}(y, (x_0, r_0))) \\ & \Delta_m^k(x_0, \dots, x_m) \mathcal{H}^k(dy) \mathcal{H}^m(dx_0) \dots \mathcal{H}^m(dx_m) \mu_m(dE) \mathbb{F}(dr_0) \dots \mathbb{F}(dr_m). \end{aligned}$$

We fix a subspace  $L \in \mathcal{L}_m^d$  and apply Theorem 3.2.1. Since  $G((x+x_0, r_0), \dots, (x+x_m, r_m)) = x + G((x_0, r_0), \dots, (x_m, r_m))$  and  $z(x+x_0, \dots, x+x_m) = x + z(x_0, \dots, x_m)$ , we get

$$\begin{aligned} & \mathbb{E}_{M_k} [h(\Phi^{P_k}, P'_k, P''_k, \Psi_k, U_k)] \\ &= \frac{\lambda^{m+1}}{(m+1)!} c_{dm}(m!)^k \int_0^\infty \cdots \int_0^\infty \int_{SO_d} \int_{\vartheta L^\perp} \int_{\vartheta L} \cdots \int_{\vartheta L} p(\text{pow}(y, (x+x_0, r_0))) \Delta_m^k(x_0, \dots, x_m) \\ & \mathbb{I}\{y \in [0, 1]^d \cap x + z((x_0, r_0), \dots, (x_m, r_m)) + \vartheta L^\perp\} \mathbb{E} \left[ h \left( \Phi^{\text{pow}(y, (x+x_0, r_0))}, \right. \right. \\ & \left. \left. \text{pow}(z((x_0, r_0), \dots, (x_m, r_m)), (x_0, r_0)), \|x + z((x_0, r_0), \dots, (x_m, r_m)) - y\|^2, \right. \right. \\ & \left. \left. \tilde{\Psi}_k((x_0, r_0), \dots, (x_m, r_m)), \tilde{U}_k(y, (x+x_0, r_0), \dots, (x+x_m, r_m)) \right) \right] \mathcal{H}^k(dy) \\ & \mathcal{H}^m(dx_0) \dots \mathcal{H}^m(dx_m) \mathcal{H}^k(dx) \nu(d\vartheta) \mathbb{F}(dr_0) \dots \mathbb{F}(dr_m). \end{aligned}$$

Now the change of coordinates introduced in Lemma 3.2.3 with  $z = z(s_0, \dots, s_m)$ ,  $t = \text{pow}(z, s_0)$  and  $r_i(t) = (t + r_i^2)^{\frac{1}{2}}$  yields

$$\begin{aligned} & \mathbb{E}_{M_k} [h(\Phi^{P_k}, P'_k, P''_k, \Psi_k, U_k)] \\ &= \frac{\lambda^{m+1}}{2(m+1)!} c_{dm}(m!)^{k+1} \int_0^\infty \cdots \int_0^\infty \int_{-\min_i r_i^2}^\infty \prod_{i=0}^m (t + r_i^2)^{\frac{m-2}{2}} \int_{SO_d} \int_{\vartheta L^\perp} \int_{\vartheta L} p(t + \|x + z - y\|^2) \end{aligned}$$

$$\begin{aligned} & \mathbb{I} \{y \in [0, 1]^d \cap x + z + \vartheta L^\perp\} \int_{S^{d-1} \cap \vartheta L} \dots \int_{S^{d-1} \cap \vartheta L} \Delta_m^{k+1} \left( (t + r_0^2)^{\frac{1}{2}} u_0, \dots, (t + r_m^2)^{\frac{1}{2}} u_m \right) \\ & \mathbb{E} \left[ h \left( \Phi^{t + \|x+z-y\|^2}, t, \|x+z-y\|^2, \{(u_0, r_0), \dots, (u_m, r_m)\}, \frac{x+z-y}{\|x+z-y\|} \right) \right] \\ & \mathbb{S}_L(du_0) \dots \mathbb{S}_L(du_m) \mathcal{H}^k(dy) \mathcal{H}^m(dz) \mathcal{H}^k(dx) \nu(d\vartheta) dt \mathbb{F}(dr_0) \dots \mathbb{F}(dr_m). \end{aligned}$$

Now substitute  $(u_0, \dots, u_m, z, x)$  by  $(\vartheta u_0, \dots, \vartheta u_m, \vartheta z, \vartheta x)$  and use that  $\Delta_m(\cdot)$  and  $\mathcal{H}^i(\cdot)$  are invariant under rotations. This yields

$$\begin{aligned} & \mathbb{E}_{M_k} [h(\Phi^{P_k}, P'_k, P''_k, \Psi_k, U_k)] \\ & = \frac{\lambda^{m+1}}{2(m+1)!} c_{dm}(m!)^{k+1} \int_0^\infty \dots \int_0^\infty \int_{-\min_i r_i^2}^\infty \prod_{i=0}^m (t + r_i^2)^{\frac{m-2}{2}} \int_{SO_d L^\perp} \int_L \int_L \int_L p(t + \|\vartheta(x+z) - y\|^2) \\ & \mathbb{I} \{y \in [0, 1]^d \cap \vartheta(x+z) + L^\perp\} \int_{S^{d-1} \cap L} \dots \int_{S^{d-1} \cap L} \Delta_m^{k+1} \left( (t + r_0^2)^{\frac{1}{2}} u_0, \dots, (t + r_m^2)^{\frac{1}{2}} u_m \right) \\ & \mathbb{E} \left[ h \left( \Phi^{t + \|\vartheta(x+z) - y\|^2}, t, \|\vartheta(x+z) - y\|^2, \{(\vartheta u_0, r_0), \dots, (\vartheta u_m, r_m)\}, \frac{\vartheta(x+z) - y}{\|\vartheta(x+z) - y\|} \right) \right] \\ & \mathbb{S}_L(du_0) \dots \mathbb{S}_L(du_m) \mathcal{H}^k(dy) \mathcal{H}^m(dz) \mathcal{H}^k(dx) \nu(d\vartheta) dt \mathbb{F}(dr_0) \dots \mathbb{F}(dr_m). \end{aligned}$$

By the change of variables  $y_0 := y - \vartheta(x+z) \in \vartheta L^\perp$  we get

$$\begin{aligned} & \mathbb{E}_{M_k} [h(\Phi^{P_k}, P'_k, P''_k, \Psi_k, U_k)] \\ & = \frac{\lambda^{m+1}}{2(m+1)!} c_{dm}(m!)^{k+1} \int_0^\infty \dots \int_0^\infty \int_{-\min_i r_i^2}^\infty \prod_{i=0}^m (t + r_i^2)^{\frac{m-2}{2}} \int_{SO_d L^\perp} \int_L \int_L \int_L p(t + \|y_0\|^2) \\ & \mathbb{I} \{y_0 + \vartheta(x+z) \in [0, 1]^d \cap \vartheta(x+z) + L^\perp\} \int_{S^{d-1} \cap L} \dots \int_{S^{d-1} \cap L} \Delta_m^{k+1} \left( (t + r_0^2)^{\frac{1}{2}} u_0, \dots, (t + r_m^2)^{\frac{1}{2}} u_m \right) \\ & \mathbb{E} \left[ h \left( \Phi^{t + \|y_0\|^2}, t, \|y_0\|^2, \{(\vartheta u_0, r_0), \dots, (\vartheta u_m, r_m)\}, \frac{-y_0}{\|y_0\|} \right) \right] \mathbb{S}_L(du_0) \dots \mathbb{S}_L(du_m) \mathcal{H}^k(dy_0) \\ & \mathcal{H}^m(dz) \mathcal{H}^k(dx) \nu(d\vartheta) dt \mathbb{F}(dr_0) \dots \mathbb{F}(dr_m). \end{aligned}$$

For fixed  $y_0 \in \vartheta L^\perp$  we have

$$\begin{aligned} & \int_{L^\perp} \int_L \mathbb{I} \{y_0 + \vartheta(x+z) \in [0, 1]^d \cap \vartheta(x+z) + L^\perp\} \mathcal{H}^m(dz) \mathcal{H}^k(dx) \\ & = \int_{L^\perp} \int_L \mathbb{I} \{y_0 + x + z \in [0, 1]^d\} \mathcal{H}^m(dz) \mathcal{H}^k(dx) = 1. \end{aligned}$$

Therefore, replacing  $-y_0$  by  $\vartheta y_0$  yields

$$\begin{aligned} & \mathbb{E}_{M_k} [h(\Phi^{P_k}, P'_k, P''_k, \Psi_k, U_k)] \\ &= \frac{\lambda^{m+1}}{2(m+1)!} c_{dm} (m!)^{k+1} \int_0^\infty \dots \int_0^\infty \int_{-\min_i r_i^2}^\infty \prod_{i=0}^m (t + r_i^2)^{\frac{m-2}{2}} \int_{L^\perp} p(t + \|y_0\|^2) \\ & \quad \int_{S^{d-1} \cap L} \dots \int_{S^{d-1} \cap L} \int_{SO_d} \mathbb{E} \left[ h \left( \Phi^{t+\|y_0\|^2}, t, \|y_0\|^2, \{(\vartheta u_0, r_0), \dots, (\vartheta u_m, r_m)\}, \frac{\vartheta y_0}{\|y_0\|} \right) \right] \nu(d\vartheta) \\ & \quad \Delta_m^{k+1} \left( (t + r_0^2)^{\frac{1}{2}} u_0, \dots, (t + r_m^2)^{\frac{1}{2}} u_m \right) \mathbb{S}_L(du_0) \dots \mathbb{S}_L(du_m) \mathcal{H}^k(dy_0) dt \mathbb{F}(dr_0) \dots \mathbb{F}(dr_m), \end{aligned}$$

which, introducing spherical coordinates  $y_0 = s^{\frac{1}{2}}u$  in  $L^\perp$ , reads

$$\begin{aligned} & \mathbb{E}_{M_k} [h(\Phi^{P_k}, P'_k, P''_k, \Psi_k, U_k)] \\ &= \frac{\lambda^{m+1}}{4(m+1)!} c_{dm} (m!)^{k+1} \int_0^\infty \dots \int_0^\infty \int_{-\min_i r_i^2}^\infty \prod_{i=0}^m (t + r_i^2)^{\frac{m-2}{2}} \int_0^\infty p(t + s) s^{\frac{k-2}{2}} \\ & \quad \int_{S^{d-1} \cap L} \dots \int_{S^{d-1} \cap L} \int_{SO_d} \int_{S^{d-1} \cap L^\perp} \mathbb{E} \left[ h \left( \Phi^{t+s}, t, s, \{(\vartheta u_0, r_0), \dots, (\vartheta u_m, r_m)\}, \vartheta u \right) \right] \mathbb{S}_{L^\perp}(du) \nu(d\vartheta) \\ & \quad \Delta_m^{k+1} \left( (t + r_0^2)^{\frac{1}{2}} u_0, \dots, (t + r_m^2)^{\frac{1}{2}} u_m \right) \mathbb{S}_L(du_0) \dots \mathbb{S}_L(du_m) ds dt \mathbb{F}(dr_0) \dots \mathbb{F}(dr_m) \end{aligned}$$

□

### Definition 3.2.5

For  $w_0, \dots, w_m \geq 0$  define

$$V_{m,k}(w_0, \dots, w_m) := (m!)^{k+1} \int_{S^{m-1}} \dots \int_{S^{m-1}} \Delta_m^{k+1}(w_0 u_0, \dots, w_m u_m) \mathbb{S}(du_0) \dots \mathbb{S}(du_m).$$

### Corollary 3.2.6 (Intensities of $M_k$ )

The intensities  $\mu_k, 0 < k < d$ , are given by the formula

$$\begin{aligned} \mu_k &= \frac{\lambda^{m+1}}{4(m+1)!} c_{dm} \sigma_k \int_0^\infty \dots \int_0^\infty \int_{-\min_i r_i^2}^\infty \prod_{i=0}^m (t + r_i^2)^{\frac{m-2}{2}} \int_0^\infty p(s+t) s^{\frac{k-2}{2}} ds \\ & \quad V_{m,k} \left( (t + r_0^2)^{\frac{1}{2}}, \dots, (t + r_m^2)^{\frac{1}{2}} \right) dt \mathbb{F}(dr_0) \dots \mathbb{F}(dr_m), \end{aligned} \tag{3.9}$$

where  $m = d - k$ . For  $k = 0$  we have

$$\begin{aligned} \mu_0 &= \frac{\lambda^{d+1}}{2(d+1)!} \int_0^\infty \dots \int_0^\infty \int_{-\min_i r_i^2}^\infty \prod_{i=0}^d (t + r_i^2)^{\frac{d-2}{2}} p(t) V_{d,0} \left( (t + r_0^2)^{\frac{1}{2}}, \dots, (t + r_d^2)^{\frac{1}{2}} \right) dt \\ & \quad \mathbb{F}(dr_0) \dots \mathbb{F}(dr_d). \end{aligned}$$

For  $k = d$  we have  $\mu_d = 1$ .

**Remarks 3.2.7**

- (i) The formulas for  $\mu_k$  cannot be evaluated further since we lack an explicit formula for  $V_{m,k}(w_0, \dots, w_m)$ . In general, it seems to be difficult to obtain such a formula. However, Miles (1971) has shown that

$$\begin{aligned} V_{m,k}(1, \dots, 1) &= (m!)^{k+1} \int_{S^{m-1}} \dots \int_{S^{m-1}} \Delta_m(u_0, \dots, u_m)^{k+1} \mathbb{S}(du_0) \dots \mathbb{S}(du_m) \\ &= 2^{m+1} \pi^{\frac{m(m+1)}{2}} \frac{\Gamma(\frac{1}{2}(m+1)(d+1) - m)}{\Gamma(\frac{md}{2}) \Gamma(\frac{d+1}{2})^{m+1}} \prod_{i=1}^m \frac{\Gamma(\frac{1}{2}(k+1+i))}{\Gamma(\frac{i}{2})}. \end{aligned} \quad (3.10)$$

For any  $r > 0$  we have

$$V_{m,k}(r, \dots, r) = r^{m(k+1)} V_{m,k}(1, \dots, 1).$$

- (ii) If the distribution of radii is degenerate we have the case of a Poisson Voronoi tessellation. This case allows for more explicit results (e.g., using (3.10)). The intensity formula (3.9) leads to the well-known values

$$\mu_k^V = \frac{\lambda^{\frac{m}{d}} 2^{m+1} \pi^{\frac{m}{2}} \Gamma(\frac{dm+k+1}{2}) \Gamma(\frac{d}{2} + 1)^{m+\frac{k}{d}} \Gamma(m + \frac{k}{d})}{d(m+1)! \Gamma(\frac{dm+k}{2}) \Gamma(\frac{d+1}{2})^m \Gamma(\frac{k+1}{2})}.$$

For the definition of the Palm probability measures  $\mathbb{Q}_k^0$  we have to make sure that the intensities  $\mu_k$  are finite. For that purpose, we first derive an estimate for the quantities  $\Delta_m(s_0 u_0, \dots, s_m u_m)^{k+1}$  and  $V_{m,k}(s_0, \dots, s_m)$ .

**Lemma 3.2.8**

Let  $0 \leq w_0 \leq w_1 \leq \dots \leq w_m$  and  $u_0, \dots, u_m \in S^{m-1}$ . Then the estimates

$$\Delta_m(w_0 u_0, \dots, w_m u_m)^{k+1} \leq \alpha_{m,k} \prod_{j=1}^m w_j^{k+1} \leq \alpha_{m,k} w_m^{m(k+1)},$$

and

$$V_{m,k}(w_0, \dots, w_m) \leq \beta_{m,k} \prod_{j=1}^m w_j^{k+1} \leq \beta_{m,k} w_m^{m(k+1)} \quad (3.11)$$

hold for suitable positive constants  $\alpha_{m,k}$  and  $\beta_{m,k}$ .

**Proof:**

For  $0 \leq w_0 \leq w_1 \leq \dots \leq w_m$  and  $u_0, \dots, u_m \in S^{m-1}$  we have

$$\begin{aligned} \Delta_m(w_0 u_0, \dots, w_m u_m) &= \Delta_m(0, w_1 u_1 - w_0 u_0, \dots, w_m u_m - w_0 u_0) \\ &= \prod_{j=1}^m w_j \Delta_m\left(0, u_1 - \frac{w_0}{w_1} u_0, \dots, u_m - \frac{w_0}{w_m} u_0\right). \end{aligned}$$

Since  $w_0 \leq w_i$  for  $i = 1, \dots, m$ , the simplex spanned by the points  $0$  and  $u_i - \frac{w_0}{w_i} u_0$ ,  $i = 1, \dots, m$ , is contained in an  $m$ -dimensional ball of radius 2. Further, the regular  $m$ -simplex

has volume  $\frac{\sqrt{m+1}}{m!\sqrt{2^m}}$  and maximizes the volume of simplices with vertices on  $S^{d-1}$  (Matoušek, 2002, p. 317). Hence,

$$\Delta_m(w_0u_0, \dots, w_mu_m) \leq \prod_{j=1}^m w_j \frac{\sqrt{2^m}\sqrt{m+1}}{m!}$$

and

$$\Delta_m(w_0u_0, \dots, w_mu_m)^{k+1} \leq \prod_{j=1}^m w_j^{k+1} \left( \frac{\sqrt{2^m}\sqrt{m+1}}{m!} \right)^{k+1}.$$

Therefore,

$$V_{m,k}(w_0, \dots, w_m) \leq \prod_{j=1}^m w_j^{k+1} \sigma_m^{m+1} \left( \sqrt{2^m}\sqrt{m+1} \right)^{k+1}.$$

□

### Theorem 3.2.9

The intensities  $\mu_k$  are finite for  $k = 0, \dots, d$ .

#### Proof:

Since  $\mu_d = 1$ , the case  $k = d$  is trivial. Hence, let  $k \in \{1, \dots, d-1\}$  and write  $m_k$  for the  $k$ -th moment of the radius distribution  $\mathbb{F}$ . Using assumption (3.3), we see that  $m_k$  is finite for any  $k \leq d$ . Further, we may assume that the radii are not almost surely equal to 0.

Assuming  $r_0 \leq r_i$  for  $i = 1, \dots, m$ , and using (3.11), we obtain

$$\prod_{i=0}^m (t + r_i^2)^{\frac{m-2}{2}} V_{m,k} \left( (t + r_0^2)^{\frac{1}{2}}, \dots, (t + r_m^2)^{\frac{1}{2}} \right) \leq \beta_{m,k} (t + r_0^2)^{\frac{m-2}{2}} \prod_{j=1}^m (t + r_j^2)^{\frac{d-1}{2}}.$$

Hence,

$$\begin{aligned} \mu_k &\leq C_{m,k} \int_0^\infty \dots \int_0^\infty \int_0^{\min_i r_i} \int_{-r_0^2}^\infty (t + r_0^2)^{\frac{m-2}{2}} \prod_{j=1}^m (t + r_j^2)^{\frac{d-1}{2}} \int_0^\infty p(s+t) s^{\frac{k-2}{2}} ds dt \mathbb{F}(dr_0) \\ &\quad \mathbb{F}(dr_1) \dots \mathbb{F}(dr_m), \end{aligned}$$

where  $C_{m,k} > 0$  is a suitable constant. Now, we split up the integral over  $s$  and  $t$  into three different cases. First, we consider  $s, t \geq 0$ . Then

$$\begin{aligned} &\int_0^\infty \dots \int_0^\infty \int_0^{\min_i r_i} \int_0^\infty (t + r_0^2)^{\frac{m-2}{2}} \prod_{j=1}^m (t + r_j^2)^{\frac{d-1}{2}} \int_0^\infty e^{-\lambda\omega_d \int_0^\infty (s+t+r^2)^{\frac{d}{2}} \mathbb{F}(dr)} s^{\frac{k-2}{2}} ds dt \mathbb{F}(dr_0) \\ &\quad \mathbb{F}(dr_1) \dots \mathbb{F}(dr_m) \\ &\leq \int_0^\infty \dots \int_0^\infty \int_0^\infty (t + r_0^2)^{\frac{m-2}{2}} \prod_{j=1}^m (t + r_j^2)^{\frac{d-1}{2}} \int_0^\infty e^{-\lambda\omega_d (s^{\frac{d}{2}} + t^{\frac{d}{2}} + m_d)} s^{\frac{k-2}{2}} ds dt \mathbb{F}(dr_0) \dots \mathbb{F}(dr_m) \\ &= e^{-\lambda\omega_d m_d} \int_0^\infty e^{-\lambda\omega_d s^{\frac{d}{2}}} s^{\frac{k-2}{2}} ds \int_0^\infty e^{-\lambda\omega_d t^{\frac{d}{2}}} \int_0^\infty (t + r^2)^{\frac{m-2}{2}} \mathbb{F}(dr) \left( \int_0^\infty (t + r^2)^{\frac{d-1}{2}} \mathbb{F}(dr) \right)^m dt. \end{aligned}$$

For any  $t > 0$  and  $n \geq -1$  we have

$$\int_0^\infty (t+r^2)^{\frac{n}{2}} \mathbb{F}(dr) \leq \begin{cases} t^{-\frac{1}{2}}, & \text{if } n = -1, \\ \int_0^\infty (t^{\frac{1}{2}}+r)^n \mathbb{F}(dr), & \text{if } n \geq 0. \end{cases}$$

The integral in the last line can be written as a polynomial in  $t^{\frac{1}{2}}$ , whose coefficients contain the moments  $m_i$ ,  $i = 1, \dots, n$ . Therefore,

$$\int_0^\infty (t+r^2)^{\frac{m-2}{2}} \mathbb{F}(dr) \left( \int_0^\infty (t+r^2)^{\frac{d-1}{2}} \mathbb{F}(dr) \right)^m \leq \sum_{i=-1}^{dm-2} a_i t^{\frac{i}{2}}$$

with suitable coefficients  $a_i \geq 0$ . Finally, with

$$\int_0^\infty t^{\alpha-1} e^{-\gamma t^\beta} dt = \frac{\Gamma(\frac{\alpha}{\beta})}{\beta \gamma^{\frac{\alpha}{\beta}}}, \quad \alpha, \beta, \gamma > 0, \quad (3.12)$$

we obtain

$$\begin{aligned} & e^{-\lambda \omega_d m d} \int_0^\infty e^{-\lambda \omega_d s^{\frac{d}{2}}} s^{\frac{k-2}{2}} ds \int_0^\infty e^{-\lambda \omega_d t^{\frac{d}{2}}} \int_0^\infty (t+r^2)^{\frac{m-2}{2}} \mathbb{F}(dr) \left( \int_0^\infty (t+r^2)^{\frac{d-1}{2}} \mathbb{F}(dr) \right)^m dt \\ & \leq e^{-\lambda \omega_d m d} \frac{2\Gamma(\frac{k}{d})}{d(\lambda \omega_d)^{\frac{k}{d}}} \sum_{i=-1}^{dm-2} a_i \frac{2\Gamma(\frac{i+2}{d})}{d(\lambda \omega_d)^{\frac{i+2}{d}}} < \infty \end{aligned}$$

As a second case, we consider the integral over the range  $-r_0^2 \leq t \leq 0$  and  $0 \leq s \leq -t$ , namely

$$\begin{aligned} & \int_0^\infty \dots \int_0^\infty \int_0^{\min_i r_i} \int_{-r_0^2}^0 (t+r_0^2)^{\frac{m-2}{2}} \prod_{j=1}^m (t+r_j^2)^{\frac{d-1}{2}} \int_0^{-t} e^{-\lambda \omega_d \int_0^{\infty} ([s+t+r^2]^+)^{\frac{d}{2}} \mathbb{F}(dr)} s^{\frac{k-2}{2}} ds dt \mathbb{F}(dr_0) \\ & \quad \mathbb{F}(dr_1) \dots \mathbb{F}(dr_m) \\ & = \int_0^\infty \dots \int_0^\infty \int_0^{\min_i r_i} \int_0^{r_0^2} t^{\frac{m-2}{2}} \prod_{j=1}^m (t+r_j^2-r_0^2)^{\frac{d-1}{2}} \int_0^{r_0^2-t} e^{-\lambda \omega_d \int_0^{\infty} ([s+t-r_0^2+r^2]^+)^{\frac{d}{2}} \mathbb{F}(dr)} s^{\frac{k-2}{2}} ds dt \mathbb{F}(dr_0) \\ & \quad \mathbb{F}(dr_1) \dots \mathbb{F}(dr_m) \\ & \leq \int_0^\infty \dots \int_0^\infty \int_0^{\min_i r_i} \int_0^{r_0^2} t^{\frac{m-2}{2}} \prod_{j=1}^m (t+r_j^2-r_0^2)^{\frac{d-1}{2}} dt \int_0^{r_0^2} s^{\frac{k-2}{2}} ds \mathbb{F}(dr_0) \mathbb{F}(dr_1) \dots \mathbb{F}(dr_m) \\ & \leq \int_0^\infty \dots \int_0^\infty \prod_{j=1}^m r_j^{d-1} \int_0^{\min_i r_i} \int_0^{r_0^2} t^{\frac{m-2}{2}} dt \int_0^{r_0^2} s^{\frac{k-2}{2}} ds \mathbb{F}(dr_0) \mathbb{F}(dr_1) \dots \mathbb{F}(dr_m). \end{aligned}$$

Disintegrating with respect to  $s$  and  $t$ , we get

$$\begin{aligned} & \int_0^\infty \dots \int_0^\infty \prod_{j=1}^m r_j^{d-1} \int_0^{\min_i r_i} \int_0^{r_0^2} t^{\frac{m-2}{2}} dt \int_0^{r_0^2} s^{\frac{k-2}{2}} ds \mathbb{F}(dr_0) \mathbb{F}(dr_1) \dots \mathbb{F}(dr_m) \\ & \leq \frac{4}{mk} \int_0^\infty \dots \int_0^\infty \prod_{j=1}^m r_j^{d-1} \int_0^\infty r_0^d \mathbb{F}(dr_0) \mathbb{F}(dr_1) \dots \mathbb{F}(dr_m) = \frac{4}{mk} m_{d-1}^m m_d. \end{aligned} \quad (3.13)$$

Finally, what remains to be investigated is the case  $-r_0^2 \leq t \leq 0$  and  $-t \leq s < \infty$ , namely

$$\begin{aligned} & \int_0^\infty \dots \int_0^\infty \int_0^{\min_i r_i} \int_{-r_0^2}^0 (t + r_0^2)^{\frac{m-2}{2}} \prod_{j=1}^m (t + r_j^2)^{\frac{d-1}{2}} \int_{-t}^\infty e^{-\lambda \omega_d \int_0^\infty (s+t+r^2)^{\frac{d}{2}} \mathbb{F}(dr)} s^{\frac{k-2}{2}} ds dt \mathbb{F}(dr_0) \\ & \mathbb{F}(dr_1) \dots \mathbb{F}(dr_m) \\ & = \int_0^\infty \dots \int_0^\infty \int_0^{\min_i r_i} \int_0^{r_0^2} t^{\frac{m-2}{2}} \prod_{j=1}^m (t + r_j^2 - r_0^2)^{\frac{d-1}{2}} \int_{r_0^2-t}^\infty e^{-\lambda \omega_d \int_0^\infty (s+t-r_0^2+r^2)^{\frac{d}{2}} \mathbb{F}(dr)} s^{\frac{k-2}{2}} ds dt \mathbb{F}(dr_0) \\ & \mathbb{F}(dr_1) \dots \mathbb{F}(dr_m) \\ & = \int_0^\infty \dots \int_0^\infty \int_0^{\min_i r_i} \int_0^{r_0^2} t^{\frac{m-2}{2}} \prod_{j=1}^m (t + r_j^2 - r_0^2)^{\frac{d-1}{2}} \int_0^\infty e^{-\lambda \omega_d \int_0^\infty (s+r^2)^{\frac{d}{2}} \mathbb{F}(dr)} (s + r_0^2 - t)^{\frac{k-2}{2}} ds dt \\ & \mathbb{F}(dr_0) \mathbb{F}(dr_1) \dots \mathbb{F}(dr_m) \\ & \leq e^{-\lambda \omega_d m_d} \int_0^\infty \dots \int_0^\infty \prod_{j=1}^m r_j^{d-1} \int_0^\infty \int_0^{r_0^2} t^{\frac{m-2}{2}} \int_0^\infty e^{-\lambda \omega_d s^{\frac{d}{2}}} (s + r_0^2 - t)^{\frac{k-2}{2}} ds dt \mathbb{F}(dr_0) \\ & \mathbb{F}(dr_1) \dots \mathbb{F}(dr_m) \end{aligned}$$

With the estimate

$$(s + r_0^2 - t)^{\frac{k-2}{2}} \leq \begin{cases} (s^{\frac{1}{2}} + r_0)^{k-2}, & \text{if } k \geq 2, \\ s^{-\frac{1}{2}}, & \text{if } k = 1, \end{cases}$$

and formula (3.12) we obtain a similar expression as in (3.13).

The case  $k = 0$  is handled similarly. □

### Corollary 3.2.10 (Marginal distributions)

Let  $\Phi$  be a stationary marked Poisson process with intensity  $\lambda > 0$  and mark distribution  $\mathbb{F}$  with property (3.3). Further, write  $m := d - k$  and let  $h$  be a non-negative measurable function defined on a suitable domain.

- (i) With respect to  $\mathbb{Q}_k^0$ , the conditional distribution of  $\Phi^{P_k}$  given  $P_k = t$  is the distribution of a marked Poisson process on  $\mathbb{R}^d \times \mathbb{R}^+$  whose intensity measure is the restriction of  $\lambda \mathcal{H}^d \otimes \mathbb{F}$  to the complement of the set  $\{(x, r) : \|x\|^2 - r^2 \leq t\}$ .

(ii) For  $1 \leq k \leq d-1$  we have

$$\begin{aligned} \mu_k \mathbb{E}_{M_k}^0 [h(P'_k, P''_k)] &= \frac{\lambda^{m+1}}{4(m+1)!} c_{dm} \sigma_k \int_0^\infty \cdots \int_0^\infty \int_{-\min_i r_i^2}^\infty \int_0^\infty p(t+s) h(t, s) \prod_{i=0}^m (t+r_i^2)^{\frac{m-2}{2}} \\ &\quad V_{m,k} \left( (t+r_0^2)^{\frac{1}{2}}, \dots, (t+r_m^2)^{\frac{1}{2}} \right) s^{\frac{k-2}{2}} ds dt \mathbb{F}(dr_0) \dots \mathbb{F}(dr_m). \end{aligned}$$

For  $k=0$  the formula reads

$$\begin{aligned} \mu_0 \mathbb{E}_{M_0}^0 [h(P_0)] &= \frac{\lambda^{d+1}}{2(d+1)!} \int_0^\infty \cdots \int_0^\infty \int_{-\min_i r_i^2}^\infty p(t) h(t) \prod_{i=0}^d (t+r_i^2)^{\frac{d-2}{2}} \\ &\quad V_{d,0} \left( (t+r_0^2)^{\frac{1}{2}}, \dots, (t+r_d^2)^{\frac{1}{2}} \right) dt \mathbb{F}(dr_0) \dots \mathbb{F}(dr_d). \end{aligned}$$

For the case  $k=d$  finally

$$\mathbb{E}_{M_d} [h(P_d)] = \frac{\lambda \sigma_d}{2} \int_0^\infty \int_{-r_0^2}^\infty p(t) (t+r_0^2)^{\frac{d-2}{2}} h(t) dt \mathbb{F}(dr_0),$$

in particular

$$\mathbb{P}(\text{pow}(0, \Phi) \leq z) = 1 - \mathbb{P}(\text{pow}(0, \Phi) > z) = 1 - p(z).$$

(iii) The random pair  $(\Psi_k, U_k)$ ,  $0 < k < d$ , has the distribution

$$\begin{aligned} &\mu_k \mathbb{E}_{M_k}^0 [h(\Psi_k, U_k)] \\ &= \frac{\lambda^{m+1}}{4(m+1)!} c_{dm} (m!)^{k+1} \int_0^\infty \cdots \int_0^\infty \int_{-\min_i r_i^2}^\infty \int_0^\infty p(t+s) \prod_{i=0}^m (t+r_i^2)^{\frac{m-2}{2}} s^{\frac{k-2}{2}} \\ &\quad \int_{S^{d-1} \cap L} \cdots \int_{S^{d-1} \cap L} \int_{S^{d-1} \cap L^\perp} \int_{SO_d} h(\{(\vartheta u_0, r_0), \dots, (\vartheta u_m, r_m)\}, \vartheta u) \nu(d\vartheta) \mathbb{S}_{L^\perp}(du) \\ &\quad \Delta_m^{k+1} \left( (t+r_0^2)^{\frac{1}{2}} u_0, \dots, (t+r_m^2)^{\frac{1}{2}} u_m \right) \mathbb{S}_L(du_0) \dots \mathbb{S}_L(du_m) ds dt \mathbb{F}(dr_0) \dots \mathbb{F}(dr_m), \end{aligned}$$

while

$$\begin{aligned} &\mu_0 \mathbb{E}_{M_0}^0 [h(\Psi_0)] \\ &= \frac{\lambda^{d+1}}{2(d+1)} \int_0^\infty \cdots \int_0^\infty \int_{-\min_i r_i^2}^\infty \prod_{i=0}^d (t+r_i^2)^{\frac{d-2}{2}} p(t) \int_{S^{d-1}} \cdots \int_{S^{d-1}} \mathbb{E}[h(\{(u_0, r_0), \dots, (u_d, r_d)\})] \\ &\quad \Delta_d \left( (t+r_0^2)^{\frac{1}{2}} u_0, \dots, (t+r_d^2)^{\frac{1}{2}} u_d \right) \mathbb{S}(du_0) \dots \mathbb{S}(du_d) dt \mathbb{F}(dr_0) \dots \mathbb{F}(dr_d). \end{aligned}$$

(iv) The random variable  $U_k$ ,  $0 < k < d$ , is independent of  $(\Phi^{P_k}, P'_k, P''_k)$ . The distribution of  $U_d$  is the uniform distribution on  $S^{d-1}$ .

**Remark 3.2.11**

For the Poisson Voronoi tessellation it is more convenient to consider the random variables  $R_k := \|X_{k,i}\|$ ,  $R'_k := \|X_{k,i} - Z_k\|$ , and  $R''_k := \|Z_k\|$  instead of  $P_k$ ,  $P'_k$ , and  $P''_k$ . Then  $\Phi^{R_k^2} = \Phi \cap \{x \in \Phi : \|x\| > R_k\}$  and the random variables  $(\Phi^{R_k^2}, R_k)$ ,  $R'_k/R_k$ , and  $(\Psi_k, U_k)$  are independent.  $R_k^d$  is Gamma distributed with shape parameter  $d - k + \frac{k}{d}$  and scale parameter  $\lambda\omega_d$ . The ratio  $\frac{R'_k}{R_k}$ ,  $k \in \{1, \dots, d-1\}$ , is Beta distributed with parameters  $\frac{d(d-k)}{2}$  and  $\frac{k}{2}$ . For details see Theorem 1.1 of Baumstark and Last (2007).

### 3.3 Further distributions

#### 3.3.1 Distributions of the typical Laguerre Delaunay simplex

In Section 1.6 we have introduced the notion of the typical cell of a random tessellation. In this section, we are going to study some distributions connected with the typical cell  $Z_0$  of the Laguerre Delaunay tessellation  $D(\Phi)$  associated with  $\Phi$ . For this purpose we define a centroid function  $c : \mathcal{C}' \rightarrow \mathbb{R}^d$  acting on the set  $\Delta^{(d)}$  of  $d$ -dimensional simplices in  $\mathbb{R}^d$ .

We denote the vertices of  $K \in \Delta^{(d)}$  numbered in lexicographic order by  $x_0(K), \dots, x_d(K)$  and assume that a weight  $r_i > 0$  is assigned to each vertex  $x_i(K)$ . Then the centroid function is defined by  $c(K) := z((x_0(K), r_0), \dots, (x_d(K), r_d))$  with  $z$  as in (3.5). For  $K \in \mathcal{C}' \setminus \Delta^{(d)}$  we set  $c(K) := 0$ . Then  $c$  is a continuous, hence measurable, function on  $\Delta^{(d)}$ .

With respect to the measure  $\mathbb{Q}_0^0$ , there is a vertex of  $L(\Phi)$  at the origin. The neighbors of this vertex are given by  $(X_{0,0}, R_{0,0}), \dots, (X_{0,d}, R_{0,d})$  as defined in (3.6). The simplex

$$Z_0 := \text{conv}\{X_{0,0}, \dots, X_{0,d}\}$$

is a cell of  $D(\Phi)$  with  $c(Z_0) = 0$ .  $Z_0$  is called the *typical cell* of  $D(\Phi)$ . Therefore, Theorem 3.2.4 can be interpreted as a distributional result for the typical Laguerre Delaunay simplex.

**Theorem 3.3.1**

Let  $h : \Delta^{(d)} \rightarrow [0, \infty)$  be a measurable function. Then

$$\begin{aligned} & \mu_0 \mathbb{E}_{M_0}^0 [h(Z_0)] \\ &= \frac{\lambda^{d+1}}{2(d+1)} \int_0^\infty \dots \int_0^\infty \int_{-\min_i r_i^2}^\infty p(t) \prod_{i=0}^d (t + r_i^2)^{\frac{d-2}{2}} \int_{S^{d-1}} \dots \int_{S^{d-1}} \Delta_d \left( (t + r_0^2)^{\frac{1}{2}} u_0, \dots, (t + r_d^2)^{\frac{1}{2}} u_d \right) \\ & \quad h \left( \text{conv} \left\{ (t + r_0^2)^{\frac{1}{2}} u_0, \dots, (t + r_d^2)^{\frac{1}{2}} u_d \right\} \right) \mathbb{S}(du_0) \dots \mathbb{S}(du_d) dt \mathbb{F}(dr_0) \dots \mathbb{F}(dr_d). \end{aligned}$$

**Corollary 3.3.2**

The  $k$ -th moment of the volume of the typical Laguerre Delaunay simplex is given by

$$\begin{aligned} \mathbb{E}_{M_0}^0 [ |Z_0|^k ] &= \frac{1}{\mu_0} \frac{\lambda^{d+1}}{2(d+1)!} \int_0^\infty \dots \int_0^\infty \int_{-\min_i r_i^2}^\infty p(t) \prod_{i=0}^d (t + r_i^2)^{\frac{d-2}{2}} V_{d,k} \left( (t + r_0^2)^{\frac{1}{2}}, \dots, (t + r_d^2)^{\frac{1}{2}} \right) \\ & \quad dt \mathbb{F}(dr_0) \dots \mathbb{F}(dr_d) \end{aligned}$$

**Remark 3.3.3**

Again, the lack of an explicit expression for  $V_{d,k}$  makes the derivation of more explicit distribution functions impossible. Only for the Poisson Voronoi case the formula for  $\mathbb{E}_{M_0}^0[h(Z_0)]$  is more tractable. Based on this formula Muche (1996a) obtained the probability density functions of the volume of the typical three-dimensional Poisson Delaunay cell, the area and the perimeter of one of its faces, the angle spanned in a face by two of its edges, and the length of an edge. He also gives formulas for higher moments of these characteristics as well as some results for the two-dimensional case.

**3.3.2 Distributions for typical faces**

We start with some definitions. For  $l, s, r_0 \geq 0$ ,  $t \in \mathbb{R}$ , and  $u, v \in S^{d-1}$  we set

$$\begin{aligned}\rho(l, t, r_0, u, v) &:= l^2 + t - 2l([t + r_0^2]^+)^{\frac{1}{2}} \langle u, v \rangle \text{ and} \\ \tau(l, t, s, u, v) &:= l^2 + t + s - 2ls^{\frac{1}{2}} \langle u, v \rangle.\end{aligned}$$

If  $\langle u, v \rangle = \cos(\theta)$  for  $\theta \in [0, \pi]$  we use the alternative definition

$$\begin{aligned}\rho(l, t, r_0, \theta) &:= l^2 + t - 2l([t + r_0^2]^+)^{\frac{1}{2}} \cos(\theta) \text{ and} \\ \tau(l, t, s, \theta) &:= l^2 + t + s - 2ls^{\frac{1}{2}} \cos(\theta).\end{aligned}$$

Let  $B_1 = b(x_1, r_1)$  and  $B_2 = b(x_2, r_2)$  be two balls in  $\mathbb{R}^d$  with centers  $x_1$  and  $x_2$  and radii  $r_1$  and  $r_2$ , respectively. The volume of their union only depends on the distance  $l = \|x_1 - x_2\|$  of the two centers and the radii  $r_1$  and  $r_2$ . It will be denoted by  $\kappa(l, r_1, r_2)$ . Further, we denote the  $d$ -volume of a truncated ball of radius  $r$  and intersection height  $w$  by  $\bar{\omega}_d(r, w)$ .

**Proposition 3.3.4**

For  $l, r_1, r_2 \geq 0$  we have

$$\kappa(l, r_1, r_2) = \begin{cases} \max(r_1, r_2)^d \omega_d, & \text{if } l < |r_1 - r_2|, \\ (r_1^d + r_2^d) \omega_d, & \text{if } l > r_1 + r_2, \\ \bar{\omega}_d(r_1, w(r_1, r_2, l)) + \bar{\omega}_d(r_2, w(r_2, r_1, l)), & \text{otherwise,} \end{cases} \quad (3.14)$$

with

$$w(r, s, l) = \frac{r^2 - s^2 + l^2}{2l}$$

and

$$\bar{\omega}_d(r, w) = r^d \omega_d \sum_{i=0}^{\lfloor d/2 \rfloor} a_i \left( \frac{w}{r} \right),$$

where  $\lfloor x \rfloor$  is the integer part of  $x$  and

$$\begin{aligned}a_0(w) &:= \begin{cases} 1 - \frac{\arccos(w)}{\pi}, & \text{if } d \text{ is even,} \\ \frac{1+w}{2}, & \text{if } d \text{ is odd,} \end{cases} \\ a_i(w) &:= \begin{cases} \frac{w}{2\sqrt{\pi}} \frac{\Gamma(i)}{\Gamma(i+\frac{1}{2})} (1-w^2)^{i-\frac{1}{2}}, & \text{if } d \text{ is even,} \\ \frac{w}{2\sqrt{\pi}} \frac{\Gamma(i+\frac{1}{2})}{\Gamma(i+1)} (1-w^2)^i, & \text{if } d \text{ is odd,} \end{cases} \quad i = 1, \dots, \lfloor d/2 \rfloor.\end{aligned}$$

**Proof:**

The formula for  $w(r, s, l)$  follows from elementary calculations. The remaining part is taken from Muche (2005, p. 291-292).  $\square$

Finally, we define

$$\xi(l, t_1, t_2) := \exp \left( -\lambda \int_0^\infty \kappa \left( l, ([t_1 + r^2]^+)^{\frac{1}{2}}, ([t_2 + r^2]^+)^{\frac{1}{2}} \right) \mathbb{F}(dr) \right) \quad (3.15)$$

for  $l \geq 0, t_1, t_2 \in \mathbb{R}$ .

**Theorem 3.3.5**

Let  $\Phi$  be a stationary marked Poisson process with intensity  $\lambda$  and mark distribution  $\mathbb{F}$  satisfying (3.3). Choose  $k \in \{1, \dots, d-1\}$  and write  $m := d - k$ . Further, let  $h$  be a non-negative measurable function defined on a suitable domain. Then the joint distribution of

$$(\mathcal{H}^k(F_k(0)), P'_k, P''_k, \Psi_k)$$

under  $\mathbb{Q}_k^0$  is given by

$$\begin{aligned} & \mu_k \mathbb{E}_{M_k}^0 [h(\mathcal{H}^k(F_k(0)), P'_k, P''_k, \Psi_k)] \\ &= \frac{\lambda^{m+1}}{4(m+1)!} c_{dm}(m!)^{k+1} \sigma_k \int_0^\infty \dots \int_0^\infty \int_{-\min_i r_i^2}^\infty \prod_{i=0}^m (t + r_i^2)^{\frac{m-2}{2}} \int_0^\infty p(t+s) s^{\frac{k-2}{2}} \\ & \int_{S^{d-1} \cap L} \dots \int_{S^{d-1} \cap L} \int_{SO_d} \mathbb{E} [h(A_{L^\perp}(t, s, \Phi^{s+t}), t, s, \{(\vartheta u_0, r_0), \dots, (\vartheta u_m, r_m)\})] \nu(d\vartheta) \\ & \Delta_m^{k+1} \left( (t + r_0^2)^{\frac{1}{2}} u_0, \dots, (t + r_m^2)^{\frac{1}{2}} u_m \right) \mathbb{S}_L(du_0) \dots \mathbb{S}_L(du_m) ds dt \mathbb{F}(dr_0) \dots \mathbb{F}(dr_m), \end{aligned} \quad (3.16)$$

with

$$A_{L^\perp}(t, s, \eta) := \int_0^\infty \int_{S^{d-1} \cap L^\perp} \mathbb{I} \{ \tau(l, t, s, v, u) \leq \text{pow}(lv, (x, r)), (x, r) \in \eta \} l^{k-1} \mathbb{S}_{L^\perp}(dv) dl$$

where  $L \in \mathcal{L}_m^d$  is a fixed subspace of  $\mathbb{R}^d$  and  $u \in S^{d-1} \cap L^\perp$ . For  $k = d$  we have

$$\begin{aligned} & \mathbb{E}_{M_d}^0 [h(\mathcal{H}^d(F_d(0)), P_d, U_d, R_{d,0})] \\ &= \frac{\lambda}{2} \int_0^\infty \int_{-r_0^2}^\infty (t + r_0^2)^{\frac{d-2}{2}} p(t) \int_{S^{d-1}} \mathbb{E} [h(A(t, r_0, u, \Phi^t), t, u, r_0)] \mathbb{S}(du) dt \mathbb{F}(dr_0), \end{aligned}$$

where

$$A(t, r_0, u, \eta) := \int_0^\infty \int_{S^{d-1}} \mathbb{I} \{ \rho(l, t, r_0, v, u) \leq \text{pow}(lv, (x, r)), (x, r) \in \eta \} l^{d-1} \mathbb{S}(dv) dl.$$

**Proof:**

We will only consider the case  $k < d$ . The case  $k = d$  is handled similarly. Since  $F_k(0) = F(S_{k,0}, \dots, S_{k,m}, \Phi)$ , the linear hull of  $F_k(0)$  is given by  $G_k(0) := G(S_{k,0}, \dots, S_{k,m})$ . For a unit vector  $v \in G_k(0) \cap S^{d-1}$  and  $l > 0$  we have

$$lv \in F_k(0) \iff \text{pow}(lv, S_{k,0}) \leq \text{pow}(lv, (x, r)), \quad (x, r) \in \Phi.$$

Now, since  $X_{k,0} = (P'_k + R_{k,0}^2)^{\frac{1}{2}}U_{k,0} + P''_k U_k$ , we have

$$\begin{aligned} \text{pow}(lv, S_{k,0}) &= \|X_{k,0} - lv\|^2 - R_{k,0}^2 \\ &= \|(P'_k + R_{k,0}^2)^{\frac{1}{2}}U_{k,0} + P''_k U_k - lv\|^2 - R_{k,0}^2 \\ &= P'_k + P''_k + l^2 - 2lP''_k \langle U_k, v \rangle \\ &= \tau(l, P'_k, P''_k, U_k, v). \end{aligned}$$

Then

$$\begin{aligned} \mathcal{H}^k(F_k(0)) &= \int_{0S^{d-1} \cap G_k(0)}^{\infty} \int \mathbb{I} \{ \tau(l, P'_k, P''_k, U_k, v) \leq \text{pow}(lv, (x, r)), (x, r) \in \Phi^{P_k} \} l^{k-1} \mathbb{S}_{G_k(0)}(dv) dl \\ &=: \tilde{A}_{G_k(0)}(P'_k, P''_k, U_k, \Phi^{P_k}). \end{aligned}$$

Now we choose a non-negative measurable function  $h$  defined on a suitable domain, apply Theorem 3.2.4 and get

$$\begin{aligned} &\mu_k \mathbb{E}_{M_k}^0 [h(\mathcal{H}^k(F_k(0)), P'_k, P''_k, \Psi_k)] \\ &= \frac{\lambda^{m+1}}{4(m+1)!} c_{dm}(m!)^{k+1} \int_0^{\infty} \dots \int_0^{\infty} \int_{-\min_i r_i^2}^{\infty} \prod_{i=0}^m (t + r_i^2)^{\frac{m-2}{2}} \int_0^{\infty} p(t+s) s^{\frac{k-2}{2}} \\ &\quad \int_{S^{d-1} \cap L} \dots \int_{S^{d-1} \cap L} \int_{S^{d-1} \cap L} \int_{SO_d} \mathbb{E} [h(\tilde{A}_{\vartheta L^\perp}(t, s, \vartheta u, \Phi^{s+t}), t, s, \{(\vartheta u_0, r_0), \dots, (\vartheta u_m, r_m)\})] \nu(d\vartheta) \\ &\quad \mathbb{S}_{L^\perp}(du) \Delta_m^{k+1} \left( (t + r_0^2)^{\frac{1}{2}} u_0, \dots, (t + r_m^2)^{\frac{1}{2}} u_m \right) \mathbb{S}_L(du_0) \dots \mathbb{S}_L(du_m) ds dt \mathbb{F}(dr_0) \dots \mathbb{F}(dr_m). \end{aligned}$$

For  $u, v \in L^\perp$  we have

$$\begin{aligned} &\mathbb{I} \{ \tau(l, t, s, \vartheta u, \vartheta v) \leq \text{pow}(l\vartheta v, (x, r)), (x, r) \in \Phi^{t+s} \} \\ &= \mathbb{I} \{ \tau(l, t, s, u, v) \leq \text{pow}(lv, (x, r)), (x, r) \in \vartheta^{-1} \Phi^{t+s} \}. \end{aligned} \tag{3.17}$$

Therefore, using the invariance under rotations of  $\Phi^{t+s}$  we have

$$\begin{aligned} &\mu_k \mathbb{E}_{M_k}^0 [h(\mathcal{H}^k(F_k(0)), P'_k, P''_k, \Psi_k)] \\ &= \frac{\lambda^{m+1}}{4(m+1)!} c_{dm}(m!)^{k+1} \int_0^{\infty} \dots \int_0^{\infty} \int_{-\min_i r_i^2}^{\infty} \prod_{i=0}^m (t + r_i^2)^{\frac{m-2}{2}} \int_0^{\infty} p(t+s) s^{\frac{k-2}{2}} \\ &\quad \int_{S^{d-1} \cap L} \dots \int_{S^{d-1} \cap L} \int_{S^{d-1} \cap L} \int_{SO_d} \mathbb{E} [h(\tilde{A}_{L^\perp}(t, s, u, \Phi^{s+t}), t, s, \{(\vartheta u_0, r_0), \dots, (\vartheta u_m, r_m)\})] \nu(d\vartheta) \\ &\quad \mathbb{S}_{L^\perp}(du) \Delta_m^{k+1} \left( (t + r_0^2)^{\frac{1}{2}} u_0, \dots, (t + r_m^2)^{\frac{1}{2}} u_m \right) \mathbb{S}_L(du_0) \dots \mathbb{S}_L(du_m) ds dt \mathbb{F}(dr_0) \dots \mathbb{F}(dr_m). \end{aligned}$$

An argument similar to (3.17) using the invariance under rotations of  $\mathbb{S}_{L^\perp}$  yields

$$\tilde{A}_{L^\perp}(t, s, \vartheta u, \Phi^{s+t}) = \tilde{A}_{L^\perp}(t, s, u, \vartheta^{-1}\Phi^{s+t})$$

for any rotation  $\vartheta$  of  $L^\perp$ . Now we can replace integration with respect to  $u$  by a fixed vector  $u \in S^{d-1} \cap L^\perp$  which yields

$$\begin{aligned} & \mu_k \mathbb{E}_{M_k}^0 [h(\mathcal{H}^k(F_k(0)), P'_k, P''_k, \Psi_k)] \\ &= \frac{\lambda^{m+1}}{4(m+1)!} c_{dm} (m!)^{k+1} \sigma_k \int_0^\infty \dots \int_0^\infty \int_{-\min_i r_i^2}^\infty \prod_{i=0}^m (t+r_i^2)^{\frac{m-2}{2}} \int_0^\infty p(t+s) s^{\frac{k-2}{2}} \\ & \quad \int_{S^{d-1} \cap L} \dots \int_{S^{d-1} \cap L} \int_{SO_d} \mathbb{E}[h(\tilde{A}_{L^\perp}(t, s, u, \Phi^{s+t}), t, s, \{(\vartheta u_0, r_0), \dots, (\vartheta u_m, r_m)\})] \nu(d\vartheta) \\ & \quad \Delta_m^{k+1} \left( (t+r_0^2)^{\frac{1}{2}} u_0, \dots, (t+r_m^2)^{\frac{1}{2}} u_m \right) \mathbb{S}_L(du_0) \dots \mathbb{S}_L(du_m) ds dt \mathbb{F}(dr_0) \dots \mathbb{F}(dr_m). \end{aligned}$$

□

### Corollary 3.3.6

The mean value  $\mathbb{E}_{M_k}^0 [\mathcal{H}^k(F_k(0))]$  for  $0 < k < d$  is given by

$$\begin{aligned} & \mu_k \mathbb{E}_{M_k}^0 [\mathcal{H}^k(F_k(0))] \\ &= \frac{\lambda^{m+1}}{4(m+1)!} c_{dm} \sigma_k \int_0^\infty \dots \int_0^\infty \int_{-\min_i r_i^2}^\infty \prod_{i=0}^m (t+r_i^2)^{\frac{m-2}{2}} V_{m,k} \left( (t+r_0^2)^{\frac{1}{2}}, \dots, (t+r_m^2)^{\frac{1}{2}} \right) \\ & \quad \int_0^\infty \int_0^\infty \int_{S^{d-1} \cap L^\perp} \xi(l, s+t, \tau(l, t, s, u, v)) l^{k-1} s^{\frac{k-2}{2}} \mathbb{S}(dv) dl ds dt \mathbb{F}(dr_0) \dots \mathbb{F}(dr_m), \end{aligned}$$

where  $u \in S^{d-1} \cap L^\perp$  is a fixed vector and the function  $\xi$  is defined in (3.15). For  $k = d$  we have

$$\begin{aligned} & \mathbb{E}_{M_d}^0 [\mathcal{H}^d(F_d(0))] \\ &= \frac{\lambda \sigma_d}{2} \int_0^\infty \int_{-r_0^2}^\infty \int_0^\infty \int_{S^{d-1}} (t+r_0^2)^{\frac{d-2}{2}} \xi(l, t, \rho(l, t, r_0, u, v)) l^{d-1} \mathbb{S}(dv) dl dt \mathbb{F}(dr_0). \end{aligned}$$

### Proof:

In this special case the expectation in the integrand of (3.16) is

$$\mathbb{E}[A_{L^\perp}(t, s, \Phi^{s+t})] = \int_{0S^{d-1} \cap L^\perp}^\infty \int \mathbb{P}(\tau(l, t, s, u, v) \leq \text{pow}(lv, (x, r)), (x, r) \in \Phi^{t+s}) l^{k-1} \mathbb{S}_{L^\perp}(dv) dl.$$

Since  $p(s+t) = \mathbb{P}(\|x\|^2 - r^2 \geq s+t, (x, r) \in \Phi)$  and by definition of  $\Phi^{s+t}$  we have

$$\begin{aligned} & p(s+t) \mathbb{P}(\tau(l, t, s, u, v) \leq \text{pow}(lv, (x, r)), (x, r) \in \Phi^{t+s}) \\ &= \mathbb{P}\left(x \notin b\left(0, ([s+t+r^2]^+)^{\frac{1}{2}}\right) \cup b\left(lv, ([\tau(l, t, s, u, v) + r^2]^+)^{\frac{1}{2}}\right), (x, r) \in \Phi\right) \\ &= \exp\left(-\lambda \int_0^\infty \kappa\left(l, ([s+t+r^2]^+)^{\frac{1}{2}}, ([\tau(l, t, s, u, v) + r^2]^+)^{\frac{1}{2}}\right) \mathbb{F}(dr)\right) \\ &= \xi(l, s+t, \tau(l, t, s, u, v)). \end{aligned}$$

Inserting this into (3.16) we obtain

$$\begin{aligned} & \mu_k \mathbb{E}_{M_k}^0 [\mathcal{H}^k(F_k(0))] \\ &= \frac{\lambda^{m+1}}{4(m+1)!} c_{dm} \sigma_k \int_0^\infty \cdots \int_0^\infty \int_{-\min_i r_i^2}^\infty \prod_{i=0}^m (t+r_i^2)^{\frac{m-2}{2}} V_{m,k}\left((t+r_0^2)^{\frac{1}{2}}, \dots, (t+r_m^2)^{\frac{1}{2}}\right) \\ & \quad \int_0^\infty \int_0^\infty \int_{S^{d-1} \cap L^\perp} \xi(l, s+t, \tau(l, t, s, u, v)) l^{k-1} s^{\frac{k-2}{2}} \mathbb{S}_{L^\perp}(dv) dl ds dt \mathbb{F}(dr_0) \cdots \mathbb{F}(dr_m). \end{aligned}$$

The proof for  $k = d$  works similarly. □

### Remark 3.3.7

For the case  $k = d$  Corollary 3.3.6 yields a formula for the mean volume  $\mathbb{E}_{M_d}[|F_d(0)|_d]$  of the (almost surely unique) Laguerre cell containing the origin. It is well known, that the cell  $F_d(0)$  is larger than the typical cell  $C_d(0)$  of the tessellation (Schneider and Weil, 2000, Satz 6.1.12). Since the volume of the typical cell is given by  $\frac{1}{\gamma_d}$ , we get the following inequalities for the cell intensity:

$$\frac{1}{\mathbb{E}_{M_d}[|F_d(0)|_d]} \leq \frac{1}{\mathbb{E}_{N_d}[|C_d(0)|_d]} = \gamma_d = p_0 \lambda \leq \lambda,$$

where  $p_0$  is the probability that the cell generated by the typical point of  $\Phi$  is not empty.

We will now have a closer look at the case  $k = 1$ . Let  $x$  be a point in the relative interior of an edge  $F \in \mathcal{S}_1(L(\Phi))$ . Then we define  $U_1^*(x, \Phi)$  to be the unique vector in the set  $\{-U_1(x, \Phi), U_1(x, \Phi)\}$  satisfying  $-U_1^*(x, \Phi) < U_1^*(x, \Phi)$  with respect to the lexicographic order on  $\mathbb{R}^d$ . Further, we write  $I_1(x, \Phi)$  for the  $\{-1, 1\}$ -valued random variable with

$$U_1(x, \Phi) = I_1(x, \Phi) U_1^*(x, \Phi).$$

Finally, let  $T'(x, \Phi)$  and  $T''(x, \Phi)$  be the two non-negative random variables such that

$$F_1(x, \Phi) = [x - T'(x, \Phi) U_1^*(x, \Phi), x + T''(x, \Phi) U_1^*(x, \Phi)].$$

Then  $T'(x, \Phi) + T''(x, \Phi) = \mathcal{H}^1(F_1(x, \Phi))$  is the length of  $F_1(x, \Phi)$ . For points  $x \in \mathbb{R}^d$  which are not contained in the relative interior of some edge the above random variables are set to some arbitrary values. With respect to  $\mathbb{Q}_1^0$  again the random variables  $T' := T'(0, \Phi)$ ,  $T'' := T''(0, \Phi)$ ,  $I_1 := I_1(0, \Phi)$ , and  $U_1^* := U_1^*(0, \Phi)$  are of special interest.

**Proposition 3.3.8**

Under the Palm probability measure  $\mathbb{Q}_1^0$  the random variables  $T'$  and  $T''$  are independent of  $\Psi_1$  and conditionally independent given  $(P'_1, P''_1, I_1)$ . We have

$$\mathbb{Q}_1^0(T' > t_1 | P'_1, P''_1, I_1) = e^{\lambda\omega_d \int_0^\infty ([P_1+r^2]^+)^{\frac{d}{2}} \mathbb{F}(dr)} \xi(t_1, P_1, P_1 + 2t_1 P_1''^{\frac{1}{2}} I_1 + t_1^2)$$

and

$$\mathbb{Q}_1^0(T'' > t_2 | P'_1, P''_1, I_1) = e^{\lambda\omega_d \int_0^\infty ([P_1+r^2]^+)^{\frac{d}{2}} \mathbb{F}(dr)} \xi(t_2, P_1, P_1 - 2t_2 P_1''^{\frac{1}{2}} I_1 + t_2^2).$$

**Proof:**

With respect to  $\mathbb{Q}_1^0$  the origin is almost surely contained in the interior of an edge  $F_1(0) \in \mathcal{S}_1(L(\Phi))$  whose neighbors  $(X_{1,0}, R_{1,0}), \dots, (X_{1,d-1}, R_{1,d-1})$  are in general position. Now

$$\begin{aligned} T' > t_1 &\iff \Phi^{P_1} \left( \left\{ (x, r) : \|x + t_1 U_1^*\|^2 - r^2 < \|X_{1,0} + t_1 U_1^*\|^2 - R_{1,0}^2 \right\} \right) = 0 \\ &\iff \|x + t_1 U_1^*\|^2 - r^2 \geq P_1 + 2t_1 P_1''^{\frac{1}{2}} I_1 + t_1^2, \quad (x, r) \in \Phi^{P_1}. \end{aligned}$$

Therefore,  $T'$  does not depend on  $\Psi_1$  and

$$\mathbb{Q}_1^0(T' > t_1 | P'_1, P''_1, I_1) = e^{\lambda\omega_d \int_0^\infty ([P_1+r^2]^+)^{\frac{d}{2}} \mathbb{F}(dr)} \xi(t_1, P_1, P_1 + 2t_1 P_1''^{\frac{1}{2}} I_1 + t_1^2).$$

A similar calculation yields the corresponding formula for  $\mathbb{Q}_1^0(T'' > t_2 | P'_1, P''_1, I_1)$ . Now for  $(x, r) \in \Phi^{P_1}$  we have  $\|x\|^2 - r^2 > P_1$ , hence

$$\begin{aligned} \|x + t_1 U_1^*\|^2 - r^2 &\leq P_1 + t_1^2 + 2t_1 P_1''^{\frac{1}{2}} I_1 \\ &\iff \|x\|^2 + 2t_1 \langle x, U_1^* \rangle - r^2 \leq P_1 + 2t_1 P_1''^{\frac{1}{2}} I_1 < \|x\|^2 - r^2 + 2t_1 P_1''^{\frac{1}{2}} I_1 \\ &\iff \langle x, U_1^* \rangle < P_1''^{\frac{1}{2}} I_1. \end{aligned}$$

Analogously we see

$$\|x - t_2 U_1^*\|^2 - r^2 \leq P_1 + t_2^2 - 2t_2 P_1''^{\frac{1}{2}} I_1 \iff \langle x, U_1^* \rangle > P_1''^{\frac{1}{2}} I_1.$$

Therefore,

$$\begin{aligned} b\left(-t_1 U_1^*, ([P_1 + t_1^2 + 2t_1 P_1''^{\frac{1}{2}} I_1 + r^2]^+)^{\frac{1}{2}}\right) &\cap b\left(t_2 U_1^*, ([P_1 + t_2^2 - 2t_2 P_1''^{\frac{1}{2}} I_1 + r^2]^+)^{\frac{1}{2}}\right) \\ &\cap \mathbb{R}^d \setminus b\left(0, ([P_1 + r^2]^+)^{\frac{1}{2}}\right) = \emptyset \end{aligned}$$

for each  $r \geq 0$ . By Corollary 3.2.10 (i) this implies that  $T'$  and  $T''$  are conditionally independent given  $(P'_1, P''_1, I_1)$ .  $\square$

So far we have only considered the face  $F_k(0)$ . In order to determine some results for the typical  $k$ -face  $C_k(0)$  of a Poisson Laguerre tessellation, we first have to define a suitable generalized centroid function. So let  $\mathcal{P}_k$  denote the system of all  $k$ -dimensional bounded polytopes in  $\mathbb{R}^d$ . Now define a measurable mapping  $c_k : \mathcal{P}_k \times \mathbf{N}(\mathbb{R}^+) \rightarrow \mathbb{R}^d$  as follows. If

$\varphi \in \mathbf{N}(\mathbb{R}^+)$  is in general position and  $F \in \mathcal{S}_k(L(\varphi))$  we choose  $y$  in the relative interior of  $F$  and set  $c_k(F, \varphi) := Z_k(y, \varphi)$  as defined in (3.6). In all other cases we define  $c_k(F, \varphi)$  as the center of the smallest ball circumscribing  $F \in \mathcal{P}_k$ . Then obviously

$$c_k(F, \varphi) = c_k(F - y, \varphi - y) + y, \quad \varphi \in \mathbf{N}(\mathbb{R}^+), F \in \mathcal{P}_k.$$

Using the fact that the factorial moment measures of a Poisson process are absolutely continuous with respect to Lebesgue measure, it can be shown that the centers of the faces  $F \in \mathcal{S}_k(L(\varphi))$  are almost surely mutually different. Due to (1.9) and the finiteness of  $\gamma_0$ , we see that

$$\varphi_k := \sum_{F \in \mathcal{S}_k(L(\varphi))} \delta_{c_k(F, \varphi)}$$

is  $\mathbb{P}$ -almost surely contained in  $\mathbf{N}_s$ . Now we define the stationary point process  $N_k$  of centers of the  $k$ -faces of  $L(\Phi)$  via  $N_k(\varphi) := \varphi_k$  if  $\varphi_k \in \mathbf{N}_s$  and  $N_k(\varphi) := 0$ , otherwise. Further, we define  $C_k(x, \varphi)$ ,  $F_k(x, \varphi)$ , and  $c_k(x, \varphi)$  for  $x \in \mathbb{R}^d$  and  $\varphi \in \mathbf{N}(\mathbb{R}^+)$  as in Section 1.6. We will often use the abbreviations  $F_k(x) := F_k(x, \Phi)$ ,  $C_k(x) := C_k(x, \Phi)$ , and  $c_k(x) := c_k(x, \Phi)$ .

For  $x \in N_k$  we define  $\rho_k(x, \Phi) := \text{pow}(x, \Phi)$ . Further, let  $V_{k,0}(x, \Phi), \dots, V_{k,m}(x, \Phi) \in S^{d-1}$  and  $R'_{k,0}(x, \Phi), \dots, R'_{k,m}(x, \Phi) \geq 0$  denote the (lexicographically ordered) unit vectors and the radii such that

$$\left( (\rho_k(x, \Phi) + R'_{k,i}(x, \Phi)^2)^{\frac{1}{2}} V_{k,i}(x, \Phi), R'_{k,i}(x, \Phi) \right), \quad i = 0, \dots, m,$$

are the neighbors of  $C_k(x)$ . For  $x \notin N_k$  these random variables can be defined arbitrarily. We write

$$\Xi_k(x, \Phi) := \left\{ (V_{k,0}(x, \Phi), R'_{k,0}(x, \Phi)), \dots, (V_{k,m}(x, \Phi), R'_{k,m}(x, \Phi)) \right\}.$$

As earlier, we will use the short-hand notations  $\rho_k := \rho_k(0, \Phi)$ ,  $V_{k,i} := V_{k,i}(0, \Phi)$ ,  $R'_{k,m} := R'_{k,m}(0, \Phi)$ , and  $\Xi_k := \Xi_k(0, \Phi)$ . With respect to the Palm measure  $\mathbb{P}_{N_d}$  we have  $0 \in N_d$ . Hence, this definition yields  $\rho_d = 0$ ,  $V_{d,0} = 0$ , and  $\Xi_d = (0, R_{d,0})$ .

### Theorem 3.3.9

Let  $h$  be a non-negative measurable function defined on a suitable domain. The distribution of  $(\mathcal{H}^k(C_k(0)), \rho_k, \Xi_k)$  with respect to  $\mathbb{P}_{N_k}^0$  for  $0 < k < d$  is given by

$$\begin{aligned} & \gamma_k \mathbb{E}_{N_k}^0 \left[ h(\mathcal{H}^k(C_k(0)), \rho_k, \Xi_k) \right] \\ &= \frac{\lambda^{m+1}}{4(m+1)!} c_{dm}(m!)^{k+1} \sigma_k \int_0^\infty \dots \int_0^\infty \int_{-\min_i r_i^2}^\infty \int_0^\infty \prod_{i=0}^m (t + r_i^2)^{\frac{m-2}{2}} p(t+s) s^{\frac{k-2}{2}} \\ & \int_{S^{d-1} \cap L} \dots \int_{S^{d-1} \cap L} \int_{SO_d} \mathbb{E} \left[ A_{L^\perp}(t, s, \Phi^{s+t})^{-1} h \left( A_{L^\perp}(t, s, \Phi^{s+t}), t, \{(\vartheta u_0, r_0), \dots, (\vartheta u_m, r_m)\} \right) \right] \\ & \Delta_m^{k+1} \left( (t + r_0^2)^{\frac{1}{2}} u_0, \dots, (t + r_m^2)^{\frac{1}{2}} u_m \right) \nu(d\vartheta) \mathbb{S}_L(du_0) \dots \mathbb{S}_L(du_m) ds dt \mathbb{F}(dr_0) \dots \mathbb{F}(dr_m), \end{aligned} \tag{3.18}$$

where  $m = d - k$  and  $A_{L^\perp}$  are defined as in Theorem 3.3.5. For  $k = d$  we have

$$\begin{aligned} & \gamma_d \mathbb{E}_{N_d}^0 [h(\mathcal{H}^d(C_d(0)), R_{d,0})] \\ &= \frac{\lambda}{2} \int_0^\infty \int_{-r_0^2}^\infty (t + r_0^2)^{\frac{d-2}{2}} p(t) \int_{S^{d-1}} \mathbb{E} [A(t, r_0, u, \Phi^t)^{-1} h(A(t, r_0, u, \Phi^t), r_0)] \mathbb{S}(du) dt \\ & \quad \mathbb{F}(dr_0) \end{aligned}$$

with the function  $A$  as defined in Theorem 3.3.5.

**Proof:**

Let  $0 < k < d$  and assume that  $0$  is contained in the relative interior of some  $k$ -face  $F_k(0)$  and that the points of  $\Phi$  are in general position. Then  $\Xi_k(0, \Phi - c_k(F_k(0))) = \Psi_k$ ,  $\rho_k(0, \Phi - c_k(F_k(0))) = P'_k$  and

$$C_k(0, \Phi - c_k(F_k(0))) = F_k(0) - c_k(F_k(0)).$$

By Corollary 1.6.4 and Theorem 3.3.5 we have for each non-negative measurable function  $h$

$$\begin{aligned} & \gamma_k \mathbb{E}_{N_k}^0 [h(\mathcal{H}^k(C_k(0)), \rho_k, \Xi_k)] \\ &= \mu_k \mathbb{E}_{M_k}^0 [\mathcal{H}^k(F_k(0))^{-1} h(\mathcal{H}^k(F_k(0)), P'_k, \Psi_k)] \\ &= \frac{\lambda^{m+1}}{4(m+1)!} c_{dm} (m!)^{k+1} \sigma_k \int_0^\infty \dots \int_0^\infty \int_{-\min_i r_i^2}^\infty \prod_{i=0}^m (t + r_i^2)^{\frac{m-2}{2}} \int_0^\infty p(t+s) s^{\frac{k-2}{2}} \\ & \quad \int_{S^{d-1} \cap L} \dots \int_{S^{d-1} \cap L} \int_{SO_d} \mathbb{E} [A_{L^\perp}(t, s, \Phi^{s+t})^{-1} h(A_{L^\perp}(t, s, \Phi^{s+t}), t, \{(\vartheta u_0, r_0), \dots, (\vartheta u_m, r_m)\})] \\ & \quad \Delta_m^{k+1} \left( (t + r_0^2)^{\frac{1}{2}} u_0, \dots, (t + r_m^2)^{\frac{1}{2}} u_m \right) \nu(d\vartheta) \mathbb{S}_L(du_0) \dots \mathbb{S}_L(du_m) ds dt \mathbb{F}(dr_0) \dots \mathbb{F}(dr_m). \end{aligned}$$

The formula for the case  $k = d$  is obtained similarly.  $\square$

**Remarks 3.3.10**

(i) For the Poisson Voronoi tessellation explicit formulas for the case  $k = 1$  exist. Formulas for the edge length distribution function have been derived by Muche (1996b) and Schlather (2000). Recently, a complete description of the distribution of the typical edge and its neighbors has been obtained by Baumstark and Last (2007). Their argumentation, however, does not carry over to the case of Laguerre tessellations.

(ii) Using formula (3.18) with  $h \equiv 1$  we get

$$\begin{aligned} \gamma_k &= \frac{\lambda^{m+1}}{4(m+1)!} c_{dm} \sigma_k \int_0^\infty \dots \int_0^\infty \int_{-\min_i r_i^2}^\infty \int_0^\infty \prod_{i=0}^m (t + r_i^2)^{\frac{m-2}{2}} p(t+s) s^{\frac{k-2}{2}} \\ & \quad V_{m,k} \left( (t + r_0^2)^{\frac{1}{2}}, \dots, (t + r_m^2)^{\frac{1}{2}} \right) \mathbb{E} [A_{L^\perp}(t, s, \Phi^{s+t})^{-1}] ds dt \mathbb{F}(dr_0) \dots \mathbb{F}(dr_m). \end{aligned}$$

The formula for the cell intensity  $\gamma_d$  reads

$$\gamma_d = \frac{\lambda \sigma_d}{2} \int_0^\infty \int_{-r_0^2}^\infty (t + r_0^2)^{\frac{d-2}{2}} p(t) \mathbb{E} [A(t, r_0, u, \Phi^t)^{-1}] dt \mathbb{F}(dr_0)$$

with fixed  $u \in S^{d-1}$ .

Unfortunately, the numerical evaluation of this formula for the cell intensity seems impossible.

### 3.3.3 Contact distributions

Given a random closed set  $X$  and a convex compact set  $B$  in  $\mathbb{R}^d$  containing the origin, the *contact distribution function*  $H_B$  is defined via

$$H_B(r) := \mathbb{P}(X \cap rB \neq \emptyset \mid 0 \notin X), \quad r \geq 0.$$

Important special cases are the *spherical contact distribution function*  $H_s$ , where  $B = b(0, 1)$  is the unit ball centered in the origin, and the *linear contact distribution function*  $H_{l(v)}$ , where  $B$  is a line segment of unit length in direction  $v \in S^{d-1}$ .

Contact and chord length distributions of the Poisson Voronoi tessellation have been studied by Muche and Stoyan (1992) while Heinrich (1998) investigated the Voronoi tessellation with respect to more general point processes. Here, we are going to consider Poisson Laguerre tessellations. In this case, the random closed set of interest is the union of cell boundaries of the tessellation. Since the origin is almost surely contained in the cell  $F_d(0)$ , we have  $H_B(r) = 1 - \mathbb{P}(rB \subset F_d(0))$  for every choice of  $B$ .

#### Lemma 3.3.11

For  $x \in \mathbb{R}^d$ ,  $v \in S^{d-1}$ , and  $s, r_1, r_2 \geq 0$  define the set

$$C(x, v, s, r_1, r_2) := b\left(sv, [||x - sv||^2 - r_1^2 + r_2^2]^{\frac{1}{2}}\right) \setminus b\left(0, ([||x||^2 - r_1^2 + r_2^2]^{\frac{1}{2}})\right).$$

Then

$$C(x, v, s_1, r_1, r_2) \subseteq C(x, v, s_2, r_1, r_2), \quad 0 \leq s_1 \leq s_2.$$

#### Proof:

Let  $x, y \in \mathbb{R}^d$ . Then

$$\begin{aligned} y \in C(x, v, s_1, r_1, r_2) \\ \iff ||y||^2 > ||x||^2 - r_1^2 + r_2^2 \text{ and } ||y - s_1 v||^2 \leq ||x - s_1 v||^2 - r_1^2 + r_2^2 \\ \iff ||y||^2 > ||x||^2 - r_1^2 + r_2^2 \text{ and } ||y||^2 - 2s_1 \langle y, v \rangle \leq ||x||^2 - 2s_1 \langle x, v \rangle - r_1^2 + r_2^2 \\ \iff ||x||^2 - r_1^2 + r_2^2 < ||x||^2 + 2s_1 \langle y - x, v \rangle - r_1^2 + r_2^2. \end{aligned}$$

Therefore,  $\langle y - x, v \rangle > 0$  and the implications above also hold for  $s_2 \geq s_1$ .  $\square$

**Lemma 3.3.12**

Let  $B$  be a compact set which is star-shaped with respect to the origin,  $r_1, r_2 \geq 0$ , and  $x \in \mathbb{R}^d$ . Then

$$\begin{aligned} & \bigcup_{y \in B} b\left(y, (\|x - y\|^2 - r_1^2 + r_2^2)^+\right)^{\frac{1}{2}} \\ &= \bigcup_{y \in \partial^* B} b\left(y, (\|x - y\|^2 - r_1^2 + r_2^2)^+\right)^{\frac{1}{2}} \cup b\left(0, (\|x\|^2 - r_1^2 + r_2^2)^+\right)^{\frac{1}{2}}, \end{aligned}$$

where  $\partial^* B := \{s_B(v)v : v \in S^{d-1}\}$  and  $s_B(v) := \sup\{s \geq 0 : sv \in B\}$ .

**Proof:**

Since  $B$  is star-shaped, we have  $B = \{sv : 0 \leq s \leq s_B(v), v \in S^{d-1}\}$ . Therefore, it is sufficient to show that

$$\bigcup_{0 \leq s \leq s_B(v)} C(x, v, s, r_1, r_2) = C(x, v, s_B(v), r_1, r_2),$$

which follows from Lemma 3.3.11. □

**Theorem 3.3.13**

Let  $\Phi$  be a stationary marked Poisson process on  $\mathbb{R}^d$  with intensity  $\lambda > 0$  and mark distribution  $\mathbb{F}$  with property (3.3). Further, let  $B \subset \mathbb{R}^d$  be a star-shaped set containing the origin. Then the contact distribution function  $H_B(r) = \mathbb{P}(\partial F_d(0) \cap rB \neq \emptyset)$  is given by

$$1 - H_B(r) = \frac{\lambda}{2} \int_0^\infty \int_{-r_0^2}^\infty (t + r_0^2)^{\frac{d-2}{2}} \int_{S^{d-1}} e^{-\lambda \int_0^\infty \nu(r, t, r_0, u, w) \mathbb{F}(dw)} \mathbb{S}(du) dt \mathbb{F}(dr_0), \quad r \geq 0,$$

where

$$\nu(r, t, r_0, u, w) = \left| \bigcup_{sv \in r\partial^* B} b\left(sv, ([\rho(s, t, r_0, u, v) + w^2]^+)^{\frac{1}{2}}\right) \cup b\left(0, ([t + w^2]^+)^{\frac{1}{2}}\right) \right|_d$$

with  $\partial^* B$  and  $s_B(v)$  as defined in Lemma 3.3.12.

**Proof:**

Assume  $F_d(0) = C((x_0, r_0), \varphi)$  for a unique point  $(x_0, r_0) \in \varphi$ . For every compact subset  $B$  of  $\mathbb{R}^d$  containing the origin we have

$$\begin{aligned} & B \subset F_d(0) \\ & \iff \|y - x_0\|^2 - r_0^2 \leq \|y - x\|^2 - r^2, \quad (x, r) \in \varphi, y \in B \\ & \iff x \notin b\left(y, (\|y - x_0\|^2 - r_0^2 + r^2)^+\right)^{\frac{1}{2}}, \quad (x, r) \in \varphi \setminus \{(x_0, r_0)\}, y \in B \\ & \iff (\varphi - \delta_{(x_0, r_0)}) \left( \left\{ (y, w) : y \in \bigcup_{x \in B} b\left(x, (\|x - x_0\|^2 - r_0^2 + w^2)^+\right)^{\frac{1}{2}} \right\} \right) = 0. \end{aligned}$$

Using the case  $k = d$  of Theorem 3.2.4 we get

$$\begin{aligned}
& \mathbb{E}[\mathbb{1}\{B \subset F_d(0)\}] \\
&= \frac{\lambda}{2} \int_0^\infty \int_{-r_0^2}^\infty (t + r_0^2)^{\frac{d-2}{2}} p(t) \\
& \quad \int_{S^{d-1}} \mathbb{P}\left(\Phi^t(\{(y, w) : y \in \bigcup_{x \in B} b(x, ([\|x - (t + r_0^2)^{\frac{1}{2}}u\|^2 - r_0^2 + w^2]^+)^{\frac{1}{2}})\}) = 0\right) \mathbb{S}(du) dt \mathbb{F}(dr_0) \\
&= \int_0^\infty \int_{-r_0^2}^\infty (t + r_0^2)^{\frac{d-2}{2}} p(t) \\
& \quad \int_{S^{d-1}} \mathbb{P}\left(\Phi^t(\{(y, w) : y \in \bigcup_{sv \in B} b(sv, ([\rho(s, t, r_0, u, v) + w^2]^+)^{\frac{1}{2}})\}) = 0\right) \mathbb{S}(du) dt \mathbb{F}(dr_0).
\end{aligned}$$

Since  $\Phi$  is a Poisson process we have

$$\begin{aligned}
& p(t) \mathbb{P}\left(\Phi^t(\{(y, w) : y \in \bigcup_{sv \in B} b(sv, ([\rho(s, t, r_0, u, v) + w^2]^+)^{\frac{1}{2}})\}) = 0\right) \\
&= \exp\left(-\lambda \int_0^\infty \left| \bigcup_{sv \in B} b(sv, ([\rho(s, t, r_0, u, v) + w^2]^+)^{\frac{1}{2}}) \cup b(0, ([t + w^2]^+)^{\frac{1}{2}}) \right|_d \mathbb{F}(dw)\right).
\end{aligned}$$

With Lemma 3.3.12 this yields

$$\begin{aligned}
1 - H_B(r) &= \mathbb{E}[(\mathbb{1}\{rB \subset F_d(0)\})] \\
&= \frac{\lambda}{2} \int_0^\infty \int_{-r_0^2}^\infty (t + r_0^2)^{\frac{d-2}{2}} \int_{S^{d-1}} e^{-\lambda \int_0^\infty \left| \bigcup_{sv \in r\partial^* B} b(sv, ([\rho(s, t, r_0, u, v) + w^2]^+)^{\frac{1}{2}}) \cup b(0, ([t + w^2]^+)^{\frac{1}{2}}) \right|_d \mathbb{F}(dw)} \mathbb{S}(du) dt \\
& \quad \mathbb{F}(dr_0).
\end{aligned}$$

□

### Corollary 3.3.14 (Linear contact distribution function)

The linear contact distribution function  $H_{l(v)}$  for  $v \in S^{d-1}$  is given by

$$1 - H_{l(v)}(r) = \frac{\lambda}{2} \int_0^\infty \int_{-r_0^2}^\infty (t + r_0^2)^{\frac{d-2}{2}} \int_{S^{d-1}} \xi(r, t, \rho(r, t, r_0, u, v)) \mathbb{S}(du) dt \mathbb{F}(dr_0), \quad r \geq 0,$$

where

$$\xi(l, t_1, t_2) = \exp\left(-\lambda \int_0^\infty \kappa\left(l, ([t_1 + r^2]^+)^{\frac{1}{2}}, ([t_2 + r^2]^+)^{\frac{1}{2}}\right) \mathbb{F}(dr)\right), \quad l \geq 0, t_1, t_2 \in \mathbb{R},$$

as defined in (3.15).

Since the Poisson Laguerre tessellation is isotropic, the values of  $H_{l(v)}(r)$  do not depend on the direction  $v$  of the line segment.

**Remark 3.3.15**

Denote the  $k$ -th moment of the linear contact distance in direction  $v$  by  $\overline{H}_{l(v)}^k$ . Then the mean volume of the cell  $F_d(0)$  can be written as

$$\mathbb{E}_{M_d}^0 [\mathcal{H}^d(F_d(0))] = \frac{1}{d} \int_{S^{d-1}} \overline{H}_{l(v)}^d \mathbb{S}(dv) = \frac{\sigma_d}{d} \overline{H}_{l(v_0)}^d,$$

where  $v_0 \in S^{d-1}$  is a fixed unit vector. For the  $k$ -th moment of any real-valued random variable  $X$  with distribution function  $F$  we have

$$\mathbb{E}[X^k] = k \int_0^\infty x^{k-1} (1 - F(x)) dx.$$

Inserting the formula for  $1 - H_{l(v)}(r)$  derived above, we obtain the formula for the mean volume of the cell  $F_d(0)$  given in Corollary 3.3.6.

**Corollary 3.3.16 (Spherical contact distribution function)**

The spherical contact distribution function  $H_s$  is given by

$$\begin{aligned} & 1 - H_s(r) \\ &= \frac{\lambda \sigma_d}{2} \int_0^\infty \int_{-r_0^2}^\infty (t + r_0^2)^{\frac{d-2}{2}} e^{-\lambda \int_0^\infty} \Big| \bigcup_{v \in S^{d-1}} b(rv, ([\rho(r, t, r_0, v, u) + w^2]^+)^{\frac{1}{2}}) \cup b(0, ([t + w^2]^+)^{\frac{1}{2}}) \Big|_d \mathbb{F}(dw) \\ & \quad dt \mathbb{F}(dr_0), \\ & r \geq 0, \end{aligned}$$

where  $u \in S^{d-1}$  is a fixed unit vector.

**Proof:**

Since

$$\left| \bigcup_{v \in S^{d-1}} b(rv, ([\rho(r, t, r_0, v, u) + w^2]^+)^{\frac{1}{2}}) \cup b(0, ([t + w^2]^+)^{\frac{1}{2}}) \right|_d$$

is independent of the unit vector  $u$ , we may replace integration with respect to this variable by a fixed choice of  $u$ .  $\square$

### 3.3.4 Chord length distribution

The chord length distribution function  $L_v$  of a random tessellation  $X$  in direction  $v$  is the distribution function of the length of the typical chord which is obtained by intersecting the system of cell boundaries with a line in direction  $v \in S^{d-1}$ . See Heinrich (1998) for a formal definition.

The relation between the chord length distribution function  $L_v$  and the linear contact distribution function  $H_{l(v)}$  is

$$H_{l(v)}(r) = \frac{1}{L_v} \int_0^r (1 - L_v(x)) dx, \quad r \geq 0, \quad (3.19)$$

where  $\bar{L}_v = \int_0^\infty (1 - L_v(x)) dx$  is the mean chord length in direction  $v$  (see Stoyan et al., 1995, Formula 6.2.5). Again, due to isotropy, the value of  $H_{l(v)}(r)$  does not depend on the choice of  $v$ . The mean chord length is equal to the mean length of a line segment in a one-dimensional section of the tessellation which can be calculated using the stereological relations given in Section 1.7. For the two- and three-dimensional case we have

$$\bar{L}_v = \begin{cases} \frac{\pi}{2L_A}, & \text{if } d = 2, \\ \frac{2}{S_V}, & \text{if } d = 3. \end{cases}$$

### Theorem 3.3.17

Let  $\Phi$  be a stationary marked Poisson process on  $\mathbb{R}^d$  with intensity  $\lambda > 0$  and mark distribution  $\mathbb{F}$  with property (3.3). The chord length distribution function  $L_v$  is given by

$$1 - L_v(r) = \bar{L}_v \frac{\lambda^2}{2} \int_0^\infty \int_{-r_0^2}^\infty (t + r_0^2)^{\frac{d-2}{2}} \int_{S^{d-1}} \int_0^\infty \kappa'(r, t, r_0, w, v, u) \mathbb{F}(dw) \xi(r, t, \rho(r, t, r_0, v, u)) \mathbb{S}(du) dt \mathbb{F}(dr_0), \quad r \geq 0,$$

where

$$\kappa'(r, t, r_0, w, u, v) = \frac{d}{dr} \kappa \left( r, ([t + w^2]^+)^{\frac{1}{2}}, ([\rho(r, t, r_0, u, v) + w^2]^+)^{\frac{1}{2}} \right).$$

### Proof:

The formula is an immediate consequence of (3.19) combined with Corollary 3.3.14.  $\square$

## 3.4 Limit theorems

We have already remarked that a Voronoi tessellation can be interpreted as a Laguerre tessellation with respect to a degenerate distribution of radii. Therefore, it seems natural to use the Poisson Voronoi tessellation as a benchmark and ask for relations between arbitrary Poisson Laguerre tessellations and this special case. One possibility is to consider Poisson Voronoi tessellations as limits of Poisson Laguerre tessellations when scaling the generating point process or changing the parameters of the mark distribution.

Let  $\Phi$  be a stationary marked Poisson process with intensity  $\lambda > 0$  and mark distribution  $\mathbb{F}$  with property (3.3). For  $c, v > 0$  define the point process

$$\Phi_{c,v} := \{(cx, vr) : (x, r) \in \Phi\}.$$

Then  $\Phi_{c,v}$  is a stationary marked Poisson process with intensity  $c^{-d}\lambda$  and  $\Phi_{1,1} = \Phi$ . Write  $L(c, v) := L(\Phi_{c,v})$  for the Laguerre tessellation generated by  $\Phi_{c,v}$  and  $M_k(c, v)$  for the corresponding random measures. The Palm measures, Palm probability measures, and intensities of  $M_k(c, v)$  are denoted by  $\mathbb{Q}_k(c, v)$ ,  $\mathbb{Q}_k^0(c, v)$ , and  $\mu_k(c, v)$ , respectively.

The following relations hold:

$$\begin{aligned}
L(1, v) &= vL(v^{-1}, 1), \\
\mathbb{Q}_k(1, v) &= v^{k-d}\mathbb{Q}_k(v^{-1}, 1), \quad k = 0, \dots, d, \\
\mu_k(1, v) &= v^{k-d}\mu_k(v^{-1}, 1), \quad k = 0, \dots, d, \\
L(c, 1) &= cL(1, c^{-1}), \\
\mathbb{Q}_k(c, 1) &= c^{k-d}\mathbb{Q}_k(1, c^{-1}), \quad k = 0, \dots, d, \text{ and} \\
\mu_k(c, 1) &= c^{k-d}\mu_k(1, c^{-1}), \quad k = 0, \dots, d.
\end{aligned} \tag{3.20}$$

For  $v = 0$  we obtain a Poisson process with degenerate mark distribution, which can be identified with an unmarked stationary Poisson process  $\Psi_\lambda$  of intensity  $\lambda$ . The corresponding random measures are denoted by  $M_{k,\lambda}^V$ , their Palm measures, Palm probability measures, and intensities are  $\mathbb{Q}_{k,\lambda}^V$ ,  $\mathbb{Q}_{k,\lambda}^{V,0}$ , and  $\mu_{k,\lambda}^V$ .

Now, we equip  $\mathbf{N}(\mathbb{R}^+)$  and  $\mathbf{N}$  with the topology of vague convergence of measures (Kallenberg, 1983, p. 169). In order to investigate weak convergence of the measures  $\mathbb{Q}_k(c, v)$ , we have to study convergence of  $\mathbb{E}_{M_k(c,v)}[f(\Phi_{c,v})]$ , where  $f : \mathbf{N}(\mathbb{R}^+) \rightarrow [0, \infty)$  is a continuous, bounded function.

#### Lemma 3.4.1

For  $k = 0, \dots, d$  define  $A_k \subset \mathbf{N}_s(\mathbb{R}^+)$  as the set of  $\varphi \in \mathbf{N}_s(\mathbb{R}^+)$  such that  $\varphi$  fulfills (R1) and that there is a real number  $t$  with

$$\begin{aligned}
\varphi(\{(x, r) \in \mathbb{R}^d \times \mathbb{R}^+ : \text{pow}(0, (x, r)) = t\}) &= d - k + 1 \text{ and} \\
\varphi(\{(x, r) \in \mathbb{R}^d \times \mathbb{R}^+ : \text{pow}(0, (x, r)) < t\}) &= 0.
\end{aligned} \tag{3.21}$$

Then the mapping

$$\varphi \mapsto (\varphi^t, t, s, \{(u_0, r_0), \dots, (u_{d-k}, r_{d-k})\}, u) \tag{3.22}$$

as suggested by (3.7) is continuous on  $A_k$ .

#### Proof:

Any  $\varphi \in A_k$  can be decomposed into the disjointed sets

$$\begin{aligned}
\varphi_t &:= \{(x, r) \in \varphi : \text{pow}(0, (x, r)) = t\} \text{ and} \\
\varphi^t &:= \{(x, r) \in \varphi : \text{pow}(0, (x, r)) > t\}.
\end{aligned}$$

For any set  $\tilde{\varphi}$  in  $\mathbb{R}^d \times \mathbb{R}^+$  which consists of exactly  $d - k + 1$  points and for which there is a number  $t \in \mathbb{R}$  such that  $\text{pow}(0, (x, r)) = t$  for all  $(x, r) \in \tilde{\varphi}$  we can define the mapping

$$\tilde{\varphi} \mapsto (t, s, \{(u_0, r_0), \dots, (u_{d-k}, r_{d-k})\}, u)$$

which is obviously continuous.

It remains to show the continuity of  $\varphi \mapsto (\varphi^t, \varphi_t)$ . So choose  $\varphi \in A_k$  and let  $t \in \mathbb{R}$  be defined by (3.21). By condition (R1),  $\min_{(x,r) \in \varphi \setminus \varphi_t} \text{pow}(0, (x, r)) =: p > t$  exists. Define the set

$$B_{t,p} := \left\{ (x, r) \in \mathbb{R}^d \times \mathbb{R}^+ : \text{pow}(0, (x, r)) \leq \frac{t+p}{2} \right\}.$$

Then  $\varphi \cap B_{t,p} = \varphi_t = \{(x_i, r_i) : i = 0, \dots, d - k + 1\}$ . Now choose a sequence  $\varphi_n \in A_k$ ,  $n \in \mathbb{N}$ , with  $\varphi_n \rightarrow \varphi$  vaguely. By Daley and Vere-Jones (1988, Proposition A2.6.II) there are sequences  $(x_i^n, r_i^n) \in \mathbb{R}^d \times \mathbb{R}^+$ ,  $n \in \mathbb{N}$ ,  $i = 0, \dots, d - k + 1$ , such that  $(x_i^n, r_i^n) \in \varphi_n$ ,  $(x_i^n, r_i^n) \rightarrow (x_i, r_i)$ , and  $\varphi_n \cap B_{t,p} = \{(x_i^n, r_i^n) : i = 0, \dots, d - k + 1\}$  for all large  $n$ . Now  $\varphi_n \in A_k$  implies  $\varphi_n \cap B_{t,p} = \varphi_{n,t}$ , hence  $\varphi_{n,t} \rightarrow \varphi_t$ , which shows the continuity of  $\varphi \mapsto (\varphi^t, \varphi_t)$ .  $\square$

### Theorem 3.4.2

Consider a stationary marked Poisson process  $\Phi$  on  $\mathbb{R}^d$  with intensity  $\lambda$  and mark distribution  $\mathbb{F}$  with property (3.3). Then  $\lim_{v \rightarrow 0} \mathbb{Q}_k^0(1, v) = \mathbb{Q}_{k,\lambda}^{V,0}$  weakly.

#### Proof:

We will show the weak convergence of the distribution of the tuple  $(\Phi_{1,v}^{P_k}, P'_k, P''_k, \Psi_k, U_k)$  under the probability measures  $\mathbb{Q}_k^0(1, v)$ , where  $P'_k, P''_k, \Psi_k$ , and  $U_k$  are defined with respect to  $\Phi_{1,v}^{P_k}$ . (The dependence on  $v$  is not captured by the notation.) In view of (3.8) it is then not difficult to derive the actual assertion of the theorem.

With respect to the measure  $\mathbb{Q}_k^0(1, v)$ ,  $\Phi_{1,v}$  is almost surely contained in  $A_k$ . By Kallenberg (1983, 15.4.1) it is therefore sufficient to show the convergence on the set  $A_k$ . As shown in Lemma 3.4.1, the decomposition (3.22) of  $\Phi_{1,v}$  is continuous on  $A_k$ .

Let  $h$  be a non-negative, continuous, bounded function defined on a suitable domain. We consider the case  $1 \leq k \leq d - 1$  first. For abbreviation, we write

$$\begin{aligned} & g(\Phi_{1,v}^{t+s}, t, s, w_0, \dots, w_m) \\ & := (m!)^{k+1} \int_{S^{d-1} \cap L} \dots \int_{S^{d-1} \cap L} \int_{S^{d-1} \cap L^\perp} \int_{SO_d} \mathbb{E}[h(\Phi_{1,v}^{t+s}, t, s, \{(\vartheta u_0, w_0), \dots, (\vartheta u_m, w_m)\}, \vartheta u)] \nu(d\vartheta) \\ & \quad \Delta_m^{k+1} \left( (t + w_0^2)^{\frac{1}{2}} u_0, \dots, (t + w_m^2)^{\frac{1}{2}} u_m \right) \mathbb{S}_{L^\perp}(du) \mathbb{S}_L(dw_0) \dots \mathbb{S}_L(dw_m). \end{aligned}$$

Then

$$\begin{aligned} & \mathbb{E}_{M_k(1,v)} \left[ h(\Phi_{1,v}^{P_k}, P'_k, P''_k, \Psi_k, U_k) \right] \\ & = \frac{\lambda^{m+1}}{4(m+1)!} c_{dm} (m!)^{k+1} \int_0^\infty \dots \int_0^\infty \int_{-\min_i v^2 r_i^2}^\infty \prod_{i=0}^m (t + v^2 r_i^2)^{\frac{m-2}{2}} \int_0^\infty e^{-\lambda \omega_d \int_0^\infty ([s+t+v^2 r^2]^+)^{\frac{d}{2}} \mathbb{F}(dr)} s^{\frac{k-2}{2}} \\ & \quad g(\Phi_{1,v}^{t+s}, t, s, vr_0, \dots, vr_m) ds dt \mathbb{F}(dr_0) \dots \mathbb{F}(dr_m). \end{aligned}$$

Here, we first consider the integral over  $t \in [0, \infty)$  and assume  $v \leq 1$ . Since  $s + t + v^2 r^2 \xrightarrow{v \rightarrow 0} s + t$  and  $s + t + v^2 r^2 \leq s + t + r^2$  for any  $s, t$ , and  $r > 0$ , Lebesgue's theorem of dominated convergence shows

$$e^{-\lambda \omega_d \int_0^\infty (s+t+v^2 r^2)^{\frac{d}{2}} \mathbb{F}(dr)} \xrightarrow{v \rightarrow 0} e^{-\lambda \omega_d (s+t)^{\frac{d}{2}}}, \quad s, t \geq 0.$$

Using the boundedness and continuity of  $h$ , Lemma 3.4.1, and again the dominated convergence theorem, we further get

$$\begin{aligned} & \mathbb{E}[h(\Phi_{1,v}^{t+s}, t, s, \{(\vartheta u_0, vr_0), \dots, (\vartheta u_m, vr_m)\}, \vartheta u)] \\ & \xrightarrow{v \rightarrow 0} \mathbb{E}[h(\Phi_{1,0}^{t+s}, t, s, \{(\vartheta u_0, 0), \dots, (\vartheta u_m, 0)\}, \vartheta u)]. \end{aligned}$$

Hence, the integrand in  $\mathbb{E}_{M_k(1,v)} \left[ h(\Phi_{1,v}^{P_k}, P'_k, P''_k, \Psi_k, U_k) \right]$  converges to

$$t^{\frac{dm-2}{2}} e^{-\lambda\omega_d(s+t)\frac{d}{2}} s^{\frac{k-2}{2}} \mathbb{E} \left[ h(\Phi_{1,0}^{t+s}, t, s, \{(\vartheta u_0, 0), \dots, (\vartheta u_m, 0)\}, \vartheta u) \right] \Delta_m^{k+1}(u_0, \dots, u_m)$$

for any  $s, t \geq 0$ ,  $u_0, \dots, u_m \in S^{d-1} \cap L$ ,  $u \in S^{d-1} \cap L^\perp$ , and  $\vartheta \in SO_d$ . Using (3.11) and assuming  $r_0 \leq r_i$  for  $i = 1, \dots, d$ , we see

$$\begin{aligned} & \prod_{i=0}^m (t + v^2 r_i^2)^{\frac{m-2}{2}} g(\Phi_{1,v}^{t+s}, t, s, vr_0, \dots, vr_m) \\ & \leq \prod_{i=1}^m (t + r_i^2)^{\frac{d-1}{2}} (t + r_0^2)^{\frac{m-2}{2}} M_h \sigma_k \beta_{m,k}, \end{aligned}$$

where  $M_h$  is an upper bound for  $h$ . Hence,

$$\begin{aligned} & \prod_{i=0}^m (t + v^2 r_i^2)^{\frac{m-2}{2}} e^{-\lambda\omega_d \int_0^\infty (s+t+v^2 r^2)\frac{d}{2} \mathbb{F}(dr)} s^{\frac{k-2}{2}} g(\Phi_{1,v}^{t+s}, t, s, vr_0, \dots, vr_m) \\ & \leq M_h \sigma_k \beta_{m,k} \prod_{i=1}^m (t + r_i^2)^{\frac{d-1}{2}} (t + r_0^2)^{\frac{m-2}{2}} e^{-\lambda\omega_d (s\frac{d}{2} + t\frac{d}{2})} s^{\frac{k-2}{2}}, \end{aligned}$$

which was shown to be integrable in Theorem 3.2.9. Therefore, the dominated convergence theorem yields

$$\begin{aligned} & \frac{\lambda^{m+1}}{4(m+1)!} c_{dm}(m!)^{k+1} \int_0^\infty \dots \int_0^\infty \prod_{i=0}^m (t + v^2 r_i^2)^{\frac{m-2}{2}} \int_0^\infty e^{-\lambda\omega_d \int_0^\infty (s+t+v^2 r^2)\frac{d}{2} \mathbb{F}(dr)} s^{\frac{k-2}{2}} \\ & g(\Phi_{1,v}^{t+s}, t, s, vr_0, \dots, vr_m) ds dt \mathbb{F}(dr_0) \dots \mathbb{F}(dr_m) \\ & \xrightarrow{v \rightarrow 0} \frac{\lambda^{m+1}}{4(m+1)!} c_{dm}(m!)^{k+1} \int_0^\infty t^{\frac{m(m-1)-2}{2}} \int_0^\infty e^{-\lambda\omega_d (s+t)\frac{d}{2}} s^{\frac{k-2}{2}} g(\Phi_{1,0}^{t+s}, t, s, 0, \dots, 0) ds dt. \end{aligned}$$

Identifying  $\Phi_{1,0}^{t+s}$  with  $\Psi_\lambda^{t+s}$  and using  $\Delta_m(tu_0, \dots, tu_m) = t^m \Delta_m(u_0, \dots, u_m)$  this yields the expectation with respect to  $\mathbb{Q}_{k,\lambda}^V$ . It remains to show the convergence to 0 of the integral over  $t \in [-v^2 \min_i r_i^2, 0]$ . With a suitable constant  $C > 0$ , we have

$$\begin{aligned} & \int_0^\infty \dots \int_0^\infty \int_{-\min_i v^2 r_i^2}^0 \prod_{i=0}^m (t + v^2 r_i^2)^{\frac{m-2}{2}} \int_0^\infty e^{-\lambda\omega_d \int_0^\infty ([s+t+v^2 r^2]^+)\frac{d}{2} \mathbb{F}(dr)} s^{\frac{k-2}{2}} \\ & g(\Phi_{1,v}^{t+s}, t, s, vr_0, \dots, vr_m) ds dt \mathbb{F}(dr_0) \dots \mathbb{F}(dr_m) \\ & \leq \beta_{m,k} M_h \sigma_k C \int_0^\infty \dots \int_0^\infty \int_0^{\min_i r_i} \int_{-v^2 r_0^2}^0 \prod_{i=1}^m (t + v^2 r_i^2)^{\frac{d-1}{2}} (t + v^2 r_0^2)^{\frac{m-2}{2}} \int_0^\infty e^{-\lambda\omega_d \int_0^\infty ([s+t+v^2 r^2]^+)\frac{d}{2} \mathbb{F}(dr)} \\ & s^{\frac{k-2}{2}} ds dt \mathbb{F}(dr_0) \mathbb{F}(dr_1) \dots \mathbb{F}(dr_m) \end{aligned}$$

$$\begin{aligned}
&= \beta_{m,k} M_h \sigma_k C \int_0^\infty \dots \int_0^\infty \int_0^{\min_i r_i} \int_0^{v^2 r_0^2} \prod_{i=1}^m (t + v^2(r_i^2 - r_0^2))^{\frac{d-1}{2}} t^{\frac{m-2}{2}} \int_0^\infty e^{-\lambda \omega_d \int_0^\infty ([s+t+v^2(r^2-r_0^2)]^+)^{\frac{d}{2}}} \mathbb{F}(dr) \\
&\quad s^{\frac{k-2}{2}} ds dt \mathbb{F}(dr_0) \mathbb{F}(dr_1) \dots \mathbb{F}(dr_m) \\
&\stackrel{v \leq 1}{\leq} \beta_{m,k} M_h \sigma_k C \int_0^\infty \dots \int_0^\infty \int_0^{\min_i r_i} \int_0^{v^2 r_0^2} \prod_{i=1}^m (t + r_i^2)^{\frac{d-1}{2}} t^{\frac{m-2}{2}} \int_0^\infty e^{-\lambda \omega_d (s+t)^{\frac{d}{2}}} \mathbf{1}_{\{s+t > r_0^2\}} s^{\frac{k-2}{2}} ds dt \mathbb{F}(dr_0) \\
&\quad \mathbb{F}(dr_1) \dots \mathbb{F}(dr_m) \\
&\xrightarrow{v \rightarrow 0} 0
\end{aligned}$$

With the special choice of  $h \equiv 1$ , the above calculations show the convergence of the intensities  $\mu_k(1, v)$  to  $\mu_{k,\lambda}^V$ . This implies weak convergence of the corresponding Palm probability measures and shows the assertion for the cases  $k = 1, \dots, d-1$ . The cases  $k = 0$  and  $k = d$  are slightly easier than the ones presented above, since there is no integration with respect to  $s$ . Otherwise, they are handled similarly.  $\square$

Now, we are going to study the case of radii tending to infinity. In order to guarantee the existence of the limits and since the radii do not play a role for Voronoi tessellations, they will be ignored in the computations below. For instance, we will consider the random variable  $\tilde{\Psi}_k := (U_{k,0}, \dots, U_{k,m})$  rather than  $\Psi_k$ . Further, we will use the following observation: If the mark distribution of a point process  $\Phi$  is degenerate, any continuous, bounded function  $h$  taking the arguments  $(\Phi^{P_k}, P'_k, P''_k, \tilde{\Psi}_k, U_k)$  can be transformed into a continuous, bounded function  $\bar{h}$  taking the arguments  $(\Phi^{R_k^2}(\cdot \times \mathbb{R}^+), R'_k, R''_k, \tilde{\Psi}_k, U_k)$  via

$$\begin{aligned}
h(\Phi^{P_k}, P'_k, P''_k, \tilde{\Psi}_k, U_k) &= \bar{h}(\Phi^{P_k + R_{k,0}^2}(\cdot \times \mathbb{R}^+), (P'_k + R_{k,0}^2)^{\frac{1}{2}}, P''_k^{\frac{1}{2}}, \tilde{\Psi}_k, U_k) \\
&= \bar{h}(\Phi^{R_k^2}(\cdot \times \mathbb{R}^+), R'_k, R''_k, \tilde{\Psi}_k, U_k).
\end{aligned} \tag{3.23}$$

### Theorem 3.4.3

Choose  $0 \leq s_0 < s_1$  and  $0 \leq p \leq 1$ . Consider a stationary marked Poisson process  $\Phi$  on  $\mathbb{R}^d$  with intensity  $\lambda$  and a mark distribution defined as a mixture  $\mathbb{F} = (1-p)\mathbb{F}_1 + p\delta_{s_1}$ , where  $\mathbb{F}_1$  is a distribution with support contained in  $[0, s_0]$ . For  $v \rightarrow \infty$  the Laguerre tessellation  $L(1, v)$  converges to the Poisson Voronoi tessellation of intensity  $p\lambda$  in the sense that

$$\mathbb{E}_{M_k(1,v)}^0 [h(P'_k, P''_k, \tilde{\Psi}_k, U_k)] \xrightarrow{v \rightarrow \infty} \mathbb{E}_{M_{k,p\lambda}^V}^0 [\bar{h}(R'_k, R''_k, \tilde{\Psi}_k, U_k)]$$

for any non-negative, bounded, and continuous function  $h$ .

#### Proof:

Let  $h$  be a non-negative, continuous, bounded function defined on a suitable domain. We consider the case  $1 \leq k \leq d-1$  and define  $N_{k,0} := \sum_{i=0}^m \mathbb{1}_{[0,s_0]}(R_{k,i})$  and  $N_{k,1} := \sum_{i=0}^m \mathbb{1}_{\{s_1\}}(R_{k,i})$ . Then  $\mathbb{E}_{M_k(1,v)} [h(P'_k, P''_k, \tilde{\Psi}_k, U_k)]$  is a sum of integrals which, given  $N_{k,0} = n_0$  and  $N_{k,1} = n_1$ , read

$$\begin{aligned}
&c_{n_0, n_1} \int_0^{s_0} \dots \int_0^{s_0} \int_{-v^2 s_0^2}^\infty \prod_{i=0}^{n_0-1} ([t + v^2 r_i^2]^+)^{\frac{(m-2)}{2}} (t + v^2 s_1^2)^{\frac{n_1(m-2)}{2}} \int_0^\infty p(t+s) s^{\frac{k-2}{2}} \\
&\quad g(t, s, vr_0, \dots, vr_{n_0-1}, vs_1, \dots, vs_1) ds dt \mathbb{F}(dr_0) \dots \mathbb{F}(dr_{n_0-1})
\end{aligned} \tag{3.24}$$

with suitable constants  $c_{n_0, n_1} > 0$  and

$$\begin{aligned} g(t, s, w_0, \dots, w_m) \\ := (m!)^{k+1} \int_{S^{d-1} \cap L} \dots \int_{S^{d-1} \cap L} \int_{S^{d-1} \cap L^\perp} \int_{SO_d} \mathbb{E}[h(t, s, \{\vartheta u_0, \dots, \vartheta u_m\}, \vartheta u)] \nu(d\vartheta) \mathbb{S}_{L^\perp}(du) \\ \Delta_m^{k+1} \left( ([t + w_0^2]^+)^{\frac{1}{2}} u_0, \dots, ([t + w_m^2]^+)^{\frac{1}{2}} u_m \right) \mathbb{S}_L(du_0) \dots \mathbb{S}_L(du_m), \end{aligned}$$

plus the expression

$$p^{m+1} \frac{\lambda^{m+1}}{4(m+1)!} c_{dm} \int_{-v^2 s_1^2}^{-v^2 s_0^2} (t + v^2 s_1^2)^{\frac{m(m-1)-2}{2}} \int_0^\infty p(t+s) s^{\frac{k-2}{2}} g(t, s, v s_1, \dots, v s_1) ds dt. \quad (3.25)$$

First, we consider the integrals (3.24). Using (3.11), we obtain the estimate

$$\begin{aligned} \prod_{i=0}^{n_0-1} ([t + v^2 r_i^2]^+)^{\frac{(m-2)}{2}} (t + v^2 s_1^2)^{\frac{n_1(m-2)}{2}} g(t, s, v r_0, \dots, v r_{n_0-1}, v s_1, \dots, v s_1) \\ \leq (t + v^2 s_1^2)^{\frac{dm-2}{2}} M_h \sigma_k \beta_{m,k}, \end{aligned}$$

where  $M_h$  is an upper bound for  $h$ . Hence, we have

$$\begin{aligned} c_{n_0, n_1} \int_0^{s_0} \dots \int_0^{s_0} \int_{-v^2 s_0^2}^\infty \prod_{i=0}^{n_0-1} ([t + v^2 r_i^2]^+)^{\frac{(m-2)}{2}} (t + v^2 s_1^2)^{\frac{n_1(m-2)}{2}} \int_0^\infty p(t+s) s^{\frac{k-2}{2}} \\ g(t, s, v r_0, \dots, v r_{n_0-1}, v s_1, \dots, v s_1) ds dt \mathbb{F}(dr_0) \dots \mathbb{F}(dr_{n_0-1}) \\ \leq c_{n_0, n_1} M_h \sigma_k \beta_{m,k} \int_{-v^2 s_0^2}^\infty (t + v^2 s_1^2)^{\frac{dm-2}{2}} \int_0^\infty p(t+s) s^{\frac{k-2}{2}} ds dt. \end{aligned}$$

Since

$$\int_0^\infty t^{\alpha-1} e^{-\gamma t^\beta} dt = \frac{\Gamma(\frac{\alpha}{\beta})}{\beta \gamma^{\frac{\alpha}{\beta}}}, \quad \alpha, \beta, \gamma > 0, \quad (3.26)$$

we have

$$\begin{aligned} \int_{-v^2 s_0^2}^\infty (t + v^2 s_1^2)^{\frac{dm-2}{2}} \int_0^\infty p(t+s) s^{\frac{k-2}{2}} ds dt \\ = \int_0^\infty (t + v^2 (s_1^2 - s_0^2))^{\frac{dm-2}{2}} \int_0^\infty e^{-\lambda \omega_d (p(s+t+v^2(s_1^2-s_0^2))^{\frac{d}{2}} + (1-p) \int_0^{s_0} ([s+t+v^2(r^2-s_0^2)]^+)^{\frac{d}{2}} \mathbb{F}(dr))} s^{\frac{k-2}{2}} ds dt \\ \leq e^{-\lambda \omega_d p v^d (s_1^2 - s_0^2)^{\frac{d}{2}}} \int_0^\infty s^{\frac{k-2}{2}} e^{-\lambda \omega_d p s^{\frac{d}{2}}} ds \int_0^\infty (t + v^2 (s_1^2 - s_0^2))^{\frac{dm-2}{2}} e^{-\lambda \omega_d p t^{\frac{d}{2}}} dt \end{aligned} \quad (3.27)$$

$$\begin{aligned}
&= e^{-\lambda\omega_d p v^d (s_1^2 - s_0^2)^{\frac{d}{2}}} \frac{2\Gamma\left(\frac{k}{d}\right)}{d(p\lambda\omega_d)^{\frac{k}{d}}} \int_0^\infty (t + v^2(s_1^2 - s_0^2))^{\frac{dm-2}{2}} e^{-\lambda\omega_d p t^{\frac{d}{2}}} dt \\
&\leq e^{-\lambda\omega_d p v^d (s_1^2 - s_0^2)^{\frac{d}{2}}} \frac{2\Gamma\left(\frac{k}{d}\right)}{d(p\lambda\omega_d)^{\frac{k}{d}}} \int_0^\infty (t^{\frac{1}{2}} + v(s_1^2 - s_0^2)^{\frac{1}{2}})^{dm-2} e^{-\lambda\omega_d p t^{\frac{d}{2}}} dt
\end{aligned}$$

Using the binomial theorem, this integral can be written as a polynomial in  $v$  with coefficients of the form (3.26). Hence, the right hand side of (3.27) tends to 0 with  $v$  to infinity.

Since all radii are equal in (3.25), we can use (3.23) and replace  $h$  by a suitable function  $\bar{h}$  and  $g$  by a function  $\bar{g}$  in the same manner. This yields

$$\begin{aligned}
&\frac{p^{m+1}\lambda^{m+1}}{4(m+1)!} c_{dm} \int_{-v^2 s_1^2}^{-v^2 s_0^2} (t + v^2 s_1^2)^{\frac{m(m-1)-2}{2}} \int_0^\infty p(t+s) s^{\frac{k-2}{2}} g(t, s, v s_1, \dots, v s_1) ds dt \\
&= \frac{p^{m+1}\lambda^{m+1}}{4(m+1)!} c_{dm} \int_{-v^2 s_1^2}^{-v^2 s_0^2} (t + v^2 s_1^2)^{\frac{m(m-1)-2}{2}} \int_0^\infty e^{-\lambda\omega_d p (s+t+v^2 s_1^2)^{\frac{d}{2}}} s^{\frac{k-2}{2}} \bar{g}(t + v^2 s_1^2, s, 0, \dots, 0) ds dt.
\end{aligned}$$

With the transformation  $r := t + v^2 s_1^2$  this formula reads

$$\begin{aligned}
&\frac{p^{m+1}\lambda^{m+1}}{4(m+1)!} c_{dm} \int_0^{v^2(s_1^2 - s_0^2)} r^{\frac{m(m-1)-2}{2}} \int_0^\infty e^{-\lambda\omega_d p (s+r)^{\frac{d}{2}}} s^{\frac{k-2}{2}} \bar{g}(r, s, 0, \dots, 0) ds dt \\
&\xrightarrow{v \rightarrow \infty} \frac{p^{m+1}\lambda^{m+1}}{4(m+1)!} c_{dm} \int_0^\infty r^{\frac{m(m-1)-2}{2}} \int_0^\infty e^{-\lambda\omega_d p (s+r)^{\frac{d}{2}}} s^{\frac{k-2}{2}} \bar{g}(r, s, 0, \dots, 0) ds dt.
\end{aligned} \tag{3.28}$$

Again, this equals the formula for  $\mathbb{E}_{M_{k,p\lambda}^V} [\bar{h}(R'_k, R''_k, \tilde{\Psi}_k, U_k)]$  for the Poisson Voronoi tessellation of intensity  $p\lambda$  (Baumstark and Last, 2007). The choice  $h \equiv 1$  shows the convergence of the intensities, and therefore of the Palm probability measures. The cases  $k = 0$  and  $k = d$  are handled similarly.  $\square$

#### Remarks 3.4.4

- (i) The result of the previous theorem cannot be formulated in terms of weak convergence of the measures  $\mathbb{Q}_k^0(1, v)$  for the following reason: Looking at the point process  $\Phi_{1,v}^{P_k}$  from a typical point on a  $k$ -face, we observe a point process of intensity  $\lambda$  containing some points whose Laguerre cell is empty. The limit point process  $\Psi_{p\lambda}$ , however, only contains the points generating non-empty cells. Therefore,  $\Psi_{p\lambda}$  could be interpreted as the limit of thinned versions of  $\Phi_{1,v}^{P_k}$ .
- (ii) The proof of Theorem 3.4.3 shows that in fact the difference  $s_1^2 - s_0^2$  is the factor determining the convergence. With increasing value of  $v$  this difference grows quadratically, thus increasing the influence of points with the larger weight.
- (iii) Theorem 3.4.3 holds in particular if  $\mathbb{F}$  is a two-atom distribution  $A(s_1, s_0, p)$  (cf. Section 1.1).

**Corollary 3.4.5**

Choose  $0 \leq s_0 < s_1$  and  $0 \leq p \leq 1$ . Consider a stationary marked Poisson process  $\Phi(s_1, s_0, p)$  on  $\mathbb{R}^d$  with intensity  $\lambda$  and mark distribution  $A(s_1, s_0, p)$  and denote the corresponding random measure  $M_k$  by  $M_k(s_1, s_0, p)$ . For  $s_1 \rightarrow \infty$  the Laguerre tessellation  $L(\Phi(s_1, s_0, p))$  converges to the Poisson Voronoi tessellation of intensity  $p\lambda$  in the sense that

$$\mathbb{E}_{M_k(s_1, s_0, p)}^0 [h(P'_k, P''_k, \tilde{\Psi}_k, U_k)] \xrightarrow{s_1 \rightarrow \infty} \mathbb{E}_{M_{k, p\lambda}^V}^0 [\bar{h}(R'_k, R''_k, \tilde{\Psi}_k, U_k)]$$

for any non-negative, bounded, and continuous function  $h$ .

**Proof:**

Imitating the steps of the previous proof, we end up with an expression similar to (3.27) which reads

$$e^{-\lambda\omega_d p(s_1^2 - s_0^2)^{\frac{d}{2}}} \frac{2\Gamma\left(\frac{k}{d}\right)}{d(\lambda\omega_d)^{\frac{k}{d}}} \int_0^\infty (t^{\frac{1}{2}} + (s_1^2 - s_0^2)^{\frac{1}{2}})^{dm-2} e^{-\lambda\omega_d t^{\frac{d}{2}}} dt. \quad (3.29)$$

Using the binomial theorem, this integral can be written as a polynomial in  $(s_1^2 - s_0^2)^{\frac{1}{2}}$  with coefficients containing integrals of the form (3.26) independent of this expression. This shows that (3.29) tends to 0 for  $s_1 \rightarrow \infty$ .

The analogue to (3.28) in the case considered here reads

$$\begin{aligned} & p^{m+1} \frac{\lambda^{m+1}}{4(m+1)!} c_{dm} \int_0^{s_1^2 - s_0^2} r^{\frac{m(m-1)-2}{2}} \int_0^\infty e^{-\lambda\omega_d p(s+r)^{\frac{d}{2}}} s^{\frac{k-2}{2}} \bar{g}(r, s, 0, \dots, 0) ds dt \\ & \xrightarrow{s_1 \rightarrow \infty} p^{m+1} \frac{\lambda^{m+1}}{4(m+1)!} c_{dm} \int_0^\infty r^{\frac{m(m-1)-2}{2}} \int_0^\infty e^{-\lambda\omega_d p(s+r)^{\frac{d}{2}}} s^{\frac{k-2}{2}} \bar{g}(r, s, 0, \dots, 0) ds dt, \end{aligned}$$

which is again the formula for  $\mathbb{E}_{M_{k, p\lambda}^V} [\bar{h}(R'_k, R''_k, \tilde{\Psi}_k, U_k)]$  for the Poisson Voronoi tessellation of intensity  $p\lambda$ .  $\square$

This result is not very surprising. With increasing value of  $s_1$  the points carrying this larger weight gain more and more influence. Finally, all cells generated by spheres with radius  $s_0$  are deleted from the tessellation.

In the following, we will apply the scaling laws given in (3.20) to deduce some limit results with dependence on the intensity  $\lambda$ .

**Corollary 3.4.6**

Consider a stationary marked Poisson process  $\Phi_\lambda$  on  $\mathbb{R}^d$  with intensity  $\lambda$  and mark distribution  $\mathbb{F}$  with property (3.3).

(i) We have

$$\lim_{\lambda \rightarrow 0} \left( \mathbb{E}_{M_{k, \lambda}}^0 [h(\Phi_\lambda^{P_k}, P'_k, P''_k, \Psi_k, U_k)] - \mathbb{E}_{M_{k, \lambda}^V}^0 [\bar{h}(\Psi_\lambda^{R_k^2}, R'_k, R''_k, \Psi_k, U_k)] \right) = 0$$

for any non-negative, continuous, bounded function  $h$  defined on a suitable domain.

(ii) Now let  $\mathbb{F}$  be a distribution as considered in Theorem 3.4.3. Then

$$\lim_{\lambda \rightarrow \infty} \left( \mathbb{E}_{M_{k,\lambda}}^0 [h(P'_k, P''_k, \tilde{\Psi}_k, U_k)] - \mathbb{E}_{M_{k,\lambda}^V}^0 [\bar{h}(R'_k, R''_k, \tilde{\Psi}_k, U_k)] \right) = 0$$

for any non-negative, continuous, bounded function  $h$  defined on a suitable domain.

**Proof:**

(i) Let  $c \geq 0$ . With (3.20) and Theorem 3.4.2 we get

$$c^{d-k} \mathbb{Q}_k(c, 1) = \mathbb{Q}_k(1, c^{-1}) \xrightarrow{c \rightarrow \infty} \mathbb{Q}_{k,\lambda}^V.$$

Now  $\mathbb{Q}_{k,\lambda}^V = c^{d-k} \mathbb{Q}_{k, \frac{\lambda}{c^d}}^V$  for any  $c > 0$ , hence  $\mathbb{Q}_k(c, 1)$  and  $\mathbb{Q}_{k, \frac{\lambda}{c^d}}^V$  approach each other for  $c \rightarrow \infty$ . The same is true if  $\mathbb{Q}_k$  is replaced by the intensities  $\mu_k$  which yields the assertion.

(ii) Let  $c \geq 0$ . Here, we use Theorem 3.4.3, which yields

$$\begin{aligned} c^{d-k} \mathbb{E}_{M_k(c,1)} [h(P'_k, P''_k, \tilde{\Psi}_k, U_k)] &= \mathbb{E}_{M_k(1,c^{-1})} [h(P'_k, P''_k, \tilde{\Psi}_k, U_k)] \\ &\xrightarrow{c \rightarrow 0} \mathbb{E}_{M_{k,p\lambda}^V} [\bar{h}(R'_k, R''_k, \tilde{\Psi}_k, U_k)]. \end{aligned}$$

Again, we use the transformation  $\mathbb{Q}_{k,p\lambda}^V = c^{d-k} \mathbb{Q}_{k, \frac{p\lambda}{c^d}}^V$ . Therefore, the expectations  $\mathbb{E}_{M_k(c,1)} [h(P'_k, P''_k, \tilde{\Psi}_k, U_k)]$  and  $\mathbb{E}_{M_{k,p\lambda}^V} [\bar{h}(R'_k, R''_k, \tilde{\Psi}_k, U_k)]$  approach each other if  $c \rightarrow 0$ . Using  $h \equiv 1$  the same holds for the intensities  $\mu_k$ , hence for the expectations with respect to the Palm probability measures. □

## 3.5 Summary and open problems

In the course of this chapter we have derived several formulas for mean values and distributions of geometric characteristics of Poisson Laguerre tessellations. Most of these results are based on the generalization of the methods developed for the analysis of Poisson Voronoi tessellations. In some cases, however, it turns out that a straightforward generalization is impossible due to the more complex geometry of Laguerre tessellations.

The main result of this chapter is a complete description of the Palm probability measure  $\mathbb{Q}_k^0$  of  $M_k$  (Theorem 3.2.4). It provides us with a description of the generating point process  $\Phi$  as seen from a randomly chosen (typical) point on a  $k$ -face of the tessellation. More precisely, we have computed the joint distribution of the  $d - k + 1$  neighbors of the  $k$ -face containing this typical point. However, the distribution formulas obtained here cannot be formulated as explicitly as the ones for the Poisson Voronoi tessellation (Baumstark and Last, 2007, Theorem 1.1). This is mainly caused by the loss of independence of some of the considered random variables when moving to the weighted case. The same is true for the formulas for the intensities  $\mu_k$ , which remain in integral form and have to be evaluated numerically.

Further random variables associated with a random tessellation are the characteristics of its typical  $k$ -faces and the point processes  $N_k$  of their centroids. It is difficult to prove

analytical formulas for these quantities directly. However, the formulas relating them to  $\mathbb{Q}_k^0$  yield some, although not very explicit, formulas (Theorem 3.3.9). An exception is the typical edge of the Poisson Voronoi tessellation. Both Schlather (2000) and Mucbe (2005) provide formulas for the distribution of its length. Baumstark and Last (2007) give a complete description of the distribution of the typical edge and its neighbors. However, each of these authors make heavy use of symmetries within a Poisson Voronoi tessellation which are no longer present in Laguerre tessellations. Therefore, the application of their methods to Poisson Laguerre tessellations is not possible.

One important quantity is the cell intensity  $\gamma_d$  which, in the Voronoi case, is easily seen to equal the intensity  $\lambda$  of the generating point process. In the Laguerre case this does no longer hold since not all points necessarily generate a cell. So far, we have not been able to derive an analytical formula for the cell intensity which allows for numerical evaluation. This has severe consequences as it implies that already for  $d = 3$  not all mean values of the cell characteristics can be computed analytically.

Based on the distribution formula for  $\mathbb{Q}_0^0$ , Mucbe (1996a) computed the distribution functions of various characteristics of the typical two- and three-dimensional Poisson Delaunay cell. In Section 3.3.1 we have deduced distribution formulas for the shape and the volume of the typical Poisson Laguerre Delaunay cell. However, the attempt to generalize Mucbe's results further fails because of the lack of an explicit formula for the volume  $\Delta_d(w_0u_0, \dots, w_du_d)$ .

Formulas for contact and chord length distributions of Poisson Laguerre tessellations have been derived in Sections 3.3.3 and 3.3.4, respectively. This generalizes results by Mucbe and Stoyan (1992). Tessellations with respect to more general point processes of generators, in the Voronoi case studied by Heinrich (1998), were not considered in this context.

Other quantities which have been studied in the case of the Poisson Voronoi tessellation include higher moments or covariances of cell characteristics (Brakke, 1986; Gilbert, 1962), distributions of several angles (Brakke, 1986; Mucbe, 1998; Baumstark and Last, 2007), or characteristics of sectional tessellations (Møller, 1994). These have not been considered here. Further, Calka (2003a,b) derived an explicit formula for the distribution of the number of faces and the area of the typical planar Poisson Voronoi cell. Our investigations have shown that, in principle, Calka's results can be generalized to the Laguerre case. However, the formulas, already looking rather complicated in the Voronoi case, did not turn out to be very explicit. Therefore, they are not given here.

Finally, we have proven some limit theorems dealing with the convergence of Poisson Laguerre to Poisson Voronoi tessellations (Section 3.4). Further relations between these two types of tessellations can be expected. Consider a Laguerre tessellation and the Voronoi tessellation generated by Poisson processes of the same intensity  $\lambda$ . Then the cell intensity of the Laguerre tessellation is at most  $\lambda$ , while the cell intensity of the Poisson Voronoi tessellation equals  $\lambda$ . Therefore, the Laguerre tessellation has fewer but larger cells than the Voronoi tessellation. We conjecture that the remaining intensities  $\gamma_k$ ,  $k = 0, \dots, d - 1$ , as well as the intensities  $\mu_k$ ,  $k = 0, \dots, d - 1$ , of a Poisson Laguerre tessellation are also bounded from above by the corresponding intensities of the Poisson Voronoi tessellation. The simulation results in the next chapter will support this conjecture. So far, however, we have not been able to prove it.

# Chapter 4

## Special cases, examples, and simulations

In this chapter we investigate planar ( $d = 2$ ) and spatial ( $d = 3$ ) Laguerre tessellations, which are the most important ones for applications. Our aim is to make the integral formulas derived in the last chapter as explicit as possible to allow for a numerical evaluation. As an example, we study Poisson Laguerre tessellations with respect to two-atom and uniform distributions of radii. We evaluate numerically the integral formulas for the intensities  $\mu_k$  and for the linear contact and chord length distributions. The resulting values for  $\mu_k$  are cross-checked with the values estimated using simulations of the particular tessellations.

Further, we show and discuss simulation results for distributions of several characteristics of the typical cells of the considered tessellations. At this point, one has to be careful with the interpretation of the notion “typical cell”. The typical cell of a Voronoi tessellation equals the cell generated by the typical point of the generating point process. For Laguerre tessellations, however, one has to distinguish between the (possibly empty) cell generated by the typical point and the typical non-empty cell drawn at random from the non-empty cells of the tessellation. Here, we will usually understand the term typical cell in the latter way. The cell generated by the typical point is then distributed as a mixture of the distribution of the typical non-empty cell (with probability  $p_0$ ) and the empty cell (with probability  $1 - p_0$ ). We start with a short survey of the simulation methods applied.

### 4.1 Simulation methods

The number of analytic formulas for distributions of characteristics of the typical Poisson Voronoi cell has grown over the last years. Nevertheless, some important distributions (e.g. the cell volume distribution of a three-dimensional tessellation) are not yet captured. The results of the last chapter indicate, that it is even harder to obtain formulas for generalized Voronoi tessellations. In addition, the variety of applications of (generalized) Voronoi tessellations requires the investigation of a wider range of processes of nuclei (e.g. hard core or cluster processes). Most of these models are completely intractable to analytic investigation. In each of these cases the desired distributions have to be studied using Monte-Carlo simulations of the tessellation models.

This fact raised the need for practical methods for the generation of realizations of random tessellations or, more precisely, their restrictions to a bounded observation window. Consequently, there have been several publications in computational geometry dealing with efficient algorithms for the computation of these structures (e.g. Aurenhammer, 1987b; Bois-

sonnat and Yvinec, 1998; Imai et al., 1985). For the simulation of Laguerre tessellations we use an algorithm discussed by Aurenhammer (1987b) and Sugihara (2000). It reduces the construction of a Laguerre Delaunay tessellation in  $\mathbb{R}^d$  to the construction of a convex hull in  $\mathbb{R}^{d+1}$ .

So let  $S$  be a finite subset of  $\mathbb{R}^d$ ,  $F$  a face of its convex hull  $\text{conv } S$ ,  $n$  the outward normal to  $F$ , and  $e_d = (0, \dots, 0, 1)$ .  $F$  is called an *upper face* if  $\langle n, e_d \rangle > 0$  and a *lower face* if  $\langle n, e_d \rangle < 0$ . The collection of the upper faces is called the *upper hull* and the collection of lower faces the *lower hull* of  $S$ . Then the basic result is the following.

**Theorem 4.1.1**

Let  $S = \{(x_i, r_i) : i = 1, \dots, n\}$  be a finite subset of  $\mathbb{R}^d \times \mathbb{R}^+$ . Define a set  $S'$  in  $\mathbb{R}^{d+1}$  via

$$S' := \{(x_i, \|x_i\|^2 - r_i^2) : i = 1, \dots, n\} \subseteq \mathbb{R}^{d+1}.$$

The projection of the lower hull of  $S'$  onto the subspace  $\mathbb{R}^d \times \{0\}$  is the Laguerre Delaunay diagram of  $S$ .

**Proof:**

Aurenhammer (1987b, Section 4). □

The corresponding algorithm for Voronoi tessellations is implemented in the QHull software package (Barber et al., 1996). We have adapted this package such that it can be used to construct Laguerre Delaunay tessellations. From these, the vertices and the systems of  $k$ -faces are derived using the system of linear equations given in (2.6).

For the simulation of the typical cell of a (generalized) Voronoi tessellation there are two main approaches. The first one is based on generating a realization of the tessellation in a single, very large window and measuring the characteristics of each of its cells. However, this straightforward approach has two main disadvantages: first, cells which are close to the boundary of the observation window may cause edge effects, which have to be removed using an appropriate edge treatment, and secondly, the generation of a sufficiently large realization might cause computational problems.

A second simulation method consists in generating a sequence of independent realizations of the typical cell and measuring the desired distributions from the aggregate of these cells. Quine and Watson (1984) introduced an efficient method for the simulation of the typical Poisson Voronoi cell based on radial generation of the Poisson process of nuclei. A generalization of this method to the Johnson-Mehl model has been published by Møller (1995). Now we will adapt the Quine-Watson approach to Poisson Laguerre tessellations.

It is well known, that the typical cell  $C_d(0)$  of a Poisson Laguerre tessellation has the same distribution as the cell  $C((0, r_0), \Phi \cup \{(0, R_0)\})$ , where  $R_0$  has the distribution of the weight of the typical point of  $\Phi$ . Therefore, we proceed as follows. Let  $\Phi$  be a stationary marked Poisson process, where the locations  $x_i$  are generated with increasing distance to the origin as described in Quine and Watson (1984) and the marks  $r_i$  are sampled from a mark distribution  $\mathbb{F}$ . In order to provide a stopping criterion for the generation of points, we will assume that an upper bound  $R > 0$  for the marks exists. In applications this is no serious restriction, since even distributions such as the gamma or log-normal distribution can be truncated at suitable values.

Then we almost surely have  $n_0 \in \mathbb{N}$  such that the (possibly empty) cell  $C(n) := C((0, r_0), \{(0, r_0), (x_1, r_1), \dots, (x_n, r_n)\})$  is bounded for all  $n \geq n_0$ . For each such  $n$  let

$d(n)$  denote the distance of the origin to the furthest vertex of  $C(n)$ . A point  $y \in \mathbb{R}^d$  belongs to  $C((0, r_0), \Phi \cup \{(0, r_0)\})$  if and only if

$$\left( [ \|y\|^2 - r_0^2 + r^2 ]^+ \right)^{\frac{1}{2}} \leq \|y - x\|, \quad (x, r) \in \Phi.$$

Therefore, the influence of a point  $(x, r)$  on  $C(n)$  depends on both the location of  $x$  and the value of  $r$ . Since the marks are bounded by  $R$ , we can formulate a criterion which is independent of the sequence of radii, namely  $C(n) = C((0, r_0), \Phi \cup \{(0, r_0)\})$  if

$$\|x_{n+1}\| > d(n) + (d(n) - r_0^2 + R^2)^{\frac{1}{2}}.$$

This yields the following algorithm for the simulation of a typical Poisson Laguerre cell: Radially generate  $x_1, \dots, x_{n+1}$  and draw the weights  $r_0, r_1, \dots, r_{n+1}$  from the mark distribution  $\mathbb{F}$  until  $C(n)$  is bounded and  $\|x_{n+1}\| > d(n) + (d(n) - r_0^2 + R^2)^{\frac{1}{2}}$ . Then  $C(n)$  yields a sample of the typical Poisson Laguerre cell  $C_d(0)$ .

## 4.2 The planar case

### 4.2.1 General formulas

In this section, we formulate the mean value formulas and distribution functions which we obtained in the last chapter explicitly for the two-dimensional case. So let  $\Phi$  be a stationary marked Poisson process on  $\mathbb{R}^2 \times \mathbb{R}^+$  with intensity  $\lambda$  and mark distribution  $\mathbb{F}$  with property (3.3).

#### Formulas for $\Delta_m^{k+1}$ and $V_{m,k}$

The main problem when working with the expressions in Theorem 3.2.4 is the lack of explicit general formulas for  $\Delta_m^{k+1}(w_0 u_0, \dots, w_m u_m)$  (p. 36) and  $V_{m,k}(w_0, \dots, w_m)$  (p. 44). However, in some special cases we are able to overcome this problem. In the two-dimensional case we have to consider  $\Delta_2$  and  $\Delta_1^2$ . Unfortunately,  $\Delta_2(w_0 u_0, w_1 u_1, w_2 u_2)$  remains intractable. But we have

$$\Delta_1^2(w_0 u_0, w_1 u_1) = w_0^2 + w_1^2 - 2\langle u_0, u_1 \rangle w_0 w_1, \quad u_0, u_1 \in S^1 \cap L, w_0, w_1 > 0,$$

and therefore

$$V_{1,1}(w_0, w_1) = 4(w_0^2 + w_1^2), \quad w_0, w_1 > 0.$$

#### The representation of $\mathbb{Q}_k$

Now we insert the expressions computed above into the distribution formulas given in Theorem 3.2.4. In each case, let  $h$  be a non-negative measurable function defined on a suitable domain. With respect to  $\mathbb{Q}_0$ , the neighborhood of the vertex in the origin is described by

the random variables  $(\Phi^{P_0}, P_0, \Psi_0)$ , whose distribution is given by

$$\begin{aligned} & \mathbb{E}_{M_0} [h(\Phi^{P_0}, P_0, \Psi_0)] \\ &= \frac{\lambda^3}{6} \int_0^\infty \int_0^\infty \int_0^\infty \int_{-\min_i r_i^2}^\infty e^{-\lambda\pi \int_0^\infty [t+r^2]^+ \mathbb{F}(dr)} \int_{S^1} \int_{S^1} \int_{S^1} \mathbb{E} [h(\Phi^t, t, \{(u_0, r_0), (u_1, r_1), (u_2, r_2)\})] \\ & \quad \Delta_2((t+r_0^2)^{\frac{1}{2}}u_0, (t+r_1^2)^{\frac{1}{2}}u_1, (t+r_2^2)^{\frac{1}{2}}u_2) \mathbb{S}(du_0) \mathbb{S}(du_1) \mathbb{S}(du_2) dt \mathbb{F}(dr_0) \mathbb{F}(dr_1) \mathbb{F}(dr_2). \end{aligned}$$

With respect to  $\mathbb{Q}_1$ , the decomposition of  $\Phi$  reads  $(\Phi^{P_1}, P'_1, P''_1, \Psi_1, U_1)$  and we have

$$\begin{aligned} & \mathbb{E}_{M_1} [h(\Phi^{P_1}, P'_1, P''_1, \Psi_1, U_1)] \\ &= \frac{\lambda^2\pi}{8} \int_0^\infty \int_0^\infty \int_{-\min_i r_i^2}^\infty \int_{S^1 \cap L} \int_{S^1 \cap L} \left( \frac{2t+r_0^2+r_1^2}{(t+r_0^2)^{\frac{1}{2}}(t+r_1^2)^{\frac{1}{2}}} - 2\langle u_0, u_1 \rangle \right) \int_0^\infty e^{-\lambda\pi \int_0^\infty [s+t+r^2]^+ \mathbb{F}(dr)} s^{-\frac{1}{2}} \\ & \quad \int_{SO_2} \int_{S^1 \cap L^\perp} \mathbb{E} [h(\Phi^{t+s}, t, s, \{(\vartheta u_0, r_0), (\vartheta u_1, r_1)\}, \vartheta u)] \mathbb{S}_{L^\perp}(du) \nu(d\vartheta) ds \mathbb{S}_L(du_0) \mathbb{S}_L(du_1) dt \\ & \quad \mathbb{F}(dr_0) \mathbb{F}(dr_1). \end{aligned}$$

When disintegrating with respect to  $\Psi_1$ , we may insert the formula for  $V_{1,1}$  and obtain

$$\begin{aligned} & \mathbb{E}_{M_1} [h(\Phi^{P_1}, P'_1, P''_1, U_1)] \\ &= \frac{\lambda^2\pi}{2} \int_0^\infty \int_0^\infty \int_{-\min_i r_i^2}^\infty \frac{2t+r_0^2+r_1^2}{(t+r_0^2)^{\frac{1}{2}}(t+r_1^2)^{\frac{1}{2}}} \int_0^\infty e^{-\lambda\pi \int_0^\infty [s+t+r^2]^+ \mathbb{F}(dr)} s^{-\frac{1}{2}} \int_{SO_2} \int_{S^1 \cap L^\perp} \mathbb{E} [h(\Phi^{t+s}, t, s, \vartheta u)] \\ & \quad \mathbb{S}_{L^\perp}(du) \nu(d\vartheta) ds dt \mathbb{F}(dr_0) \mathbb{F}(dr_1). \end{aligned}$$

### The intensities $\mu_k$

For the intensities  $\mu_0$  and  $\mu_1$  we get

$$\begin{aligned} \mu_0 &= \frac{\lambda^3}{12} \int_0^\infty \int_0^\infty \int_0^\infty \int_{-\min_i r_i^2}^\infty e^{-\lambda\pi \int_0^\infty [t+r^2]^+ \mathbb{F}(dr)} V_{2,0} \left( (t+r_0^2)^{\frac{1}{2}}, (t+r_1^2)^{\frac{1}{2}}, (t+r_2^2)^{\frac{1}{2}} \right) dt \mathbb{F}(dr_0) \\ & \quad \mathbb{F}(dr_1) \mathbb{F}(dr_2) \end{aligned}$$

and

$$\mu_1 = \lambda^2\pi \int_0^\infty \int_0^\infty \int_{-\min_i r_i^2}^\infty \frac{2t+r_0^2+r_1^2}{(t+r_0^2)^{\frac{1}{2}}(t+r_1^2)^{\frac{1}{2}}} \int_0^\infty e^{-\lambda\pi \int_0^\infty [t+s+r^2]^+ \mathbb{F}(dr)} s^{-\frac{1}{2}} ds dt \mathbb{F}(dr_0) \mathbb{F}(dr_1).$$

These two formulas provide all parameters which are required for computing the mean values of the cell characteristics using Theorem 1.6.6. In particular, we can derive a formula

for the probability  $p_0$  that the typical point of  $\Phi$  generates a non-empty cell: Since the intensity of cells is given by  $\gamma_2 = p_0\lambda$  and  $\gamma_0 = 2\gamma_2$ , we have

$$\begin{aligned} p_0 &= \frac{\gamma_2}{\lambda} = \frac{\gamma_0}{2\lambda} = \frac{\mu_0}{2\lambda} = \\ &= \frac{\lambda^2}{24} \int_0^\infty \int_0^\infty \int_0^\infty \int_{-\min_i r_i^2}^\infty e^{-\lambda\pi \int_0^\infty [t+r^2]^+ \mathbb{F}(dr)} V_{2,0} \left( (t+r_0^2)^{\frac{1}{2}}, (t+r_1^2)^{\frac{1}{2}}, (t+r_2^2)^{\frac{1}{2}} \right) dt \mathbb{F}(dr_0) \\ &\quad \mathbb{F}(dr_1) \mathbb{F}(dr_2). \end{aligned}$$

Denote the intensities of the point process of centers of the  $k$ -faces of a Poisson Voronoi tessellation with intensity  $\lambda$  by  $\gamma_k^V$ . Then, since  $\gamma_2 = \lambda p_0 \leq \lambda = \gamma_2^V$ , we see that  $\gamma_1 = 3\gamma_2 \leq 3\gamma_2^V = \gamma_1^V$  and  $\gamma_0 = 2\gamma_2 \leq 2\gamma_2^V = \gamma_0^V$ . Therefore, the estimates conjectured in Section 3.5 hold in the planar case.

### The mean content of $F_k(0)$

For the mean length of the edge  $F_1(0)$  we obtain

$$\begin{aligned} \mathbb{E}_{M_1}^0 [\mathcal{H}^1(F_1(0))] &= \frac{\lambda^2 \pi}{\mu_1} \sum_{\theta \in \{0, \pi\}} \int_0^\infty \int_0^\infty \int_{-\min_i r_i^2}^\infty \frac{2t + r_0^2 + r_1^2}{(t+r_0^2)^{\frac{1}{2}} (t+r_1^2)^{\frac{1}{2}}} \int_0^\infty \int_0^\infty \xi(l, s+t, \tau(l, t, s, \theta)) \\ &\quad s^{-\frac{1}{2}} dl ds dt \mathbb{F}(dr_0) \mathbb{F}(dr_1). \end{aligned}$$

The mean area of the cell  $F_2(0)$  containing the origin is

$$\mathbb{E}_{M_2}^0 [\mathcal{H}^2(F_2(0))] = \lambda \pi \int_0^\infty \int_{-r_0^2}^\infty \int_0^\infty \int_0^{2\pi} \xi(l, t, \rho(l, t, r_0, \theta)) l d\theta dl dt \mathbb{F}(dr_0).$$

### The linear contact distribution

The formula for the linear contact distribution function is given by

$$H_l(r) = 1 - \frac{\lambda}{2} \int_0^\infty \int_{-r_0}^\infty \int_0^{2\pi} \xi(r, t, \rho(r, t, r_0, \theta)) d\theta dt \mathbb{F}(dr_0), \quad r \geq 0,$$

where we recall that

$$\xi(r, t, \rho) = \exp \left( -\lambda \int_0^\infty \kappa \left( r, ([t+w^2]^+)^{\frac{1}{2}}, ([\rho+w^2]^+)^{\frac{1}{2}} \right) \mathbb{F}(dr) \right), \quad r \geq 0, t, \rho \in \mathbb{R}.$$

In the two-dimensional case, formula (3.14) for  $\kappa\left(r, (t+w^2)^{\frac{1}{2}}, (\rho+w^2)^{\frac{1}{2}}\right)$  with  $r > 0$ ,  $t+w^2 > 0$ , and  $\rho+w^2 > 0$  reads

$$\begin{aligned} & \kappa\left(r, (t+w^2)^{\frac{1}{2}}, (\rho+w^2)^{\frac{1}{2}}\right) \\ &= (t+w^2) \left( \pi - \arccos\left(\frac{t-\rho+r^2}{2r(t+w^2)^{\frac{1}{2}}}\right) + \frac{t-\rho+r^2}{2r(t+w^2)^{\frac{1}{2}}} \left(1 - \frac{(t-\rho+r^2)^2}{4r^2(t+w^2)}\right)^{\frac{1}{2}} \right) \\ &+ (\rho+w^2) \left( \pi - \arccos\left(\frac{\rho-t+r^2}{2r(\rho+w^2)^{\frac{1}{2}}}\right) + \frac{\rho-t+r^2}{2r(\rho+w^2)^{\frac{1}{2}}} \left(1 - \frac{(\rho-t+r^2)^2}{4r^2(\rho+w^2)}\right)^{\frac{1}{2}} \right) \end{aligned}$$

if  $|(t+w^2)^{\frac{1}{2}} - (\rho+w^2)^{\frac{1}{2}}| < r < (t+w^2)^{\frac{1}{2}} + (\rho+w^2)^{\frac{1}{2}}$ . The formulas for the other cases in (3.14) are obvious.

### The chord length distribution

The formula for the chord length distribution function reads

$$L(r) = 1 - \frac{\lambda^2 \pi}{4\mu_1} \int_0^\infty \int_{-r^2}^\infty \int_0^{2\pi} \int_0^\infty \kappa'(r, t, r_0, w, \theta) \mathbb{F}(dw) \xi(r, t, \rho(r, t, r_0, \theta)) d\theta dt \mathbb{F}(dr_0), \quad r \geq 0,$$

where  $\xi$  and  $\kappa$  are defined as above and

$$\kappa'(r, t, r_0, w, \theta) = \frac{d}{dr} \kappa\left(r, ([t+w^2]^+)^{\frac{1}{2}}, ([\rho(r, t, r_0, \theta) + w^2]^+)^{\frac{1}{2}}\right)$$

for  $r, r_0, w \geq 0, t \in \mathbb{R}$ , and  $\theta \in [0, 2\pi]$ .

### 4.2.2 Two-atom distribution

In the following we investigate formula (3.9) for a two-dimensional Poisson Laguerre tessellation where  $\mathbb{F}$  is the two-atom distribution  $A(s_1, s_0, p)$  with  $0 \leq s_0 < s_1$  and  $0 \leq p \leq 1$ . Consider a stationary marked Poisson process  $\Phi$  on  $\mathbb{R}^2$  with intensity  $\lambda$  and mark distribution  $\mathbb{F} = A(s_1, s_0, p)$ . Let  $m_2 := ps_1^2 + (1-p)s_0^2$  be the second moment of the radii.

The cells, edges, and vertices of  $L(\Phi)$  can be partitioned into several classes depending on how many of the generating nuclei carry the smaller or the larger radius. In the following formulas we will condition on the number of nuclei with radius  $s_0$  and  $s_1$ , respectively. This yields explicit information on the contribution of the different classes of  $k$ -faces to  $\mathbb{Q}_k$ .

We recall that  $\Psi_k = \{(U_{k,0}, R_{k,0}), \dots, (U_{k,m}, R_{k,m})\}$  and define the random variables

$$N_{k,j} := \sum_{i=0}^m \mathbb{1}_{\{s_j\}}(R_{k,i}), \quad k = 0, 1, j = 0, 1, \quad (4.1)$$

as the random number of nuclei carrying weight  $s_j$ . Then the formulas for the expectations  $\mathbb{E}_{M_0} [h(\Phi^{P_0}, P_0, \Psi_0)]$  conditioned on a specific choice of radii are

$$\begin{aligned}
& \mathbb{E}_{M_0} [h(\Phi^{P_0}, P_0, \Psi_0) \mid N_{0,1} = 3] \\
&= \frac{\lambda^3}{6} p^3 e^{-\lambda\pi m_2} \int_{-s_0^2}^{\infty} e^{-\lambda\pi t} (t + s_1^2) \int_{S^1} \int_{S^1} \int_{S^1} \mathbb{E} [h(\Phi^t, t, \{(u_0, s_1), (u_1, s_1), (u_2, s_1)\})] \\
&\quad \Delta_2(u_0, u_1, u_2) \mathbb{S}(du_0) \mathbb{S}(du_1) \mathbb{S}(du_2) dt \\
&+ \frac{\lambda^3}{6} p^3 e^{-\lambda\pi s_1^2} \int_{-s_1^2}^{-s_0^2} e^{-\lambda\pi t} (t + s_1^2) \int_{S^1} \int_{S^1} \int_{S^1} \mathbb{E} [h(\Phi^t, t, \{(u_0, s_1), (u_1, s_1), (u_2, s_1)\})] \\
&\quad \Delta_2(u_0, u_1, u_2) \mathbb{S}(du_0) \mathbb{S}(du_1) \mathbb{S}(du_2) dt,
\end{aligned}$$

$$\begin{aligned}
& \mathbb{E}_{M_0} [h(\Phi^{P_0}, P_0, \Psi_0) \mid N_{0,0} = 1, N_{0,1} = 2] \\
&= \frac{\lambda^3}{2} p^2 (1-p) e^{-\lambda\pi m_2} \int_{-s_0^2}^{\infty} e^{-\lambda\pi t} \int_{S^1} \int_{S^1} \int_{S^1} \mathbb{E} [h(\Phi^t, t, \{(u_0, s_0), (u_1, s_1), (u_2, s_1)\})] \\
&\quad \Delta_2((t + s_0^2)^{\frac{1}{2}} u_0, (t + s_1^2)^{\frac{1}{2}} u_1, (t + s_1^2)^{\frac{1}{2}} u_2) \mathbb{S}(du_0) \mathbb{S}(du_1) \mathbb{S}(du_2) dt,
\end{aligned}$$

$$\begin{aligned}
& \mathbb{E}_{M_0} [h(\Phi^{P_0}, P_0, \Psi_0) \mid N_{0,0} = 2, N_{0,1} = 1] \\
&= \frac{\lambda^3}{2} p (1-p)^2 e^{-\lambda\pi m_2} \int_{-s_0^2}^{\infty} e^{-\lambda\pi t} \int_{S^1} \int_{S^1} \int_{S^1} \mathbb{E} [h(\Phi^t, t, \{(u_0, s_1), (u_1, s_0), (u_2, s_0)\})] \\
&\quad \Delta_2((t + s_1^2)^{\frac{1}{2}} u_0, (t + s_0^2)^{\frac{1}{2}} u_1, (t + s_0^2)^{\frac{1}{2}} u_2) \mathbb{S}(du_0) \mathbb{S}(du_1) \mathbb{S}(du_2) dt,
\end{aligned}$$

and

$$\begin{aligned}
& \mathbb{E}_{M_0} [h(\Phi^{P_0}, P_0, \Psi_0) \mid N_{0,0} = 3] \\
&= \frac{\lambda^3}{6} (1-p)^3 e^{-\lambda\pi m_2} \int_{-s_0^2}^{\infty} e^{-\lambda\pi t} (t + s_0^2) \int_{S^1} \int_{S^1} \int_{S^1} \mathbb{E} [h(\Phi^t, t, \{(u_0, s_0), (u_1, s_0), (u_2, s_0)\})] \\
&\quad \Delta_2(u_0, u_1, u_2) \mathbb{S}(du_0) \mathbb{S}(du_1) \mathbb{S}(du_2) dt.
\end{aligned}$$

For the formulas with respect to  $\mathbb{Q}_1$  we note that  $\Delta_1^2(u_0, u_1) = 4 \mathbb{I}\{u_0 = -u_1\}$  and  $\Delta_1^2(w_0 u_0, w_1 u_1) = \Delta_1^2(w_1 u_0, w_0 u_1)$  for unit vectors  $u_0, u_1 \in S^1 \cap L$  and  $w_0, w_1 > 0$ . Therefore,

we may keep  $u_0 \in S^1 \cap L$  fixed in two of the following formulas and get

$$\begin{aligned}
& \mathbb{E}_{M_1} [h(\Phi^{P_1}, P'_1, P''_1, \Psi_1, U_1) \mid N_{1,1} = 2] \\
&= \lambda^2 \pi p^2 e^{-\lambda \pi m_2} \int_{-s_0^2}^{\infty} e^{-\lambda \pi t} \int_0^{\infty} e^{-\lambda \pi s} s^{-\frac{1}{2}} \int_{SO_2} \int_{S^1 \cap L^\perp} \mathbb{E} [h(\Phi^{t+s}, t, s, \{(\vartheta u_0, s_1), (-\vartheta u_0, s_1)\}, \vartheta u)] \\
&\quad \mathbb{S}_{L^\perp}(du) \nu(d\vartheta) ds dt \\
&+ \lambda^2 \pi p^2 e^{-\lambda \pi s_1^2} \int_{-s_1^2}^{-s_0^2} e^{-\lambda \pi t} \int_0^{-(t+s_0^2)} e^{-\lambda \pi s} s^{-\frac{1}{2}} \int_{SO_2} \int_{S^1 \cap L^\perp} \mathbb{E} [h(\Phi^{t+s}, t, s, \{(\vartheta u_0, s_1), (-\vartheta u_0, s_1)\}, \vartheta u)] \\
&\quad \mathbb{S}_{L^\perp}(du) \nu(d\vartheta) ds dt \\
&+ \lambda^2 \pi p^2 e^{-\lambda \pi m_2} \int_{-s_1^2}^{-s_0^2} e^{-\lambda \pi t} \int_{-(t+s_0^2)}^{\infty} e^{-\lambda \pi s} s^{-\frac{1}{2}} \int_{SO_2} \int_{S^1 \cap L^\perp} \mathbb{E} [h(\Phi^{t+s}, t, s, \{(\vartheta u_0, s_1), (-\vartheta u_0, s_1)\}, \vartheta u)] \\
&\quad \mathbb{S}_{L^\perp}(du) \nu(d\vartheta) ds dt,
\end{aligned}$$

$$\begin{aligned}
& \mathbb{E}_{M_1} [h(\Phi^{P_1}, P'_1, P''_1, \Psi_1, U_1) \mid N_{1,0} = 1, N_{1,1} = 1] \\
&= \frac{\lambda^2 \pi}{4} p(1-p) e^{-\lambda \pi m_2} \int_{-s_0^2}^{\infty} \left( \frac{2t + s_1^2 + s_0^2}{(t + s_1^2)^{\frac{1}{2}} (t + s_0^2)^{\frac{1}{2}}} - 2\langle u_0, u_1 \rangle \right) e^{-\lambda \pi t} \int_0^{\infty} e^{-\lambda \pi s} s^{-\frac{1}{2}} \\
&\quad \int_{SO_2} \int_{S^1 \cap L} \int_{S^1 \cap L} \int_{S^1 \cap L^\perp} \mathbb{E} [h(\Phi^{t+s}, t, s, \{(\vartheta u_0, s_1), (\vartheta u_1, s_0)\}, \vartheta u)] \mathbb{S}_{L^\perp}(du) \mathbb{S}_L(du_0) \mathbb{S}_L(du_1) \\
&\quad \nu(d\vartheta) ds dt,
\end{aligned}$$

and

$$\begin{aligned}
& \mathbb{E}_{M_1} [h(\Phi^{P_1}, P'_1, P''_1, \Psi_1, U_1) \mid N_{1,0} = 2] \\
&= \lambda^2 \pi (1-p)^2 e^{-\lambda \pi m_2} \int_{-s_0^2}^{\infty} e^{-\lambda \pi t} \int_0^{\infty} e^{-\lambda \pi s} s^{-\frac{1}{2}} \int_{SO_2} \int_{S^1 \cap L^\perp} \mathbb{E} [h(\Phi^{t+s}, t, s, \{(\vartheta u_0, s_0), (-\vartheta u_0, s_0)\}, \vartheta u)] \\
&\quad \mathbb{S}_{L^\perp}(du) \nu(d\vartheta) ds dt.
\end{aligned}$$

We are now going to investigate the intensities  $\mu_k$  of the measures  $M_k$ . As above, we may not only ask for the total value of  $\mu_k$  but also for the contribution of each class of  $k$ -faces to this value. Hence, write  $\mu_0(r_0, r_1, r_2)$  for the intensity of vertices whose neighbors carry the weights  $r_0, r_1$ , and  $r_2$  and  $\mu_1(r_0, r_1)$  for the total length of edges whose neighbors carry the

weights  $r_0$  and  $r_1$ . Then the intensities  $\mu_0$  and  $\mu_1$  have the decomposition

$$\begin{aligned} \mu_0 &= \mu_0(s_0, s_0, s_0) + \mu_0(s_1, s_0, s_0) + \mu_0(s_1, s_1, s_0) + \mu_0(s_1, s_1, s_1) \\ &= (1-p)^3 2\lambda e^{-\lambda\pi p(s_1^2 - s_0^2)} \\ &\quad + \frac{(1-p)^2 p}{4} \lambda^3 e^{-\lambda\pi m_2} \int_{-s_0^2}^{\infty} e^{-\lambda\pi t} V_{2,0} \left( (t + s_1^2)^{\frac{1}{2}}, (t + s_0^2)^{\frac{1}{2}}, (t + s_0^2)^{\frac{1}{2}} \right) dt \\ &\quad + \frac{(1-p)p^2}{4} \lambda^3 e^{-\lambda\pi m_2} \int_{-s_0^2}^{\infty} e^{-\lambda\pi t} V_{2,0} \left( (t + s_1^2)^{\frac{1}{2}}, (t + s_1^2)^{\frac{1}{2}}, (t + s_0^2)^{\frac{1}{2}} \right) dt \\ &\quad + 2p\lambda \left( 1 - e^{-\lambda\pi p(s_1^2 - s_0^2)} (1-p)(1+p + \lambda\pi p(s_1^2 - s_0^2)) \right) \end{aligned}$$

and

$$\begin{aligned} \mu_1 &= \mu_1(s_0, s_0) + \mu_1(s_1, s_0) + \mu_1(s_1, s_1) \\ &= (1-p)^2 2e^{-\lambda\pi p(s_1^2 - s_0^2)} \lambda^{\frac{1}{2}} + 2(1-p)p\lambda^{\frac{3}{2}}\pi e^{-\lambda\pi m_2} \int_{-s_0^2}^{\infty} \frac{2t + s_1^2 + s_0^2}{(t + s_1^2)^{\frac{1}{2}}(t + s_0^2)^{\frac{1}{2}}} e^{-\lambda\pi t} dt \\ &\quad + 4p^2\lambda^2\pi \left[ \int_0^{s_1^2 - s_0^2} e^{-\lambda\pi s} s^{\frac{1}{2}} ds + e^{-\lambda\pi p(s_1^2 - s_0^2)} \int_0^{\infty} e^{-\lambda\pi s} (s + s_1^2 - s_0^2)^{\frac{1}{2}} ds \right]. \end{aligned}$$

### Example 4.2.1

As an example, we consider the Poisson Laguerre tessellation for the parameters  $\lambda = 100$ ,  $s_0 = 0.01$ ,  $s_1 = 0.01, 0.05, 0.1, 0.15, 0.2, 0.25, 0.3$ , and  $p = 0.5$ . This means we start with a Poisson Voronoi tessellation of intensity  $\lambda = 100$  and gradually increase the value of the larger radius. By Corollary 3.4.5, the tessellations obtained this way will approach the Poisson Voronoi tessellation of intensity  $\lambda = 50$  for large values of  $s_1$ . Some realizations are shown in Figure 4.3.

The formulas for  $\mu_0 (= \gamma_0)$  and  $\mu_1 (= L_A)$  are evaluated using the numerical integration functions of Mathematica. From these, the mean values of characteristics of the typical non-empty cell are computed using the relations given in Theorem 1.6.6. The results are summarized in Table 4.1. The contributions of the different types of cells to  $\mu_0$  and  $\mu_1$  are listed in Tables 4.2 and 4.3, respectively.

Plots of the linear contact distribution function, its density, and the chord length distribution function, also evaluated with Mathematica, are shown in Figures 4.1 and 4.2.

In each of these representations, the convergence to a Poisson Voronoi tessellation of intensity  $\lambda = 50$  with increasing  $s_1$  is clearly visible. It turns out that already for  $r_1 = 0.3$  nearly all of the cells generated by points with the smaller weight have disappeared.

Due to the lack of analytic formulas, distributions of characteristics of the typical cells have to be studied by simulation. For each value of  $s_1$  we generated 200,000 realizations of the typical non-empty cell using the algorithm discussed in the previous section. The results for the means, variances, minima, and maxima of their area, perimeter, and number of edges are presented in Table 4.5. The histograms of the corresponding distributions are shown in

Figures 4.4, 4.5, and 4.6, respectively. Besides the distributions for the total number of cells we also included the histograms conditioned on the radius of the generators.

The histograms of the area distributions show a large amount of very small cells generated by spheres with radius  $s_0$ . The values of the minima of area and perimeter indicate that cells can in principle become arbitrarily small. From the distribution of edge numbers we see that small cells have less edges with an increasing amount of triangles and quadrangles. However, besides the peak for small cells in the area distributions it is hard to distinguish between the two cell types in the histograms.

In order to investigate the situation for different choices of  $p$  we have computed the mean values  $\gamma_0$ ,  $\gamma_2$ , and  $L_A$  for the same choices of  $\lambda$ ,  $s_0$ , and  $s_1$  as above and  $p = 0.1, 0.3, 0.5, 0.7$ , and  $0.9$ . To check the accuracy of the numerical integration, the results are compared to the values obtained by simulation of the model. For each set of parameters, we generate 10,000 realizations of the Laguerre tessellations within the unit cube using periodic boundary conditions. As a reference value, we use the mean of the values measured from the single realizations. The results are summarized in Table 4.4. We observe that the values obtained by simulation are in good agreement with the results from numerical integration. Further, it turns out that the convergence to the Poisson Voronoi tessellation is slower for smaller values of  $p$ .

$s_1$	$PV_{100}$	0.05	0.1	0.15	0.2	0.25	0.3	$PV_{50}$
$\gamma_0$	200.000	192.406	148.398	110.968	101.050	100.043	100.001	100.000
$\gamma_1$	300.000	288.609	222.597	166.452	151.574	150.065	150.001	150.000
$\gamma_2$	100.000	96.203	74.199	55.484	50.525	50.022	50.001	50.000
$L_A$	20.000	19.203	16.283	14.529	14.173	14.143	14.142	14.142
$l_1$	0.06667	0.06654	0.07315	0.08729	0.09351	0.09425	0.09428	0.09428
$a_2$	0.0100	0.0104	0.0135	0.0180	0.0198	0.0200	0.0200	0.0200
$u_2$	0.4000	0.3992	0.4389	0.5237	0.5610	0.5655	0.5657	0.5657

Table 4.1: Mean values of cell characteristics of a Laguerre tessellation in  $\mathbb{R}^2$  generated by a stationary marked Poisson process with intensity  $\lambda = 100$ . The mark distribution is a two-atom distribution with  $s_1$  as given in the table,  $s_0 = 0.01$ , and  $p = 0.5$ . For comparison, the values for Poisson Voronoi tessellations with intensity  $\lambda = 100$  and  $\lambda = 50$  are included.

$s_1$	$PV_{100}$	0.05	0.1	0.15	0.2	0.25	0.3	$PV_{50}$
$\mu_0(s_1, s_1, s_1)$	25.000	35.627	67.743	92.562	99.263	99.969	99.999	100.000
$\mu_0(s_0, s_1, s_1)$	75.000	77.291	48.678	12.652	1.331	0.058	0.001	0.000
$\mu_0(s_0, s_0, s_1)$	75.000	62.341	26.699	5.013	0.408	0.015	0.000	0.000
$\mu_0(s_0, s_0, s_0)$	25.000	17.148	5.279	0.741	0.047	0.001	0.000	0.000

Table 4.2: Contributions to  $\mu_0$  of different cell types in a Laguerre tessellation in  $\mathbb{R}^2$  generated by a stationary marked Poisson process with intensity  $\lambda = 100$ . The mark distribution is a two-atom distribution with  $s_1$  as given in the table,  $s_0 = 0.01$ , and  $p = 0.5$ . For comparison, the values for Poisson Voronoi tessellations with intensity  $\lambda = 100$  (interpreted as a Laguerre tessellation with mark distribution  $A(0.01, 0.01, 0.5)$ ) and  $\lambda = 50$  (interpreted as a Laguerre tessellation with mark distribution  $A(0.01, 0.01, 1)$ ) are included.

$s_1$	$PV_{100}$	0.05	0.1	0.15	0.2	0.25	0.3	$PV_{50}$
$\mu_1(s_1, s_1)$	5.000	6.935	11.239	13.615	14.100	14.141	14.142	14.142
$\mu_1(s_0, s_1)$	10.000	8.839	3.987	0.766	0.063	0.002	0.000	0.000
$\mu_1(s_0, s_0)$	5.000	3.430	1.056	0.148	0.010	0.000	0.000	0.000

Table 4.3: Contributions to  $\mu_1$  of different cell types in a Laguerre tessellation in  $\mathbb{R}^2$  generated by a stationary marked Poisson process with intensity  $\lambda = 100$ . The mark distribution is a two-atom distribution with  $s_1$  as given in the table,  $s_0 = 0.01$ , and  $p = 0.5$ . For comparison, the values for Poisson Voronoi tessellations with intensity  $\lambda = 100$  (interpreted as a Laguerre tessellation with mark distribution  $A(0.01, 0.01, 0.5)$ ) and  $\lambda = 50$  (interpreted as a Laguerre tessellation with mark distribution  $A(0.01, 0.01, 1)$ ) are included.

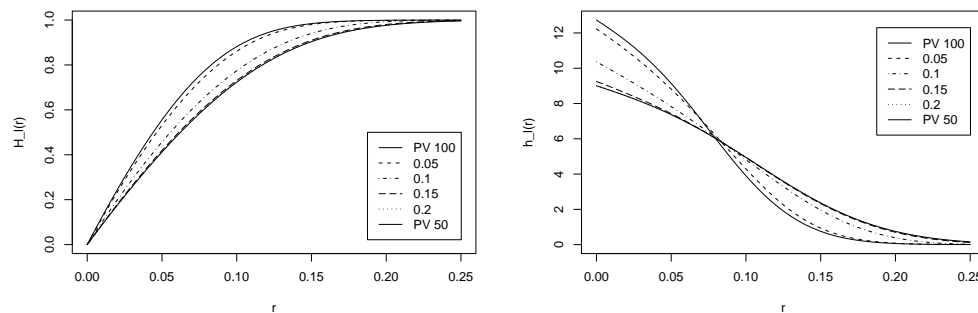


Figure 4.1: Linear contact distribution function (left) and its density (right) for a Laguerre tessellation in  $\mathbb{R}^2$  generated by a stationary marked Poisson process with intensity  $\lambda = 100$  and radius distribution  $A(s_1, 0.01, 0.5)$  with  $s_1 = 0.05, 0.1, 0.15,$  and  $0.2$ . The solid lines correspond to the Poisson Voronoi tessellations with intensities  $\lambda = 100$  and  $\lambda = 50$ . The line for  $s_1 = 0.2$  is so close to the Poisson Voronoi line that they cannot be distinguished.

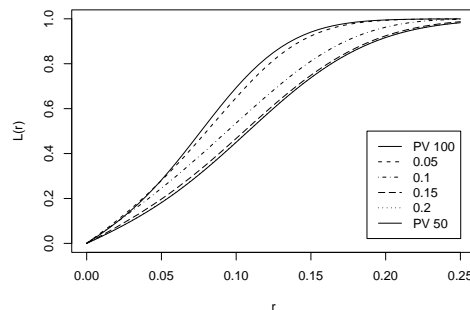


Figure 4.2: Chord length distribution function for a Laguerre tessellation in  $\mathbb{R}^2$  generated by a stationary marked Poisson process with intensity  $\lambda = 100$  and radius distribution  $A(s_1, 0.01, 0.5)$  with  $s_1 = 0.05, 0.1, 0.15,$  and  $0.2$ . The solid lines correspond to the Poisson Voronoi tessellations with intensities  $\lambda = 100$  and  $\lambda = 50$ .

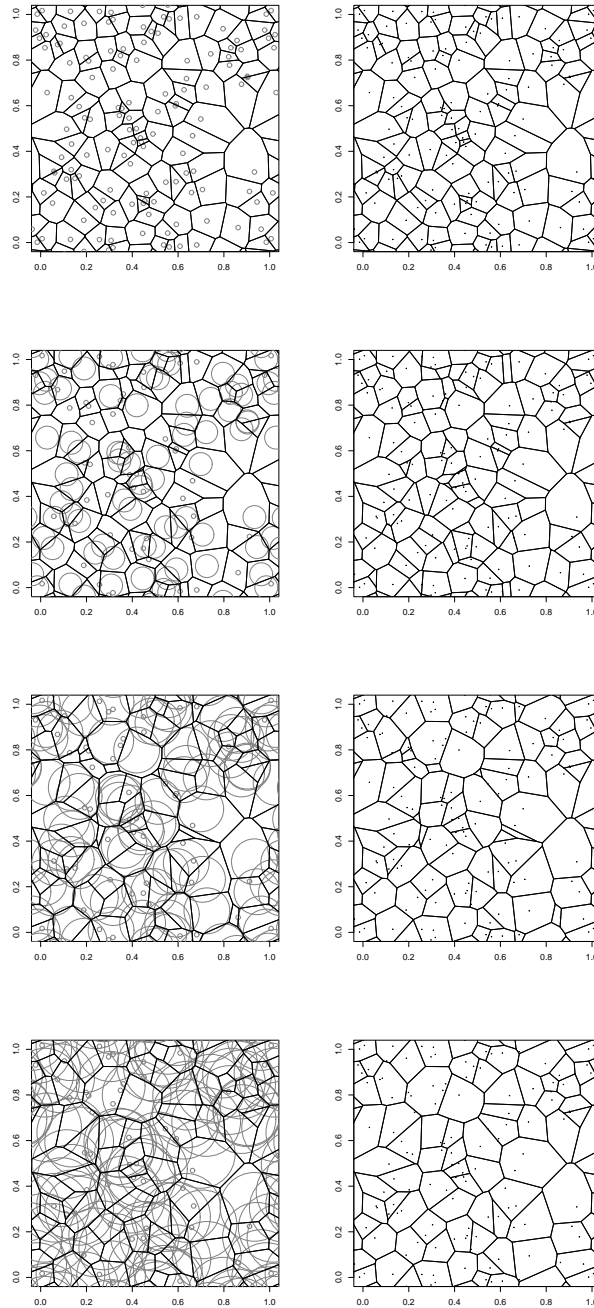


Figure 4.3: Realizations of Poisson Laguerre tessellations of a fixed realization of a stationary marked Poisson process with intensity  $\lambda = 100$ . The radii are equal (top) or have distribution  $A(0.05, 0.01, 0.5)$ ,  $A(0.1, 0.01, 0.5)$ , and  $A(0.15, 0.01, 0.5)$ . The last image equals the Voronoi tessellation of the points carrying the larger weights.

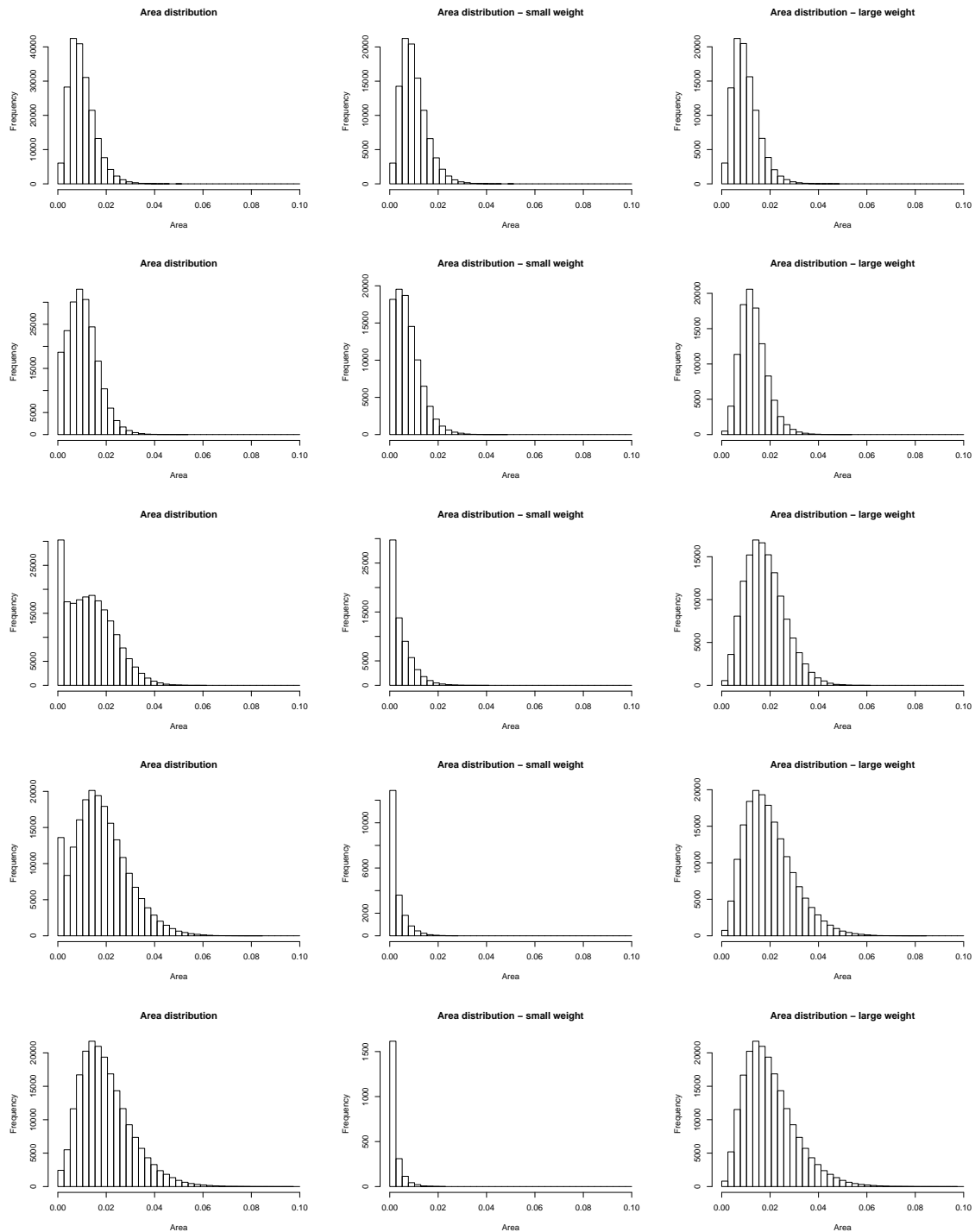


Figure 4.4: Area distribution of the typical non-empty cell of a Laguerre tessellation in  $\mathbb{R}^2$  generated by a stationary marked Poisson process with intensity  $\lambda = 100$  and mark distribution  $A(s_1, 0.01, 0.5)$ . The rows correspond to the parameters  $s_1 = 0.01$  (Voronoi case) and  $s_1 = 0.05, 0.1, 0.15, 0.2$ . The columns show the area distributions of the typical non-empty cell (left) and of the typical non-empty cells whose generators carry the weights 0.01 (middle) and  $s_1$  (right).

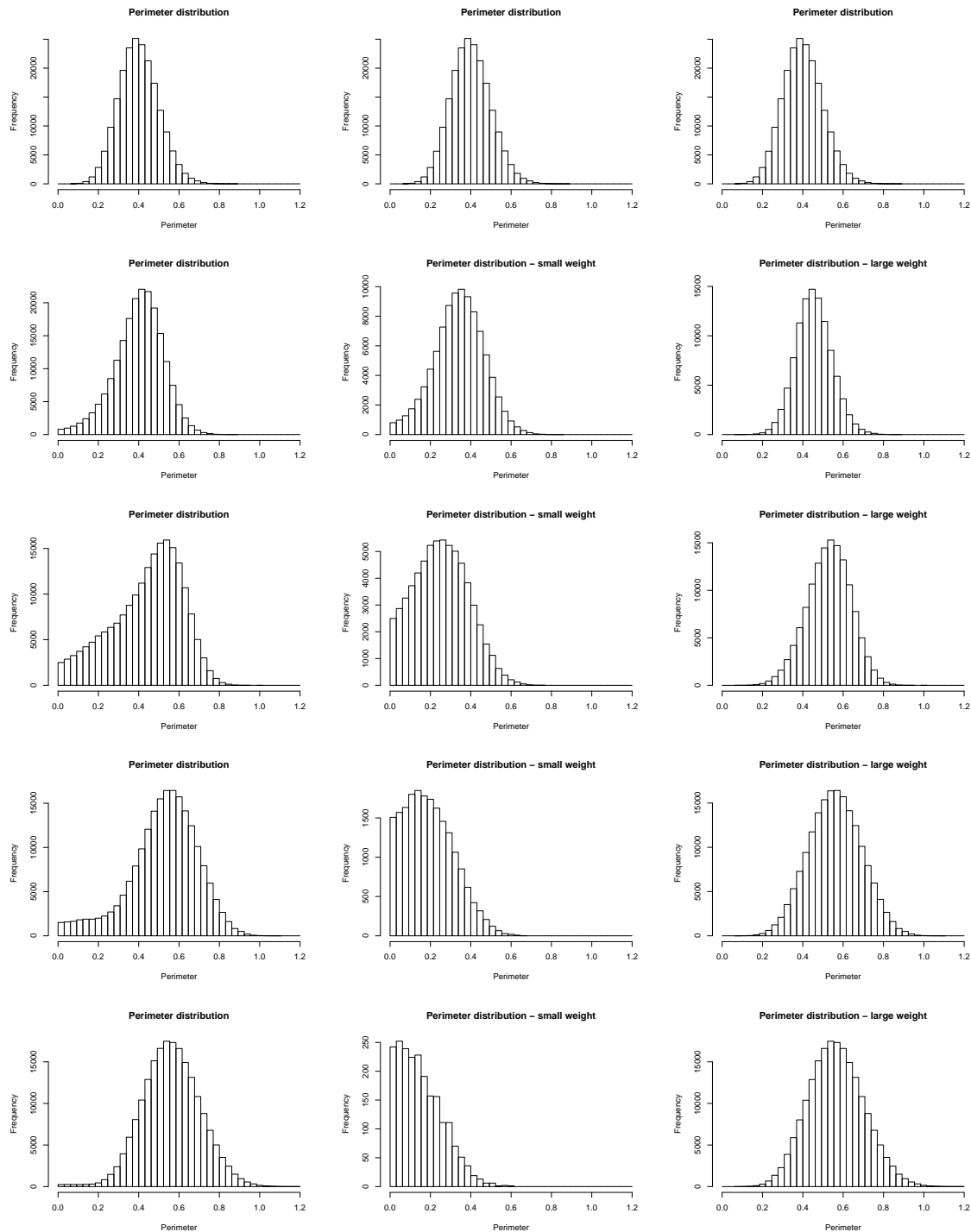


Figure 4.5: Perimeter distribution of the typical non-empty cell of a Laguerre tessellation in  $\mathbb{R}^2$  generated by a stationary marked Poisson process with intensity  $\lambda = 100$  and mark distribution  $A(s_1, 0.01, 0.5)$ . The rows correspond to the parameters  $s_1 = 0.01$  (Voronoi case) and  $s_1 = 0.05, 0.1, 0.15, 0.2$ . The columns show the perimeter distributions of the typical non-empty cell (left) and of the typical non-empty cells whose generators carry the weights 0.01 (middle) and  $s_1$  (right).

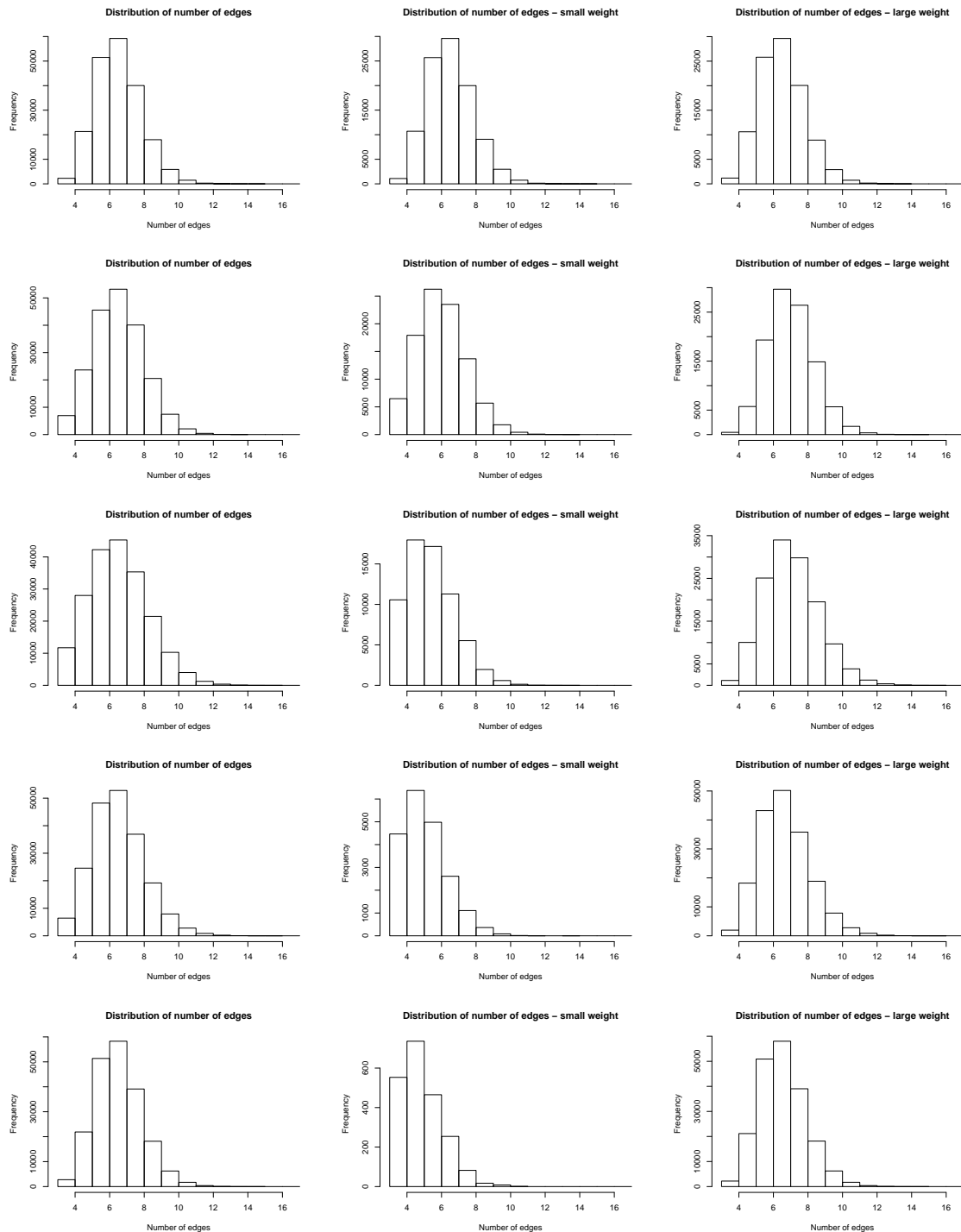


Figure 4.6: Distribution of the number of edges of the typical non-empty cell of a Laguerre tessellation in  $\mathbb{R}^2$  generated by a stationary marked Poisson process with intensity  $\lambda = 100$  and mark distribution  $A(s_1, 0.01, 0.5)$ . The rows correspond to the parameters  $s_1 = 0.01$  (Voronoi case) and  $s_1 = 0.05, 0.1, 0.15, 0.2$ . The columns show the edge number distributions of the typical non-empty cell (left) and of the typical non-empty cells whose generators carry the weights 0.01 (middle) and  $s_1$  (right).

$p$	$s_1$	$\gamma_2$	$\gamma_2^S$	$\gamma_0$	$\gamma_0^S$	$L_A$	$L_A^S$
0.1	0.05	98.865	98.711	197.730	197.422	19.688	19.671
0.1	0.10	90.204	90.201	180.408	180.401	17.870	17.866
0.1	0.15	72.748	72.883	145.496	145.767	14.805	14.826
0.1	0.20	51.855	51.870	103.709	103.741	11.598	11.607
0.1	0.25	33.694	33.557	67.387	67.113	9.104	9.092
0.1	0.30	21.373	21.328	42.746	42.656	7.569	7.561
0.1	0.35	14.630	14.715	29.260	28.430	6.798	6.808
0.1	0.40	11.600	11.595	23.199	23.190	6.478	6.473
0.3	0.05	97.065	97.176	194.129	194.354	19.301	19.312
0.3	0.10	77.138	77.112	154.276	154.224	16.078	16.075
0.3	0.15	50.548	50.587	101.095	101.175	12.853	12.860
0.3	0.20	35.381	35.396	70.762	70.791	11.380	11.388
0.3	0.25	30.848	30.807	61.695	61.615	11.013	10.998
0.3	0.30	30.081	30.049	60.162	60.098	10.959	10.958
0.3	0.35	30.005	30.013	60.009	60.027	10.955	10.960
0.3	0.40	30.000	29.986	60.000	59.972	10.955	10.952
0.5	0.05	96.203	95.937	192.406	191.875	19.203	19.176
0.5	0.10	74.199	74.274	148.398	148.548	16.283	16.287
0.5	0.15	55.484	55.477	110.968	110.954	14.529	14.522
0.5	0.20	50.525	50.468	101.050	100.937	14.173	14.165
0.5	0.25	50.022	50.021	100.043	100.043	14.143	14.143
0.5	0.30	50.001	49.997	100.001	99.993	14.142	14.144
0.7	0.05	96.591	96.713	193.182	193.426	19.359	19.368
0.7	0.10	80.054	80.049	160.107	160.097	17.485	17.482
0.7	0.15	71.140	71.195	142.280	142.389	16.798	16.804
0.7	0.20	70.039	70.018	140.077	140.036	16.735	16.732
0.7	0.25	70.001	70.015	140.001	140.030	16.733	16.735
0.7	0.30	70.000	70.010	140.000	140.020	16.733	16.734
0.9	0.05	98.459	98.518	196.918	197.035	19.737	19.747
0.9	0.10	92.255	92.408	184.509	184.816	19.120	19.138
0.9	0.15	90.125	90.133	180.250	180.265	18.980	18.978
0.9	0.20	90.002	90.097	180.003	180.193	18.974	18.985
0.9	0.25	90.000	90.024	180.000	180.048	18.974	18.977
0.9	0.30	90.000	90.062	180.000	180.125	18.974	18.981

Table 4.4: Intensities for a Laguerre tessellation in  $\mathbb{R}^2$  generated by a stationary marked Poisson process with intensity  $\lambda = 100$  and radius distribution  $A(s_1, 0.01, p)$ . The characteristics with superscript S are obtained by simulation (mean of 10,000 realizations), characteristics without superscript by numerical integration.

	$s_1$	mean	var	min	max
area	0.01	0.01001	2.837e-5	0.00017	0.05065
	0.05	0.01042	3.831e-5	0	0.05146
	0.10	0.01350	9.102e-5	0	0.06110
	0.15	0.01800	1.186e-4	0	0.08345
	0.20	0.01978	1.139e-4	0	0.09525
perimeter	0.01	0.40012	0.00955	0.06488	0.87680
	0.05	0.39972	0.01464	1.5e-5	0.88848
	0.10	0.43929	0.03040	5.0e-6	0.99135
	0.15	0.52317	0.02876	1.0e-6	1.10381
	0.20	0.56073	0.02047	1.5e-5	1.18035
number of edges	0.01	6.002	1.775	3	14
	0.05	6.005	2.197	3	14
	0.10	6.004	2.933	3	15
	0.15	5.999	2.338	3	16
	0.20	6.001	1.861	3	14

Table 4.5: Characteristics of the typical cell of a Laguerre tessellation in  $\mathbb{R}^2$  generated by a stationary marked Poisson process with intensity  $\lambda = 100$  and radius distribution  $A(s_1, 0.01, 0.5)$ .

### 4.2.3 Uniform distribution

As a second example we investigate planar Poisson Laguerre tessellations with uniformly distributed radii. In contrast to the two-atom case we will not explicitly formulate the integral formulas but only consider the results of numerical integrations and simulations.

As in the two-atom case we choose  $\lambda = 100$ , while the radius distribution is  $U(0.01, b)$ , where  $b$  starts at 0.05 and increases in steps of 0.05. Again, we evaluate numerically the formulas for  $\mu_0$  and  $\mu_1$ , compare the results to the mean values measured from 10,000 simulations, and compute the mean values of the cell characteristics. The results are shown in Tables 4.7 and 4.6. Here, also, the values are in good agreement.

$s_1$	$PV_{100}$	0.05	0.1	0.15	0.2	0.25	0.3
$\gamma_0$	200.000	196.976	172.513	129.974	92.506	69.431	55.785
$\gamma_1$	300.000	295.464	258.770	194.961	138.759	104.147	83.678
$\gamma_2$	100.000	98.488	86.113	64.619	46.253	34.715	27.893
$L_A$	20.000	19.615	17.477	14.546	12.201	10.641	9.566
$l_1$	0.06667	0.06639	0.06754	0.07461	0.08793	0.10217	0.11432
$a_2$	0.0100	0.0102	0.0116	0.0155	0.0216	0.0288	0.0359
$u_2$	0.4000	0.3983	0.4052	0.4477	0.5276	0.6130	0.6859

Table 4.6: Mean values of cell characteristics of a Laguerre tessellation in  $\mathbb{R}^2$  generated by a Poisson process with intensity  $\lambda = 100$  and mark distribution  $U(0.01, b)$ .

In order to study distributions of cell characteristics of the typical cell, we simulate 200,000 realizations of the typical non-empty cell. Means, variances, minima, and maxima of their area, perimeter, and number of edges are contained in Table 4.8. The corresponding distributions together with the distribution of the radii of their generators are shown in Figure 4.7. Again, we observe decreasing values of the intensities  $\mu_0$  and  $\mu_1$ . This time, however, there is no obvious limiting distribution. The histograms for the first steps show a rapid change in the shapes of the distributions. For larger values of  $b$  the changes are more even and the distributions seem to stabilize at a certain shape while their support increases. As in the two-atom case we find a large number of very small cells.

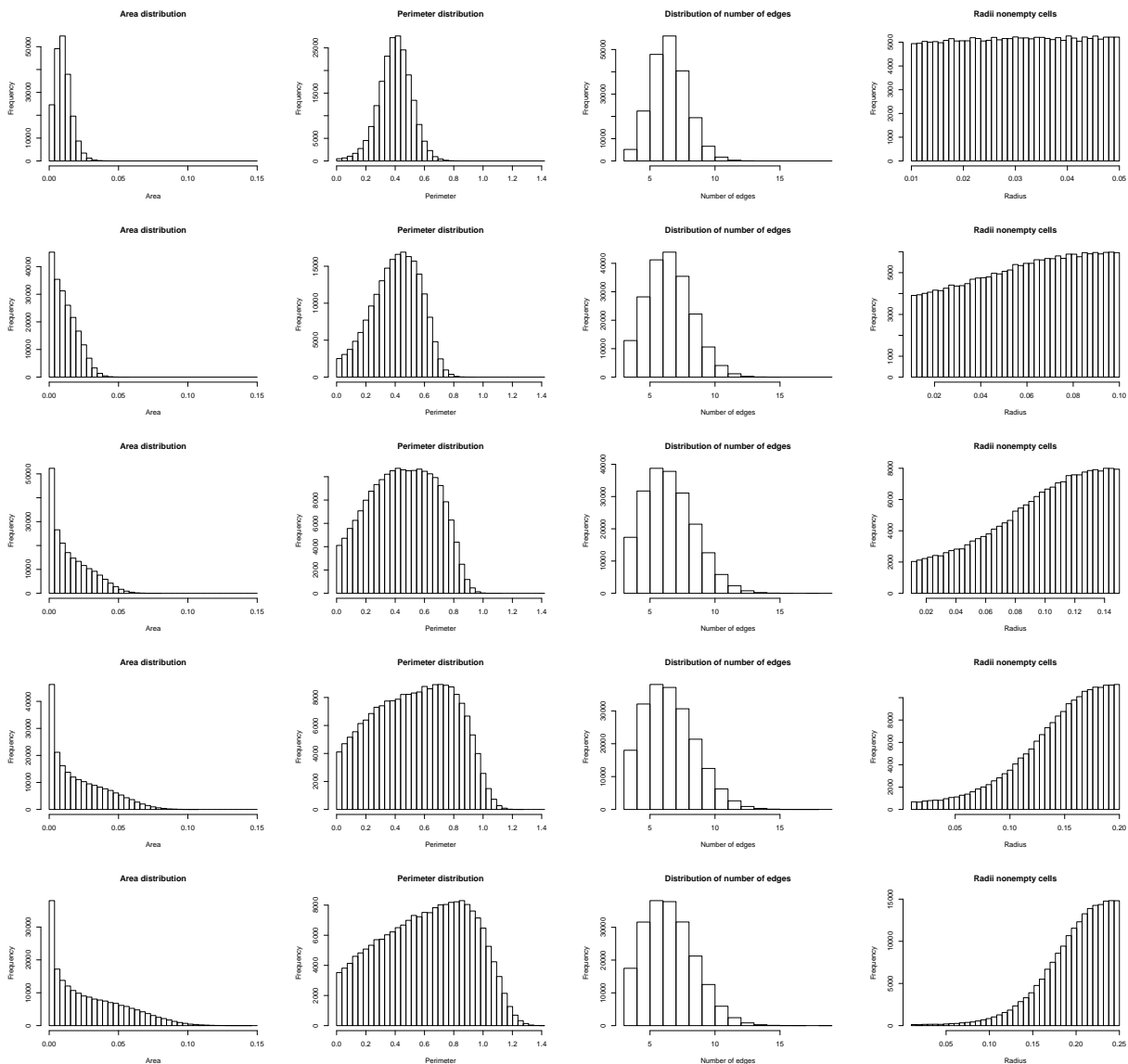


Figure 4.7: Distribution of area, perimeter, number of edges, and radius of the generating circle (from left to right) of the typical non-empty cell of a Laguerre tessellation in  $\mathbb{R}^2$  generated by a Poisson process with intensity  $\lambda = 100$  and mark distribution  $U(0.01, b)$ . The rows correspond to the parameters  $b = 0.05, 0.1, 0.15, 0.2, 0.25$ .

$a$	$b$	$\gamma_2$	$\gamma_2^S$	$\gamma_0$	$\gamma_0^S$	$L_A$	$L_A^S$
0.01	0.05	98.488	98.459	196.976	197.918	19.615	19.617
0.01	0.10	86.113	86.057	172.226	172.115	17.477	17.476
0.01	0.15	64.619	64.705	129.237	129.411	14.546	14.541
0.01	0.20	46.253	46.344	92.506	92.688	12.201	12.204
0.01	0.25	34.715	34.814	69.431	69.628	10.641	10.639
0.01	0.30	27.893	27.810	55.785	55.619	9.566	9.560
0.01	0.35	23.195	23.295	46.391	46.589	8.767	8.773
0.01	0.40	20.032	19.981	40.064	39.962	8.148	8.140

Table 4.7: Intensities for a Laguerre tessellation in  $\mathbb{R}^2$  generated by a Poisson process with intensity  $\lambda = 100$  and radius distribution  $U(a, b)$ . The characteristics with superscript S are obtained by simulation (mean of 10,000 realizations), characteristics without superscript by numerical integration.

	$a$	$b$	mean	var	min	max
area	0.01	0.05	0.010158	3.2892e-5	0	0.05385
	0.01	0.10	0.011601	7.6127e-5	0	0.06399
	0.01	0.15	0.015474	1.9257e-4	0	0.08425
	0.01	0.20	0.021659	3.8921e-4	0	0.11881
	0.01	0.25	0.028860	6.5194e-4	0	0.14515
perimeter	0.01	0.05	0.39841	0.01218	0.00012	0.88004
	0.01	0.10	0.40554	0.02597	5.8e-5	0.94447
	0.01	0.15	0.44923	0.04854	1.4e-5	1.09619
	0.01	0.20	0.52728	0.07216	3.0e-6	1.27365
	0.01	0.25	0.61234	0.09250	3.0e-6	1.41067
number of edges	0.01	0.05	5.9997	2.0007	3	13
	0.01	0.10	5.9981	2.9830	3	15
	0.01	0.15	5.9959	3.7364	3	17
	0.01	0.20	6.0063	3.8906	3	17
	0.01	0.25	6.0072	3.7834	3	18

Table 4.8: Characteristics of the typical cell of a Laguerre tessellation in  $\mathbb{R}^2$  generated by a Poisson process with intensity  $\lambda = 100$  and radius distribution  $U(a, b)$ .

### 4.3 The spatial case

Now we will have a closer look at the three-dimensional case. We proceed as for  $d = 2$ . Let  $\Phi$  be a stationary marked Poisson process on  $\mathbb{R}^3 \times \mathbb{R}^+$  with intensity  $\lambda > 0$  and mark distribution  $\mathbb{F}$  with property (3.3).

### 4.3.1 General formulas

#### Formulas for $\Delta_m^{k+1}$ and $V_{m,k}$

The first step is again the derivation of explicit formulas for  $\Delta_m^{k+1}$  and  $V_{m,k}$ . This time,  $\Delta_3$ ,  $\Delta_2^2$ , and  $\Delta_1^3$  are required. Again,  $\Delta_3(w_0u_0, \dots, w_3u_3)$  is intractable. A formula for  $\Delta_2^2(w_0u_0, w_1u_1, w_2u_2)$  can in principle be computed but looks rather complicated. Nevertheless, we get

$$V_{2,1}(w_0, w_1, w_2) = 4\pi^3(w_0^2w_1^2 + w_0^2w_2^2 + w_1^2w_2^2), \quad w_0, w_1, w_2 > 0,$$

and for  $0 \leq w_0 \leq w_1$  we obtain

$$\Delta_1^3(w_0u_0, w_1u_1) = w_1(w_1^2 + 3w_0^2) - w_0(3w_1^2 + w_0^2) \langle u_0, u_1 \rangle, \quad u_0, u_1 \in S^2 \cap L, w_0, w_1 > 0$$

and

$$V_{1,2}(w_0, w_1) = 4w_1(w_1^2 + 3w_0^2), \quad w_0, w_1 > 0.$$

Note that the last two expressions are not symmetric in  $w_0$  and  $w_1$ . Therefore, one has to be careful which of the occurring radii is the smaller one when applying these formulas.

#### The representation of $\mathbb{Q}_k$

Now we insert the formulas derived above in the distribution formulas given in Theorem 3.2.4. In each case let  $h$  be a non-negative measurable function defined on a suitable domain. With respect to  $\mathbb{Q}_0$ , the neighborhood of the vertex in the origin is described by the random variables  $(\Phi^{P_0}, P_0, \Psi_0)$ , whose distribution function is given by

$$\begin{aligned} & \mathbb{E}_{M_0} [h(\Phi^{P_0}, P_0, \Psi_0)] \\ &= \frac{\lambda^4}{8} \int_0^\infty \int_0^\infty \int_0^\infty \int_0^\infty \int_{-\min_i r_i^2}^\infty \prod_{i=0}^3 (t + r_i^2)^{\frac{1}{2}} e^{-\frac{4}{3}\pi\lambda \int_0^\infty ([t+r^2]^+)^{\frac{3}{2}} \mathbb{F}(dr)} \\ & \int_{S^2} \int_{S^2} \int_{S^2} \int_{S^2} \mathbb{E} [h(\Phi^t, t, \{(u_0, r_0), (u_1, r_1), (u_2, r_2), (u_3, r_3)\})] \Delta_3 \left( (t + r_0^2)^{\frac{1}{2}} u_0, \dots, (t + r_3^2)^{\frac{1}{2}} u_3 \right) \\ & \mathbb{S}(du_0) \dots \mathbb{S}(du_3) dt \mathbb{F}(dr_0) \mathbb{F}(dr_1) \mathbb{F}(dr_2) \mathbb{F}(dr_3). \end{aligned}$$

With respect to  $\mathbb{Q}_1$ , the point process  $\Phi$  is determined by the tuple  $(\Phi^{P_1}, P_1', P_1'', \Psi_1, U_1)$  and we have

$$\begin{aligned} & \mathbb{E}_{M_1} [h(\Phi^{P_1}, P_1', P_1'', \Psi_1, U_1)] \\ &= \frac{\lambda^3 \pi}{3} \int_0^\infty \int_0^\infty \int_0^\infty \int_{-\min_i r_i^2}^\infty \int_0^\infty e^{-\frac{4}{3}\pi\lambda \int_0^\infty ([s+t+r^2]^+)^{\frac{3}{2}} \mathbb{F}(dr)} s^{-\frac{1}{2}} \\ & \int_{S^2 \cap L} \int_{S^2 \cap L} \int_{S^2 \cap L} \int_{S^2 \cap L^\perp} \int_{SO_3} \mathbb{E} [h(\Phi^{t+s}, t, s, \{(\vartheta u_0, r_0), (\vartheta u_1, r_1), (\vartheta u_2, r_2)\}, \vartheta u)] \\ & \Delta_2^2 \left( (t + r_0^2)^{\frac{1}{2}} u_0, (t + r_1^2)^{\frac{1}{2}} u_1, (t + r_2^2)^{\frac{1}{2}} u_2 \right) \nu(d\vartheta) \mathbb{S}_{L^\perp}(du) \mathbb{S}_L(du_0) \mathbb{S}_L(du_1) \mathbb{S}_L(du_2) ds dt \\ & \mathbb{F}(dr_0) \mathbb{F}(dr_1) \mathbb{F}(dr_2). \end{aligned}$$

Again, we disintegrate with respect to  $\Psi_1$ , which yields

$$\begin{aligned} & \mathbb{E}_{M_1} [h(\Phi^{P_1}, P'_1, P''_1, U_1)] \\ &= \frac{\lambda^3 \pi^4}{3} \int_0^\infty \int_0^\infty \int_{-\min_i r_i^2}^\infty \int_0^\infty e^{-\frac{4}{3}\pi\lambda \int_0^\infty ([s+t+r^2]^+)^{\frac{3}{2}} \mathbb{F}(dr)} s^{-\frac{1}{2}} \int_{S^2 \cap L^\perp} \int_{SO_3} \mathbb{E} [h(\Phi^{t+s}, t, s, \vartheta u)] \\ & \quad (r_1^2 r_2^2 + r_0^2 r_1^2 + r_0^2 r_2^2 + 2t(r_0^2 + r_1^2 + r_2^2) + 3t^2) \nu(d\vartheta) \mathbb{S}_{L^\perp}(du) ds dt \mathbb{F}(dr_0) \mathbb{F}(dr_1) \mathbb{F}(dr_2). \end{aligned}$$

With respect to  $\mathbb{Q}_2$ , the point process  $\Phi$  is determined by the tuple  $(\Phi^{P_2}, P'_2, P''_2, \Psi_2, U_2)$ . As remarked earlier, the formulas for  $\Delta_1^3$  and  $V_{1,2}$  require information on the order of the radii  $r_0$  and  $r_1$ . Therefore, we arrange integration in a way that  $r_0 \leq r_1$  always holds. To do so, we have to distinguish between continuous and discrete distributions of radii. If we assume a continuous distribution the corresponding formulas read

$$\begin{aligned} & \mathbb{E}_{M_2} [h(\Phi^{P_2}, P'_2, P''_2, \Psi_2, U_2)] \\ &= \frac{\lambda^2 \pi}{2} \int_0^\infty \int_0^{r_1} \int_{-r_0^2}^\infty \left( \frac{4t + r_1^2 + 3r_0^2}{(t + r_0^2)^{\frac{1}{2}}} - \frac{(4t + 3r_1^2 + r_0^2)\langle u_0, u_1 \rangle}{(t + r_1^2)^{\frac{1}{2}}} \right) \int_0^\infty e^{-\frac{4}{3}\pi\lambda \int_0^\infty ([s+t+r^2]^+)^{\frac{3}{2}} \mathbb{F}(dr)} \\ & \quad \int_{S^2 \cap L} \int_{S^2 \cap L} \int_{SO_3} \int_{S^2 \cap L^\perp} \mathbb{E} [h(\Phi^{t+s}, t, s, \{(\vartheta u_0, r_0), (\vartheta u_1, r_1)\}, \vartheta u)] \mathbb{S}_{L^\perp}(du) \nu(d\vartheta) \mathbb{S}_L(du_0) \\ & \quad \mathbb{S}_L(du_1) ds dt \mathbb{F}(dr_0) \mathbb{F}(dr_1) \end{aligned}$$

and

$$\begin{aligned} & \mathbb{E}_{M_2} [h(\Phi^{P_2}, P'_2, P''_2, U_2)] \\ &= 2\lambda^2 \pi \int_0^\infty \int_0^{r_1} \int_{-r_0^2}^\infty \int_0^\infty e^{-\frac{4}{3}\pi\lambda \int_0^\infty ([s+t+r^2]^+)^{\frac{3}{2}} \mathbb{F}(dr)} \frac{4t + r_1^2 + 3r_0^2}{(t + r_0^2)^{\frac{1}{2}}} \int_{SO_3} \int_{S^2 \cap L^\perp} \mathbb{E} [h(\Phi^{t+s}, t, s, \vartheta u)] \\ & \quad \mathbb{S}_{L^\perp}(du) \nu(d\vartheta) ds dt \mathbb{F}(dr_0) \mathbb{F}(dr_1). \end{aligned}$$

For a discrete distribution  $\mathbb{F}$  which takes the values  $r_i, i = 0, \dots, n$ , such that  $0 \leq r_0 < r_1 < \dots < r_n$  with probability  $p_i \in [0, 1]$  we get

$$\begin{aligned} & \mathbb{E}_{M_2} [h(\Phi^{P_2}, P'_2, P''_2, \Psi_2, U_2)] \\ &= \frac{\lambda^2 \pi}{2} \sum_{i=0}^n \sum_{j=i+1}^n p_i p_j \int_{-r_i^2}^\infty \left( \frac{4t + r_j^2 + 3r_i^2}{(t + r_i^2)^{\frac{1}{2}}} - \frac{(4t + 3r_j^2 + r_i^2)\langle u_0, u_1 \rangle}{(t + r_j^2)^{\frac{1}{2}}} \right) \int_0^\infty e^{-\frac{4}{3}\pi\lambda \sum_{k=0}^n p_k ([s+t+r_k^2]^+)^{\frac{3}{2}}} \\ & \quad \int_{S^2 \cap L} \int_{S^2 \cap L} \int_{SO_3} \int_{S^2 \cap L^\perp} \mathbb{E} [h(\Phi^{t+s}, t, s, \{(\vartheta u_0, r_i), (\vartheta u_1, r_j)\}, \vartheta u)] \mathbb{S}_{L^\perp}(du) \nu(d\vartheta) \mathbb{S}_L(du_0) \\ & \quad \mathbb{S}_L(du_1) ds dt \\ & + 4\lambda^2 \pi \sum_{i=0}^n p_i^2 \int_{-r_i^2}^\infty (t + r_i^2)^{\frac{1}{2}} \int_0^\infty e^{-\frac{4}{3}\pi\lambda \sum_{k=0}^n p_k ([s+t+r_k^2]^+)^{\frac{3}{2}}} \end{aligned}$$

$$\int_{SO_3} \int_{S^2 \cap L^\perp} \mathbb{E} [h(\Phi^{t+s}, t, s, \{(\vartheta u_0, r_i), (-\vartheta u_0, r_i)\}, \vartheta u)] \mathbb{S}_{L^\perp}(du) \nu(d\vartheta) ds dt,$$

where  $u_0 \in S^2 \cap L$  is fixed, and

$$\begin{aligned} & \mathbb{E}_{M_2} [h(\Phi^{P_2}, P'_2, P''_2, U_2)] \\ &= 2\lambda^2 \pi \sum_{i=0}^n \sum_{j=i+1}^n p_i p_j \int_{-r_i^2}^{\infty} \int_0^{\infty} e^{-\frac{4}{3}\pi\lambda \sum_{k=0}^n p_k ([s+t+r_k^2]^+)^{\frac{3}{2}}} \frac{4t + r_j^2 + 3r_i^2}{(t + r_i^2)^{\frac{1}{2}}} \int_{SO_3} \int_{S^2 \cap L^\perp} \mathbb{E} [h(\Phi^{t+s}, t, s, \vartheta u)] \\ & \quad \mathbb{S}_{L^\perp}(du) \nu(d\vartheta) ds dt \\ &+ 4\lambda^2 \pi \sum_{i=0}^n p_i^2 \int_{-r_i^2}^{\infty} \int_0^{\infty} e^{-\frac{4}{3}\pi\lambda \sum_{k=0}^n p_k ([s+t+r_k^2]^+)^{\frac{3}{2}}} (t + r_i^2)^{\frac{1}{2}} \int_{SO_3} \int_{S^2 \cap L^\perp} \mathbb{E} [h(\Phi^{t+s}, t, s, \vartheta u)] \mathbb{S}_{L^\perp}(du) \\ & \quad \nu(d\vartheta) ds dt. \end{aligned}$$

### The intensities $\mu_k$

For the intensities  $\mu_k$  we have

$$\begin{aligned} \mu_0 &= \frac{\lambda^4}{48} \int_0^\infty \int_0^\infty \int_0^\infty \int_0^\infty \int_{-\min_i r_i^2}^\infty \prod_{i=0}^3 (t + r_i^2)^{\frac{1}{2}} e^{-\frac{4}{3}\pi\lambda \int_0^\infty ([t+r^2]^+)^{\frac{3}{2}} \mathbb{F}(dr)} V_{3,0} \left( (t + r_0^2)^{\frac{1}{2}}, \dots, (t + r_3^2)^{\frac{1}{2}} \right) dt \\ & \quad \mathbb{F}(dr_0) \mathbb{F}(dr_1) \mathbb{F}(dr_2) \mathbb{F}(dr_3), \\ \mu_1 &= \frac{2\lambda^3 \pi^4}{3} \int_0^\infty \int_0^\infty \int_{0-\min_i r_i^2}^\infty \int_0^\infty (r_1^2 r_2^2 + r_0^2 r_1^2 + r_0^2 r_2^2 + 2t(r_0^2 + r_1^2 + r_2^2) + 3t^2) \int_0^\infty e^{-\frac{4}{3}\pi\lambda \int_0^\infty ([s+t+r^2]^+)^{\frac{3}{2}} \mathbb{F}(dr)} \\ & \quad s^{-\frac{1}{2}} ds dt \mathbb{F}(dr_0) \mathbb{F}(dr_1) \mathbb{F}(dr_2) \end{aligned}$$

and, if  $\mathbb{F}$  is a continuous distribution,

$$\mu_2 = 4\lambda^2 \pi^2 \int_0^\infty \int_0^{r_1} \int_{-r_0^2}^\infty \frac{4t + 3r_0^2 + r_1^2}{(t + r_0^2)^{\frac{1}{2}}} \int_0^\infty e^{-\frac{4}{3}\pi\lambda \int_0^\infty ([s+t+r^2]^+)^{\frac{3}{2}} \mathbb{F}(dr)} ds dt \mathbb{F}(dr_0) \mathbb{F}(dr_1).$$

For a discrete distribution  $\mathbb{F}$  as described above we get

$$\begin{aligned} \mu_2 &= 4\lambda^2 \pi^2 \sum_{i=0}^n \sum_{j=i+1}^n p_i p_j \int_{-r_i^2}^\infty \frac{4t + 3r_i^2 + r_j^2}{(t + r_i^2)^{\frac{1}{2}}} \int_0^\infty e^{-\frac{4}{3}\pi\lambda \sum_{k=0}^n p_k ([s+t+r_k^2]^+)^{\frac{3}{2}}} ds dt \\ & \quad + 8\lambda^2 \pi^2 \sum_{i=0}^n p_i^2 \int_{-r_i^2}^\infty (t + r_i^2)^{\frac{1}{2}} \int_0^\infty e^{-\frac{4}{3}\pi\lambda \sum_{k=0}^n p_k ([s+t+r_k^2]^+)^{\frac{3}{2}}} ds dt. \end{aligned}$$

**Remark 4.3.1**

For a spatial Poisson Laguerre tessellation formula (3.9) only yields  $\gamma_0$ ,  $L_V$ , and  $S_V$ . For a complete determination of the mean cell characteristics, we still lack the value of  $\gamma_3$  or, equivalently, of the probability  $p_0$ . So far the only way to determine this value is by simulation.

**The mean content of  $F_k(0)$** 

The mean length of the edge  $F_1(0)$  is given by

$$\begin{aligned} \mathbb{E}_{M_1}^0 [\mathcal{H}^1(F_1(0))] &= \frac{2\lambda^3\pi^4}{3\mu_1} \int_0^\infty \int_0^\infty \int_0^\infty \int_{-\min_i r_i^2}^\infty (r_1^2 r_2^2 + r_0^2 r_1^2 + r_0^2 r_2^2 + 2t(r_0^2 + r_1^2 + r_2^2) + 3t^2) \\ &\quad \sum_{\theta \in \{0, \pi\}} \int_0^\infty \int_0^\infty \xi(l, s+t, \tau(l, t, s, \theta)) s^{-\frac{1}{2}} dl ds dt \mathbb{F}(dr_0) \mathbb{F}(dr_1) \mathbb{F}(dr_2). \end{aligned}$$

The mean area of the facet  $F_2(0)$  for a continuous distribution  $\mathbb{F}$  is

$$\begin{aligned} \mathbb{E}_{M_2}^0 [\mathcal{H}^2(F_2(0))] &= \frac{4\lambda^2\pi^2}{\mu_2} \int_0^\infty \int_0^{r_1} \int_{-r_0}^\infty \frac{(4t + r_1^2 + 3r_0^2)}{(t + r_0^2)^{\frac{1}{2}}} \int_0^{2\pi} \int_0^\infty \int_0^\infty \xi(l, s+t, \tau(l, t, s, \theta)) l dl ds d\theta dt \mathbb{F}(dr_0) \mathbb{F}(dr_1). \end{aligned}$$

For a discrete distribution we get

$$\begin{aligned} \mathbb{E}_{M_2}^0 [\mathcal{H}^2(F_2(0))] &= \frac{4\lambda^2\pi^2}{\mu_2} \sum_{i=0}^n \sum_{j=i+1}^n p_i p_j \int_{-r_i}^\infty \frac{(4t + r_j^2 + 3r_i^2)}{(t + r_i^2)^{\frac{1}{2}}} \int_0^\infty \int_0^\infty \int_0^{2\pi} \xi(l, s+t, \tau(l, t, s, \theta)) l dl ds d\theta dt \\ &\quad + \frac{8\lambda^2\pi^2}{\mu_2} \sum_{i=0}^n p_i^2 \int_{-r_i}^\infty (t + r_i^2)^{\frac{1}{2}} \int_0^\infty \int_0^\infty \int_0^{2\pi} \xi(l, s+t, \tau(l, t, s, \theta)) l dl ds d\theta dt. \end{aligned}$$

Finally, the mean volume of the cell  $F_3(0)$  containing the origin is given by

$$\mathbb{E}_{M_3}^0 [\mathcal{H}^3(F_3(0))] = 4\pi^2\lambda \int_0^\infty \int_{-r_0^2}^\infty (t + r_0^2)^{\frac{1}{2}} \int_0^\infty \int_0^\pi \xi(l, t, \rho(l, t, r_0, \theta)) l^2 \sin(\theta) d\theta dl dt \mathbb{F}(dr_0).$$

**The linear contact distribution**

The formula for the linear contact distribution function is

$$H_l(r) = 1 - \lambda\pi \int_0^\infty \int_{-r_0^2}^\infty (t + r_0^2)^{\frac{1}{2}} \int_0^\pi \xi(r, t, \rho(r, t, r_0, \theta)) \sin(\theta) d\theta dt \mathbb{F}(dr_0), \quad r \geq 0,$$

where again

$$\xi(r, t, \rho) = \exp \left( -\lambda \int_0^\infty \kappa(r, ([t+w^2]^+)^\frac{1}{2}, ([\rho+w^2]^+)^\frac{1}{2}) \mathbb{F}(dr) \right), \quad r \geq 0, t, \rho \in \mathbb{R}.$$

This time, we have

$$\begin{aligned} \kappa \left( r, (t+w^2)^\frac{1}{2}, (\rho+w^2)^\frac{1}{2} \right) &= \frac{2\pi}{3} \left( (t+w^2)^\frac{3}{2} \left( 1 + \frac{t-\rho+r^2}{4r(t+w^2)^\frac{1}{2}} \left( 3 - \frac{(t-\rho+r^2)^2}{4r^2(t+w^2)} \right) \right) \right. \\ &\quad \left. + (\rho+w^2)^\frac{3}{2} \left( 1 + \frac{\rho-t+r^2}{4r(\rho+w^2)^\frac{1}{2}} \left( 3 - \frac{(\rho-t+r^2)^2}{4r^2(\rho+w^2)} \right) \right) \right) \end{aligned}$$

for  $r > 0$ ,  $t+w^2 > 0$ , and  $\rho+w^2 > 0$  if  $|(t+w^2)^\frac{1}{2} - (\rho+w^2)^\frac{1}{2}| < r < (t+w^2)^\frac{1}{2} + (\rho+w^2)^\frac{1}{2}$ . The formulas for the other cases in (3.14) are again obvious.

### The chord length distribution

The formula for the chord length distribution function reads

$$\begin{aligned} L(r) &= 1 - \frac{2\pi\lambda^2}{\mu_2} \int_0^\infty \int_{-r_0^2}^\infty (t+r_0^2)^\frac{1}{2} \int_0^\pi \int_0^\infty \kappa'(r, t, r_0, w, \theta) \mathbb{F}(dw) \xi(r, t, \rho(r, t, r_0, \theta)) \sin(\theta) d\theta dt \\ &\quad \mathbb{F}(dr_0), \quad r \geq 0, \end{aligned}$$

where  $\xi$  and  $\kappa$  are defined as above and

$$\kappa'(r, t, r_0, w, \theta) = \frac{d}{dr} \kappa \left( r, ([t+w^2]^+)^\frac{1}{2}, ([\rho(r, t, r_0, \theta) + w^2]^+)^\frac{1}{2} \right)$$

for  $r, r_0, w \geq 0, t \in \mathbb{R}$ , and  $\theta \in [0, 2\pi]$ .

### 4.3.2 Two-atom distribution

Choose  $0 \leq s_0 < s_1$  and  $0 \leq p \leq 1$ . Consider a stationary Poisson process  $\Phi$  on  $\mathbb{R}^2$  with intensity  $\lambda$  and mark distribution  $A(s_1, s_0, p)$ . Then

$$p(t) = \begin{cases} p_1(t) := e^{-\frac{4}{3}\lambda\pi(p(t+s_1^2)^\frac{3}{2} + (1-p)(t+s_0^2)^\frac{3}{2})}, & \text{if } -s_0^2 < t, \\ p_2(t) := e^{-\frac{4}{3}\lambda\pi p(t+s_1^2)^\frac{3}{2}}, & \text{if } -s_1^2 \leq t \leq -s_0^2. \end{cases}$$

Again, we consider random variables  $N_{k,j}$  defined analogously to (4.1) and distinguish between different configurations of radii. Let  $h$  be a non-negative measurable function defined on a suitable domain. Then the distribution formulas with respect to  $\mathbb{Q}_0$  for the corresponding Laguerre tessellation are given by

$$\begin{aligned} &\mathbb{E}_{M_0} [h(\Phi^{P_0}, P_0, \Psi_0) | N_{0,0} = 4] \\ &= \frac{\lambda^4(1-p)^4}{8} \int_{-s_0^2}^\infty (t+s_0^2)^\frac{7}{2} p_1(t) \int_{s^2} \int_{s^2} \int_{s^2} \int_{s^2} \mathbb{E} [h(\Phi^t, t, \{(u_0, s_0), (u_1, s_0), (u_2, s_0), (u_3, s_0)\})] \\ &\quad \Delta_3(u_0, u_1, u_2, u_3) \mathbb{S}(du_0) \mathbb{S}(du_1) \mathbb{S}(du_2) \mathbb{S}(du_3) dt, \end{aligned}$$

$$\begin{aligned}
& \mathbb{E}_{M_0} [h(\Phi^{P_0}, P_0, \Psi_0) \mid N_{0,1} = 4] \\
&= \frac{\lambda^4 p^4}{8} \int_{-s_0^2}^{\infty} (t + s_1^2)^{\frac{7}{2}} p_1(t) \int_{S^2} \int_{S^2} \int_{S^2} \int_{S^2} \mathbb{E} [h(\Phi^t, t, \{(u_0, s_1), (u_1, s_1), (u_2, s_1), (u_3, s_1)\})] \\
&\quad \Delta_3(u_0, u_1, u_2, u_3) \mathbb{S}(du_0) \mathbb{S}(du_1) \mathbb{S}(du_2) \mathbb{S}(du_3) dt \\
&+ \frac{\lambda^4 p^4}{8} \int_{-s_1^2}^{-s_0^2} (t + s_1^2)^{\frac{7}{2}} p_2(t) \int_{S^2} \int_{S^2} \int_{S^2} \int_{S^2} \mathbb{E} [h(\Phi^t, t, \{(u_0, s_1), (u_1, s_1), (u_2, s_1), (u_3, s_1)\})] \\
&\quad \Delta_3(u_0, u_1, u_2, u_3) \mathbb{S}(du_0) \mathbb{S}(du_1) \mathbb{S}(du_2) \mathbb{S}(du_3) dt,
\end{aligned}$$

$$\begin{aligned}
& \mathbb{E}_{M_0} [h(\Phi^{P_0}, P_0, \Psi_0) \mid N_{0,0} = 3, N_{0,1} = 1] \\
&= \frac{\lambda^4 (1-p)^3 p}{2} \int_{-s_0^2}^{\infty} (t + s_1^2)^{\frac{1}{2}} (t + s_0^2)^{\frac{3}{2}} p_1(t) \\
&\quad \int_{S^2} \int_{S^2} \int_{S^2} \int_{S^2} \mathbb{E} [h(\Phi^t, t, \{(u_0, s_1), (u_1, s_0), (u_2, s_0), (u_3, s_0)\})] \\
&\quad \Delta_3((t + s_1)^{\frac{1}{2}} u_0, (t + s_0)^{\frac{1}{2}} u_1, (t + s_0)^{\frac{1}{2}} u_2, (t + s_0)^{\frac{1}{2}} u_3) \mathbb{S}(du_0) \mathbb{S}(du_1) \mathbb{S}(du_2) \mathbb{S}(du_3) dt,
\end{aligned}$$

$$\begin{aligned}
& \mathbb{E}_{M_0} [h(\Phi^{P_0}, P_0, \Psi_0) \mid N_{0,0} = 1, N_{0,1} = 3] \\
&= \frac{\lambda^4 (1-p)^3 p^3}{2} \int_{-s_0^2}^{\infty} (t + s_1^2)^{\frac{3}{2}} (t + s_0^2)^{\frac{1}{2}} p_1(t) \\
&\quad \int_{S^2} \int_{S^2} \int_{S^2} \int_{S^2} \mathbb{E} [h(\Phi^t, t, \{(u_0, s_1), (u_1, s_1), (u_2, s_1), (u_3, s_0)\})] \\
&\quad \Delta_3((t + s_1)^{\frac{1}{2}} u_0, (t + s_1)^{\frac{1}{2}} u_1, (t + s_1)^{\frac{1}{2}} u_2, (t + s_0)^{\frac{1}{2}} u_3) \mathbb{S}(du_0) \mathbb{S}(du_1) \mathbb{S}(du_2) \mathbb{S}(du_3) dt,
\end{aligned}$$

and

$$\begin{aligned}
& \mathbb{E}_{M_0} [h(\Phi^{P_0}, P_0, \Psi_0) \mid N_{0,0} = 2, N_{0,1} = 2] \\
&= \frac{3\lambda^4 (1-p)^2 p^2}{4} \int_{-s_0^2}^{\infty} (t + s_1^2) (t + s_0^2) p_1(t) \\
&\quad \int_{S^2} \int_{S^2} \int_{S^2} \int_{S^2} \mathbb{E} [h(\Phi^t, t, \{(u_0, s_1), (u_1, s_1), (u_2, s_0), (u_3, s_0)\})] \\
&\quad \Delta_3((t + s_1)^{\frac{1}{2}} u_0, (t + s_1)^{\frac{1}{2}} u_1, (t + s_0)^{\frac{1}{2}} u_2, (t + s_0)^{\frac{1}{2}} u_3) \mathbb{S}(du_0) \mathbb{S}(du_1) \mathbb{S}(du_2) \mathbb{S}(du_3) dt.
\end{aligned}$$

With respect to  $\mathbb{Q}_1$ , we obtain

$$\begin{aligned} & \mathbb{E}_{M_1} [h(\Phi^{P_1}, P'_1, P''_1, \Psi_1, U_1) \mid N_{1,0} = 3] \\ &= \frac{\lambda^3 \pi}{3} (1-p)^3 \int_{-s_0^2}^{\infty} (t+s_0^2)^2 \int_0^{\infty} p_1(s+t) s^{-\frac{1}{2}} \int_{S^2 \cap L} \int_{S^2 \cap L} \int_{S^2 \cap L} \Delta_2^2(u_0, u_1, u_2) \\ & \quad \int_{SO_3} \int_{S^2 \cap L^\perp} \mathbb{E}[h(\Phi^{s+t}, s, t, \{(\vartheta u_0, s_0), (\vartheta u_1, s_0), (\vartheta u_2, s_0)\}, \vartheta u)] \mathbb{S}_{L^\perp}(du) \nu(d\vartheta) \mathbb{S}_L(du_0) \\ & \quad \mathbb{S}_L(du_1) \mathbb{S}_L(du_2) ds dt, \end{aligned}$$

$$\begin{aligned} & \mathbb{E}_{M_1} [h(\Phi^{P_1}, P'_1, P''_1, \Psi_1, U_1) \mid N_{1,1} = 3] \\ &= \frac{\lambda^3 \pi}{3} p^3 \int_{-s_0^2}^{\infty} (t+s_1^2)^2 \int_0^{\infty} p_1(s+t) s^{-\frac{1}{2}} \int_{S^2 \cap L} \int_{S^2 \cap L} \int_{S^2 \cap L} \Delta_2^2(u_0, u_1, u_2) \\ & \quad \int_{SO_3} \int_{S^2 \cap L^\perp} \mathbb{E}[h(\Phi^{s+t}, s, t, \{(\vartheta u_0, s_1), (\vartheta u_1, s_1), (\vartheta u_2, s_1)\}, \vartheta u)] \mathbb{S}_{L^\perp}(du) \nu(d\vartheta) \mathbb{S}_L(du_0) \\ & \quad \mathbb{S}_L(du_1) \mathbb{S}_L(du_2) ds dt \\ &+ \frac{\lambda^3 \pi}{3} p^3 \int_{-s_1^2}^{-s_0^2} (t+s_1^2)^2 \int_0^{-(t+s_0^2)} p_2(s+t) s^{-\frac{1}{2}} \int_{S^2 \cap L} \int_{S^2 \cap L} \int_{S^2 \cap L} \Delta_2^2(u_0, u_1, u_2) \\ & \quad \int_{SO_3} \int_{S^2 \cap L^\perp} \mathbb{E}[h(\Phi^{s+t}, s, t, \{(\vartheta u_0, s_1), (\vartheta u_1, s_1), (\vartheta u_2, s_1)\}, \vartheta u)] \mathbb{S}_{L^\perp}(du) \nu(d\vartheta) \mathbb{S}_L(du_0) \\ & \quad \mathbb{S}_L(du_1) \mathbb{S}_L(du_2) ds \\ &+ \frac{\lambda^3 \pi}{3} p^3 \int_{-s_1^2}^{-s_0^2} (t+s_1^2)^2 \int_{-(t+s_0^2)}^{\infty} p_1(s+t) s^{-\frac{1}{2}} \int_{S^2 \cap L} \int_{S^2 \cap L} \int_{S^2 \cap L} \Delta_2^2(u_0, u_1, u_2) \\ & \quad \int_{SO_3} \int_{S^2 \cap L^\perp} \mathbb{E}[h(\Phi^{s+t}, s, t, \{(\vartheta u_0, s_1), (\vartheta u_1, s_1), (\vartheta u_2, s_1)\}, \vartheta u)] \mathbb{S}_{L^\perp}(du) \nu(d\vartheta) \mathbb{S}_L(du_0) \\ & \quad \mathbb{S}_L(du_1) \mathbb{S}_L(du_2) ds dt, \end{aligned}$$

$$\begin{aligned} & \mathbb{E}_{M_1} [h(\Phi^{P_1}, P'_1, P''_1, \Psi_1, U_1) \mid N_{1,0} = 1, N_{1,1} = 2] \\ &= \lambda^3 \pi p^2 (1-p) \int_{-s_0^2}^{\infty} \int_0^{\infty} p_1(s+t) s^{-\frac{1}{2}} \int_{S^2 \cap L} \int_{S^2 \cap L} \int_{S^2 \cap L} \Delta_2^2((t+s_0^2)^{\frac{1}{2}} u_0, (t+s_1^2)^{\frac{1}{2}} u_1, (t+s_1^2)^{\frac{1}{2}} u_2) \\ & \quad \int_{SO_3} \int_{S^2 \cap L^\perp} \mathbb{E}[h(\Phi^{s+t}, s, t, \{(\vartheta u_0, s_0), (\vartheta u_1, s_1), (\vartheta u_2, s_1)\}, \vartheta u)] \mathbb{S}_{L^\perp}(du) \nu(d\vartheta) \mathbb{S}_L(du_0) \mathbb{S}_L(du_1) \\ & \quad \mathbb{S}_L(du_2) ds dt, \end{aligned}$$

and

$$\begin{aligned}
& \mathbb{E}_{M_1} [h(\Phi^{P_1}, P'_1, P''_1, \Psi_1, U_1) \mid N_{1,0} = 2, N_{1,1} = 1] \\
&= \lambda^3 \pi p (1-p)^2 \int_{-s_0^2}^{\infty} \int_0^{\infty} p_1(s+t) s^{-\frac{1}{2}} \int_{S^2 \cap L} \int_{S^2 \cap L} \int_{S^2 \cap L} \Delta_2^2((t+s_1^2)^{\frac{1}{2}} u_0, (t+s_0^2)^{\frac{1}{2}} u_1, (t+s_0^2)^{\frac{1}{2}} u_2) \\
&\quad \int_{SO_3} \int_{S^2 \cap L^\perp} \mathbb{E}[h(\Phi^{s+t}, s, t, \{(\vartheta u_0, s_1), (\vartheta u_1, s_0), (u\vartheta_2, s_0)\}, \vartheta u)] \mathbb{S}_{L^\perp}(du) \nu(d\vartheta) \mathbb{S}_L(du_0) \\
&\quad \mathbb{S}_L(du_1) \mathbb{S}_L(du_2) ds dt.
\end{aligned}$$

Finally, with respect to  $\mathbb{Q}_2$  we have

$$\begin{aligned}
& \mathbb{E}_{M_2} [h(\Phi^{P_2}, P'_2, P''_2, \Psi_2, U_2) \mid N_{2,0} = 2] \\
&= 4\lambda^2 \pi (1-p)^2 \int_{-s_0^2}^{\infty} (t+s_0^2)^{\frac{1}{2}} \int_0^{\infty} p_1(s+t) \int_{S^2 \cap L^\perp} \int_{SO_3} \mathbb{E}[h(\Phi^{s+t}, s, t, \{(\vartheta u_0, s_0), (-\vartheta u_0, s_0)\}, \vartheta u)] \\
&\quad \mathbb{S}_{L^\perp}(du) \nu(d\vartheta) ds dt,
\end{aligned}$$

$$\begin{aligned}
& \mathbb{E}_{M_2} [h(\Phi^{P_2}, P'_2, P''_2, \Psi_2, U_2) \mid N_{2,1} = 2] \\
&= 4\lambda^2 \pi p^2 \int_{-s_0^2}^{\infty} (t+s_1^2)^{\frac{1}{2}} \int_0^{\infty} p_1(s+t) \int_{SO_3} \int_{S^2 \cap L^\perp} \mathbb{E}[h(\Phi^{s+t}, s, t, \{(\vartheta u_0, s_1), (-\vartheta u_0, s_1)\}, \vartheta u)] \\
&\quad \mathbb{S}_{L^\perp}(du) \nu(d\vartheta) ds dt \\
&+ 4\lambda^2 \pi p^2 \int_{-s_1^2}^{-s_0^2} (t+s_1^2)^{\frac{1}{2}} \int_0^{-(t+s_0^2)} p_2(s+t) \int_{SO_3} \int_{S^2 \cap L^\perp} \mathbb{E}[h(\Phi^{s+t}, s, t, \{(\vartheta u_0, s_1), (-\vartheta u_0, s_1)\}, \vartheta u)] \\
&\quad \mathbb{S}_{L^\perp}(du) \nu(d\vartheta) ds dt \\
&+ 4\lambda^2 \pi p^2 \int_{-s_1^2}^{-s_0^2} (t+s_1^2)^{\frac{1}{2}} \int_{-(t+s_0^2)}^{\infty} p_1(s+t) \int_{SO_3} \int_{S^2 \cap L^\perp} \mathbb{E}[h(\Phi^{s+t}, s, t, \{(\vartheta u_0, s_1), (-\vartheta u_0, s_1)\}, \vartheta u)] \\
&\quad \mathbb{S}_{L^\perp}(du) \nu(d\vartheta) ds dt,
\end{aligned}$$

and

$$\begin{aligned}
& \mathbb{E}_{M_2} [h(\Phi^{P_2}, P'_2, P''_2, \Psi_2, U_2) \mid N_{2,0} = 1, N_{2,1} = 1] \\
&= \frac{\lambda^2 \pi}{2} p (1-p) \int_{-s_0^2}^{\infty} \left( \frac{4t+s_1^2+3s_0^2}{(t+s_0^2)^{\frac{1}{2}}} - \frac{(4t+3s_1^2+s_0^2)\langle u_0, u_1 \rangle}{(t+s_1^2)^{\frac{1}{2}}} \right) \int_0^{\infty} p_1(s+t) \\
&\quad \int_{S^2 \cap L} \int_{S^2 \cap L} \int_{SO_3} \int_{S^2 \cap L^\perp} \mathbb{E}[h(\Phi^{s+t}, s, t, \{(\vartheta u_0, s_0), (\vartheta u_1, s_1)\}, \vartheta u)] \mathbb{S}_{L^\perp}(du) \nu(d\vartheta) \mathbb{S}_L(du_0) \mathbb{S}_L(du_1) \\
&\quad ds dt.
\end{aligned}$$

Then the intensities  $\mu_k$  are given by

$$\begin{aligned} \mu_0 = & \frac{2^7 \lambda^4 \pi^5}{105} \left[ (1-p)^4 \int_{-s_0^2}^{\infty} (t+s_0^2)^{\frac{7}{2}} p_1(t) dt + p^4 \int_{-s_0^2}^{\infty} (t+s_1^2)^{\frac{7}{2}} p_1(t) dt + p^4 \int_{-s_1^2}^{-s_0^2} (t+s_1^2)^{\frac{7}{2}} p_2(t) dt \right] \\ & + \frac{\lambda^4 (1-p)^3 p}{12} \int_{-s_0^2}^{\infty} (t+s_1^2)^{\frac{1}{2}} (t+s_0^2)^{\frac{3}{2}} p_1(t) V_{3,0} \left( (t+s_1^2)^{\frac{1}{2}}, (t+s_0^2)^{\frac{1}{2}}, (t+s_0^2)^{\frac{1}{2}}, (t+s_0^2)^{\frac{1}{2}} \right) dt \\ & + \frac{\lambda^4 (1-p) p^3}{12} \int_{-s_0^2}^{\infty} (t+s_1^2)^{\frac{3}{2}} (t+s_0^2)^{\frac{1}{2}} p_1(t) V_{3,0} \left( (t+s_1^2)^{\frac{1}{2}}, (t+s_1^2)^{\frac{1}{2}}, (t+s_1^2)^{\frac{1}{2}}, (t+s_0^2)^{\frac{1}{2}} \right) dt \\ & + \frac{\lambda^4 (1-p)^2 p^2}{8} \int_{-s_0^2}^{\infty} (t+s_1^2) (t+s_0^2) p_1(t) V_{3,0} \left( (t+s_1^2)^{\frac{1}{2}}, (t+s_1^2)^{\frac{1}{2}}, (t+s_0^2)^{\frac{1}{2}}, (t+s_0^2)^{\frac{1}{2}} \right) dt, \end{aligned}$$

$$\begin{aligned} \mu_1 = & 2\lambda^3 \pi^4 (1-p)^3 \int_{-s_0^2}^{\infty} (t+s_0^2)^2 \int_0^{\infty} p_1(s+t) s^{-\frac{1}{2}} ds dt \\ & + 2\lambda^3 \pi^4 p^3 \left[ \int_{-s_0^2}^{\infty} (t+s_1^2)^2 \int_0^{\infty} p_1(s+t) s^{-\frac{1}{2}} ds dt + \int_{-s_1^2}^{-s_0^2} (t+s_1^2)^2 \int_0^{-(t+s_0^2)} p_2(s+t) s^{-\frac{1}{2}} ds dt \right. \\ & \left. + \int_{-s_1^2}^{-s_0^2} (t+s_1^2)^2 \int_{-(t+s_0^2)}^{\infty} p_1(s+t) s^{-\frac{1}{2}} ds dt \right] \\ & + 2\lambda^3 \pi^4 p^2 (1-p) \int_{-s_0^2}^{\infty} (t+s_1^2) (s_1^2 + 2s_0^2 + 3t) \int_0^{\infty} p_1(s+t) s^{-\frac{1}{2}} ds dt \\ & + 2\lambda^3 \pi^4 p (1-p)^2 \int_{-s_0^2}^{\infty} (t+s_0^2) (2s_1^2 + s_0^2 + 3t) \int_0^{\infty} p_1(s+t) s^{-\frac{1}{2}} ds dt, \end{aligned}$$

and

$$\begin{aligned} \mu_2 = & 8\lambda^2 \pi^2 (1-p)^2 \int_{-s_0^2}^{\infty} (t+s_0^2)^{\frac{1}{2}} \int_0^{\infty} p_1(s+t) ds dt \\ & + 8\lambda^2 \pi^2 p^2 \left[ \int_{-s_0^2}^{\infty} (t+s_1^2)^{\frac{1}{2}} \int_0^{\infty} p_1(s+t) ds dt + \int_{-s_1^2}^{-s_0^2} (t+s_1^2)^{\frac{1}{2}} \int_0^{-(t+s_0^2)} p_2(s+t) ds dt \right. \\ & \left. + \int_{-s_1^2}^{-s_0^2} (t+s_1^2)^{\frac{1}{2}} \int_{-(t+s_0^2)}^{\infty} p_1(s+t) ds dt \right] \end{aligned}$$

$$+ 4\lambda^2\pi^2p(1-p) \int_{-s_0^2}^{\infty} \frac{4t + s_1^2 + 3s_0^2}{(t + s_0^2)^{\frac{1}{2}}} \int_0^{\infty} p_1(s+t) ds dt.$$

### Example 4.3.2

As in the planar case we will now discuss an example. This time, we choose  $\lambda = 1000$ ,  $s_0 = 0.01$  and  $s_1$  starting at 0.01 and then taking the values between 0.05 and 0.3 at steps of 0.05. In order to keep the extend of this chapter limited, observations are slightly reduced compared to the planar case.

Due to the lack of a tractable formula for the cell intensity  $\gamma_3$ , we are not able to compute all the mean values of cell characteristics only based on numerical integration. Table 4.9 shows the values of  $\gamma_0$ ,  $L_V$ , and  $S_V$  for  $p = 0.1, 0.3, 0.5, 0.7$ , and  $0.9$ . The values obtained by numerical integration are again compared to the mean values measured from 10,000 realizations of the corresponding tessellations. For  $\gamma_3$  only the simulated value is given.

For  $p = 0.5$  the mean values of the limiting Poisson Voronoi tessellation are reached for  $s_1 = 0.20$ . As in the two-dimensional case convergence is faster for larger values of  $p$ .

The plots of the linear contact distribution function, its density, and the chord length distribution function for the case  $p = 0.5$  are shown in Figures 4.13 and 4.14. The curves rapidly approach the one for the Poisson Voronoi tessellation of intensity  $\lambda = 500$ . It is almost impossible to distinguish between the lines already for  $s_1 = 0.15$ .

Finally, the distributions of volume  $v$ , surface area  $s$ , total edge length  $l$ , and number of faces  $n$  of the typical non-empty cell are studied by simulation. As a further characteristic we include the sphericity (or isoperimetric shape factor)  $g = \frac{6\sqrt{\pi}v}{\sqrt{s^3}}$  of the cells. For each set of parameters we generate 200,000 realizations of the typical non-empty cell. The means, variances, minima, and maxima of the observed characteristics are shown in Table 4.13. The histograms of  $v$ ,  $s$ ,  $l$ ,  $n$ , and  $g$  are displayed in Figures 4.8, 4.9, 4.10, 4.11, and 4.12, respectively.

The histograms for  $s_1 = 0.05$  are still close to both the ones for the Poisson Voronoi tessellation and to the corresponding histograms of the planar tessellation. For  $s_1 = 0.1$ , however, the two classes of cells are clearly visible especially in the histograms for  $s$  and  $l$ . Already for  $s_1 = 0.15$  the influence of the cells with smaller weight has decreased a lot. Looking at the histogram for the shape factor we observe that the cells generated by points with smaller weight tend to be much more irregular than cells whose generator carries the larger weight.

$p$	$s_1$	$\gamma_3^S$	$\gamma_0$	$\gamma_0^S$	$L_V$	$L_V^S$	$S_V$	$S_V^S$
0.1	0.05	998.090	6703.969	6703.907	577.182	577.182	28.776	28.775
0.1	0.10	929.936	5863.007	5862.817	501.083	501.007	25.252	25.250
0.1	0.15	624.804	3582.998	3584.842	315.166	315.208	18.484	18.485
0.1	0.20	246.347	1407.210	1407.059	165.555	165.564	14.337	14.340
0.1	0.25	112.111	732.295	733.788	128.080	128.209	13.548	13.554
0.1	0.30	100.342	677.653	678.680	125.674	125.776	13.509	13.515
0.3	0.05	994.516	6613.913	6618.535	569.013	569.041	28.385	28.385
0.3	0.10	791.390	4809.509	4813.489	422.236	422.307	23.126	23.127
0.3	0.15	373.931	2391.778	2393.539	276.374	276.541	19.712	19.719
0.3	0.20	300.782	2033.237	2034.211	261.431	261.537	19.484	19.489
0.3	0.25	300.055	2030.319	2030.469	261.349	261.368	19.483	19.483
0.3	0.30	300.034	2030.319	2030.361	261.349	261.341	19.483	19.483
0.5	0.05	991.877	6582.627	6584.787	566.198	566.195	28.300	28.300
0.5	0.10	738.288	4657.602	4659.877	427.898	428.883	24.177	24.176
0.5	0.15	506.250	3413.997	3412.675	368.270	368.196	23.110	23.106
0.5	0.20	499.887	3383.870	3382.616	367.384	367.304	23.100	23.097
0.5	0.25	499.900	3383.864	3382.724	367.384	367.311	23.100	23.097
0.5	0.30	499.880	3383.864	3382.609	367.384	367.299	23.100	23.097
0.7	0.05	992.027	6610.021	6611.158	568.883	568.892	28.470	28.470
0.7	0.10	789.504	5200.652	5199.942	478.175	478.190	26.111	26.111
0.7	0.15	700.503	4739.167	4740.349	459.808	459.864	25.842	25.844
0.7	0.20	699.987	4737.410	4737.445	459.768	459.760	25.842	25.842
0.7	0.25	699.777	4737.410	4736.683	459.768	459.660	25.842	25.839
0.7	0.30	699.949	4737.410	4737.131	459.768	459.744	25.842	25.841
0.9	0.05	996.034	6698.905	6698.458	577.066	577.034	28.849	28.848
0.9	0.10	917.453	6180.176	6178.456	546.653	546.581	28.137	28.135
0.9	0.15	900.130	6091.007	6091.888	543.629	543.677	28.100	28.101
0.9	0.20	899.334	6090.956	6090.185	543.628	543.574	28.100	28.098
0.9	0.25	899.589	6090.956	6089.589	543.628	543.554	28.100	28.098
0.9	0.30	899.828	6090.956	6089.697	543.628	543.555	28.100	28.098

Table 4.9: Intensities for a Laguerre tessellation in  $\mathbb{R}^3$  generated by a Poisson process with intensity  $\lambda = 1000$  and radius distribution  $A(s_1, 0.01, p)$ . The characteristics with superscript S are obtained by simulation (mean of 10,000 realizations), characteristics without superscript by numerical integration.

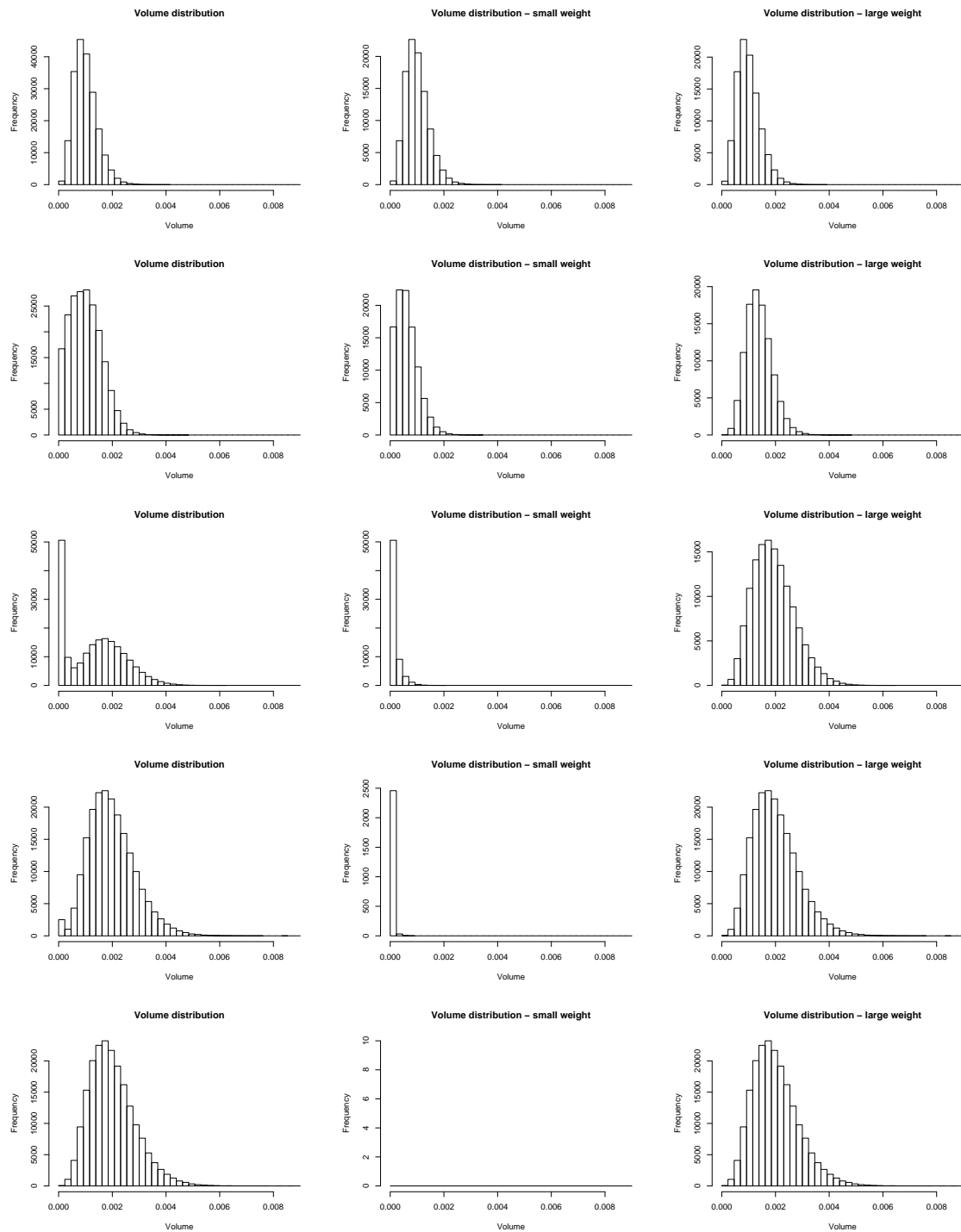


Figure 4.8: Volume distribution of the typical non-empty cell of a Laguerre tessellation in  $\mathbb{R}^3$  generated by a Poisson process with intensity  $\lambda = 1000$  and mark distribution  $A(s_1, 0.01, 0.5)$ . The rows correspond to the parameters  $s_1 = 0.01$  (Voronoi case) and  $s_1 = 0.05, 0.1, 0.15, 0.2$ . The columns show the volume distributions of the typical non-empty cell (left) and of the typical non-empty cells whose generators carry the weights 0.01 (middle) and  $s_1$  (right).

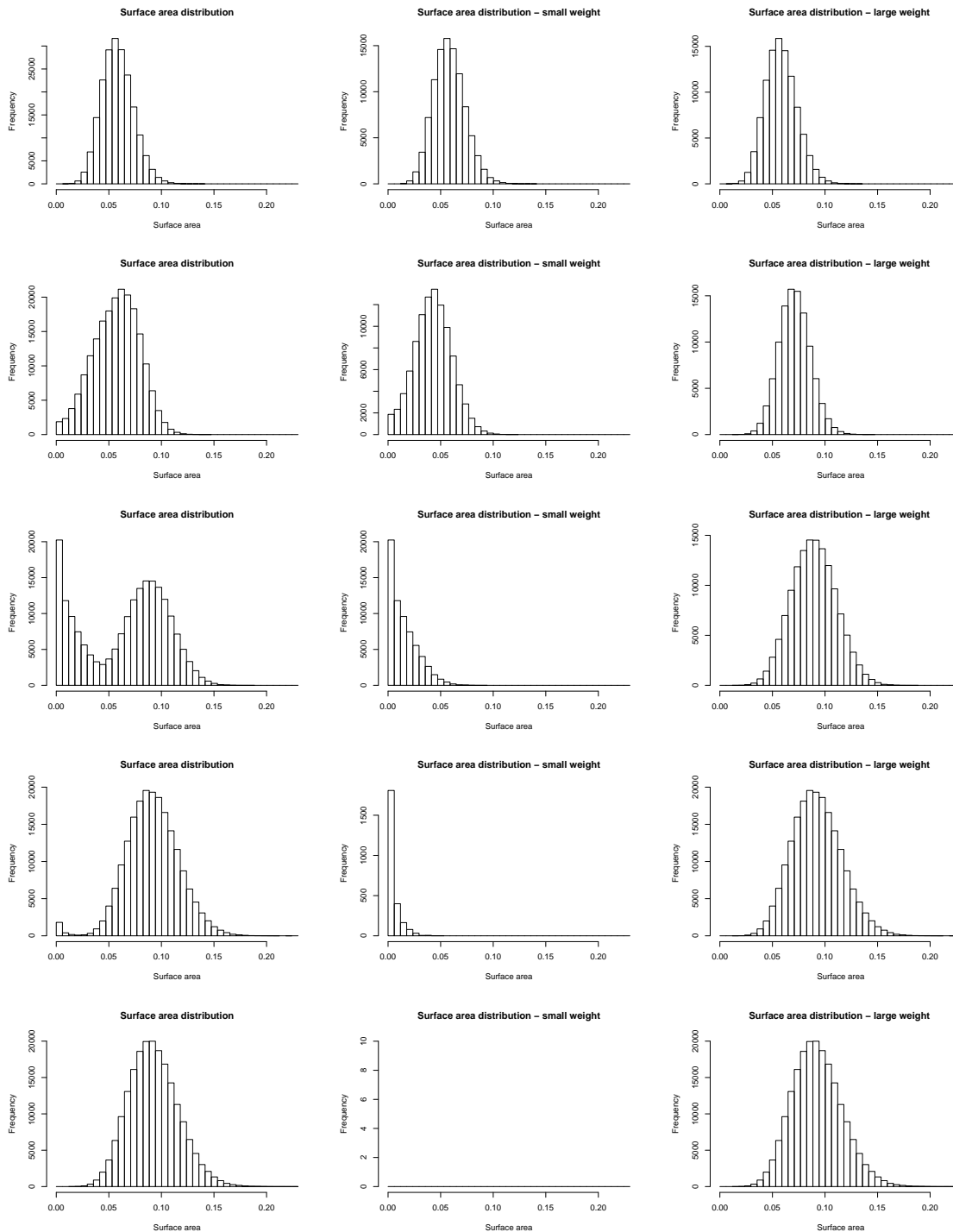


Figure 4.9: Surface area distribution of the typical non-empty cell of a Laguerre tessellation in  $\mathbb{R}^3$  generated by a Poisson process with intensity  $\lambda = 1000$  and mark distribution  $A(s_1, 0.01, 0.5)$ . The rows correspond to the parameters  $s_1 = 0.01$  (Voronoi case) and  $s_1 = 0.05, 0.1, 0.15, 0.2$ . The columns show the surface area distributions of the typical non-empty cell (left) and of the typical non-empty cells whose generators carry the weights 0.01 (middle) and  $s_1$  (right).

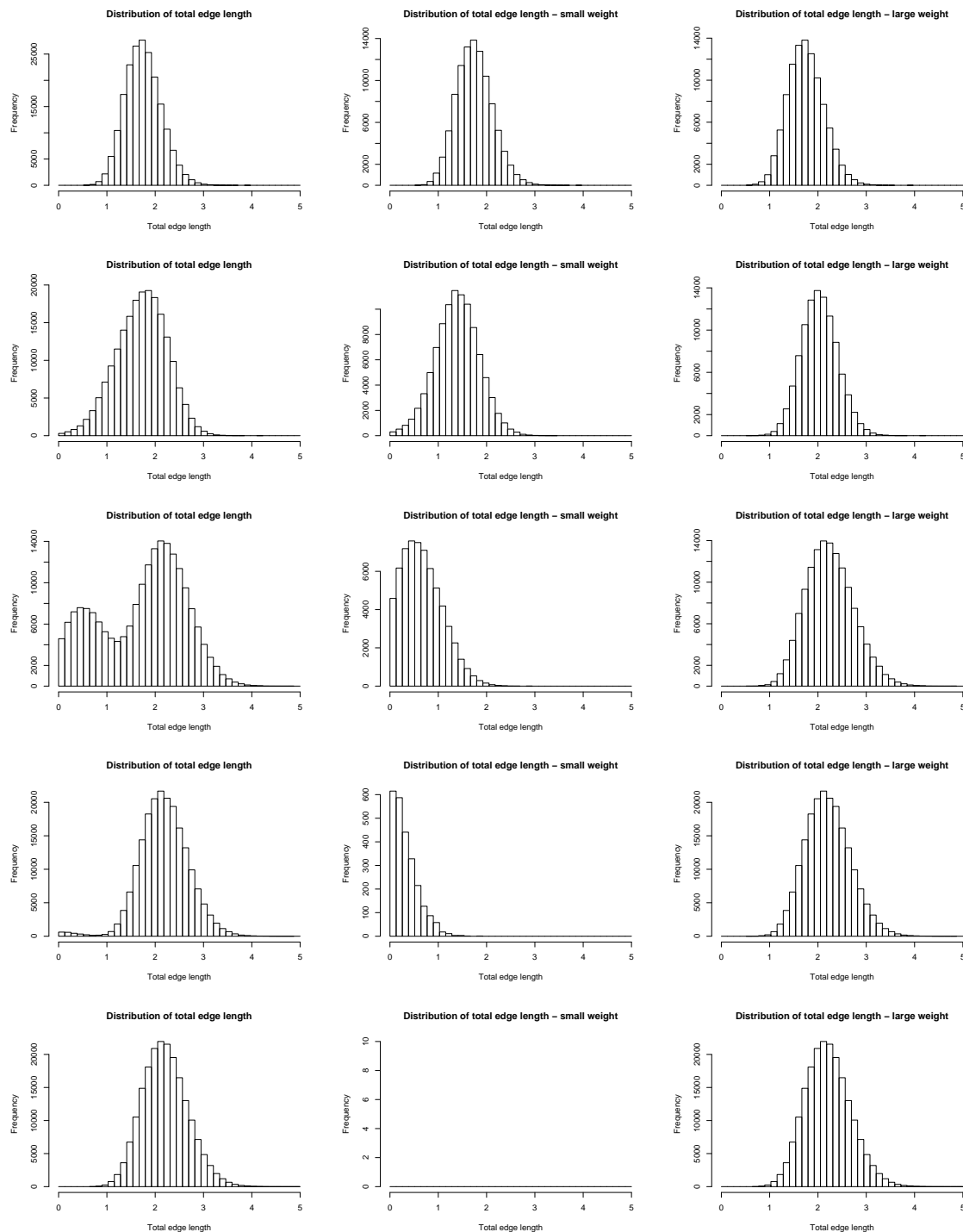


Figure 4.10: Distribution of the total edge length of the typical non-empty cell of a Laguerre tessellation in  $\mathbb{R}^3$  generated by a Poisson process with intensity  $\lambda = 1000$  and mark distribution  $A(s_1, 0.01, 0.5)$ . The rows correspond to the parameters  $s_1 = 0.01$  (Voronoi case) and  $s_1 = 0.05, 0.1, 0.15, 0.2$ . The columns show the edge length distributions of the typical non-empty cell (left) and of the typical non-empty cells whose generators carry the weights 0.01 (middle) and  $s_1$  (right).

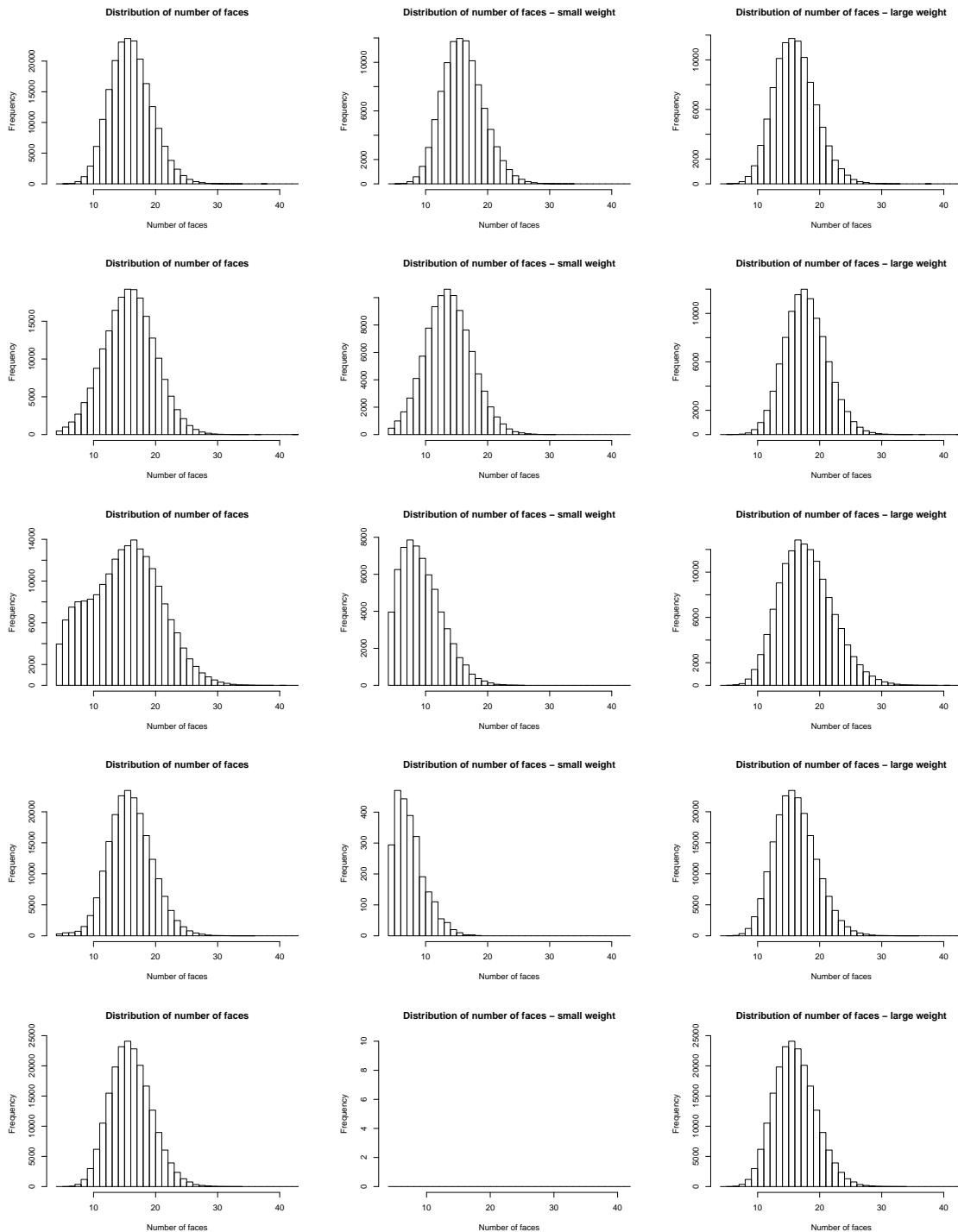


Figure 4.11: Distribution of the number of faces of the typical non-empty cell of a Laguerre tessellation in  $\mathbb{R}^3$  generated by a Poisson process with intensity  $\lambda = 1000$  and mark distribution  $A(s_1, 0.01, 0.5)$ . The rows correspond to the parameters  $s_1 = 0.01$  (Voronoi case) and  $s_1 = 0.05, 0.1, 0.15, 0.2$ . The columns show the face number distributions of the typical non-empty cell (left) and of the typical non-empty cells whose generators carry the weights  $0.01$  (middle) and  $s_1$  (right).

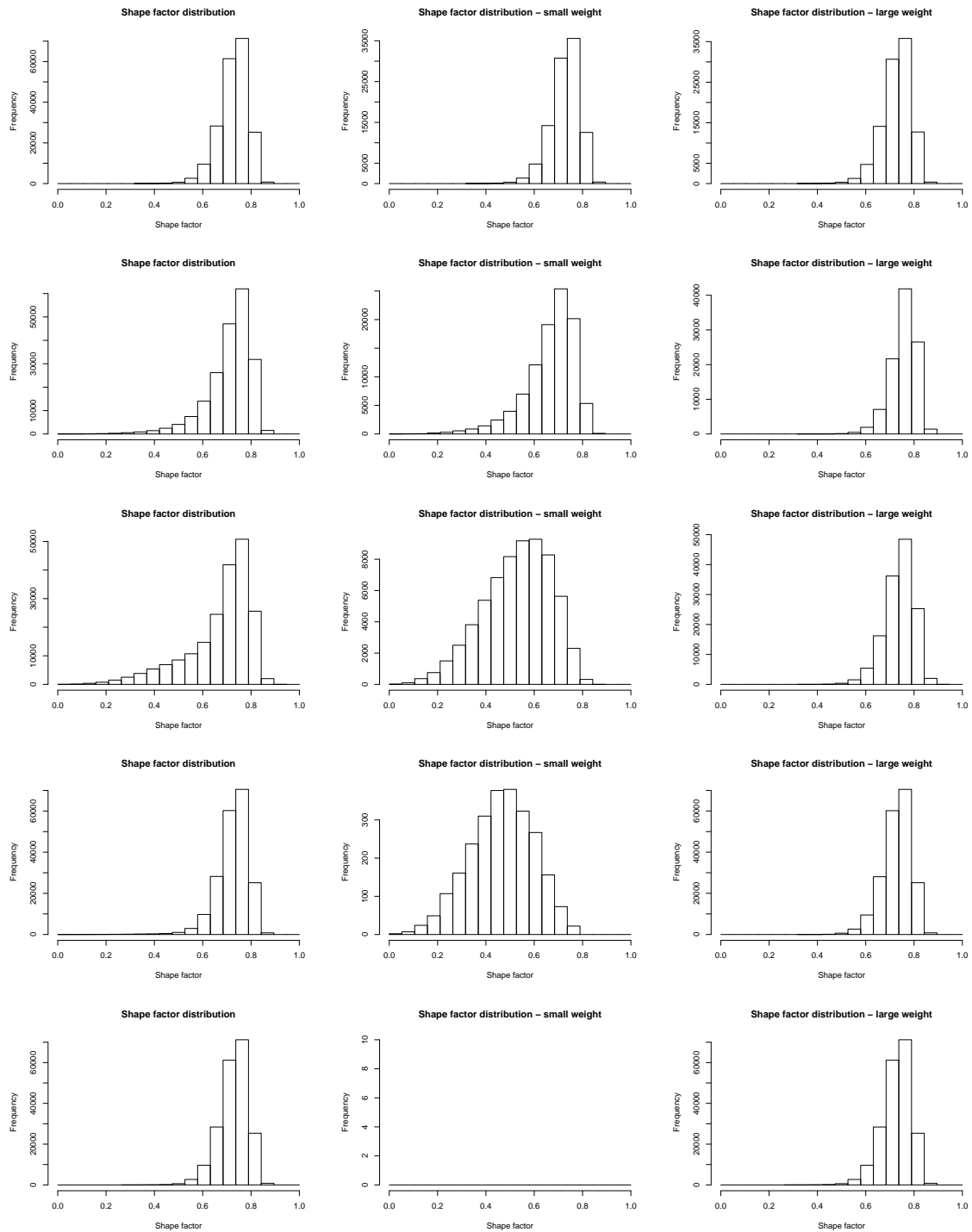


Figure 4.12: Shape factor distribution of the typical non-empty cell of a Laguerre tessellation in  $\mathbb{R}^3$  generated by a Poisson process with intensity  $\lambda = 1000$  and mark distribution  $A(s_1, 0.01, 0.5)$ . The rows correspond to the parameters  $s_1 = 0.01$  (Voronoi case) and  $s_1 = 0.05, 0.1, 0.15, 0.2$ . The columns show the shape factor distributions of the typical non-empty cell (left) and of the typical non-empty cells whose generators carry the weights 0.01 (middle) and  $s_1$  (right).

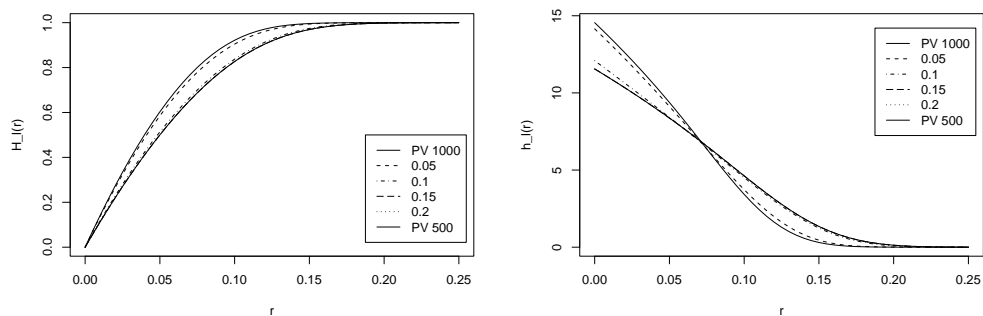


Figure 4.13: Linear contact distribution function (left) and its density (right) for a Laguerre tessellation in  $\mathbb{R}^3$  generated by a Poisson process with intensity  $\lambda = 1000$  and radius distribution  $A(s_1, 0.01, 0.5)$  with  $s_1 = 0.05, 0.1, 0.15,$  and  $0.2$ . The solid lines correspond to the Poisson Voronoi tessellations with intensities  $\lambda = 1000$  and  $\lambda = 500$ . The lines for  $s_1 = 0.15$  and  $s_1 = 0.2$  are so close to the Poisson Voronoi line that they cannot be distinguished.

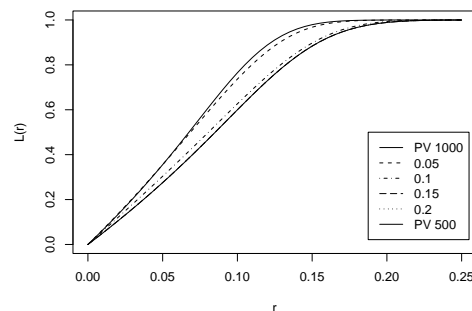


Figure 4.14: Chord length distribution function for a Laguerre tessellation in  $\mathbb{R}^3$  generated by a Poisson process with intensity  $\lambda = 1000$  and radius distribution  $A(s_1, 0.01, 0.5)$  with  $s_1 = 0.05, 0.1, 0.15,$  and  $0.2$ . The solid lines correspond to the Poisson Voronoi tessellations with intensities  $\lambda = 1000$  and  $\lambda = 500$ . The lines for  $s_1 = 0.15$  and  $s_1 = 0.2$  are so close to the Poisson Voronoi line that they cannot be distinguished.

	$s_1$	mean	var	min	max
volume	0.01	0.00100	1.795e-7	3.322e-05	0.00405
	0.05	0.00101	3.434e-7	6.515e-13	0.00465
	0.10	0.00135	1.114e-6	8.333e-18	0.00631
	0.15	0.00197	7.521e-7	3.833e-17	0.00832
	0.20	0.00200	7.199e-7	1.165e-04	0.00863
surface area	0.01	0.05823	0.00022	0.00875	0.13570
	0.05	0.05710	0.00047	1.440e-07	0.14645
	0.10	0.06554	0.00157	5.030e-11	0.18579
	0.15	0.09126	0.00064	1.228e-10	0.22315
	0.20	0.09243	0.00055	0.01622	0.22916
total edge length	0.01	1.75004	0.13605	0.54345	3.87302
	0.05	1.71358	0.27484	0.00239	4.18984
	0.10	1.74015	0.75631	5.0e-5	4.83475
	0.15	2.18177	0.25936	6.5e-5	4.86945
	0.20	2.20532	0.21661	0.66430	4.92969
number of faces	0.01	15.540	11.091	5	37
	0.05	15.286	16.930	4	42
	0.10	14.633	31.450	4	40
	0.15	15.485	12.407	4	35
	0.20	15.534	11.103	5	33
shape factor	0.01	0.72774	0.00341	0.32331	0.88563
	0.05	0.71072	0.00889	0.02882	0.89174
	0.10	0.67049	0.01838	0.02089	0.90484
	0.15	0.72452	0.00445	0.03287	0.88187
	0.20	0.72768	0.00343	0.28647	0.89110

Table 4.10: Characteristics of the typical non-empty cell of a Laguerre tessellation in  $\mathbb{R}^3$  generated by a Poisson process with intensity  $\lambda = 1000$  and radius distribution  $A(s_1, 0.01, 0.5)$ .

### 4.3.3 Uniform distribution

As for the two-dimensional case we study the case of uniformly distributed radii as a second example. Here, we choose  $\lambda = 1000$  and a radius distribution  $U(0.01, b)$ , where  $b$  takes values between 0.05 and 0.25 (or 0.30) in steps of 0.05. As for the discrete distribution, we evaluate numerically the formulas for  $\gamma_0$ ,  $L_V$ , and  $S_V$  and compare the results to the mean values measured from 10,000 simulations. We also use these simulations to determine the value of  $\gamma_3$ . The results are shown in Table 4.11.

Further, we simulate 200,000 realizations of the typical non-empty cell. As in the previous sections we measure the volume  $v$ , surface area  $s$ , total edge length  $l$ , number of faces  $n$ , and shape factor  $g$  of each of the cells. The means, variances, minima, and maxima are summarized in Table 4.12. The corresponding histograms are shown in Figures 4.15 and 4.16. As in the planar case, the shape of the histograms rapidly changes during the first steps. In the later steps some kind of stabilization occurs and the changes are less obvious.

$a$	$b$	$\gamma_3^S$	$\gamma_0$	$\gamma_0^S$	$L_V$	$L_V^S$	$S_V$	$S_V^S$
0.01	0.05	998.306	6706.899	6704.146	577.284	577.196	28.800	28.791
0.01	0.10	919.005	5817.862	5815.773	501.165	501.325	25.689	25.758
0.01	0.15	619.285	3745.935	3754.156	356.206	356.372	21.236	21.276
0.01	0.20	383.809	2340.349	2346.283	263.072	262.971	18.400	18.408
0.01	0.25	274.842	1690.610	1689.321	212.865	212.693	16.572	16.610
0.01	0.30	213.464	1303.043	1315.433	180.515	180.516	15.310	15.325

Table 4.11: Intensities for a Laguerre tessellation in  $\mathbb{R}^3$  generated by a Poisson process with intensity  $\lambda = 1000$  and radius distribution  $U(a, b)$ . The characteristics with superscript S are obtained by simulation (mean of 10,000 realizations), characteristics without superscript by numerical integration.

	$a$	$b$	mean	var	min	max
volume	0.01	0.05	0.00100	2.470e-7	5.0e-14	0.00399
	0.01	0.10	0.00109	1.065e-6	2.4e-17	0.00623
	0.01	0.15	0.00162	3.503e-6	2.0e-18	0.01110
	0.01	0.20	0.00262	8.001e-6	8.1e-17	0.01692
	0.01	0.25	0.00364	1.460e-5	5.7e-17	0.02415
surface area	0.01	0.05	0.05769	0.00032	1.093e-08	0.13931
	0.01	0.10	0.05601	0.00127	8.562e-11	0.17898
	0.01	0.15	0.06877	0.00323	1.900e-11	0.26118
	0.01	0.20	0.09622	0.00557	2.725e-10	0.34477
	0.01	0.25	0.12087	0.00824	1.235e-10	0.44358
total edge length	0.01	0.05	1.73446	0.19107	5.0e-4	3.84100
	0.01	0.10	1.63534	0.66397	5.8e-5	4.74310
	0.01	0.15	1.72638	1.25302	2.1e-5	6.03187
	0.01	0.20	2.06038	1.60204	1.1e-4	6.86152
	0.01	0.25	2.32245	1.91240	2.0e-6	7.60894
number of faces	0.01	0.05	15.429	13.424	4	33
	0.01	0.10	14.644	31.888	4	42
	0.01	0.15	14.121	44.114	4	45
	0.01	0.20	14.251	41.295	4	45
	0.01	0.25	14.301	39.708	4	42
shape factor	0.01	0.05	0.72068	0.00581	0.04453	0.88186
	0.01	0.10	0.67082	0.01828	0.03801	0.91074
	0.01	0.15	0.63871	0.02389	0.01932	0.91075
	0.01	0.20	0.64597	0.02286	0.01068	0.90765
	0.01	0.25	0.64953	0.02228	0.02061	0.90274

Table 4.12: Characteristics of the typical cell of a Laguerre tessellation in  $\mathbb{R}^3$  generated by a Poisson process with intensity  $\lambda = 1000$  and radius distribution  $U(a, b)$ .

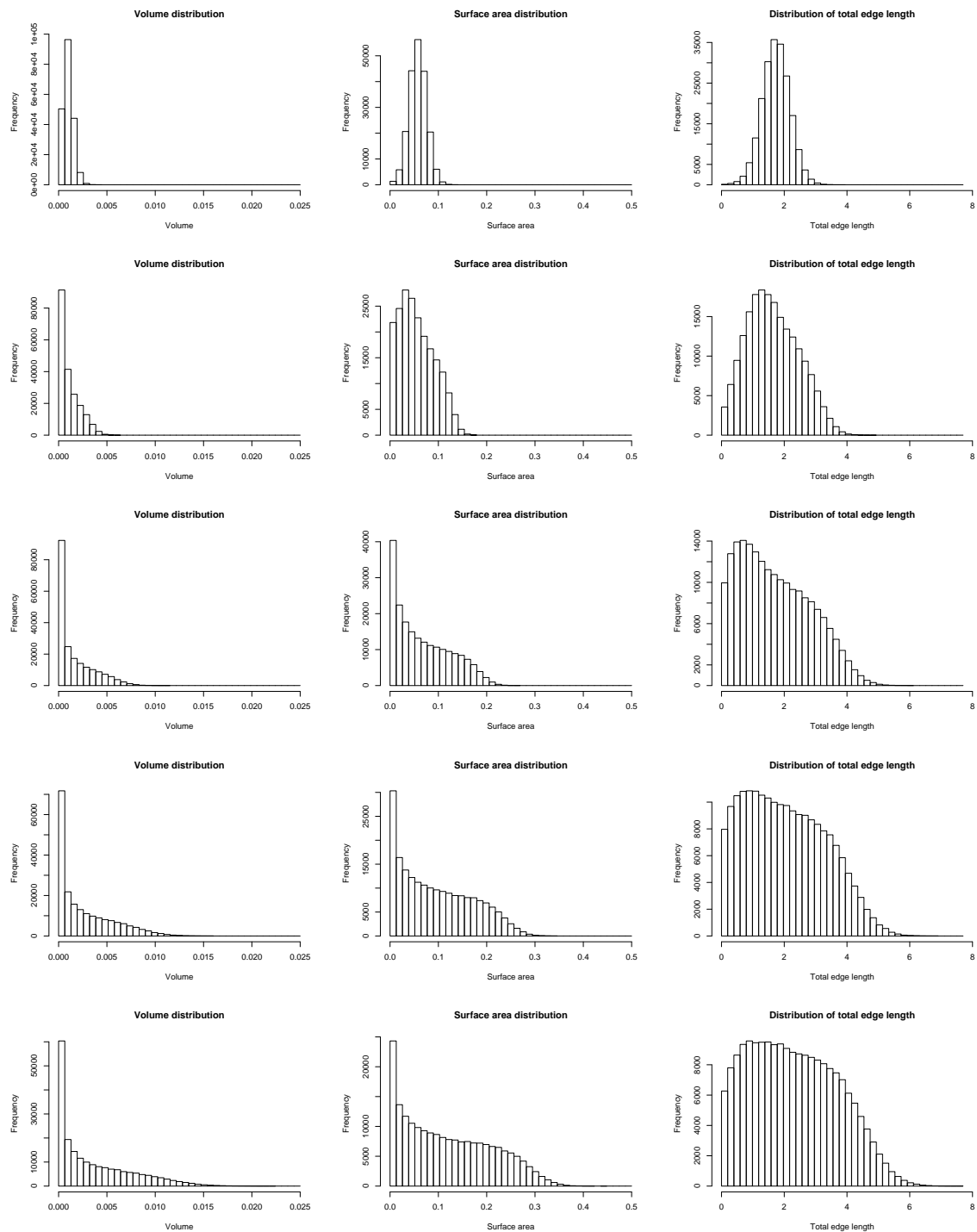


Figure 4.15: Distribution of volume, surface area, and total edge length (from left to right) of the typical non-empty cell of a Laguerre tessellation in  $\mathbb{R}^3$  generated by a Poisson process with intensity  $\lambda = 1000$  and mark distribution  $U(0.01, b)$ . The rows correspond to the parameters  $b = 0.05, 0.1, 0.15, 0.2, 0.25$ .

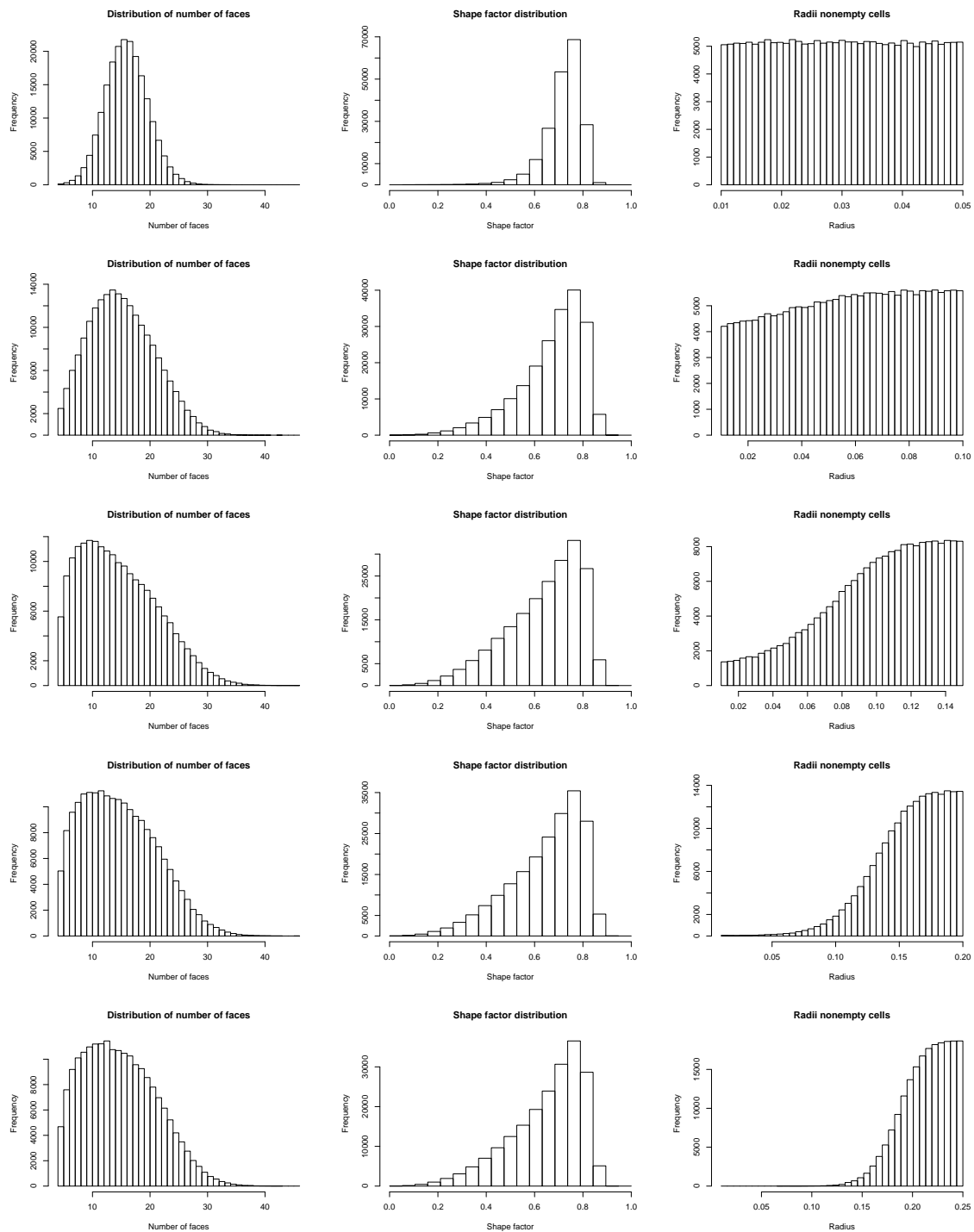


Figure 4.16: Distribution of number of faces, shape factor, and radius of the generating sphere (from left to right) of the typical non-empty cell of a Laguerre tessellation in  $\mathbb{R}^3$  generated by a Poisson process with intensity  $\lambda = 1000$  and mark distribution  $U(0.01, b)$ . The rows correspond to the parameters  $b = 0.05, 0.1, 0.15, 0.2, 0.25$ .

# Chapter 5

## Modeling of cellular materials

The microstructure of a material highly affects its macroscopic properties such as elasticity, thermal conductivity or permeability. Therefore, the design of modern high-performance materials requires insight into the microstructure of the given material as well as an understanding of its influence on physical properties. Even more, this knowledge is required when optimizing materials for the construction of components.

Microstructural geometry is usually described by mean values or distributions of suitable geometric characteristics which are statistically estimated from images of the material. In order to capture all spatial information, these measurements are ideally performed on volume images. Thanks to the rapid development of imaging techniques such as micro-computer tomography ( $\mu$ CT) or laser scanning microscopy, more and more high quality three-dimensional images become available. Nevertheless, many materials can not yet be handled by 3d imaging devices due to resolution restrictions or low contrast. For example, the current limit resolution in  $\mu$ CT imaging is about  $1\ \mu\text{m}$ , while typical grain diameters in sintered ceramics, are about  $150 - 200\ \text{nm}$ . For these materials, the classical method of sectional analysis has to be used. Therefore, it is not possible to measure all desired quantities directly from the image. The answer to this problem might be the use of model assumptions. The model parameters can be estimated from sectional images, further characteristics are then derived using stereological formulas for the model structure under consideration.

Another application area for modeling of materials, which is just starting to develop, is the so-called “virtual design” of materials. Using the model structure, physical properties of the corresponding material are computed or simulated. Repeated calculations with varying model parameters allow to investigate the reaction of the material’s properties to changes of the microstructure. Thus, instead of producing many sample structures and choosing the best one for a given application, suggestions for good candidates can be obtained by simulation. The increasing capability of simulation algorithms as well as computer power allows for high precision in the simulation results. In return, this requires more and more sophisticated model structures and model-fitting procedures.

Random closed sets are classical models from stochastic geometry which are used to describe the microstructure of materials (see Matheron, 1975; Stoyan et al., 1995; Ohser and Mücklich, 2000). The variety of these models makes them applicable for various types of materials. Processes of lines or cylinders are used to model fibrous materials (Schladitz et al., 2006). Systems of balls are used for porous materials as they appear in the beginning of the sinter process (Lautensack et al., 2006) or the system of grains and pores in concrete

(Ballani et al. (2006) and Kadashevich et al. (2005), respectively). Boolean models with various kinds of grain shapes are used for example for cast iron (line segments, Stoyan et al. (1995, p. 92)), calcium ferrite (quadrangles, Serra (1982, Chapter XIII)) or the pore phase in carbonate rock (ellipsoids, Arns et al. (2003)). Finally, random tessellations are popular models for cellular or polycrystalline materials such as foams or sintered ceramics. Further information on the modeling of materials can be found in the books by Ohser and Mücklich (2000), Stoyan et al. (1995) or Torquato (2002).

## 5.1 Modeling the microstructure of materials by random tessellations

Random tessellations are typically used as models for polycrystalline or cellular materials. So far, however, mainly the Voronoi and the Johnson-Mehl tessellation have been considered. We will give only a few examples here which nevertheless indicate the wide range of possibilities arising from the use of tessellation models. Kumar and Kurtz (1994) used three-dimensional Poisson Voronoi tessellations to study the thermal expansion coefficients of polycrystalline materials. Schwertel and Stamm (1997) investigated sectional images of an austenitic steel. From measurements in the 2d images they estimated the cell intensities of corresponding Poisson Voronoi and Johnson-Mehl tessellations. Their results suggest that the weighted tessellation gives the better fit. Roberts and Garboczi (2001) as well as Ribeiro-Ayeh (2005) modeled closed cell solid foam structures by Voronoi tessellations with respect to hard core point processes. From these models, they computed elastic moduli of the foam structures. Andersson (2005) used two-dimensional Poisson Voronoi tessellations to simulate crack growth in metals. Finally, Coster et al. (2005) constructed a three-dimensional Johnson-Mehl model for a sintered ceramic (Cerine).

The wish for a model structure which is easy to handle both analytically and computationally often suggests the use of the Poisson Voronoi tessellation. However, for some applications, the Poisson Voronoi model can be rejected right away (see Stoyan et al., 1995). Also, the range of distributions which can be realized by Voronoi tessellations with respect to changing seed distributions is limited. As indicated by Coster et al. (2005) or Schwertel and Stamm (1997) the use of weighted tessellations provides a powerful alternative. In many cases the Johnson-Mehl model is proposed (Chu et al., 2000; Coster et al., 2005; Schwertel and Stamm, 1997). This seems to be a good choice for materials with strongly curved cell faces.

For structures with (nearly) planar faces, Laguerre tessellations should be favored for the following reasons: The results stated in Section 2.4 suggest that each normal and regular cell structure with convex or nearly convex cells can be realized as or at least approximated by a Laguerre tessellation. The mean value relations for normal and regular tessellations (Section 1.6) allow for a computation of the mean values of the cell characteristics based on only few measurements. As described in Section 4.1, efficient algorithms for the construction of Laguerre tessellations are available. Since the Laguerre cells are bounded by planar faces (in contrast to the curved faces of Johnson-Mehl cells), the computation of their characteristics such as volume or surface area is much easier. The same is true when sectional tessellations have to be studied. Using its representation as a Laguerre tessellation (Okabe et al., 2000, p.132), it is possible to simulate the sectional tessellation without actually constructing the

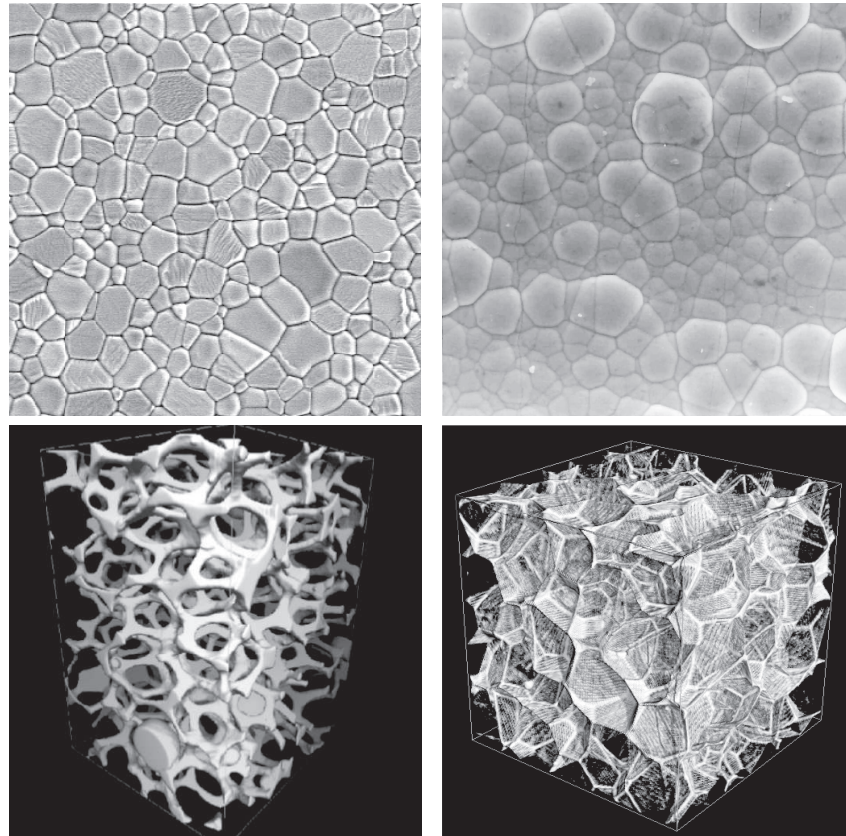


Figure 5.1: Examples for cellular materials: sectional image of sintered alumina ( $\text{Al}_2\text{O}_3$ , A. Krell, Fraunhofer IKTS, top left), alkaline zinc-nickel layers on steel (D. Peisker, Institute of Iron and Steel Technology, Freiberg University of Mining and Technology, top right), reconstructed tomographic images of an open aluminum foam (Mpore, bottom left) and a closed polymer foam (L. Helfen, ESRF, bottom right).

three-dimensional structure. Johnson-Mehl tessellations do not possess this property. For the simulation of physical properties of a material, finite element methods are applied, which usually require a triangulation of the cell faces. This is again much easier for the planar Laguerre faces than for the curved ones appearing in Johnson-Mehl tessellations. Finally, like Voronoi or Johnson-Mehl tessellations, Laguerre tessellations can be defined as the result of a growth process (Edelsbrunner and Seidel, 1986, Note 3.3). Therefore, this model can also be used for porous structures as they typically appear in intermediate states of a sinter process.

As a consequence, Laguerre tessellations should be regarded as a powerful tool for the modeling of materials. First applications can be found for example in several publications by the group of T. Liebling in Lausanne (Telley et al., 1996a,b; Xue et al., 1997) or in Kühn (2005) and Kanaun and Tkachenko (2006).

## 5.2 Modeling a foam structure

Foamed materials made of ceramics, metals or polymers are of interest in many application areas. Due to properties such as light weight, porosity, and stiffness, they are used for filters, crash absorbers, insulators or as cores of sandwich constructions. On the other hand, they can also be found in many natural structures such as bone, wood or sponge and in food structures like bread or cereals.

Foams consist of spherical or polyhedral cells separated by liquid or solid cell boundaries together building a space-filling structure. They are characterized as “open-cell” when forming a continuous network of cell edges or “closed-cell” if the cells are bounded by solid membrane-like faces.

The physical properties of a foam (e.g., elasticity or thermal conductivity) heavily depend on its microstructure. However, the influence of certain geometric characteristics of the foam cells on these properties is far from being understood. Many of the formulas for the computation of physical properties of a foam are gained from simplifications of the foam cells such as the cubic unit cell used by Gibson and Ashby (1988). Other approaches are mainly based on the observation of liquid foams, leading to deterministic models such as the Kelvin (Thomson, 1887) and the Weaire-Phelan foam (Weaire and Phelan, 1994) or the tetrakaidekahedral cell model (i.e., the Voronoi tessellation of the bcc lattice, Kusner and Sullivan (1996)).

For a long time the only way of studying the structure of real foams consisted in tediously observing single foam cells as done by Matzke (1946). Today, three-dimensional images of foam structures obtained by micro-computer tomography provide a powerful source of information on the microstructure of a foam sample. Several tools for processing these images and measuring cell characteristics have been developed during the last years (see Godehardt et al. (2004), Montminy et al. (2004) or Lambert et al. (2005)). Investigations of various samples of solid foams have shown that these structures show a great variety of cell shapes and sizes (Montminy et al. (2004), Dillard et al. (2005)) which is not captured by deterministic models.

Information on the macroscopic properties of a given foam can be gained from experiments (e.g., mechanical testing, Benouali et al. (2005) or Dillard et al. (2005)) or simulation of these properties in images of its microstructure (Knackstedt et al., 2005). However, these techniques only mirror the behavior of a given foam sample. The virtual design approach allows to study the reaction of physical properties to changes of certain geometric characteristics and to optimize a foam for particular applications. Therefore, finite element analyses are carried out using model foams featuring various microstructures. Models which are typically used for these purposes are randomly disturbed variations of the deterministic models discussed above (see e.g., Grenestedt and Tanaka (1999) or Ribeiro-Ayeh (2005)) or Voronoi tessellations with respect to the centers of sphere packings generated by random sequential adsorption or other random close packing algorithms (see e.g., Roberts and Garboczi (2001), Zhu et al. (2000) or Ribeiro-Ayeh (2005)).

Most studies on physical properties of foam structures are concerned with elastic properties. From both experiments and the use of model structures it is well known that the volume fraction and cell anisotropy of the foam play an important role (Gibson and Ashby (1988), Benouali et al. (2005), Knackstedt et al. (2005) or Roberts and Garboczi (2001)). Results of Brezny and Green (1990), Zhu et al. (2000), and Kanaun and Tkachenko (2006)

further indicate that cell size and irregularity (measured e.g., by the variation of shape or size) are of importance as well.

So far, most of the publications on foam structures are devoted to either the analysis of real foam structures or the observation of model foams. In some of these model studies the values of physical properties are compared to real foam samples without, however, investigating the geometric fit of the model (Roberts and Garboczi (2001, 2002) or Ribeiro-Ayeh (2005)).

In this chapter, we are going to use geometric characteristics measured from a three-dimensional image of a foam structure for fitting a model to its geometric microstructure. We are not going to investigate physical properties of the foam under consideration. However, we expect that a better fit of the geometry of a material will also improve the results obtained for its macroscopic properties.

### 5.2.1 The data

The material considered here is a polymer foam used for the thermal insulation of buildings. A three-dimensional gray value image of the material taken at the European Synchrotron Radiation Facility in Grenoble was provided by the producer of the material. The original image size is  $1024 \times 1024 \times 2000$  voxels with a voxel edge length of  $5 \mu m$  such that the image shows  $5.12 \text{ mm} \times 5.12 \text{ mm} \times 10 \text{ mm}$  of material. The average thickness of the facets of the cells in the material is  $1.7 \mu m$ , the volume fraction is 3.6%.

### 5.2.2 Cell reconstruction

The microstructure of the foam sample will be described using geometric characteristics of its cells which are extracted from the image of the material. This image, however, only shows the system of cell boundaries. In order to measure geometric characteristics of single foam cells, the cells have to be separated. The straightforward approach of binarizing and labeling the image does not work here because of the coarse resolution of the image. Instead, the cells have to be reconstructed using a chain of image processing algorithms.

To reduce computational effort, the reconstruction procedure is restricted to a cube of a side length of 578 voxels. First, the wall system of the foam is segmented by simple thresholding. To the resulting black-and-white image, the Euclidean distance transformation is applied, assigning to each background pixel its distance to the wall system (Cuisenaire, 1999). Ideally, this yields local maxima exactly at the cell centers. In practice, superfluous local maxima have to be removed using filters or morphological transformations. Here, the h-maxima transformation (Soille, 1999, Section 6.4.4) is applied. The watershed algorithm (Vincent and Soille, 1991) divides the inverted distance image into cells. Due to the coarse resolution of the image some of the cell walls are hardly visible and therefore not captured in the binarization step. In a post-processing step, these errors are corrected manually. Finally, in order to make measurements comparable to the space-filling tessellation models, the black cell facets are removed from the image by dilation.

Planar sections of the volume images obtained during this procedure are shown in Figure 5.2. All image processing steps are performed on volume images using the MAVI software package developed at the Fraunhofer ITWM (2005). For further information on the reconstruction method see Godehardt et al. (2004) and Lautensack and Sych (2006).

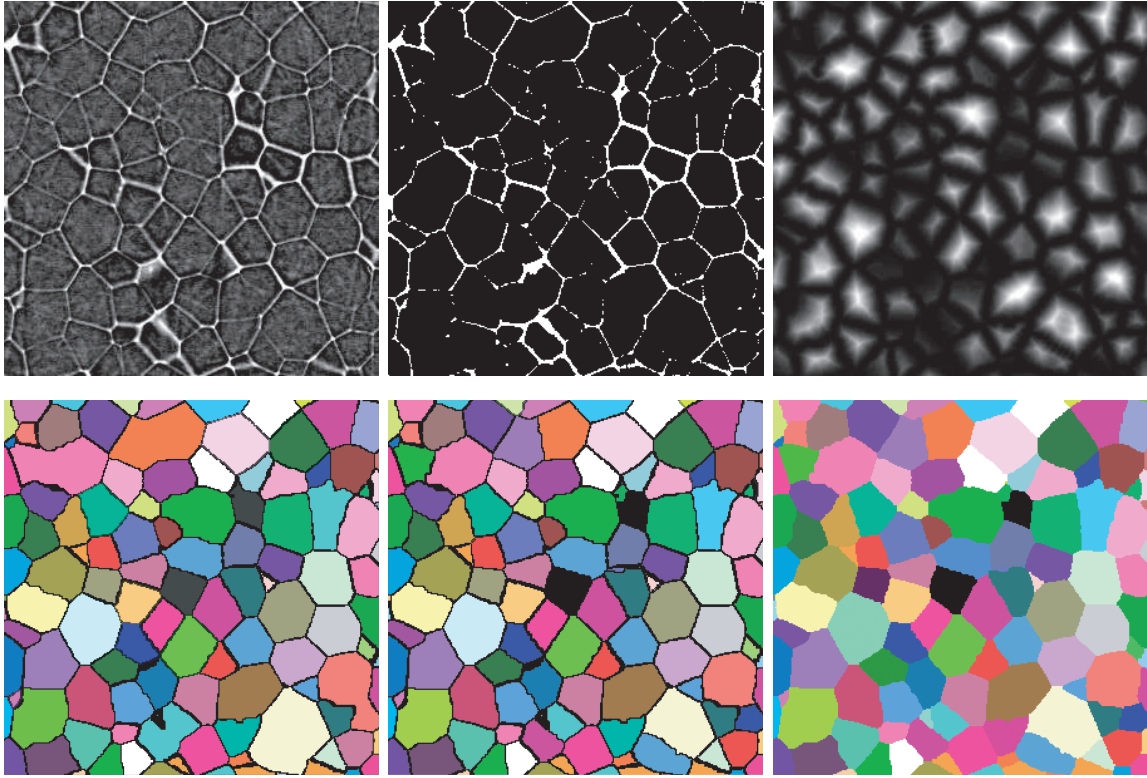


Figure 5.2: Planar sections of the original image, the segmented system of cell walls, the distance image, the reconstructed cells, the reconstructed cells after manual correction, and the dilated image.

### 5.2.3 Statistical analysis

The difference between a proposed tessellation model and the foam sample will be measured by the deviation of several geometric characteristics of the typical cell of the model from the characteristics of the foam cells. Similar approaches are discussed for example in Gloaguen et al. (2006) and in Kühn (2005). Both are based on optimization with respect to distance measures defined on vectors of cell characteristics of the tessellations. Let  $\hat{c}$  be the vector of characteristics estimated from the input structure and  $c$  the vector of the same characteristics for one of the model structures under consideration. For measuring the distance between  $\hat{c}$  and  $c$  we adopt the approach of Gloaguen et al. (2006) who define relative distance measures based on the Euclidean, the absolute, and the maximum metric via

$$\begin{aligned}
 d_e(\hat{c}, c) &= \sqrt{\sum_{i=1}^n \left( \frac{\hat{c}_i - c_i}{\hat{c}_i} \right)^2}, \\
 d_a(\hat{c}, c) &= \sum_{i=1}^n \left| \frac{\hat{c}_i - c_i}{\hat{c}_i} \right|, \text{ and} \\
 d_m(\hat{c}, c) &= \max_{i=1, \dots, n} \frac{|\hat{c}_i - c_i|}{\hat{c}_i}.
 \end{aligned} \tag{5.1}$$

Although a large number of characteristics can in principle be computed, our model-

fit will be based on only four of them. The mean value formulas for three-dimensional tessellations in Theorem 1.6.7 suggest the use of  $\gamma_0$ ,  $\gamma_3$ ,  $L_V$ , and  $S_V$ . However, we will use some characteristics which are more easily and robustly estimated from both the volume image and the analytic representation of the tessellation models: the volume  $v$ , surface area  $s$ , mean width  $\bar{b}$ , and number of faces  $f$  of the cells. Moreover, for fixed  $\gamma_3$  the values of  $s$  and  $\bar{b}$  are proportional to  $S_V$  and  $L_V$ , respectively, and  $f$  only depends on  $\gamma_0$ .

While  $f$  already holds some information on the regularity of the cells, the sphericity (or isoperimetric shape factor)  $g = \frac{6\sqrt{\pi}v}{\sqrt{s^3}}$  is additionally investigated. Measurements are again performed using MAVI. A rough approximation of the mean width  $\bar{b}$  is obtained as the mean of the diameters  $d_x$ ,  $d_y$ , and  $d_z$  in coordinate directions. In order to avoid boundary effects we use a minus sampling edge correction whereby 1823 cells with a total volume of 10.123 mm<sup>3</sup> are included in the statistics. The mean values of the cell characteristics are given in Table 5.1, histograms of the corresponding distributions are displayed in Figure 5.3.

data	$v$	$s$	$f$	$b$	$d_x$	$d_y$	$d_z$	$g$
mean	0.0055532	0.17586	14.637	0.24698	0.23773	0.24785	0.23951	0.77124
var	6.54219e-6	0.00280	10.378	0.00143	0.00192	0.00222	0.00195	0.00173
PV	$v$	$s$	$f$	$b$	$d_x$	$d_y$	$d_z$	$g$
mean	0.0055532	0.18254	15.535	0.25819	0.25819	0.25819	0.25819	0.72790
var	5.55081e-6	0.00215	11.012	0.00095	0.00095	0.00095	0.00095	0.00340

Table 5.1: Mean values and variances of geometric characteristics of the reconstructed foam cells. For comparison the values for the Poisson Voronoi tessellation of the same intensity  $\lambda = 180.077$  are given. The values for the Poisson Voronoi tessellation are taken from (Okabe, Boots, Sugihara, and Chiu, 2000) except for  $g$  which is obtained by simulation.

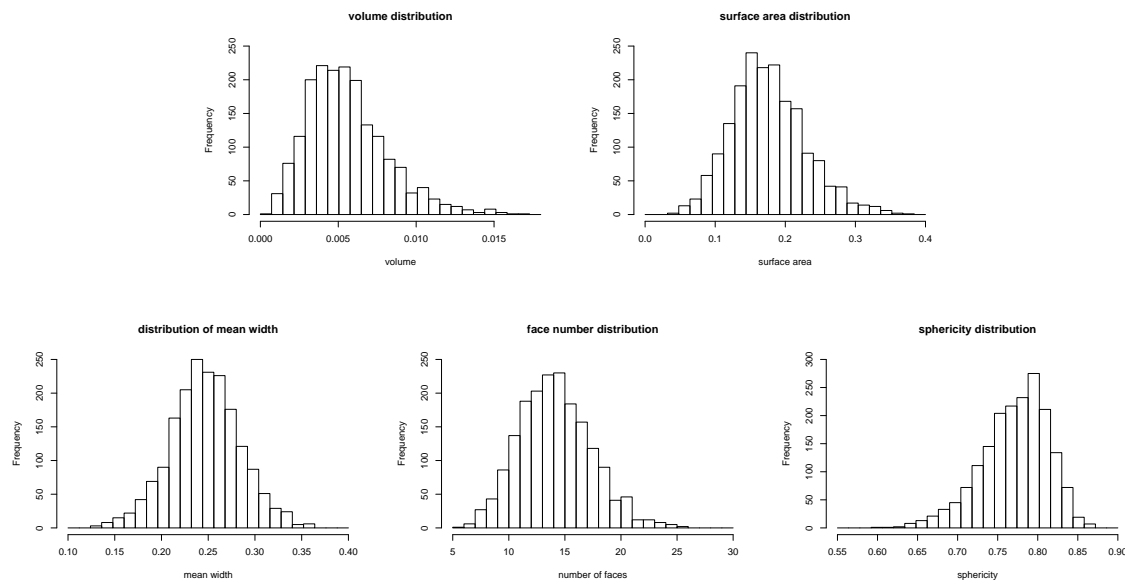


Figure 5.3: Distributions of cell characteristics of the foam sample.

### 5.2.4 Choice of model structures

We are planning to model the given foam sample by a Laguerre tessellation with respect to a marked point process. First of all, we note that the small deviation in the values for  $d_x$ ,  $d_y$ , and  $d_z$  justifies the use of an isotropic model. Working with a Poisson process of generators would of course hold the advantage of having analytic formulas for at least some of the mean values at hand. However, the lack of a formula for the cell intensity requires simulation studies even for these structures. The comparison of Figure 5.3 with the simulation results given in Chapter 4 yields several further arguments against Poisson distributed generators. In particular, the existence of very small and highly irregular cells in the Poisson Laguerre tessellations does not fit the distributions measured for the foam structure.

For this application, Laguerre tessellations generated by marked point processes defined by the centers and radii of hard sphere systems are a more promising choice. In this case, the cell intensity is equal to the intensity of the generating process while the remaining cell characteristics have to be measured from simulations. Up to now, simulation studies for such structures are still rare. Gervois et al. (2002) investigated Laguerre tessellations with respect to packings of binary mixtures of spheres. Fan et al. (2004) studied Laguerre tessellations of random dense packings of spheres with log-normal volume distribution. Their results indicate that the volume distribution of the Laguerre cells is closely determined by the distribution of the ball volumes. However, they observe mean face numbers in a range of 13.0 to 14.2 which demonstrates that these structures are too regular for our application. Further, the generation of dense packings is computationally very complex. An algorithm which is less time consuming would be preferable for the optimization procedure.

In conclusion, we are looking for a hard sphere point process which is less regular than a dense packing of balls, easy to implement, has acceptable run times and does not depend on too many parameters. If the volume fraction is not chosen too high, a system of balls generated by random sequential adsorption (RSA, Torquato (2002, Section 3.4), or SSI, Stoyan et al. (1995)) fulfills these requirements. This point process is generated within a bounded observation window  $W$  as follows: Proposals for the position of ball centers and radii are successively drawn from the uniform distribution on  $W$  and a given radius distribution, respectively. If a newly proposed ball does not overlap with any of the previously placed balls, the proposal is accepted, otherwise it is rejected and a new proposal is made. This procedure is repeated until the desired number of balls has been placed.

However, since small balls are accepted with a higher probability than large ones, the radius distribution of the accepted balls will differ from the distribution of the proposed radii. In order to generate a system of balls with a radius distribution equal to the proposal distribution, the RSA algorithm should be implemented in a way that a new radius is only proposed if a ball with the previously proposed radius has been placed successfully. In contrast to the Poisson processes discussed in the previous chapters, the marks of an RSA process are no longer independent. Nevertheless, the proposal distribution of the radii may be interpreted as the distribution of the radius of the typical ball. In the following, we will consider Laguerre tessellations generated by an RSA point process (RSA Laguerre tessellations).

In the literature both log-normal and gamma distributions are reported for the cell volume distribution of cellular materials (see Fan et al., 2004, and references therein). Hence, we estimate the parameters of both distributions from the foam data using maximum likelihood.

For the gamma distribution we obtain shape parameter  $a = 4.6705$  and scale parameter  $s = 0.001189$ , for the log-normal distribution we get  $\mu = -5.3043$  and  $\sigma = 0.4907$ . Figure 5.4 shows the density of the volume distribution of the foam cells together with the densities of the estimated distributions. The plot shows an acceptable fit for the gamma distribution while the log-normal distribution performs worse. Therefore, we choose a gamma distribution for the ball volumes  $v_b$ . Denoting the mean number of balls per unit volume by  $N_V$  and the volume fraction of the ball system by  $V_V$ , the mean ball volume is given by  $\mathbb{E}[v_b] = V_V/N_V$ . Therefore, the fit of the tessellation structure requires an optimization with respect to  $V_V$  and the variance  $\text{Var}[v_b]$ .

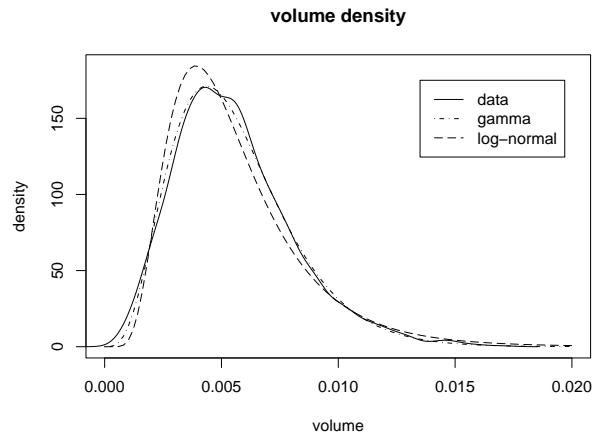


Figure 5.4: The volume density of the foam cells and the density of the fitted gamma and log-normal distributions.

### 5.2.5 Model fitting procedure

In the following, we will discuss how the model described above will be fitted to the foam data using the distance measures defined in (5.1). In the application discussed in Gloaguen et al. (2006), all three measures performed similarly. Since we do not see any reasons why one of them should be preferred, we will run the optimization procedure with all three measures and compare the results.

The vectors  $c$  and  $\hat{c}$  will in our case consist of eight entries, namely the means and variances of  $v$ ,  $s$ ,  $\bar{b}$  (measured as the mean of  $d_x, d_y$ , and  $d_z$ ), and  $f$ . The reference values for the proposed RSA Laguerre tessellations have to be determined by simulation. As a direct simulation of the typical cell is not possible in this case we use the approach working with large aggregates of cells. We simulate Laguerre tessellations of RSA systems consisting of 18230 balls within a cube of volume  $101.23 \text{ mm}^3$ , which is ten times the size of the original sample. For the ball volumes we simulate a gamma distribution with mean  $0.0055532 \text{ mm}^3$  (the mean cell volume) and a coefficient of variation (CV) varying between 0.80 and 1.20 with a step width of 0.01. Scaling these values with the volume fraction  $V_V$  yields an expected ball volume of  $V_V/N_V$ . For the volume fraction  $V_V$  we use the values 0.20, 0.25, and 0.30. For each combination of CV and  $V_V$  we generate five realizations yielding a total number of

91150 cells per set of parameters. All simulations use periodic boundary conditions to avoid edge effects.

In the simulations it turned out that for each of the three  $V_V$ -values all four cell characteristics show the same monotonous behavior with increasing value of CV: While the mean values decrease, we observe increasing variances. Therefore, including both in the optimization procedure is crucial for the minimization.

In order to compare the Laguerre model to some widely used Voronoi models we will also investigate the Poisson Voronoi (PV) tessellation as well as a Voronoi tessellation with respect to a hard core (HCV) point pattern generated by random sequential adsorption. For this purpose we simulate Voronoi tessellations of RSA systems consisting of 18230 equal balls within a cube of volume  $101.23 \text{ mm}^3$ . The volume fraction  $V_V$  of the balls varies between 0.1 and 0.3 in steps of 0.05. Again, we consider five realizations for each choice of  $V_V$ .

### 5.2.6 Test of the optimization method using simulated data

Before applying the proposed optimization method to the foam sample we test the method using simulated data. For that purpose we choose several values for CV and  $V_V$  from the range of our reference structures. For each set of parameters we generate a realization of the corresponding RSA Laguerre tessellation of the same size as the foam sample, i.e. containing 1823 cells within a cube of volume  $10.123 \text{ mm}^3$ . Again, periodic boundary conditions are used to avoid edge effects. To these realizations, we apply the optimization method described in the last section. The minimal distances  $d_e$ ,  $d_a$ , and  $d_m$  and the corresponding parameters are shown in Table 5.2.

It turns out that in most cases the value of  $V_V$  is fitted correctly when using distances  $d_e$  and  $d_a$  while more errors occur for distance  $d_m$ . Otherwise, especially  $d_e$  and  $d_a$  perform similarly. When interpreting the results, one should keep in mind that the reference values also result from simulations and therefore deviate from the true values.

### 5.2.7 Results for foam data

Now we use the optimization method described above for fitting a tessellation model to the polymer foam. The minimal distances for each of the three  $V_V$ -values are shown in Table 5.3. In all three cases the smallest CV-value is obtained using  $d_a$ , while  $d_m$  returns the largest value. The total minimum over the range of simulations is obtained for  $V_V = 0.20$  irrespective of the distance measure applied. This means that the most irregular structure is chosen as the best model. However, the distances between the results for different  $V_V$ -values appear rather small when compared to the distances obtained for the Poisson Voronoi tessellation. The hard core Voronoi tessellation, usually a very popular model for foam structures, performs even worse than the Poisson Voronoi model. This is mainly caused by the low variances of the considered characteristics compared to the real data. Consequently, the best results are obtained for the smallest value of  $V_V$ , which again produces the most irregular structures. Table 5.4 shows the mean values and the variances for the cell characteristics of the best fit models under the different distance measures.

To further validate the model fit we examine the distributions of the cell characteristics of interest. Their densities are plotted in Figure 5.6. The differences between the best fit models for the three distance measures are small compared to the difference of one of them

simulation		result $d_e$			result $d_a$			result $d_m$		
CV	$V_V$	$d_e^{\min}$	$CV_e^{\min}$	$V_{V_e}^{\min}$	$d_a^{\min}$	$CV_a^{\min}$	$V_{V_a}^{\min}$	$d_m^{\min}$	$CV_m^{\min}$	$V_{V_m}^{\min}$
0.83	0.20	0.00835	0.83	0.20	0.01878	0.83	0.20	0.00575	0.83	0.20
0.86	0.25	0.01267	0.85	0.25	0.02866	0.85	0.25	0.00868	0.85	0.25
0.91	0.20	0.03249	0.90	0.20	0.05686	0.90	0.20	0.02520	0.90	0.20
0.94	0.30	0.01907	1.00	0.30	0.03109	1.00	0.30	0.01256	1.12	0.25
0.95	0.25	0.03400	0.96	0.25	0.05728	0.96	0.25	0.02310	0.86	0.30
1.01	0.25	0.02370	1.08	0.20	0.03525	0.95	0.25	0.01243	1.08	0.20
1.05	0.20	0.02076	1.09	0.20	0.03898	1.09	0.20	0.01541	1.09	0.20
1.08	0.30	0.02578	1.10	0.30	0.04496	1.10	0.30	0.01907	1.09	0.30
1.12	0.30	0.01252	1.14	0.30	0.02549	1.14	0.30	0.00881	1.14	0.30
1.14	0.25	0.02401	1.17	0.25	0.04485	1.17	0.25	0.01892	1.16	0.25
1.17	0.20	0.03278	1.01	0.25	0.07600	1.14	0.20	0.02198	1.01	0.25

Table 5.2: Result of the fitting procedure for simulated input data. The first two columns show the parameters of the simulated data sets. The remaining columns contain the minimal distances and the corresponding parameters  $CV$  and  $V_V$  with respect to each of the distance measures  $d_e$ ,  $d_a$ , and  $d_m$ .

to the Voronoi tessellations or the real data. Therefore, only the results for  $d_a$  are included in the plots.

For each of the considered distributions it is obvious that the Laguerre model performs better than both Voronoi tessellations. Especially the difference between the data and the hard core Voronoi tessellation is striking. This model is not able to capture the variability of the characteristics observed in the material. The Poisson Voronoi tessellation fits the volume density of the foam cells quite nicely, which is due to the fact that both volume distributions can be approximated by a gamma distribution (Kumar et al., 1992). For the other characteristics, however, the Laguerre models provides much better results. 3D visualizations and sections of both the real and the model foam are shown in Figure 5.5.

$V_V$	$d_e^{\min}$	$CV_e^{\min}$	$d_a^{\min}$	$CV_a^{\min}$	$d_m^{\min}$	$CV_m^{\min}$
0.20	0.26031	1.10	0.51813	1.03	0.17392	1.14
0.25	0.26544	0.99	0.52428	0.94	0.17895	1.00
0.30	0.27097	0.90	0.52052	0.85	0.17553	0.91
PV	0.44882	-	0.92655	-	0.33695	-
HCV	1.19135	-	2.43360	-	0.67866	-

Table 5.3: Result of the fitting procedure for the foam data. The columns contain the minimal distances and corresponding values of  $CV$  with respect to each of the distance measures  $d_e$ ,  $d_a$ , and  $d_m$ . For comparison the distances for the Poisson Voronoi tessellation and for the hard core Voronoi tessellation with  $V_V = 0.1$  are shown.

### 5.3 Discussion

In this chapter we have reconstructed the cells of a closed polymer foam from a tomographic image of the material. From the reconstructed image we have extracted information on the distributions of various cell characteristics of the foam. Using an optimization method based on relative distance measures defined on vectors of means and variances of cell characteristics, we have fitted a Laguerre tessellation model to the foam structure. Comparison of our model to some widely used Voronoi tessellation models shows that it allows for a better fit of the geometric characteristics of the foam sample.

The results presented in this chapter indicate that Laguerre tessellations are promising models for the microstructure of cellular materials. However, the area of model fitting still holds many open questions. So far, little is known about geometric characteristics of the typical cell of Laguerre tessellations with respect to different processes of generators (e.g., hard core point processes or random dense packings of spheres) and different distributions of radii. Therefore, the decision for a certain model structure will at the moment mainly be based on “smart guessing”.

Comparing the density of cell volumes in our example to the fitted gamma distribution in Figure 5.4 we observe that the gamma distribution shows a slight deviation to the left. The same tendency is even more clearly visible in both the volume and the surface area density of the model structures. Consequently, the question arises whether the choice of another distribution type for the ball volumes would yield better results. The two-peaked structure of the volume distribution suggests using a mixture of different distributions. However, by increasing the number of model parameters, this would also increase the complexity of the fitting procedure.

Once the decision for a certain model structure has been made, the parameters of the model are optimized with respect to distance measures. Here, one has to decide for the characteristics which are included in the optimization procedure. At this point a better knowledge of the correlations between microstructure and physical properties would be helpful when designing the fitting procedures. If the degree of influence of the geometric characteristics on a certain macroscopic property was known, one could concentrate on the more important characteristics and neglect the less influential ones.

When moving through the space of model parameters, we have to ask for a suitable range and step width. In our example it turned out that the differences between the Laguerre tessellations for neighboring CV-values are small. Therefore, one could have chosen a larger step width for the CV-values in the optimization procedure which would have reduced the run time. In general, the step widths should be chosen such that they allow for both acceptable accuracy and run time.

data	$v$	$s$	$f$	$b$	$g$
mean	0.0055532	0.17586	14.637	0.24698	0.77124
variance	6.54219e-6	0.00280	10.378	0.00143	0.00173
$d_e$	$v$	$s$	$f$	$b$	$g$
mean	0.0055532	0.17507	15.111	0.24920	0.76560
variance	7.29116e-6	0.00251	11.079	0.00115	0.00307
$d_a$	$v$	$s$	$f$	$b$	$g$
mean	0.0055532	0.17532	15.129	0.24951	0.76752
variance	6.62352e-6	0.00231	10.444	0.00107	0.00281
$d_m$	$v$	$s$	$f$	$b$	$g$
mean	0.0055532	0.17494	15.113	0.24913	0.76463
variance	7.68002e-6	0.00263	11.419	0.00120	0.00317
PV	$v$	$s$	$f$	$b$	$g$
mean	0.0055532	0.18254	15.535	0.25819	0.72790
var	5.55081e-6	0.00215	11.012	0.00095	0.00340
HCV	$v$	$s$	$f$	$b$	$g$
mean	0.0055532	0.17990	15.402	0.25492	0.76257
variance	2.32507e-6	0.00090	7.033	0.00049	0.00140

Table 5.4: Mean values and variances of geometric characteristics of the reconstructed foam cells and the fitted Laguerre and Voronoi tessellations.

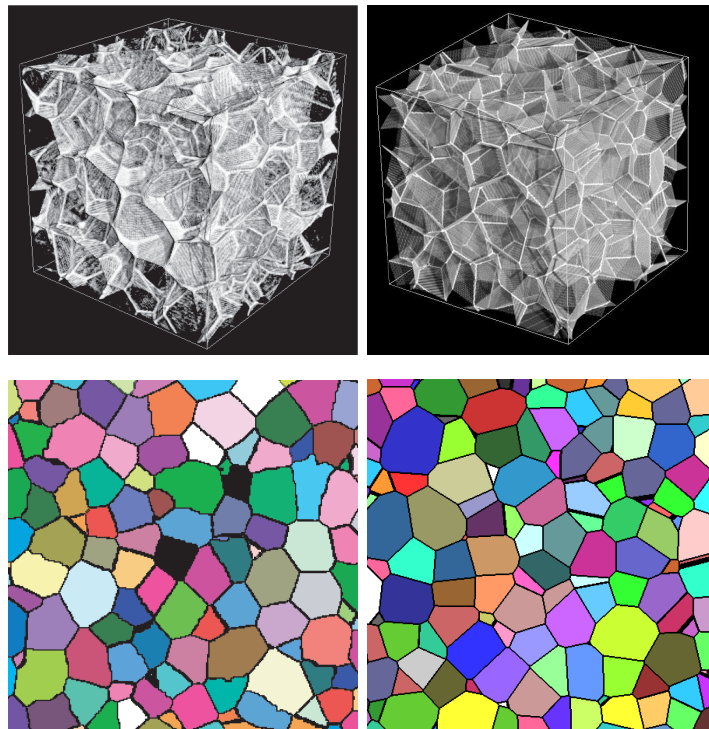


Figure 5.5: Visualizations (top) and planar sections (bottom) of the reconstructed foam cells (left) and of the model foam (right).

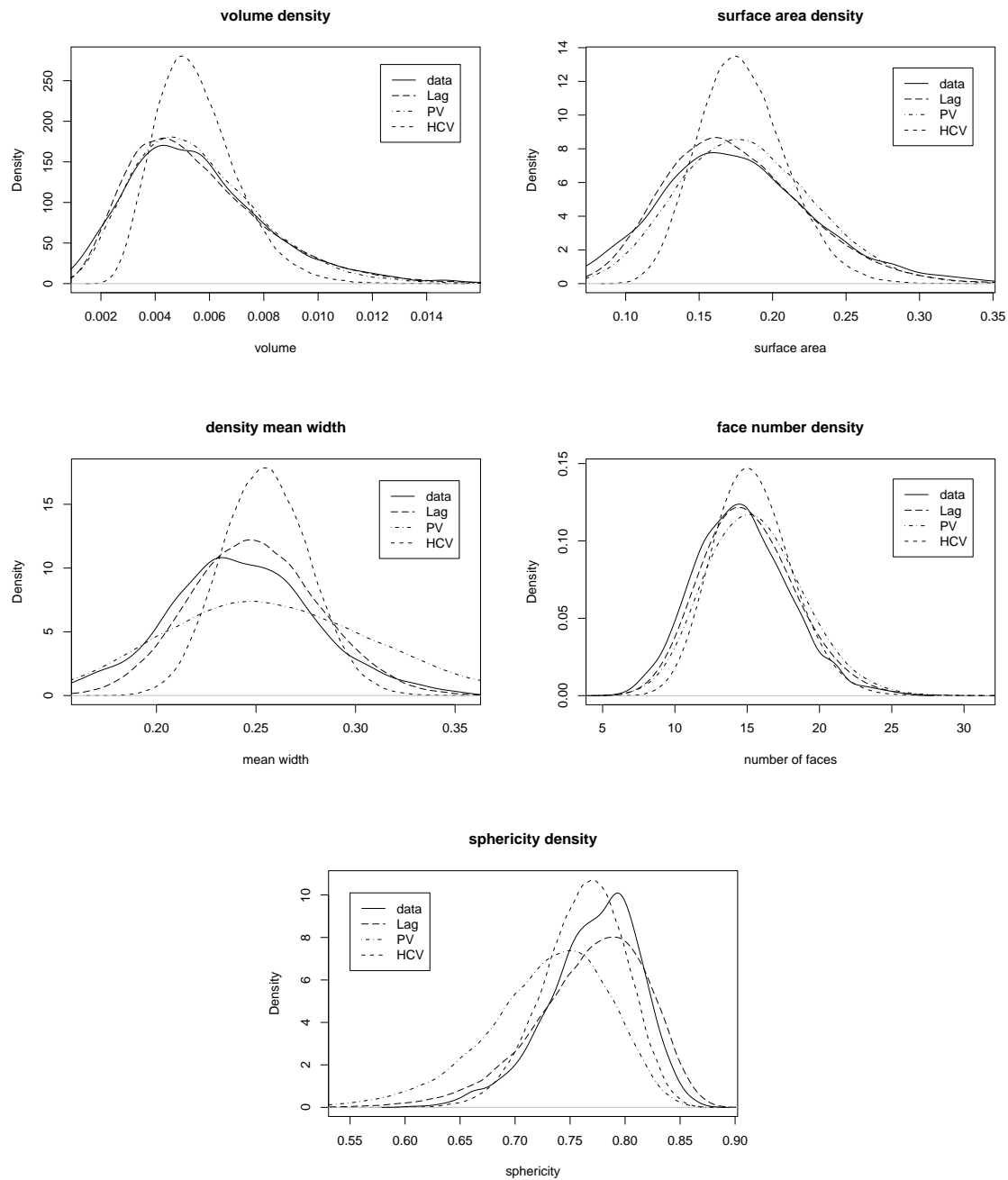


Figure 5.6: Distributions of cell characteristics of the foam sample, the fitted Laguerre tessellation using distance  $d_a$ , and the Voronoi tessellations with respect to a Poisson and an RSA hard core point process.

# Bibliography

- J. Andersson. The influence of grain size variation on metal fatigue. *International Journal of Fatigue*, 27:847–852, 2005.
- C. H. Arns, M. A. Knackstedt, and K. R. Mecke. Reconstructing Complex Materials via Effective Grain Shapes. *Physical Review Letters*, 91(21):215506, 2003.
- P. Ash and E. Bolker. Generalized Dirichlet tessellations. *Geometriae Dedicata*, 20:230–243, 1986.
- F. Aurenhammer. A Criterion for the Affine Equivalence of Cell Complexes in  $\mathbb{R}^d$  and Convex Polyhedra in  $\mathbb{R}^{d+1}$ . *Discrete & Computational Geometry*, 2:49–64, 1987a.
- F. Aurenhammer. Power Diagrams: Properties, Algorithms and Applications. *SIAM Journal on Computing*, 16:78–96, 1987b.
- D. Avis, B. K. Bhattacharya, and H. Imai. Computing the volume of the union of spheres. *The Visual Computer*, 3:323–328, 1988.
- F. Ballani, D. J. Daley, and D. Stoyan. Modelling the microstructure of concrete with spherical grains. *Computational Materials Science*, 35:399–407, 2006.
- C. B. Barber, D. P. Dobkin, and H. T. Huhdanpaa. The Quickhull Algorithm for Convex Hulls. *ACM Transactions on Mathematical Software*, 22, 1996.
- V. Baumstark and G. Last. Some distributional results for Poisson Voronoi tessellations. *Advances in Applied Probability*, 39, 2007. to appear.
- A.-H. Benouali, L. Froyen, T. Dillard, S. Forest, and F. N’Guyen. Investigation on the influence of cell shape anisotropy on the mechanical performance of closed cell aluminium foams using micro-computed tomography. *Journal of Materials Science*, 40:5801–5811, 2005.
- W. Blaschke. *Vorlesungen über Differentialgeometrie und geometrische Grundlagen von Einsteins Relativitätstheorie*. Springer, Berlin, 1929.
- J.-D. Boissonnat and M. Yvinec. *Algorithmic Geometry*. Cambridge University Press, Cambridge, 1998.
- K. A. Brakke. Statistics of random plane Voronoi tessellations. URL <http://www.susqu.edu/facstaff/b/brakke/papers/voronoi.htm>. 1986.

- R. Brezny and D. J. Green. The effect of cell size on the mechanical behavior of cellular materials. *Acta metall. mater.*, 38(12):2517–2526, 1990.
- P. Calka. Precise formulae for the distribution of the principal geometric characteristics of the typical cell of a two-dimensional Poisson-Voronoi tessellation and a Poisson line process. *Adv. Appl. Probab.*, 35:551–562, 2003a.
- P. Calka. An explicit expression for the distribution of the number of sides of the typical Poisson-Voronoi cell. *Adv. Appl. Probab.*, 35:863–870, 2003b.
- Z. Chu, R. L. Mullen, and R. Ballarini. Monte Carlo Simulation of Elastic Properties of Polycrystalline Materials using the Johnson-Mehl Model. In *Proceedings of the 14th ASCE Engineering Mechanics Division Conference*, Austin, May 2000.
- M. Coster, X. Arnould, J.-L. Chermant, A. El Moataz, and T. Chartier. A microstructural model by space tessellation for a sintered ceramic: cerine. *Image Anal. Stereol.*, 24:105–116, 2005.
- H. S. M. Coxeter. *Introduction to geometry*. Wiley, New York, 1969.
- O. Cuisenaire. *Distance transformations: fast algorithms and applications to medical image processing*. PhD thesis, Universite catholique de Louvain, Louvain, 1999. URL <http://ltswww.epfl.ch/~cuisenai>.
- D. J. Daley and D. Vere-Jones. *An Introduction to the Theory of Point Processes*. Springer, New York, 1988.
- T. Dillard, F. N’Guyen, E. Maire, L. Salvo, S. Forest, Y. Bienvenu, J.-D. Bartout, M. Croset, R. Dendievel, and P. Cloetens. 3d quantitative image analysis of open-cell nickel foams under tension and compression loading using X-ray microtomography. *Philosophical Magazine*, 85(19):2147–2175, 2005.
- G. L. Dirichlet. über die Reduction der positiven quadratischen Formen mit drei unbestimmten ganzen Zahlen. *Journal für die Reine und Angewandte Mathematik*, 40:209–227, 1850.
- H. Edelsbrunner and R. Seidel. Voronoi Diagrams and Arrangements. *Discrete Comp. Geom*, 1:25–44, 1986.
- Z. Fan, Y. Wu, X. Zhao, and Y. Lu. Simulation of polycrystalline structure with Voronoi diagram in Laguerre geometry based on random closed packing of spheres. *Computational Materials Science*, 29:301–308, 2004.
- W. Fischer, E. Koch, and E. Hellner. Zur Berechnung von Wirkungsbereichen in Strukturen anorganischer Verbindungen. *Neues Jahrbuch für Mineralogie Monatshefte*, pages 227–237, 1971.
- A. Gervois, L. Oger, P. Richard, and J. P. Troadec. Voronoi and radical tessellations of packings of spheres. In *Computational Geometry and Applications*, pages 95–104, Amsterdam, April 2002.

- A. Gervois, L. Oger, and J.-P. Troadec. Random cuts in binary mixtures of spheres. *Physical Review E*, 70:031112, 2004.
- L. J. Gibson and M. F. Ashby. *Cellular Solids: Structure and Properties*. Cambridge University Press, Cambridge, 1988.
- E. N. Gilbert. Random subdivision of space into crystals. *Ann. Math. Statist.*, 33:958–972, 1962.
- C. Gloaguen, F. Fleischer, H. Schmidt, and V. Schmidt. Fitting of stochastic telecommunication network models via distance measures and Monte-Carlo tests. *Telecommunications Systems*, 31:353–377, 2006.
- M. Godehardt, K. Schladitz, and T. Sych. Analysis of volume images - a tool for understanding the microstructure of foams. In *Symposium Cellular Metals and Polymers*, Fürth, October 2004.
- J. L. Grenstedt and K. Tanaka. Influence of cell shape variations on elastic stiffness of closed cell cellular solids. *Scripta Materialia*, 40(1):71–77, 1999.
- P. Hall. *Introduction to the Theory of Coverage Processes*. Wiley, New York, 1988.
- L. Heinrich. Contact and chord length distribution of a stationary Voronoi tessellation. *Adv. Appl. Prob.*, 30:603–618, 1998.
- H. Imai, M. Iri, and K. Murota. Voronoi diagram in the Laguerre geometry and its applications. *SIAM Journal on Computing*, 14:93–105, 1985.
- Fraunhofer ITWM. MAVI - Modular Algorithms for Volume Images, 2005. URL <http://www.itwm.fhg.de/mab/projects/MAVI>.
- W. A. Johnson and R. F. Mehl. Reaction kinetics in processes of nucleation and growth. *Trans. Amer. Inst. Min. Engrs.*, 135:416–458, 1939.
- I. Kadashevich and D. Stoyan. Aerated autoclaved concrete: Stochastic structure model and elastic properties. *Proc. Appl. Math. Mech.*, 5:419–420, 2005.
- I. Kadashevich, H.-J. Schneider, and D. Stoyan. Statistical modeling of the geometrical structure of the system of artificial air pores in autoclaved aerated concrete. *Cement and Concrete Research*, 35:1495–1502, 2005.
- O. Kallenberg. *Random Measures*. Akademie-Verlag, Berlin, 1983.
- S. Kanaun and O. Tkachenko. Mechanical properties of open cell foams: simulations by Laguerre tessellation procedure. *International Journal of Fracture*, 140:305–312, 2006.
- M. Knackstedt, C. Arns, M. Saadatfar, T. Senden, A. Sakellariou, A. Sheppard, R. Sok, W. Schrof, and H. Steininger. Virtual Materials Design: Properties of Cellular Solids Derived from 3D Tomographic Images. *Advanced Engineering Materials*, 7(4):238–243, 2005.

- M. Kühn. Optimierung von Power-Diagrammen zur Modellierung keramischer Mikrostrukturen. Master's thesis, Fernuniversität Hagen, Fraunhofer EMI, Freiburg i. Br., 2005.
- S. Kumar and S. K. Kurtz. Simulation of material microstructure using a 3D Voronoi tessellation: calculation of effective thermal expansion coefficient of polycrystalline materials. *Acta metall. mater.*, 42(2):3917–3927, 1994.
- S. Kumar, S. K. Kurtz, J. R. Banavar, and M. G. Sharma. Properties of a Three-Dimensional Poisson-Voronoi Tessellation: A Monte-Carlo Study. *Journal of Statistical Physics*, 67(3/4):523–551, 1992.
- R. Kusner and J. M. Sullivan. Comparing the Weaire-Phelan Equal-Volume Foam to Kelvin's Foam. In *The Kelvin Problem: Foam Structures of Minimal Surface Area*, pages 71–80, London, Bristol, 1996. Taylor & Francis.
- J. Lambert, I. Cantat, R. Delannay, A. Renault, F. Graner, J. A. Glazier, I. Veretennikov, and P. Cloetens. Extraction of relevant physical parameters from 3d images of foams obtained by x-ray tomography. *Colloids and Surfaces A: Physiochem. Eng. Aspects*, 263:295–302, 2005.
- C. Lautensack and T. Sych. 3d image analysis of open foams using random tessellations. *Image Analysis and Stereology*, 25:87–93, 2006.
- C. Lautensack, K. Schladitz, and A. Särkkä. Modeling the microstructure of sintered copper. In *Proceedings of the 6th International Conference on Stereology, Spatial Statistics and Stochastic Geometry*, Prague, June 2006.
- G. Matheron. *Random Sets and Integral Geometry*. John Wiley & Sons, New York, 1975.
- J. Matoušek. *Lectures on Discrete Geometry*. Springer, New York, 2002.
- E. B. Matzke. The three-dimensional shape of bubbles in foam - an analysis of the role of surface forces in three-dimensional cell shape determination. *Am. J. Bot.*, 33:58–80, 1946.
- J. Mecke. Parametric representation of mean values for stationary random mosaics. *Math. Operationsforsch. u. Statistik, ser. stat.*, 3:437–442, 1984.
- J. L. Meijering. Interface area, edge length and number of vertices in crystal aggregates with random nucleation. *Philips Res. Rep.*, 8:270–290, 1953.
- R. E. Miles. Isotropic random simplices. *Adv. Appl. Probab.*, 3:353–382, 1971.
- R. E. Miles. The random division of space. *Adv. Appl. Probab. Suppl.*, 4:243–266, 1972.
- J. Møller. Random tessellations in  $\mathbb{R}^d$ . *Adv. Appl. Probab.*, 21:37–73, 1989.
- J. Møller. Random Johnson-Mehl tessellations. *Adv. Appl. Probab.*, 24:814–844, 1992.
- J. Møller. *Lectures on Random Voronoi Tessellations*, volume 87 of *Lect. Notes Statist.* Springer, New York, 1994.

- J. Møller. Generation of Johnson-Mehl crystals and comparative analysis of models for random nucleation. *Adv. Appl. Prob.*, 27:367–383, 1995.
- M. D. Montminy, A. R. Tannenbaum, and C. W. Macosko. The 3D structure of real polymer foams. *Journal of Colloid and Interface Science*, 280:202–211, 2004.
- L. Muche. The Poisson Voronoi tessellation: Relationships for edges. *Adv. Appl. Prob.*, 37:279–296, 2005.
- L. Muche. Distributional properties of the three-dimensional Poisson Delaunay cell. *J. Stat. Phys.*, 84:147–167, 1996a.
- L. Muche. The Poisson-Voronoi tessellation. II. edge length distribution functions. *Math. Nachrichten*, 178:271–283, 1996b.
- L. Muche. The Poisson Voronoi tessellation. III. Miles’ formula. *Math. Nachrichten*, 191:247–267, 1998.
- L. Muche and D. Stoyan. Contact and chord length distributions of the Poisson Voronoi tessellation. *J. Appl. Probab.*, 29:467–471, 1992.
- J. Neveu. Processus ponctuels. In *École d’Été de Probabilités de Saint-Flour VI. Lecture Notes in Mathematics 598*, pages 249–445, Berlin, 1977. Springer.
- J. Ohser and F. Mücklich. *Statistical Analysis of Microstructures in Materials Science*. J. Wiley & Sons, Chichester, 2000.
- A. Okabe, B. Boots, K. Sugihara, and S. N. Chiu. *Spatial Tessellations — Concepts and Applications of Voronoi Diagrams*. Wiley, Chichester, second edition, 2000.
- M. P. Quine and D. F. Watson. Radial generation of n-dimensional poisson processes. *J. Appl. Prob.*, 21:548–557, 1984.
- S. Ribeiro-Ayeh. *Finite Element Modelling of the Mechanics of Solid Foam Materials*. PhD thesis, Kungliga Tekniska Högskolan, Stockholm, 2005.
- A. P. Roberts and E. J. Garboczi. Elastic moduli of model random three-dimensional closed-cell cellular solids. *Acta materialia*, 49:189–197, 2001.
- A. P. Roberts and E. J. Garboczi. Elastic properties of model random three-dimensional open-cell solids. *Journal of the Mechanics and Physics of Solids*, 50(1):33–55, 2002.
- J. F. Sadoc, R. Jullien, and N. Rivier. The Laguerre polyhedral decomposition: application to protein folds. *Eur. Phys. J. B*, 33:355–363, 2003.
- K. Schladitz, S. Peters, D. Reinel-Bitzer, A. Wiegmann, and J. Ohser. Design of acoustic trim based on geometric modeling and flow simulation for non-woven. *Computational Materials Science*, 38:56–66, 2006.
- M. Schlather. A Formula for the Edge Length Distribution Function of the Poisson Voronoi Tessellation. *Math. Nachrichten*, 214:113–119, 2000.

- M. Schlottmann. Periodic and quasi-periodic Laguerre tilings. *International Journal of Modern Physics B*, 7:1351–1363, 1993.
- R. Schneider. *Convex bodies: the Brunn-Minkowski theory*. Cambridge University Press, Cambridge, 1993.
- R. Schneider and W. Weil. *Stochastische Geometrie*. Teubner, Leipzig, 2000.
- R. Schneider and W. Weil. *Integralgeometrie*. B. G. Teubner, Stuttgart, 1992.
- E. Schüle. A justification of the Hillert distribution by spatial grain growth simulation performed by modifications of Laguerre tessellations. *Computational Materials Science*, 5:277–285, 1996.
- J. Schwertel and H. Stamm. Analysis and modelling of tessellations by means of image analysis methods. *Journal of Microscopy*, 186:198–209, 1997.
- J. Serra. *Image Analysis and Mathematical Morphology*. Academic Press, London, 1982.
- P. Soille. *Morphological image analysis*. Springer Verlag, 1999.
- D. Stoyan, W. S. Kendall, and J. Mecke. *Stochastic Geometry and its Applications*. Wiley, Chichester, second edition, 1995.
- K. Sugihara. Three-dimensional Convex Hull as a Fruitful Source of Diagrams. *Theoretical Computer Science*, 235:325–337, 2000.
- H. Telley, T. M. Liebling, and A. Mocellin. The Laguerre model of grain growth in two dimensions, I. Cellular structures viewed as dynamical laguerre tessellations. *Philosophical Magazine B*, 73(3):395–408, 1996a.
- H. Telley, T. M. Liebling, and A. Mocellin. The Laguerre model of grain growth in two dimensions, II. Examples of coarsening simulations. *Philosophical Magazine B*, 73(3):409–427, 1996b.
- Sir W. Thomson. On the division of space with minimum partitional area. *Phil. Mag.*, 24:503–614, 1887.
- S. Torquato. *Random Heterogeneous Materials: microstructure and macroscopic properties*. Springer-Verlag, New York, 2002.
- L. Vincent and P. Soille. Watersheds in digital spaces: an efficient algorithm based on immersion simulations. *IEEE Transactions on Pattern Analysis and Machine Intelligence*, 13:583–598, 1991.
- G. Voronoi. Nouvelles applications des paramètres continus à la théorie des formes quadratiques. premier mémoire: Sur quelques propriétés des formes quadratiques positives parfaites. *Journal für die Reine und Angewandte Mathematik*, 133:97–178, 1907.
- G. Voronoi. Nouvelles applications des paramètres continus à la théorie des formes quadratiques. Deuxième Mémoire: Recherches sur les paralléloèdres primitifs. *Journal für die Reine und Angewandte Mathematik*, 134:198–287, 1908.

- G. Voronoi. Nouvelles applications des paramètres continus à la théorie des formes quadratiques. Deuxième Mémoire: Recherches sur les paralléloèdres primitifs. second partie. domaines des formes quadratiques correspondant aux différents types de paralléloèdres primitifs. *Journal für die Reine und Angewandte Mathematik*, 136:67–181, 1909.
- D. Weaire and R. Phelan. A counter-example to Kelvin's conjecture on minimal surfaces. *Phil. Mag. Lett.*, 69:107–110, 1994.
- X. Xue, F. Righetti, H. Telley, and T. M. Lieblich. The Laguerre model for grain growth in three dimensions. *Philosophical Magazine B*, 75(4):567–585, 1997.
- H. X. Zhu, J. R. Hobdell, and A. H. Windle. Effects of cell irregularity on the elastic properties of open-cell foams. *Acta materialia*, 48:4893–4900, 2000.
- S. Zuyev. Poisson power tessellations. unpublished, 2004.

# List of symbols

$A(r_0, r_1, p)$ .....	6	$P_k(x, \varphi)$ .....	35
$A(t, r_0, u, \eta)$ .....	52	$R_k$ .....	50
$A_{L^\perp}(t, s, \eta)$ .....	52	$R'_k$ .....	50
$B + x$ .....	6	$R''_k$ .....	50
$C((x, w), \varphi)$ .....	20	$R_{k,i}$ .....	36
$C_k(0)$ .....	15	$R_{k,i}(x, \varphi)$ .....	35
$C_k(x)$ .....	57	$R'_{k,m}$ .....	57
$C_k(x, T), C_k(x, \varphi)$ .....	15, 57	$R'_{k,m}(x, \Phi)$ .....	57
$D(\varphi)$ .....	27	$SO_d$ .....	6
$D(z, \varphi)$ .....	26	$S^{d-1}$ .....	6
$F(s_0, \dots, s_k, \varphi)$ .....	22	$S_V$ .....	17
$F(y)$ .....	14	$S_{k,i}(x, \varphi)$ .....	35
$F_k(0)$ .....	36	$T'$ .....	55
$F_k(x)$ .....	57	$T''$ .....	55
$F_k(x, T), F_k(x, \varphi)$ .....	15, 57	$T''(x, \Phi)$ .....	55
$G(s_0, \dots, s_k)$ .....	22	$T'(x, \Phi)$ .....	55
$G_\Phi$ .....	8	$U(a, b)$ .....	6
$H(s_1, s_2)$ .....	22	$U_1^*$ .....	55
$H_B(r)$ .....	59	$U_1^*(x, \Phi)$ .....	55
$H_s(r)$ .....	59	$U_k$ .....	36
$H_{l(v)}(r)$ .....	59	$U_k(x, \varphi)$ .....	35
$I_1$ .....	55	$U_{k,i}$ .....	36
$I_1(x, \Phi)$ .....	55	$U_{k,i}(x, \varphi)$ .....	35
$L(\varphi)$ .....	20	$V_{k,i}$ .....	57
$L(c, v)$ .....	64	$V_{k,i}(x, \Phi)$ .....	57
$L_A$ .....	17	$V_{m,k}(s_0, \dots, s_m)$ .....	44
$L_V$ .....	17	$X_s$ .....	18
$L_v(r)$ .....	62	$X_{k,i}(x, \varphi)$ .....	35
$M_k(\cdot)$ .....	15, 34	$Z_k$ .....	36
$M_{k,\lambda}^V(\cdot)$ .....	64	$Z_k(x, \varphi)$ .....	35
$N_k(X)$ .....	15	$\Delta_m(x_0, \dots, x_m)$ .....	36
$N_k(\varphi)$ .....	57	$\Delta_s(P)$ .....	14
$N_{k,j}$ .....	78	$\Delta_s(T)$ .....	14
$P_k$ .....	36	$\mathbb{E}_M$ .....	13
$P'_k$ .....	36	$\mathbb{E}_{M_k}$ .....	34
$P''_k$ .....	36	$\mathbb{E}_{M_k}^0$ .....	34
$P''_k(x, \varphi)$ .....	35	$\Lambda(\cdot)$ .....	7, 12
$P'_k(x, \varphi)$ .....	35	$\mathbb{P}^0(\cdot)$ .....	8, 11

$\mathbb{P}^{0,!}(\cdot)$ .....	8	$\mathcal{S}_s(T)$ .....	14
$\mathbb{P}_M(\cdot)$ .....	13	$\delta_x(\cdot)$ .....	6
$\mathbb{P}_M^0(\cdot)$ .....	13	$\gamma_k$ .....	15
$\Phi - y$ .....	7, 10	$\kappa(l, r_1, r_2)$ .....	51
$\Phi_{c,v}$ .....	64	$\lambda_M$ .....	12
$\Psi_k$ .....	36	$\lambda_d$ .....	6
$\mathbb{Q}_k(\cdot)$ .....	34	$\langle \cdot, \cdot \rangle$ .....	6
$\mathbb{Q}_k(c, v)$ .....	64	$\mu_k$ .....	15, 34
$\mathbb{Q}_k^0(\cdot)$ .....	34	$\mu_k(c, v)$ .....	64
$\mathbb{Q}_k^0(c, v)$ .....	64	$\mu_m$ .....	36
$\mathbb{Q}_{k,\lambda}^V(\cdot)$ .....	64	$\mu_{k,\lambda}^V$ .....	64
$\mathbb{Q}_{k,\lambda}^{V,0}(\cdot)$ .....	64	$\nu$ .....	6
$\mathbb{R}^d$ .....	5	$\nu_m$ .....	36
$\mathbb{S}$ .....	6	$\omega_d$ .....	6
$\mathbb{S}_L$ .....	38	$\partial B$ .....	6
$\Xi_k$ .....	57	$\text{pow}(y, s)$ .....	20
$\Xi_k(x, \Phi)$ .....	57	$\text{pow}(y, (x, w))$ .....	20
$\alpha_{m,k}$ .....	45	$\text{Ra}(s_1, s_2)$ .....	21
$\mathbf{M}$ .....	12	$\rho(l, t, r_0, \theta)$ .....	51
$\mathbf{N}$ .....	6	$\rho(l, t, r_0, u, v)$ .....	51
$\mathbf{N}(E)$ .....	10	$\rho_k$ .....	57
$\mathbf{N}_s$ .....	6	$\rho_k(x, \Phi)$ .....	57
$\mathbf{T}$ .....	14	$\sigma_d$ .....	6
$\mathbf{T}_f$ .....	14	$\tau(l, t, s, \theta)$ .....	51
$\mathbf{T}_n$ .....	14	$\tau(l, t, s, u, v)$ .....	51
$\beta_{m,k}$ .....	45	$\text{int } B$ .....	6
$\mathcal{B}(E)$ .....	5	$\varphi^t$ .....	32
$\mathcal{B}^d$ .....	5	$\vartheta\Phi$ .....	8, 10
$\mathcal{C}$ .....	5	$\xi(l, t_1, t_2)$ .....	52
$\mathcal{C}'$ .....	5	$b(x, r)$ .....	6
$\mathcal{C}'(E)$ .....	5	$c(C)$ .....	14
$\mathcal{C}(E)$ .....	5	$c(C, \eta)$ .....	14
$\mathcal{F}$ .....	5	$c_k(F, X)$ .....	15
$\mathcal{F}'$ .....	5	$c_k(x)$ .....	57
$\mathcal{F}'(E)$ .....	5	$c_k(x, T), c_k(x, \varphi)$ .....	15, 57
$\mathcal{F}(E)$ .....	5	$c_{dm}$ .....	37
$\mathcal{F}^C$ .....	5	$m_2$ .....	78
$\mathcal{F}_C$ .....	5	$p(t)$ .....	32
$\mathcal{G}$ .....	5	$p_0$ .....	55
$\mathcal{G}(E)$ .....	5	$p_1(t)$ .....	96
$\mathcal{H}^k$ .....	6	$p_2(t)$ .....	96
$\mathcal{M}$ .....	12	$s(x, r)$ .....	20
$\mathcal{N}$ .....	6	$t^+$ .....	32
$\mathcal{N}(E)$ .....	10	$z(s_0, \dots, s_m)$ .....	35
$\mathcal{P}_k$ .....	57	$\mathcal{E}_m^d$ .....	36
$\mathcal{S}_s(C)$ .....	14	$\mathcal{L}_m^d$ .....	36